DYNAMIC MODELING, CONTROL AND ADAPTIVE ENVELOPE PROTECTION SYSTEM FOR HORIZONTAL AXIS WIND TURBINES

A THESIS SUBMITTED TO
THE GRADUATE SCHOOL OF NATURAL AND APPLIED SCIENCES
OF
MIDDLE EAST TECHNICAL UNIVERSITY

BY

MUSTAFA ŞAHİN

IN PARTIAL FULFILLMENT OF THE REQUIREMENTS
FOR
THE DEGREE OF DOCTORATE OF PHILOSOPHY
IN
AEROSPACE ENGINEERING

DECEMBER 2018

Approval of the thesis:

DYNAMIC MODELING, CONTROL AND ADAPTIVE ENVELOPE PROTECTION SYSTEM FOR HORIZONTAL AXIS WIND TURBINES

submitted by **MUSTAFA ŞAHİN** in partial fulfillment of the requirements for the degree of **Doctor of Philosophy in Aerospace Engineering Department, Middle East Technical University** by,

Prof. Dr. Halil Kalıpçılar
Dean, **Graduate School of Natural and Applied Sciences** ______________

Prof. Dr. İsmail Hakkı Tuncer
Head of Department, **Aerospace Engineering Dept., METU** ______________

Assoc. Dr. İlkay Yavrucuk
Supervisor, **Aerospace Engineering Dept., METU** ______________

Examining Committee Members:

Prof. Dr. Oğuz Uzol ______________
Aerospace Engineering Dept., METU

Assoc. Prof. Dr. İlkay Yavrucuk ______________
Aerospace Engineering Dept., METU

Assoc. Prof. Dr. M. Metin Yavuz ______________
Aerospace Engineering Dept., METU

Prof. Dr. Mehmet Önder Efe ______________
Computer Engineering Dept.,
Hacettepe University

Prof. Dr. Metin U. Salamcı ______________
Mechanical Engineering Dept.,
Gazi University

Date: 04.12.2018

I hereby declare that all information in this document has been obtained and presented in accordance with academic rules and ethical conduct. I also declare that, as required by these rules and conduct, I have fully cited and referenced all material and results that are not original to this work.

Name, Last name: Mustafa Şahin

Signature :

ABSTRACT

DYNAMIC MODELING, CONTROL AND ADAPTIVE ENVELOPE PROTECTION SYSTEM FOR HORIZONTAL AXIS WIND TURBINES

Şahin, Mustafa

PhD, Department of Aerospace Engineering

Supervisor : Assoc. Prof. Dr. İlkay Yavrucuk

December 2018, 270 pages

In this thesis study, a wind turbine envelope protection system is introduced to protect turbines throughout the below and above rated regions. The proposed protection system, which is based on a neural network, adapts to various turbines and operational conditions. It can keep the turbine within pre-defined envelope limits whenever a safe operation is about to be violated. The avoidance is realized by control limiting technique applied to the blade pitch controller output, thereby adjusting the blade pitch angle. To achieve the purpose, a horizontal axis wind turbine (HAWT) dynamic (simulation) model based on Blade Element Momentum (BEM) theory is developed using MATLAB and Simulink programs. It is named as MS (Mustafa Sahin) Bladed simulation model. The MS Bladed model includes important aerodynamic corrections and particular coordinate systems etc. for a more realistic turbine behavior. It is validated using experimental data or program/model performance predictions of various turbines belong to National Renewable Energy Laboratory, or NREL. Eventually, NREL 5 MW wind turbine is adopted in the MS Bladed model. Baseline controllers such as generator torque and collective blade pitch controllers are designed for NREL 5MW turbine, and then their simulations are evaluated. Afterward, the proposed protection system is designed and added on to the controlled MS Bladed

model for NREL 5 MW turbine. Thrust force is selected as the pre-defined envelope limit. Simulations under normal turbulent winds with different mean values have shown that the newly proposed system shows a promising capability to keep the 5 MW turbine within the pre-defined thrust limit throughout the below and above rated regions. In this thesis study, three example cases under normal turbulent winds with mean values of 8, 11 and 15 m/s are given to show the effectivity of the proposed algorithm.

Keywords: Wind turbine aerodynamics, Dynamic modeling of wind turbines, Wind turbine control and protection system designs, Neural network, Limit detection and avoidance, Ultimate load reduction.

ÖZ

YATAY EKSENLİ RÜZGAR TÜRBİNİN DİNAMİK MODELLENMESİ, KONTROLÜ VE ADAPTİVE ZARF KORUMASI SİSTEMİ

Şahin, Mustafa
Doktora, Havacılık ve Uzay Mühendisliği Bölümü
Tez Yöneticisi : Doç. Dr. İlkay Yavrucuk

Aralık 2018, 270 sayfa

Bu tez çalışmasında, türbinleri kısmı ve tam yük bölgelerinde önceden belirlenen güvenli limitler içerisinde tutmak için bir zarf koruma sistemi önerilmiştir. Önerilen sistem, adaptif bir yapay sinir ağı kullanmakta olup, rüzgar türbinlerinde oluşan değişikliğe ve farklı çalışma şartlarına adapte olabilmektedir. Önceden belirlenen limitin aşılma olasılığı durumunda, sistem türbini koruyabilecek bir özelliğe sahiptir. Koruma/sakınma işlemi, kanat yunuslama açısı kontrolcüsünün çıkışı ve sonucunda da kanatların yunuslama açışının değiştirilmesi ile sağlanmıştır. Önerilen sistemi tasarlamak ve test etmek için, Pal Elemanı Momentum (BEM) teorisine dayanan dinamik bir yatay eksenli rüzgar türbin modeli, MATLAB ve Simulink programları kullanılarak geliştirilmiştir. Geliştirilen model, MS (Mustafa Şahin) Bladed olarak isimlendirilmiştir. Modellemede, BEM teorisinin dışında, önemli aerodinamik düzeltme formülleri ve özel koordinat sistemlerinden de faydalanılarak, daha gerçekçi bir rüzgar türbin modeli elde edilmiştir. Amerika Birleşik Devletlerine ait Milli Yenilenebilir Enerji Laboratuvarının (NREL) türbinlerine ait test verileri ve mevcut program/model performans tahminleri kullanılarak, geliştirilen model doğrulanmıştır. En nihayetinde, NREL'in 5 MW'lık rüzgar türbini MS Bladed türbin simülasyon modelinde kullanılmış olup, bu türbine göre, temel kontrolcülerden jeneratör tork ve kanat yunuslama açısı kontrolcüleri tasarlanmış ve simülasyonları incelenmiştir.

Ardından, önerilen zarf koruma sistemi de tasarlanarak kontrol edilen 5 MW'lık türbin modeline eklenmiştir. İtki kuvveti, limitlenecek parametre olarak seçilmiştir. Normal türbülanslı farklı ortalama rüzgar hızlarındaki simülasyonlarda, önerilen sistemin 5 MW'lık türbini kısmı ve tam yük bölgeleri boyunca önceden belirlenen itki değeri içinde tutarak, umut verici bir performans sergilediği gözlemlenmiştir. Bu tez çalışmasında, 8, 15 ve 11 m/s ortalama rüzgar hızlarındaki simülasyonlara yer verilerek sistemin etkinliği gösterilmiştir.

Anahtar Kelimeler: Rüzgar türbin aerodinamiği, Rüzgar türbinlerinin dinamik modellenmesi, Rüzgar türbin kontrol ve koruma sistemleri tasarımı, Yapay sinir ağı, Limit sezme ve sakınma, Azami yük azaltma

To the youth who long for a better education, never give up!

ACKNOWLEDGMENTS

First and foremost, I would like to thank my supervisor Assoc. Prof. Dr. İlkay Yavrucuk not only for accepting me as a doctorate student and giving me a change to study at METU Aerospace Engineering, Graduate School of Natural and Applied Sciences, but also for guiding me to study envelope protection systems on wind turbines along with his constant support, guidance, and patience throughout the periods during the one-year scientific prep school and the doctorate study.

I am also very grateful to the senior design engineer, Dr. Jason Jonkman at National Renewable Energy Laboratory, NREL for his precious help, comments and sharing his experiences during the turbine modeling and designs of baseline controllers.

I am also very thankful to my Thesis Monitoring Committee Members, Prof. Dr. Oğuz Uzol and Assoc. Prof. Dr. Metin Yavuz for their valuable help and beneficial comments during committee meetings.

I am very appreciated to Asst. Prof. Dr. Ali Türker Kutay, Prof. Dr. Ozan Tekinalp, Prof. Dr. Altan Kayran, Prof. Dr. Dilek Funda Kurtuluş, Assoc. Prof. Dr. Nilay Oğuz Uzol for their valuable support, and to my colleagues, Dr. Touraj Farsadi, Dr. Hooman Amiri Hazaveh, Doctorate candidate Can Muyan, Doctorate candidate Sinan Ekinci, and Doctorate candidate Aydın Amirali for the scientific discussions related to control, aerodynamics, structures etc. and lastly Doctorate student İrem Nalça, Michael McMillan for their valuable help during checking this thesis study.

Finally, I am very grateful to my family for their valuable supports throughout my life.

TABLE OF CONTENTS

LIST OF TABLES

TABLES

LIST OF FIGURES

FIGURES

LIST OF ABBREVIATIONS

HAWT	Horizontal Axis Wind Turbine
VAWT	Vertical Axis Wind Turbine
LSS	Low Speed Shaft
HSS	High Speed Shaft
WRSG	Wound Rotor Synchronous Generator
DC	Direct Current
SCIG	Squirrel Cage Induction Generator
DFIG	Doubly Fed Induction Generator
WRIG	Wound Rotor Induction Generator
PMSG	Permanent Magnet Synchronous Generator
BEM	Blade Element Momentum
TSR	Tip Speed Ratio
RPM	Revolutions Per Minute
NREL	National Renewable Energy Laboratory
DOE	US Department of Energy Office
SERI	Solar Energy Research Institute
NWTC	National Wind Technology Center
PROPID	Inverse Design and Analysis Program
PROPGA	Genetic Algorithm-Based Optimization
FAST	NREL HAWT Simulation Model
SHLNN	Single Hidden Layer Neural Network
LPNN	Linearly Parameterized Neural Network
PI	Proportional-Integral
PID	Proportional-Integral-Derivative
AOA	Angle of Attack
HOT	High Order Terms
DU	Delft University
NACA	National Advisory Committee for Aeronautics

AR	Aspect Ratio
kW	Kilowatt
MW	Megawatt
$O_i x_i y_i z_i$	Inertial Coordinate System
$O_w x_w y_w z_w$	Wind-aligned Coordinate System
$O_y x_y y_y z_y$	Yaw-aligned Coordinate System
$O_h x_h y_h z_h$	Hub-aligned Coordinate System
$O_z x_z y_z z_z$	Azimuth-aligned Coordinate System
$O_b x_b y_b z_b$	Blade-aligned Coordinate System
$O_{ae} x_{ae} y_{ae} z_{ae}$	Aerodynamic-aligned Coordinate System
U, V_{wind}	Freestream Velocity or Wind Speed
ρ	Air Density
A	Turbine Rotor Disk Area
$\dot{m}$	Mass Flow Rate
p	Static Pressure
a	Axial Induction Factor
a_{skew}	Corrected Axial Induction Factor due to Skewed Wake
a'	Tangential Induction Factor
a_c	Critical Axial Induction Factor
C_p, Cp	Turbine Power Coefficient
C_{pmax}	Maximum Power Coefficient
C_T	Turbine Thrust Coefficient
U_{rel}	Relative Wind
T	Turbine Thrust Force
dT	Elemental Thrust Force
P_{wind}	Power in Wind
$F_{dynamics}$	Dynamic Wind Force
P	Turbine Power
dP	Elemental Turbine Power
ω	Flow Angular Velocity behind the Turbine

Ω	Turbine Rotor Speed
Ω_u	Upper Limit for Generator or Rotor Speed
Ω_l	Lower Limit for Generator or Rotor Speed
S	Number of Blade Sections
R	Rotor Radius
R_{hub}	Rotor Hub Radius
r	Local Rotor Radius
c	Local Chord Length
dr	Elemental Thickness or Length
b	Fixed Structural Angle between Turbine Blades
λ	Tip Speed Ratio
λ_*	Optimum Tip Speed Ratio
λ_r	Local Speed Ratio
α	Angle of Attack
$\Delta\alpha$	Stall Delay Angle
$\alpha C_{l,max}$	Angle for Maximum Lift
αC_{l0}	Angle for Lift Coefficient of Zero
K'	External Flow Velocity Gradient
θ_{TE}	Position of the Trailing Edge
φ	Local Inflow Angle
β	Blade Pitch Angle
β_*	Optimum Blade Pitch Angle
β_T	Elemental Twist Angle
β_{p}	Total of Elemental Blade Twist and Pitch Angle
β_{ref}	Blade Pitch Reference
B_n	Blade Element Number
Cl	Lift Coefficient
Cd	Drag Coefficient
C_n	Normal Force Coefficient

C_t	Tangential Force Coefficient
dF_L	Elemental Lift Force
dF_D	Elemental Drag Force
dF_N	Elemental Normal (Thrust) Force or Flap Shear Force
dF_T	Elemental Tangential Force or Lead-Lag Shear Force
dM_T	Lead-Lag Moment
dM_N	Flap Moment
dF'_N, dT	Elemental Total Thrust Force
dF'_T	Elemental Total Tangential Force
dQ	Elemental Total Torque
F_{hub}	Hub Loss Factor
F_{tip}	Tip Loss Factor
F	Total Loss Factor
σ	Local Solidity
φ	Inflow Angle
X	Wake Skew Angle
Λ	Azimuth Angle
β_{wind}	Wind Angle
Ψ	Turbine Yaw Angle
θ	Nacelle Tilt Angle
Φ	Rotor Precone Angle
J_t	Total Turbine Inertia
dM_T	Elemental Aerodynamic Torque due to Tangential Force
dM_N	Elemental Aerodynamic Torque due to Normal Force
F_{bx}	Flap Shear Force
F_{by}	Lead-Lag Force
F_{hx}	Axial/Thrust Force at Rotor Hub Center
F_{hy}	Lateral Force at Rotor Hub Center
F_{hz}	Vertical Force at Rotor Hub Center
M_{hx}	Rotor/Aerodynamic Torque at Rotor Hub Center

M_{hy}	Tilt Moment at Rotor Hub Center
M_{hz}	Yaw Moment at Rotor Hub Center
J_{rotor}	Rotor Inertia
J_{gen}	Generator Inertia
N_{gear}	Gearbox Ratio
τ_{aero}	Aerodynamic Rotor Torque
τ_{gen}	Generator Torque with Gearbox Ratio Effect
τ_l	Lower Limit of Generator Torque on LSS or HSS
τ_u	Upper Limit of Generator Torque on LSS or HSS
τ_g	Generator Torque Actuator Output
V_{ef}	Effective Wind Speed
K_g	Generator Torque Controller Gain
Re	Reynolds Number
U_e	Equilibrium Wind Speed
Ω_e	Equilibrium Rotor Speed
β_e	Equilibrium Blade Pitch Angle
ɣ	Partial Derivative of Aerodynamic Torque wrt Rotor Speed
η	Partial Derivative of Aerodynamic Torque wrt Blade Pitch Angle
μ	Partial Derivative of Aerodynamic Torque wrt Wind Speed
K_p	Proportional Gain
K_i	Integral Gain
A	System Gain or Matrix
B	Input Gain or Matrix
B_d	Disturbance Gain or Matrix
w_n	Natural Frequency
ζ	Damping Ratio
EP	Equilibrium Point
GK	Gain Correction Factor
Y	Measurable System Outputs

y_l	Limit Parameter
$\hat{y}_l$	Approximate or Estimate Limit Parameter
$y_{l_{UD}}$	Unsteady Dynamics Value of Limit Parameter
u	System Input
x	States
x_s	Slow States
x_f	Fast States
ξ	Modelling Error
$\hat{r}$	Approximate Model for Limit Parameter Dynamics
e	Error Term
Δ	Neural Network Term, Output Vector
W	Neural Network Weights
ϵ	Reconstruction Error
δ	Basis Functions
μ	Input Vector
k	e-modification Term
Γ	Learning Rate
Γ_{min}	Lower Bound for Learning Rate
Γ_{max}	Upper Bound for Learning Rate
$\oplus$	Kronecker Product
K	Observer Gain Matrix
u_{env}	Envelope Wind Speed
ε	Design Parameter for Effective Limit Avoidance

CHAPTER 1

INTRODUCTION

Energies are the essence for a comfortable and an easy life. They are almost everywhere, but the important point is to explore the energy type first and then change it into a way that the desired purpose is realized properly. One kind of energy is the wind, which has been utilized for ages in order to fulfill various purposes. The advantages of wind over other energy sources are that it is a totally free, abundant and clean energy source. Therefore, it is a wise choice to utilize this energy as much as possible in our daily life.

1.1 Wind Energy Usage and Current Worldwide Status of Wind Power

Wind generally occurs because of the sun heating the atmosphere unevenly, earth surface roughness and earth rotation[1]. It includes a large amount of useful energy that does not need any pre-processing. Therefore, wind energy has played a role in human civilization for centuries. Starting from the first usage to the 20th century, it was utilized for different purposes by means of machines referred to as windmills or windwheels. However, the main purpose of these machines was not the generation of electricity. They were simply constructed for various purposes such as milling grain, pumping water, land draining, sawing woods, hammering, grounding spices, olive oil extraction or even gunpowder manufacturing. As examples, Figure 1-1 shows a very primitive windmill used in Afghanistan for milling grain. Figure 1-2, on the other hand, shows a more modern windmill used in Europe during the 16th and 17th centuries. This windmill was used for different purposes such as milling grain, sawing woods etc.

Figure 1-1 A primitive windmill, Afghanistan[2]

Today, these duties are easily overcome with the usage of electrical devices or machines. Therefore, from the late 19th century until today, the main usage of wind energy has changed the route into the production of electricity[2].

Figure 1-2 Paltrock windmill, Europe[2]

There are many ways to produce electrical energy such as hydropower, fossil-fueled power, nuclear power etc. But the wind is a significant method and finally thought as a leading energy source for electricity production[3]. Currently, machines which produce electrical energy from wind are mostly known as wind turbines, not as windmills or windwheels. Wind turbines are cost-effective solutions to generate electrical energy without pollution releases and greenhouse effects. In addition, the usage of turbines eliminates the dependence of costly oil and gas used for electricity generation. Furthermore, the cost of electricity generation by wind turbines is much lower than other electricity generation methods such as coal-fired turbo-alternators, hydrothermal-, geothermal-, biofuel-based electricity generators, tidal wave turbines, nuclear reactor-based generators etc.[1].

Wind turbine technology has been improved over the years. But, the last four decades have seen unprecedented advancement in wind turbines because they have reached today's technology within this short period. This quick improvement has occurred since the major aim is to produce electricity for industrial applications. These applications require higher technologies compared to old duties such as milling grain, pumping water, sawing wood etc.[2]. Within this period, turbine designs have moved from the fixed speed operation with a gearbox to the variable speed operation with an active blade pitch control property, with and without a gearbox, with a power electronics unit and the latest aerodynamically shaped blades[4]. For instance, with advanced controllers, turbines work much more efficiently than ones with simple controllers. Thus, modern turbines capture more energy and have less structural loads as well as longer life spans[5].

In parallel to technological advances, there are now many companies designing and installing wind turbines in the world such as Vestas, General Electric, Siemens. Usually, wind turbines are erected as on-shore, but modern turbine technologies have allowed manufacturers to build wind turbines for off-shore applications as well[6]. For instance, VESTAS Wind Systems A/S, the Danish wind turbine manufacturer, has installed an off-shore wind turbine with a rated power of 8.0 MW off the coast of

Liverpool, The United Kingdom. This turbine has a rotor diameter of 164 meters and tip height of 187 meters[7].

Table 1-1 Top ten countries according to the new and installed capacity in 2017[8]

New Installed Capacity		**Cumulative Installed Capacity**	
Country	**MW**	**Country**	**MW**
PR China	19,660	PR China	188,392
USA	7,017	USA	89,077
Germany	6,581	Germany	56,132
UK	4,270	India	32,848
India	4,148	Spain	23,170
Brazil	2,022	UK	18,872
France	1,694	France	13,759
Turkey	766	Brazil	12,763
South Africa	618	Canada	12,239
Finland	535	Italy	9,479
Rest of the World	5,182	Rest of the World	82,391
Total Top Ten	**47,310**	**Total Top Ten**	**456,732**
World Total	**52,492**	**World Total**	**539,123**

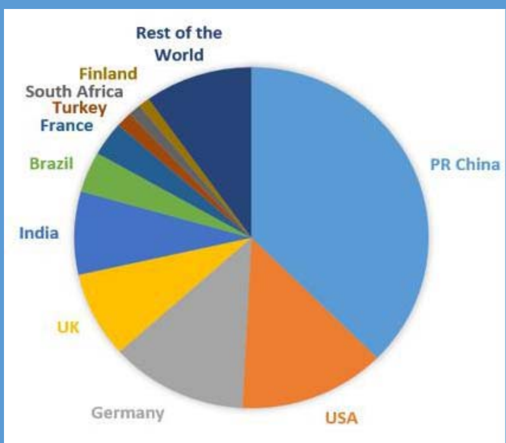

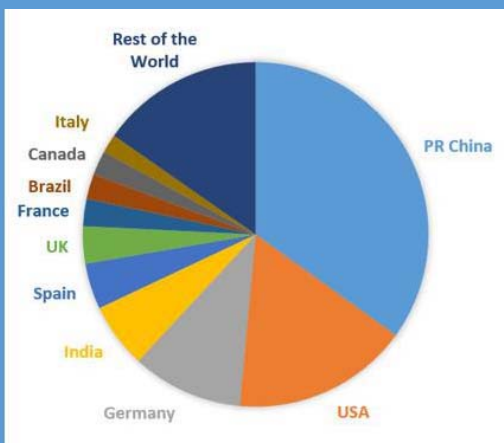

The usage of wind turbines started in California in the 1970s, and later separated to other countries such as Denmark, Germany, Spain, Netherlands and China and so on[9]. Today, similar efforts to use turbine technology for electricity generation may be observed in some other countries such as Turkey. Table 1-1 shows the top ten countries with the new installed capacity and the cumulative installed capacity in the year 2017. The Republic of China comes is the world leader with the largest cumulative installed capacity and continues to erect new turbines. As seen in Table 1-1, this is followed by the USA, Germany, India and so on. Turkey is not among the top ten countries with the total cumulative capacity, but it places among the top ten counters with the new installed capacity in 2017.

Figure 1-3 Horizontal axis wind turbine[10]

In order to generate more electrical energy, wind turbines are installed in a particular organization, referred to as a wind farm or wind power plant. The most commonly seen wind turbine in wind farms is the horizontal wind turbine (HAWT) with three blades (Figure 1-3). This is the most preferred turbine type by the wind power industry due to their efficiency and practicality[5]. Figure 1-4 shows an example of wind farms consisting of three-bladed turbines in Turkey, which is located in Soma, Manisa.

Figure 1-4 Soma wind farm, Manisa, Turkey

Wind turbine technology is an exceptionally sophisticated technology requiring multi-disciplinary and comprehensive engineering knowledge such as aerodynamics, mechanics, structural dynamics, electrical and electronics engineering. Electrical and electronics engineering is as important as aerodynamic engineering since electricity generation, transmission and connection of wind turbines to the electrical grid are also other major problems for these machines[4].

This thesis study deals with the upwind HAWT configuration and focuses on the development of a nonlinear dynamic HAWT model or simulation model. It is named as MS (Mustafa SAHIN) Bladed simulation model. The thesis study also focuses on baseline controller designs and a new adaptive envelope protection control system design. Since the proposed adaptive envelope protection control system is not available for wind turbines, this thesis study has introduced a novel protection system to wind turbine industry and the literature. Simulations have shown that the proposed protection algorithm has demonstrated successful performance results to reduce the wind turbine loads, by not allowing the turbine to operate beyond a pre-defined envelope limit, i.e. the thrust force. Therefore, it is eventually expected to see an increase in the service life of turbines and may be applied to the operating turbines.

With the help of a turbine simulation model, the performance of an already-designed HAWT with any configuration or size is predicted before starting its mass production. New control algorithms may be developed and be simulated on the simulation model. Further, time-depended turbine behavior under various operation and wind conditions may also be observed through the simulations.

Here, the developed MS Bladed turbine simulation model includes a rotating turbine rotor, a gearbox and a simple generator with a rotating rotor. It uses blade element momentum (BEM) theory, particular coordinate systems, aerodynamic corrections, Newton second law of motion, generator and rotor inertias etc. All these are included to get a more modern turbine and a better aerodynamic behavior at various wind speeds. The electrical generator is modeled in a way that it can produce a variable electromagnetic torque depending on the rotor speed/generator input. The transformer and other components such as a rectifier, inverters etc. are not modeled. Therefore, the turbine model has the properties of nacelle yawing and blade pitching, individually or collectively. The MS Bladed simulation model does not consider elasticity in any turbine structural parts and therefore assumes everything such as blades, shafts etc. as rigid structures. In addition, it allows the selection of rotor precone and nacelle tilt angles. Some of the coordinate systems are locally defined to simulate turbines with even swept or curved blades. However, this may require some extra modifications to the developed simulation model if it is going to be utilized for those particular turbines.

The development of the MS Bladed simulation model is carried out by MATLAB and Simulink software. Validation of MS Bladed model is realized by comparing the predicted outputs with the test data of NREL Phase II and III experimental wind turbines, Phase VI wind turbine rotor design performance results (PROPID outputs) as well as NREL 5 MW wind turbine performance data published in the literature. After validating aerodynamic part of the model, the MS Bladed simulation model is obtained by utilizing the properties of aerodynamic model with those of electrical generator through the Newton second law. NREL 5 MW wind turbine is adopted eventually in the MS Bladed simulation model. According to 5 MW turbine, baseline controllers (generator torque and collective blade pitch controllers) are designed intensively. Their simulation results are given in terms of various turbine parameters such as turbine rotor speed, torque, blade pitch angle etc. Lastly, the theory and design of new adaptive approach for protecting the HAWT are investigated. The effectivity of the proposed approach is proven here by the simulation results for the below and above rated regions as well as around the rated wind speed. Lastly, conclusions and suggestions are added.

Before focusing on the details of turbine modeling or MS Bladed model, baseline controller designs and so on, it is useful to briefly discuss wind turbines, their types and working principles. Furthermore, a particular subchapter is prepared for discussion of HAWTs since it is the focus of this thesis study. It defines the turbine electrical, mechanical components, the control system and contemporary technologies etc.

1.2 Wind Turbine and Their Types

Wind turbines are basically a system that extracts the kinetic energy in the wind by a rotor to produce mechanical energy, which is directly converted into electrical power through an electrical generator[3], [11]. Turbines may be seen with different designs or configurations, which this and the proceeding subchapters are about. Usually, when a wind turbine design is considered, the rotor is taken into account in the first place. However, there are also other turbine components that require rigorous designs. These are basically the electrical generator, gearbox, power electronics and control systems etc.[2].

Wind turbines are manufactured with different dimensions and capacities. Although small-scale wind turbines, on the order of 10 kW or less, are common, large-scale turbines, on the order of 1 MW or more, constitutes the major cumulative capacity in the world[12]. Further, turbines are designed as various types such as the H type, Darrieus type, Savonius type and the propeller type turbines. These may be classified depending on the aerodynamic working principles as lift-based (lift type) and drag-based (drag type) turbines or depending on the constructional installation layouts as the vertical or horizontal axis. Nevertheless, it is more practical to classify the turbines according to their constructional designs as vertical axis wind turbines (or VAWTs) and horizontal axis wind turbines (or HAWTs)[2][13]. Figure 1-5 shows some examples of these turbine types.

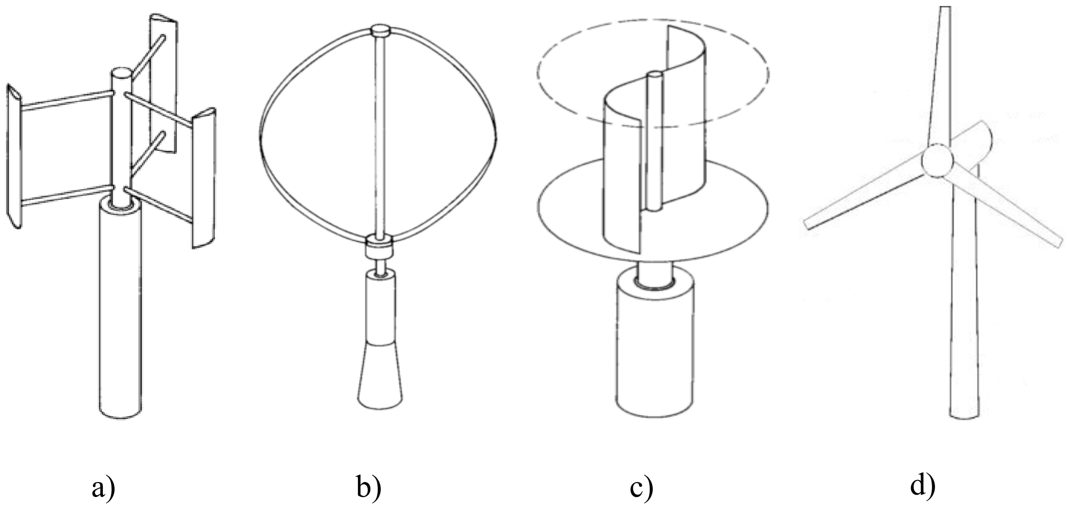

Figure 1-5 Vertical and horizontal axis wind turbines, a) H type turbine, b) Darrieus type turbine, c) Savonius type turbine, d) Propeller turbine[2].

VAWTs can capture the wind flow from any direction, while HAWTs have a sensitivity to wind direction. HAWTs are more efficient than the VAWTs. VAWTs are mostly designed for low output power applications such as battery charging particularly for rural areas with no electrical grids, whereas HAWTs are used both for low and high power applications[13][1].

1.2.1 H Type Turbine

This type of turbine (Figure 1-5-a) works based on lift force and captures the wind energy from any direction. It is a VAWT type turbine with the shape of the letter H. The active airfoil shaped-blades are connected to the main shaft with the middle segments. One or two or more segments may be utilized depending on the turbine design. Having more than two blades results in a smoother operation of this type of turbine[13].

1.2.2 Darrieus Type Turbine

The Darrieus type turbine (Figure 1-5-b) is very similar to the H type turbine since it is also a vertical axis turbine, using the lift force to produce the power. The main difference from the H type turbine is their curved blades attached to the turbine shaft from both of their tips. Guy wires are required to increase the strength of the turbine. This allows the use of a less strong turbine shaft contrary to the H type turbine. The disadvantage of this turbine is that it has an improper starting torque at low wind speeds. However, when it starts rotating, it has enough torque to generate electricity[13].

1.2.3 Savonius Type Turbine

Unlike the H and Darrieus type turbines, the Savonius type turbine (Figure 1-5-c) is a drag force-based turbine. It is much simpler to manufacture because its rotor consists of two half cylinder sections attached to the rotor shaft. They jointly form a cross section with the shape of letter S. During turbine operation, one blade captures the energy, while the other one opposes the wind flow. Therefore, the net torque is the result of these two blades. The number of blades may be increased to achieve a smoother operation. Compared to the Darrieus type turbine, it has a good starting torque at low wind speeds. Furthermore, the Savonius turbine may operate horizontally as well. In that case, the direction of the wind becomes important. This type of turbine may be seen with some modifications such as a space between blade joints to the rotor shaft, or twisted half cylinders to harvest much more power from wind. The Savonius turbines are largely employed as motors to start the Darius type turbines in the field as they have an improper self-starting torque at low wind speeds[13][1].

1.2.4 Horizontal Axis Wind Turbine or Propeller Turbine

The last turbine type is the HAWT configuration, which is a frequently seen turbine with a three-bladed rotor. The rotor is placed on top of a tower in order to capture more energy from the wind. This turbine type is also referred to as propeller turbine because of its similarity to an aircraft propeller. It may have more than three blades, while at other times only two. But, the best combination is the three-bladed turbines due to its balance, efficiency, and practicality etc.[13].

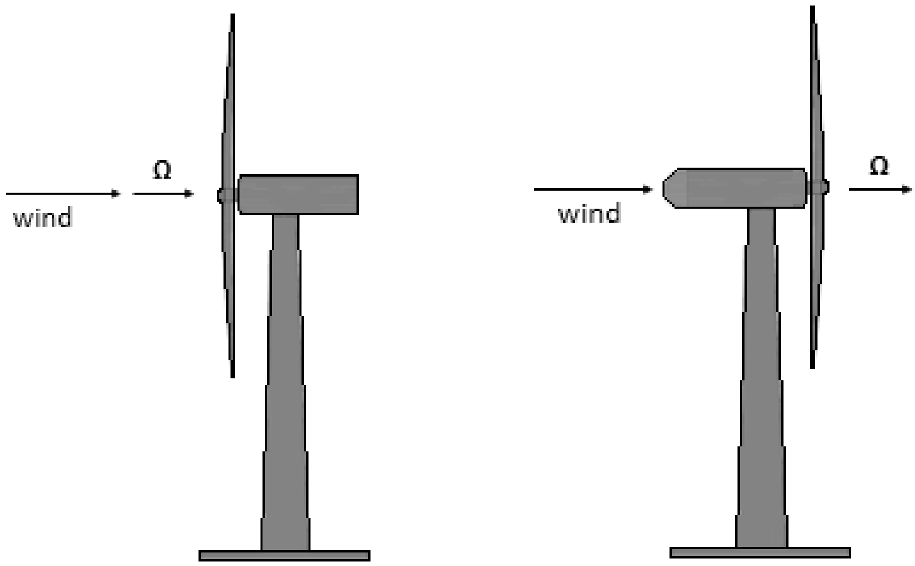

a) b)

Figure 1-6 Upwind and downwind oriented HAWTs, a) Upwind orientation,
b) Downwind orientation

Two-bladed HAWTs are less expensive, yet rotate faster, which results in a production of the visual flickering effect. They are also aerodynamically less efficient than the three-bladed HAWTs. Exceptionally, this type of turbine has also a potential to operate with just one blade[1]. Further, they can be designed as upwind or downwind oriented (Figure 1-6).

The upwind oriented wind turbine is the turbine with the rotor spinning on the upwind side of the tower, whereas the downwind ones have the opposite orientation. Two-bladed HAWTs are mostly installed as downwind. In downwind turbines, the wind firstly hits the tower then reaches the turbine blades. This produces a low-frequency noise as each blade passes the tower at every one-per-revolution. Thus, the most commonly designed wind turbine for wind farms is the three-bladed upwind utility-scale HAWTs due to their less disturbing effects on humans. A downwind configured turbine aligns itself with wind direction compared to upwind turbines. However, they inevitably require a control system when the turbine size gets larger[1], [5], [11], [13], [14].

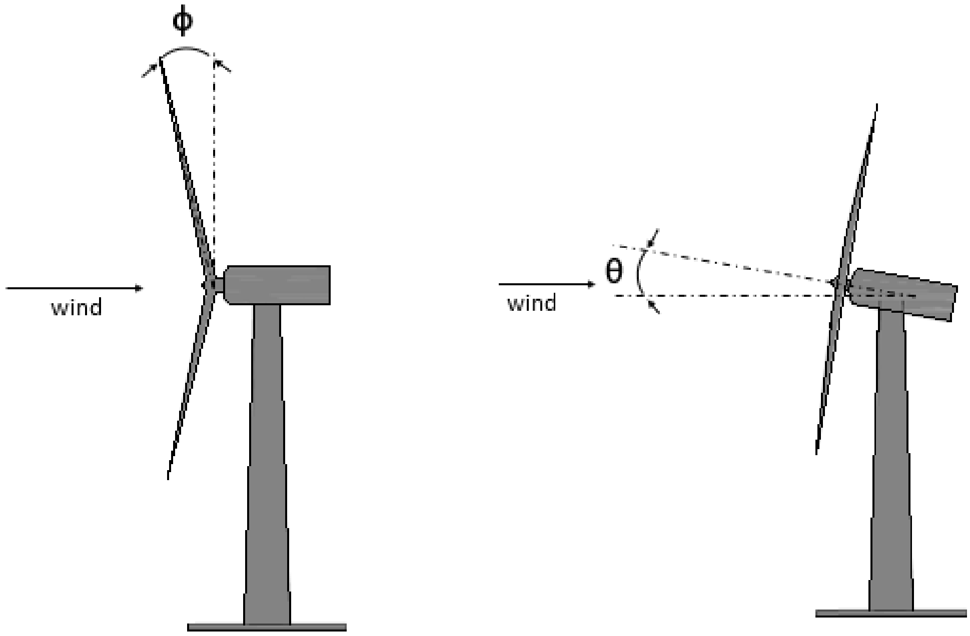

a) b)

Figure 1-7 Geometric fixed angles, a) Rotor precone angle, b) Nacelle tilt angle

A blade-tower clearance is required for large-scale turbines. This is achieved by employing some fixed structural angles such as rotor precone and nacelle tilt angles, which are seen respectively in Figure 1-7-a and b. A negative precone angle is used to keep the blade away from the tower, therefore putting a clearance between blade tips and tower. A positive tilt angle helps to increase this clearance more.

Figure 1-8 shows power coefficients or aerodynamic efficiencies of VAWT types and HAWT types with one, two and three blades. It also includes the Betz limit or ideal C_p as well as the theoretical C_p for an infinite number of blades with respect to Tip Speed Ratio, or TSR, i.e the ratio of blade tip speed to the freestream wind speed. As seen from the figure, the three-bladed HAWT is more efficient than other turbines considering its maximum C_p.

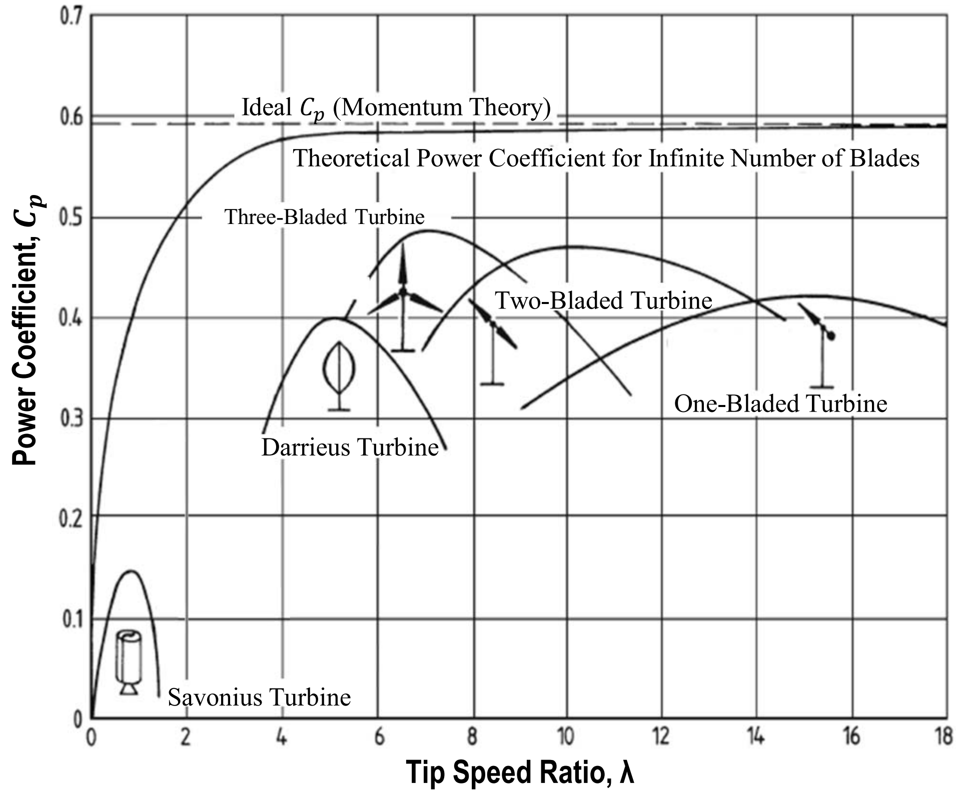

Figure 1-8 Power coefficients for different turbines[2]

As a result, HAWTs are more advantageous turbines than the VAWTs. Having the rotor on top of the tower allows the HAWTs to take larger wind speeds, resulting in more power. Furthermore, with pitchable blades, they have a greater energy capturing capability, reduced loads and thus a longer lifetime etc. All of these benefits make the HAWTs a more attractive alternative than other turbines to the wind power industry[5].

1.3 More about Horizontal Axis Wind Turbines

When viewed from the outside of a general HAWT, tower, nacelle and the rotor (blades) are the visible parts. However, there are other turbine components such as a generator, a gearbox, brakes etc. existing inside the nacelle, a foundation buried underground, and a transformer inside the nacelle or outside on the ground[1], [13] Figure 1-9 shows the main components of a general HAWT system.

Figure 1-9 Wind turbine main components[15][16]

Basically, the rotating rotor in front of the turbine nacelle captures the kinetic energy in the wind and turns that energy into rotational kinetic energy. This energy is later applied to an electrical generator via a shaft. This type of HAWT with only one shaft is referred to as the direct drive turbine. But, generally, most HAWTs have a gearbox between the turbine rotor and the generator to increase the rotational speed of the rotor shaft (or low speed shaft, LSS) to drive the generator shaft (or high speed shaft, HSS)[5], [13].

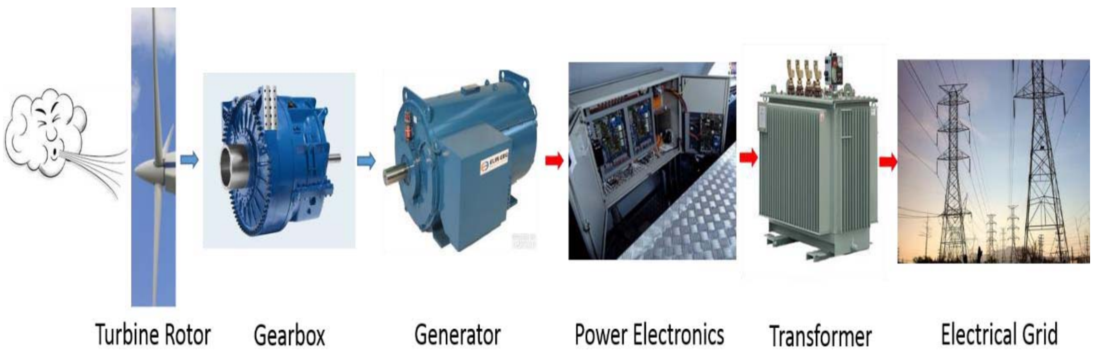

Figure 1-10 Wind energy conversion process[17][18][19][20][21][22][23]

Figure 1-10 summarizes the wind energy conversion process of a wind turbine system into the electrical energy. It shows respectively, the turbine rotor, gearbox, electrical generator, power electronics and control systems, transformer and lastly the electrical grid. Essentially, the wind passes through the turbine rotor, where its kinetic energy is converted into rotational mechanic energy or motion. This rotational motion is mostly speeded up by a gearbox to drive the electrical generator. Turbine control systems and power electronics as well as their related parts are used for a better aerodynamic performance from the turbine and a reliable grid connection purpose. The generator output voltage is usually increased by a step-up transformer, and then is connected to the electrical grid.

Mainly, HAWTs consist of mechanical and electrical components. These components may be grouped into primary and secondary components considering their size and importance. Primary components are the indispensable components for every HAWT design, whereas secondary components are optional to the turbine manufacturers[13]. Therefore, turbine components are grouped into

- Mechanical Components
    - Primary Components: Foundation, Tower, Nacelle and Rotor (a hub with blades)
    - Secondary Components: Transmission System or Gearbox, Shaft(s) and Brake(s)
- Electrical Components
    - Primary Components: Generator and Transformer
    - Secondary Components: Power Electronics Unit-Rectifier, and Inverter, Anemometer, Vane[13].

1.3.1 Primary Mechanical Components

A HAWT consists of four primary mechanical components. These, from the ground up to the turbine, are the foundation, tower, nacelle and rotor. Following are the definitions of these main mechanical components seen in Figure 1-9.

1.3.1.1 Foundation

Wind turbines are similar to multi-storey buildings, but their foundations are quite different than those of these buildings. Turbines are mounted on a number of piles inserted into the ground. Due to having lower base areas than those of these buildings, the most practical method for a wind turbine foundation is to use a large and heavy mass that can keep the turbine in the upright position. The foundation size is directly related to the turbine dimension. Large-scale turbines require large foundation size and vice versa. Soil type, weather conditions, and terrain topology are also other factors affecting the foundation size[13].

1.3.1.2 Tower

The turbine tower supports and holds the other turbine components up in the air such as nacelle, rotor and so on. It must be structurally strong enough to carry the weights of turbine components and the forces exerted on the turbine due to the wind. The tower height is extremely important to expose the rotor to high winds. Previous turbine designs consisted of lattice towers with jointed metallic bars. On the other hand, modern turbines use tubular towers which are made of rolled steel in the shape of a cylinder or slightly tapered in the form of a conic section. Moreover, modern turbine towers are manufactured as segments for easier transportation. During the turbine erection, these segments are connected to each other by bolts starting from the lowest segment to the highest segment, with the lowest segment bolted to the turbine foundation[13] [1].

1.3.1.3 Nacelle

Located between the rotor and the tower is the nacelle, which houses various electrical and mechanical components such as shafts, gearbox, generators and other components. These components are, for instance, the heaters for winter operation, brake system, coolers for gearbox oil, yaw system gears, wind direction and speed measuring system etc. The nacelle moves about the tower to put the turbine into the wind, which is referred to as yawing motion that is realized by a yaw control system[13].

1.3.1.4 Rotor

The rotor is the rotating part of the turbine due to the wind flow. It is basically a hub with a number of airfoil shaped-blades, which captures the energy from the wind and turn the turbine rotor shaft. The rotor blades may be constructed using one or more different shaped airfoils throughout the blade span. From the blade root to the tip, chord lengths of the airfoil(s) decreases due to mainly an aerodynamic reason or partially a structural reason. Thus, the root section of the turbine blade is constructed wider and thicker than the tip section. Furthermore, modern blades are also twisted throughout the blade span. They are constructed in large dimensions, which necessitates the blades and the hub be manufactured individually. These separate parts are later attached to each other during the wind turbine installation. In order to capture more energy from the wind, so as to produce more mechanical power, blade sizes are getting progressively larger and larger with time. In addition, modern turbines have rotors with a blade-turning capability around blade pitching axis relative to the rotor hub, referred to as blade pitching. Therefore, those turbines are referred to as variable pitch turbines[4]. However, old turbines do not have this property as their blades are firmly attached to the rotor hub. A blade pitch control system adjusts the amount of energy harvested by the turbine rotor. When the blades are moved in a direction in which the blades produce no power is referred to as feathered blades. Finally, in a structural sense, the blades are hollow structures and are made of composite materials[13].

1.3.2 Secondary Mechanical Components

The transmission system consists of a shaft(s), gearbox as well as a brake(s). It transmits the aerodynamic rotor power to the generator.

A braking system usually exists on the generator shaft in order not to operate the turbine in the case of storms, maintenance, or component malfunction etc. When a turbine is shut down, turbine blades are feathered to 90 degrees and the turbine nacelle is yawed out of the wind. With these precautions, the turbine rotor may not be entirely prevented from rotating. Therefore, a pin is usually inserted into the generator shaft, which strictly locks the turbine rotor[4], [13].

Another important part of the turbine is the gearbox. In wind turbines, the gearbox increases the rotor speed since the generator shaft must turn faster than that of the rotor. Typical generator speed ranges from 900 to 1800 rpms. But rotor speed of modern turbines lies in the range of 12-24 rpms. For this reason, most modern turbines use a gearbox between the rotor and the generator. As mentioned previously, these turbines have two different shafts; the LSS attached to the rotor and the HSS attached to the generator. The middle component is the gearbox which is the heaviest component of the turbine system. Gearboxes may be manufactured as multi-input and multi-outputs to drive more generators[13] [1] and have their own lubrication and cooling systems. They have a very short life span-approximately around two years- since they are subjected to significant changes in torques of large turbines. This problem is solved by increasing the number of generator pole pairs over one hundred, which eliminates the usage of a gearbox[4].

1.3.3 Primary Electrical Components

As electrical components, the generator and transformer are the main parts of the wind turbines. Turbines have other electrical components such as yaw motors, pitch motors, oil circulation motor pumps, electrical heaters, lights etc. Modern wind turbine control systems include various electrical, electromechanical and electronic components. For instance, one is the power electronics unit. Here, the power electronics unit is considered as a secondary electrical component, as it is largely used in most modern turbines.

1.3.3.1 Electrical Generators

Generators are the electromechanical part of wind turbines, responsible for converting mechanical rotor power into electrical power. Their size depends on the generator power output; the larger the desired electrical power output the larger the generator size is. Generators are simply made of a stationary and a rotating component referred to as respectively as stator and rotor. The stator includes windings mounted in a certain pattern while rotor may have a permanent magnet or an electromagnet-windings. Particularly, the rotor with permanent magnets is not suitable for large electrical power outputs. Therefore, the generator rotor may have an electromagnet-windings for higher power outputs. The rotor produces a magnetic field for generator during its rotation. This magnetic field affects the stator windings and induces a voltage at the stator terminals. The stator is later connected to the utility grid usually via a transformer. If the stator magnetic field follows that of the rotor, that type of generator is referred to as synchronous generator, otherwise, it is an asynchronous generator since a relative motion referred to as slip is available between the rotor speed and the speed of rotating stator field. These are the two main generator types used by the electrical power industry. Synchronous generators are also referred to as alternators, whereas asynchronous generators are referred to as induction generators. Most power plants such as hydro, fossil fuels or nuclear power plants use synchronous generators, whereas wind turbines exceptionally utilize both generator types[4], [13][1]. Following are the detail of these two main generator types.

1.3.3.1.1 Synchronous Generator

Synchronous generators operate at synchronous speed and are directly connected to the electrical grid without a dependency on the applied torque quantity. Most often, the wind power industry uses two classical synchronous generators, Wound Rotor Synchronous Generator (WRSG) or Permanent Magnet Synchronous Generator (PMSG). The WRSG generates a constant frequency power output and is therefore directly connected to the electrical grid. The winding of WRSG rotor requires a DC current to generate a constant magnetic field. This is realized by permanent magnet poles on PMSGs. Therefore, they do not need an external energy supply, which makes them more efficient than WRSGs. Generator speed is determined by the rotating field frequency and the number of pole pairs. A generator with an appropriate number of poles eliminates the usage of a gearbox to increase the turbine rotor speed[4][1].

1.3.3.1.2 Asynchronous (Induction) Generator

These generators are manufactured in large series because they are robust, stable mechanically simple and inexpensive. The shortcoming of these generators is that their stators require a reactive magnetizing current and therefore consume reactive power to get its magnetic excitation. This reactive power is supplied by the power electronics unit or the electrical grid.[4].

The rotor of this generator type is a short circuit (squirrel-cage rotor) or wound rotor. The squirrel-cage induction generator (SCIG) has been utilized by the industry for many years due to its high efficiency, mechanical simplicity as well as low maintenance requirements. The rotor, which consists of embedded bars in slots with their endpoints shortened by rings, does not give any opportunity to change generator electrical characteristics from outside. The speed of SCIGs changes only with a few percents as its slip varies with changing wind speed. Turbines with SCIGs typically include a soft-starter mechanism along with a reactive power compensation[4].

Wound Rotor Induction Generator (WRIG) has a rotor with windings. Slip rings and brushes are used for the external connection of rotor windings. This feature permits the user to change the generator characteristics externally unlike SCIGs[4].

In the wind power industry, WRIGs may have two different configurations, OptiSlip or FlexiSlip Induction Generators and Doubly Fed Induction Generators or DFIGs. The OptiSlip or FlexiSlip Induction Generators were largely used in the 1990s as WRIGs with a variable rotor resistance connected to their rotor windings. This technology is depicted in Figure 1-11-b. The size of rotor resistance determines the dynamic speed control range and is adjusted by an optically controlled converter located on the rotor shaft. The slip for OptiSlip is 10%, whereas for FlexiSlip, it is approximately 16%[4]. In DFIG type generators, the stator is directly connected to the utility grid, while the rotor is connected to the grid over a back to back power converter (Figure 1-11-c). Most advanced turbines employ the DFIG-type generators since they efficiently harness energy in the wind[13].

1.3.3.2 Transformers

The duty of a transformer in an electrical system is similar to that of a gearbox in a mechanical system. Transformers increase or decrease the voltage level, whereas a gearbox increases or decreases the mechanical rotary motion. The transformer decreasing voltage level is referred to as a step-down transformer, while the one increasing output voltage is referred to as a step-up transformer. For connecting the turbines to the electrical grids, generator outputs are mostly increased to have higher voltage levels, ranging from 11000 to 25000 volts or more. Therefore, most turbines have step-up transformers, which are located at the tower bottom, either inside or outside, sometimes inside the nacelle[13].

1.3.4 Secondary Electrical Components

The anemometer and wind vane are particularly important devices, generally mounted on the top of the nacelle roof and sense wind speed and direction, respectively. This information is evaluated by turbine controllers, and accordingly the generator torque or blade pitch angles are adjusted, the nacelle is directed into the wind etc.[13]. Another important component is the power electronics unit, located between the generator and the electrical grid. This unit, available in most modern turbines, allows the connection of generator output to the electrical grid. It must satisfy the generator and grid side requirements. On the generator side, this unit assures that the rotor speed is adjusted in such a way that the turbine extracts maximum power from the changing wind speed. On the grid side, however, this unit must comply with the grid codes regardless of wind speed. The usage of the power electronics unit improves the turbine performance, not only decreasing the structural loadings/stresses, but also increasing the harvested energy[4].

1.4 Wind Turbine Control System and Contemporary Technologies

A wind turbine must have a control system for efficient operation under different operating conditions. Generally, controls are realized by a passive or an active method. Passive control uses its own sensing mechanism to realize a control action and does not necessitate external energy. For instance, rotor stall phenomena, which decreases the rotor efficiency, is a passive control method. In active control, however, electrical, hydraulic or pneumatic power along with some sensors are required to fulfill a control action[4].

The passive control of wind turbines is a very simple and robust, known as stall control. The turbines with stall control are referred to as stall-regulated turbines. They have firmly fixed blades to the rotor hub and do not need any complex control systems. However, it is very difficult to design stall-regulated turbines due to their sophisticated aerodynamics. Scientist and engineers are still trying to understand both 2D and 3D dynamic stall delay effects. This is due to the fact that the post-stall lift and drag coefficients measured in wind tunnels alters because of centrifugal and Coriolis forces occurring during the rotation of turbine blades. Therefore, a significant engineering talent as well as experience are required to prepare reliable airfoil data that include 3D stall delay effect. When wind exceeds a certain speed, stall-regulated turbine blades start naturally going into stall as they are firmly fixed to the rotor hub. This decreases the efficiency of the turbine rotor, resulting in a regulated power[4][1][11]. The larger the wind speed is, the more sections of the blades will go into deeper stall.

The active control method, on the other hand, includes pitching the turbine blades to stall or feather, which respectively increases and decreases the angle of attacks (AOAs) of blade sections in order to regulate rotor power. Whole or some parts of the blades are designed with pitching capability, but the whole blade pitching is the most commonly used method in today’s wind turbines.

In a pitch to stall control, leading edges of turbine blades are turned out of the wind, which causes the blades to have negative pitch angles, resulting in large AOAs and stall. This control method is referred to as active stall control since it utilizes both blade pitch control and stall phenomenon together. Therefore, increasing AOAs increases the drag force of each blade section, i.e. the thrust force of the turbines. Both the thrust and torque of turbines are more stable than the one obtained with pitching to feather technique.

Further, a very small amount of change in pitch angle is enough to regulate turbine power output at the rated value. Therefore, pitch to stall control requires a small amount of movement of pitch mechanism and a smaller pitch rate, compared to pitch to feather control[24]. This active stall control strategy allows turbines to produce more power, compared to stall-regulated turbines. Furthermore, turbines run at their rated power at all high wind speeds[25].

Turning blade leading edges into the wind is referred to as pitch to feather control. This method requires large pitch angles, for which blade actuators have to act very quickly with high pitch rates. In this method, the pitch angles of turbine blades are increased as wind speed increases. This process decreases the AOAs of all the blade sections, resulting in limiting turbine power output during an increasing wind speed[24].

In addition, wind turbines are also designed to operate at fixed or variable rotor speeds. Fixed speed turbines are equipped with SCIGs that are connected to the grid with a soft starter. These turbines operate at almost fixed rotor speed regardless of wind speed. They are designed to get their maximum power efficiency at only one certain wind speed. This is most probably the wind speed in the place where turbines are to be erected. At all other wind speeds, they produce a lower power output. These turbines encounter large mechanical stresses, uncontrollable reactive power consumption and limited power output quality[26]. Nowadays, the wind power industry uses variable speed wind turbines most commonly since they use their rotors more efficiently and therefore maximize their power output at low wind speeds[26] [27]. Due to their variable rotor speed operation, they require a power electronics unit to decouple the electrical grid frequency and mechanical rotor frequency. Variable speed wind turbines are more efficient than the fixed speed turbines. Around 5% more annual energy capturing is achievable, compared to fixed speed turbines[4]. Furthermore, they have also fewer mechanical stresses, a better power output quality, and a more grid friendliness, which is an important issue for the large wind farms.

Hence, turbines may be manufactured with the above control properties as fixed speed fixed pitched turbines, fixed speed variable pitch turbines, variable speed fixed pitch turbines, and finally as variable speed variable pitch turbines. The last turbine is the most modern turbine used in today's wind farms, which is the focus of this thesis.

Fixed speed fixed pitch or fixed speed variable pitch (pitch to feather or pitch to stall) turbines have been utilized by the industry. Until the mid-1990s, the dominant turbines in wind farms were fixed speed fixed pitch turbines. Pitch to feather control application to fixed speed turbines has not been popular due to their large inherent power fluctuations at large wind speeds. This is due to the deficiency of the pitch mechanism to prevent power fluctuations during a gust at high wind speed[4].

Fixed speed pitch to stall controlled turbines have been largely used in the 1990s due to their smooth power regulation. However, due to strict requirements imposed by the utility companies, today the success of these turbines are conditioned since they have a very slow control. Pitch to feather control has proven to be a very attractive technique for variable speed wind turbines with a capacity of larger than 1 MW. Variable speed turbines come with fast pitching capability in power regulation. Variable speed fixed pitch or variable speed pitch to stall-controlled turbines are not considered due to their inability for fast power reduction[4].

Considering the contemporary technologies, wind turbines may also be classified into four types

- Fixed Speed Wind Turbines (Type 1)
- Limited Variable Speed Wind Turbines (Type 2)
- Variable Speed Wind Turbine with Partial-Scale Power Converter (Type 3)
- Variable Speed Wind Turbine with Full-Scale Power Converter (Type 4)

As stated above, fixed speed turbines are the most fundamental turbines operating at nearly fixed rotor speed and are directly connected to the grid. Variable speed turbines, on the other hand, may operate at different rotor speeds and generally have the blade pitching capability. Type 2, 3 and 4 turbines are variable speed variable pitch turbines with different technologies.

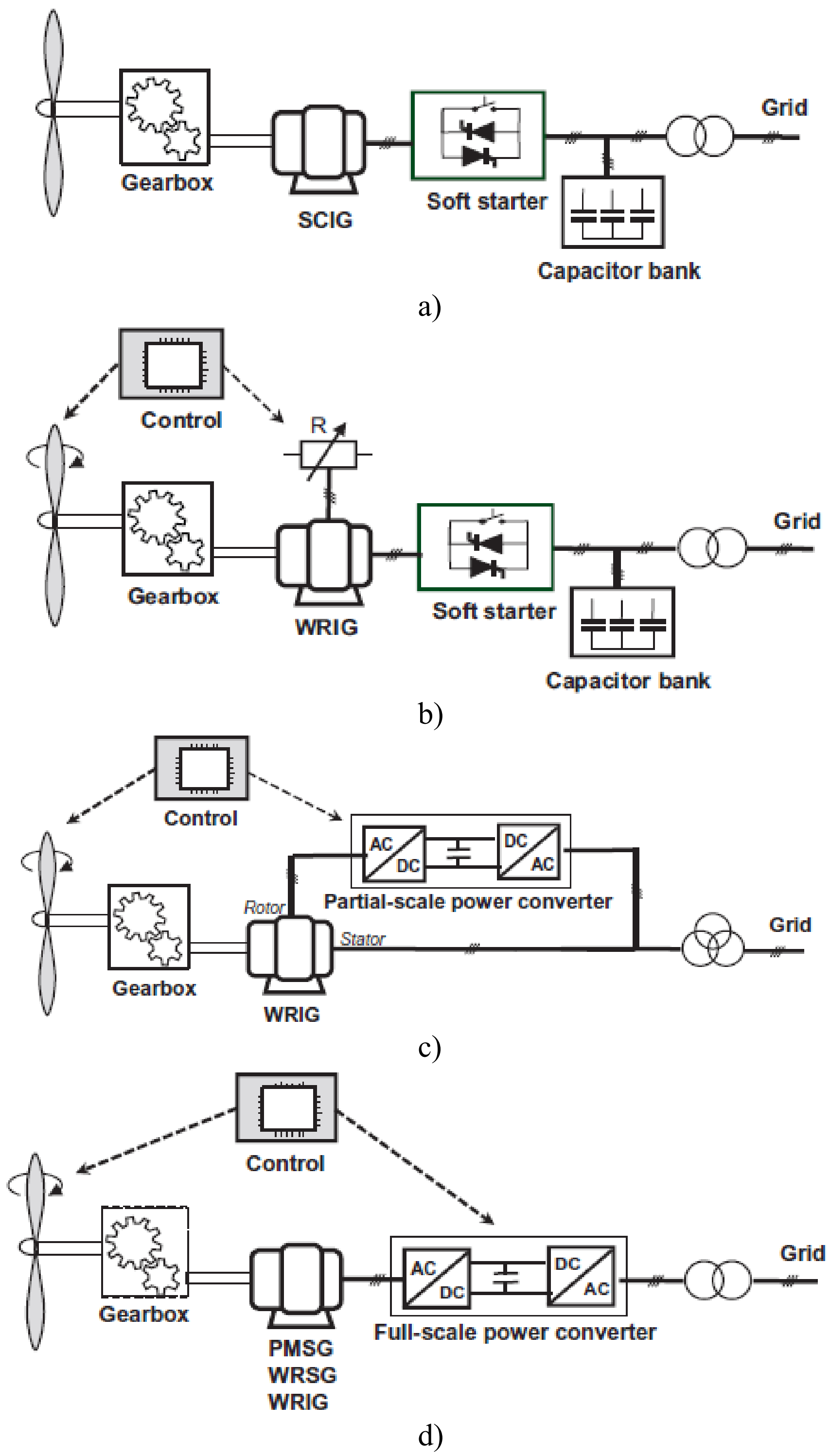

Figure 1-11 Turbine contemporary technologies, a) Type 1, b) Type 2, c) Type 3, d) Type 4[4]

Type 1 turbine configuration includes a multi-stage gearbox and a SCIG. This concept is referred to as the 'Danish concept' because it was largely utilized by Danish wind turbine manufacturers in 1980s and 1990s. As seen in Figure 1-11-a, SCIG is directly connected to the grid via a transformer. In this turbine system, a soft starter is employed for a smoother grid connection and a capacitor bank is employed to compensate the reactive power. The turbine operates almost at a fixed rotor speed at any wind speed. Therefore, it is less efficient in an aerodynamical sense due to the fixed speed operation and experiences high mechanical stresses and fatigue loads[4].

Figure 1-11-b is a Type 2 turbine configuration allows a limited variable speed operation, typically from 0 to 10%. This concept was used by the Danish manufacturer, VESTAS from the mid-1990s to 2006 and later by the Indian manufacturer, SUZLON. WRIG is employed in this configuration. Generator stator is directly connected to the electrical grid via a transformer, while a variable resistance is connected to the rotor windings in series. The resistance is controlled optically and is varied dynamically by power electronics. Type 2 configuration has an improved speed operation, reduced mechanical stresses, power fluctuations etc. As in the Type 1 configuration, it requires a soft starter and capacitors to compensate the reactive power. Since the speed range depends on the resistance, some power is inevitably lost due to varying the value of resistance and due to the improper active and reactive power controls. This configuration may be considered as a first step to the variable speed rotor operation, since it partially increases the turbine rotor efficiency[4].

Type 3 is a variable speed turbine with a DFIG, through whose slip rings are connected to a partial scale back-to-back converter. This configuration permits a wide range of variable rotor speeds depending on power converter size. Generator stator, as in Type 1 and Type 2 configurations, is directly connected to the grid, while the rotor is connected through a partial scale back to back converter. The power rating of the converter gives a ±30% speed about the synchronous speed. The converter decouples the electrical and mechanical frequencies and allows the turbine to run at variable rotor speeds. Furthermore, the converter is also responsible for the soft starting and compensation of reactive power. The converter controls the rotor frequency, and therefore the rotor speed[4], [28]–[30]. This concept is more expensive and commonly used than those of Type 1 and 2[4].

Type 4 configuration uses a full-scale power converter. Different from Type 1, 2 and 3, the stator is connected to the grid through a full-scale power converter. With this converter, the speed range is extended to 100%. Thus, all rotor speeds allow a smooth grid connection and reactive power compensation. As in Type 3, the control system in Type 4 is responsible for active and reactive power controls. This concept may be applied to different types of generators such as PMSG, WRSG, and WRIG [4]. Today, most commercial wind turbines in wind farms are Type 3 and 4 configurations[27].

To summarize, HAWTs are designed to operate at fixed or variable rotor speeds. However, modern HAWTs are designed to operate at variable rotor speeds. With this feature, they operate almost at their maximum efficiency for most of the operational time. HAWTs may have fixed or pitchable blades, which are respectively referred to as stall-regulated or pitch-regulated turbines. Modern turbines have pitchable blades in order to control the loads and vary the aerodynamic rotor torque.

In order to connect the variable speed turbine to the grid, power electronics units are used to convert the variable frequency power to that of the electrical grid. However, fixed speed turbines do not need such extra components and are directly connected to the grid. Nevertheless, power electronics units are cost-effective components due to their positive impacts on turbine efficiency and loads[14]. The power electronics unit realizes the generator torque control to maximize the energy capture. Therefore, the rotor speed is adjusted by this unit to changing wind speeds in order to obtain the maximum power possible at low winds[25]. Design of a standard generator torque controller is given in Chapter 5.

1.5 Control and Operation Regions of Variable Speed Variable Pitch HAWTs

The addition of advanced controllers to wind turbines increases the power efficiency and reduces the structural loadings. Therefore, the turbines with advanced controllers can capture more energy from the wind and possess a longer life span[5].

In modern HAWTs, control systems consist of different layers; the highest level, middle level and the lowest level controllers. The highest level controller, also referred to as supervisory control, determines when to start or stop turbines according to wind speed level. Turbines start producing electricity at a certain wind speed, which is referred to as cut-in wind speed. At a certain wind speed, usually 25 m/s, they stop in order to prevent damages to the turbine components due to very high wind speeds, i.e. storms. This wind speed is referred to as cut-out wind speed. Middle-level control is about the turbine's own control and is referred to as operational control. This control level includes generator torque, turbine blade pitch and turbine yaw controllers. The generator torque is realized by means of a power electronics unit as mentioned in the previous subchapters. This component decides how much torque is to be given by the generator to the turbine rotor to get the optimum turbine efficiency. The blade pitch control is utilized to keep the rotor speed at the rated speed in order to produce the rated power. Yaw control is employed to direct the nacelle into the wind direction. However, yaw control is not so valued for control engineers compared to the generator torque and the blade pitch controls. For this reason, this thesis has focused on the generator torque and blade pitch controllers. Lastly, the lowest control level includes an internal generator control, actuator control etc., which must run faster than the turbine other level controls[14].

Variable speed variable pitch turbines have basically three different operational regions. Region 1 stays below the cut-in wind speed. In this region, turbines do not generate electrical energy due to very low wind speeds. Wind speeds are not sufficient even to produce electrical power even for turbines' own systems. Electrical power generation starts at the cut-in wind speed and ends up at the cut-out wind speed. Between these two wind speeds, there are two operational regions, referred to as Region 2 and Region 3. The region between the cut-in and rated wind speeds is referred as to Region 2, whereas the region between the rated and cut-out wind speeds is referred as to Region 3. The main objective in Region 2 is to maximize the energy capture of turbines since wind speeds in this region are low to produce the rated power. This maximum energy generation is achieved by keeping blade pitch angle fixed and using generator torque to vary the rotor speed. In Region 3, on the other hand, turbines limit their powers to their rated value due to high wind speeds in order not to exceed certain mechanical and electrical loads. This is generally achieved by keeping generator torque fixed at the rated torque and adjusting blade pitch angles to regulate the rotor speed. In addition, Region 2 and 3 are also referred to as the partial or below-rated and the full load or above-rated regions of the turbines, respectively. Some articles such as the Ref.[27] considers the region above the cut–out wind speed as an extra region, Region 4. Above the cut-out wind speed, wind turbines are normally not allowed to operate due to the extreme turbine loadings. However, most modern turbines operate even beyond the cut-out wind speed with offline-shaped strategies such as ramp shaping, stepwise shaping etc.[31] [14] [32] [33] [34] [35].

As an example, Figure 1-12 depicts all these regions and their boundaries for a 5 MW turbine. The dashed red line is the rated power of 5 MW wind turbine. The blue curve represents the power in wind. The green, on the other hand, represents the controlled power curve of the turbine. As seen in Figure 1-12, not all the power in wind is extracted into electrical power due to the Betz limit (subchapter 2.1.1) and losses in turbine mechanical and electrical components.

There are also transitional regions between Region 1 and 2, as well as Region 2 and Region 3, which are respectively referred to as Region 1.5 and 2.5. During the generator torque controller design, the transition from Region 1 to Region 2 or Region 2 to 3 is not realized by a simple switching, but rather a dynamic scheme depending on the generator speed[36] or rotor speed. The controllers in these transition regions are referred to as Region 1.5 and 2.5 transition controllers. Region 1 covers an operation from start-up to the cut-in wind speed. Just above the cut-in wind speeds, turbines may not give the maximum power possible (Region 2.5), yet still, it is said to be operating in Region 2[27].

Region 2 typically includes a generator torque controller in order to gain the maximum energy possible from the available wind. This is achieved by variable rotor speed operation, which allows the turbines to operate at the peak of the Cp-TSR-Pitch surface, whose extraction is defined extensively in subchapter 4.4.1. Therefore, the turbine operates at the optimum TSR, resulting in operation with the maximum power coefficient, C_{pmax}. With the C_{pmax}, the turbine produces the maximum power at any wind speeds. This is realized by keeping the blades at their optimum pitch settings and adjusting the generator torque to change the rotor speed to the changing wind speed. During turbine operation, the Cp-TSR-Pitch surface may change and usually get a lower maximum C_p due to residue buildup, blade erosion and blade icing etc. This undesired phenomenon negatively affects the Cp-TSR-Pitch surface, which potentially requires an adaptive control technique. However, here, the rotor blades are assumed to be clean during the generator torque controller design. Region 3, however, usually includes a Proportional and Integral (PI) or Proportional-Integral-Derivative (PID) based blade pitch controller[14][32]. The primary purpose in Region 3 is to obtain the rated power. To ensure that, the generator torque is held constant at its rated value and blade pitch angle is varied.

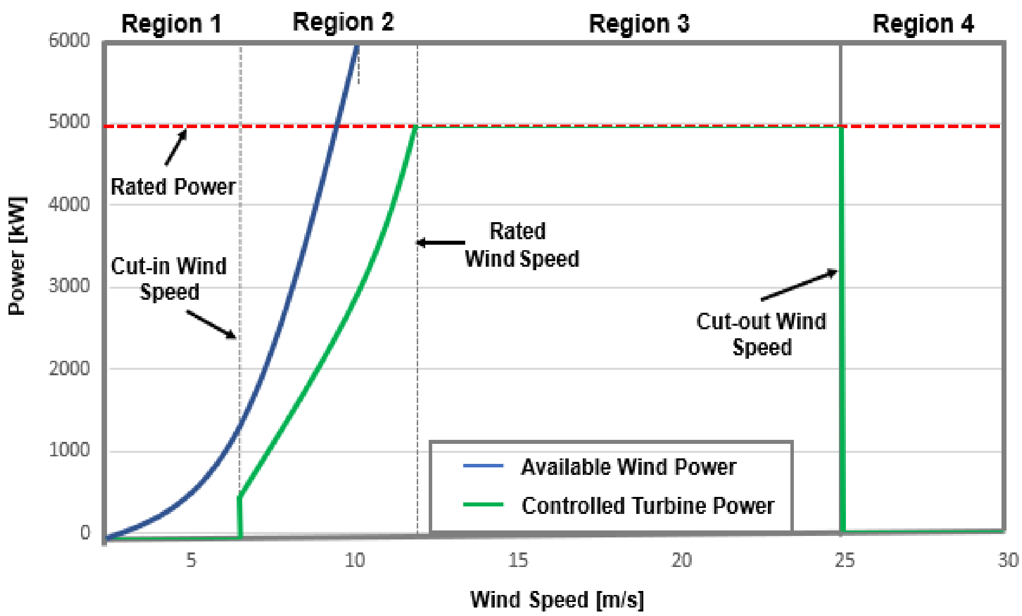

Figure 1-12 Illustration of wind turbine operation region[37]

Generator torque control may be realized in two different ways; torque-mode control or speed mode control. In the standard torque controller scheme, an optimal gain is calculated and the torque demand of the generator is generated proportional to the square of generator speed, which is employed in the present thesis study for the baseline generator torque controller. However, the rotor speed is used rather than that of the generator. In the speed control mode, on the other hand, there is usually a PI-based controller to produce the required torque demand of the generator[38].

1.6 Literature Survey on Wind Turbine Envelope Protection.

Operational conditions have a direct impact on wind turbine life spans. Excessive loadings are one undesired condition that occurs on turbines in the field. There are numerous control studies in the literature in order to reduce wind turbine loads in terms of both fatigue[39]–[42] and ultimate loads[36], [39], [43]–[45]. This thesis focuses on ultimate load reduction and proposes an adaptive envelope protection control algorithm that intervenes only with the standard collective blade pitch control systems whenever an envelope violation is detected throughout the below and above rated regions, Region 1.5, 2, 2.5 and 3.

Power reduction is a useful method to alleviate turbine loads[35]. For instance, Ref.[45] uses this idea to avoid excessive turbine loadings not only around the rated wind speed but also throughout the entire operational regions. Thus, it keeps the turbine always in the pre-defined safe envelope limits. There, an online optimization-based procedure monitors the current wind and turbine states and is employed for the prediction of wind speed variations that would lead the turbine response to reach the boundary of the safe operation region. Later, this wind speed, which is referred to as envelope wind speed, is compared with the actual wind passing through the turbine. This comparison determines whether the turbine operates with the excessive loadings or not, in which case the power reference is altered accordingly.

The online optimization-based control algorithm in Ref.[45] is the extension of the study in Ref.[44], which focuses on the optimal soft cut-out control strategy to prevent high structural loadings that typically occurs during storms. That optimal soft cut-out strategy enhances the power generation in Region 4, compared to the standard soft cut-out strategies such as ramp shaping, stepwise shaping etc.[35]. These are offline-shaped strategies and are based on mean wind speed. They do not take into account the current wind and turbine conditions. However, the optimal soft cut-out strategy utilizes a dynamic optimization which takes into account the wind and turbine states in the soft cut-out process. In the soft cut-out strategy, the power reference is adjusted depending on the current loadings of the turbine. When the turbine operates with lower loads than the limits of allowable loads, then the power reference is increased. Conversely, the power reference is decreased whenever the turbine loading exceeds the limit of allowable limits. Power reference adjustment is realized by means of varying the rotor speed reference while keeping the generator torque constant at its rated value. Thus, the turbine is safely operated within the allowable limits, thereby obtaining a soft envelope protecting cut-out with the enhanced power generation, less fatigue and minimized disturbance to the electrical grid. A similar idea on soft cut-out is investigated in Ref.[46], but an assumption is required on wind characteristics. Therefore, an incorrect assumption may result in an excessively low power reference or high loads, which inevitably requires online monitoring of wind characteristics to obtain a proper performance from the suggested control algorithm[44].

In Ref.[36], the same optimization-based algorithm is re-investigated with the generalized formulation under the name of wind turbine envelope protection control for the full speed range, i.e. Region 2, 2.5, 3 and, lastly the optional region, Region 4. It also describes the overall robustness of the algorithm using load measurements. The capability of the mentioned algorithm is determined against the available modified load reduction methods such as the thrust clipping around the rated wind speed and the soft cut algorithm used for Region 4, which are based on static characteristics computed off-line.

The algorithm used in Ref.[36], [44], [45] is an add-on to the baseline power control algorithms such as generator torque and collective blade pitch controllers. This property allows reusing the available turbine controllers, likely making it attractive to the wind power industry. In the algorithm, as far as the turbine operates in the pre-defined safe limits, the control algorithm carries out no action. But, any exceedance detection of the pre-defined limits results in an intervention of the protection system with turbine control systems to keep it within the desired limits. The employed optimization algorithm in the above references consists of two linear optimization procedures. The main part of the algorithm is the linear optimization for the worst case prediction which calculates the envelope wind speed. The other part of the algorithm is the linear optimization for power reference selection that utilizes the optimization procedure for envelope wind speed as a constraint. In all of these Ref.[36], [44], [45], the thrust force is chosen as the limit parameter since it is a meaningful proxy for the vital design driving loads on some wind turbine components.

In this thesis study, similarly, the thrust force is limited and is directly taken from the controlled turbine simulation model. However, in actual turbine implementation, the turbine thrust information may be taken from blade root load sensors, which are utilized on modern turbines for other forms of load mitigation control purposes[36].

In contrast to the previous optimization-based algorithm in Ref.[36], [44], [45], this thesis study utilizes a different theoretical approach-the wind turbine envelope protection control system based on neural networks. This new approach originates from the idea of adaptive envelope protection system for fly-by-wire manned/unmanned fixed or rotary wing aircraft[47]–[50]. However, the implementation of the approach to wind turbines is quite different than those of manned/unmanned aircraft, which is based on the dynamic trim concept and requires estimations of limit and control margins to be used in envelope protection system[47]–[49]. The newly proposed approach employs an online learning neural network. Since the learning is realized in real time, this algorithm does not require any prior training process of neural networks using a large amount of data, which would be difficult to generate for all turbine operating conditions. Besides, it does not require an excessive computation compared to off-line trained neural networks. The algorithm has the adaptation capability to any turbine operating conditions since neural network weights are updated in real-time based on Lyapunov analysis[49]. Therefore, the algorithm may potentially be used with any turbine configurations, from small to large scale turbines, i.e. rigid to flexible structures. Furthermore, the currently suggested adaptive envelope protection system seems more straightforward in implementation than the optimization-based algorithm in Ref.[36], [44], [45]. The optimization-based algorithm requires the addition of baseline control laws to the reduced wind turbine model for the below and above rated regions. An issue may arise requiring the best knowledge of the algorithm used for the baseline turbine controllers on different turbines. Otherwise, application/design of the optimization-based algorithm may not be possible. However, the newly proposed adaptive envelope protection control algorithm is independent of algorithms for baseline controllers since the measurements of wind or turbine states are taken directly from the turbine itself, i.e. from the controlled turbine. Moreover, the turbine gains the ability to efficiently ride at the desired envelope boundary at all times. This study also differs from those of Ref.[36], [44], [45] in terms of the utilized avoidance method. In those studies, to prevent the turbine from excessive loading, both blade pitch angle and generator torque, i.e. controller gain is varied in the below-rated region, while rotor speed reference is adjusted for the above rated region. Here, this protection/avoidance is realized only through output change of blade pitch control system i.e. blade pitch reference via a control limiting technique[48]. This avoidance technique is most probably much simpler in application to the available turbines in the field since there is no need for the intervention with the generator torque controller, i.e. power electronics unit.

Neural networks may approximate any continuous function to any desired level of accuracy. Therefore, a neural network is used in this thesis to augment an approximate linear dynamic model of the limit parameter to enhance the estimation of limit parameter dynamics in real time. Therefore, in this thesis, Linearly Parameterized Neural Network (LPNN), one type of neural network, is employed to approximate the nonlinear dynamics of the limit parameter. Here, it is the thrust of the turbine. Weight update laws are designed in such a way that the modeling uncertainty of the approximate limit parameter dynamic model is eliminated by neural network output. The proposed approach is adopted here to protect the turbine throughout the entire operational regions, i.e. from the cut-in to cut-out wind speed.

Unlike the algorithm in Ref.[36], [44], [45], the utilized adaptive algorithm is an add-on to the baseline blade pitch controller only and basically monitors the wind and turbine states at all times. Therefore, it learns online the current situations of the wind turbine and adapts the learning weights to estimate accurate limit parameter dynamics.

This estimated limit parameter dynamics is used to calculate the envelope wind speed at the same time via a fixed point iteration method. By comparing the envelope wind speed with the actual wind speed, a proper protection/avoidance action is applied to the standard blade pitch control system of the turbine. This corresponds to the power output reduction whenever the safe operational region is about to be abandoned. The developed turbine simulation model[51] here is equipped with a standard generator torque controller in the below rated region and a gain-scheduled PI-based collective blade pitch control system, pitch to feather for the above rated region. More information about the proposed system and its implementation and simulation results are given in Chapter 6.

1.7 The Contribution of the Thesis

The main contribution of this thesis study is the adaptive envelope protection system based on a neural network that can adapt online to wind and turbine states. The protection system is utilized here to prevent the turbine from having larger thrust values than the pre-defined value since it is a meaningful proxy for the vital design driving loads on some turbine components. The proposed system protects the turbine from the cut-in to cut-out wind speeds, i.e. throughout the below and above rated operational regions. In this thesis study, an LPNN has used as a neural network and a new concept referred to as unsteady dynamics is introduced to the literature. This concept is utilized to estimate the envelope wind speed that would take the turbine to the pre-defined envelope boundary. The dynamic trim concept, used in designing the envelope protection system for manned/unmanned fixed/rotary wing aircraft, has been experienced as an invalid concept for wind turbines due to the turbulent nature of wind. This is due to the fact that all the states of the controlled turbine, i.e. fast and slow states, are being always in transient phases.

With this thesis study, a new avoidance method to wind turbines is applied via blade pitch control system output, i.e. a control limiting technique both for the below and above rated regions. This design/implementation of the proposed system is also easier in application to the operating turbines since the only intervention is the blade pitch controller output, in contrast to available methods in the literature[36], [45] varying the generator torque, i.e. controller gain and blade pitch angle for the below rated region, adjusting the rotor speed reference for the above-rated region, while keeping generator torque at its rated value.

Simulations show a promising capability to reduce excessive turbine loadings, i.e. keeping the turbine within the pre-defined limit value in both regions under normal turbulent winds with different mean values. The proposed system may be used to limit other critical turbine variables.

In addition, this protection system may replace the already known method "Thrust Clipping" or "Peak Shaving", which are off-line shaped strategies[35] and protects turbines only around the rated wind speed where the thrust force peaks for pitch to feather controlled turbines. The proposed system protects turbines not only around the rated wind speed but also throughout the below and above rated regions. Therefore, these significant benefits are quite likely to appeal to the wind power industry. Furthermore, it is also an alternative to the available envelope protection control algorithm in Ref.[36], [45] and is easier to implement to the operating turbines since the proposed algorithm is independent of the baseline controllers. Lastly, it is also more straightforward in terms of avoidance method, i.e. intervening with only the blade pitch controller output, and does not require any intervention with the generator torque controller, i.e the power electronics unit that is widely utilized in modern turbines.

1.8 Structure of the Thesis Study

This thesis study is organized as follows. Chapter 1 provides information about the wind and wind energy usage, worldwide wind power status, wind turbine types and their operational principles. It focuses largely on Horizontal Axis Wind Turbines (HAWT) since this turbine type is utilized in this thesis study. It defines the primary and secondary HAWT mechanical and electrical components, and defines wind turbine control systems, contemporary technologies, as well as control and operational regions of variable speed variable pitch HAWTs. It also includes a literature survey about the load reductions, i.e. fatigue and ultimate loads, envelope riding and envelope protection systems as well as the contributions of the current thesis study. Chapter 2 defines wind turbine aerodynamics, blade element momentum (BEM) theory, and particular aerodynamic corrections for a more realistic turbine behavior. Chapter 3 focuses on the dynamic modeling and overall wind turbine system, i.e developing the MS Bladed simulation model, turbine coordinate systems and their transformation matrices. It provides information about the iteration process, which is the main part of the MS Bladed simulation model, to calculate the elemental forces and therefore the moments. Validation of the developed MS Bladed simulation model is carried out in Chapter 4 by comparing the estimated performance results with those of experimental turbines, Phase II and Phase III, NREL Phase VI rotor blade designs-PROPID predictions as well as NREL 5 MW turbine data published in the literature. Baseline controller designs and implementations are given in Chapter 5 with their thoughtfully investigated simulations. The chapter also provides information about the turbine linearization for the above rated region with frozen wake and equilibrium wake assumptions etc. Finally, Chapter 6 defines the new envelope protection system. It addresses the main idea and theory behind the proposed system, estimating the linear parameter dynamics, calculating the envelope wind speed, detecting excessive loadings and lastly realizing the limit avoidance action. In addition, it presents the simulations of the developed envelope protection system both in the below and above rated regions as well as around the rated wind speed under normal turbulent wind speeds with a mean of 8, 15 and 11 m/s, respectively. Eventually, conclusions and suggestions are drawn in Chapter 7.

CHAPTER 2

BEM BASED AERODYNAMIC MODELING OF A HORIZONTAL AXIS WIND TURBINE

A layman may believe that wind turbine aerodynamics is less sophisticated than the fixed or rotary wing aircraft. However, some of the most fundamental wind turbine aerodynamic aspects are still not completely understood even though the wind turbine is one of the oldest machines in the world. This is because of the fact that the inflow is exposed to stochastic wind fields during the turbine operation. In particular, when the turbine is not pitch-regulated, the stall is an inherent part of the operational envelope. With the stall phenomenon, the airflow is separated from the upper surface of the blades with turbulent mixing and a flow reversal occurring close to the turbine blade surface[52], resulting in a very quiet complex aerodynamic phenomenon.

As stated before, the turbine rotor is one of the main turbine components whose duty is to convert the kinetic energy in wind into a useful rotational mechanic energy to drive an electrical generator. The amount of mechanical rotor power depends on the interaction between the rotor and the wind passing through the rotor. Therefore, modern wind turbine rotor blades are particularly designed to be twisted, tapered and swept/curved structures, usually consisting of multiple airfoils throughout their blade spans. Thus, the more efficient the rotor blades, the higher the energy obtained by the turbine, which eventually results in more mechanical power available to be converted into the electricity.

The wind flow, which passes through the rotor, may be thought as a mean air flow with turbulent fluctuations. The mean wind flow determines the wind turbine mean power output and the mean loads on the turbine components. Wind shear, off-axis winds or rotor rotation may cause periodically changing forces on the wind turbines. Turbulence and dynamic effects induce randomly fluctuating forces, which have similar effects on the turbine structures as well. Therefore, turbines mostly work under unsteady aerodynamic conditions. However, the steady-state aerodynamics is particularly important to develop a wind turbine simulation model, which represents an actual wind turbine in a computer environment. A simulation model may not only include the models of turbine mechanical parts such as rotor blades, gearbox etc., but also the electrical parts such as generator, transformer and power electronics unit etc. In this thesis study, the focus is more on the mechanical side of wind turbine, less on the electrical side. The developed MS Bladed simulation model basically consists of a rotor, a simple variable torque electrical generator as well as a gearbox.

Here, in this chapter, dynamic modeling or simulation model of a horizontal axis wind turbine (HAWT) is carried out, i.e MS Bladed model. Therefore, all the aerodynamic derivations, i.e. blade element momentum (BEM) theory, aerodynamic corrections, coordinate systems etc. belong to the HAWT type or propeller type turbine.

In order to develop a turbine simulation model, BEM theory is a commonly used method. With BEM theory, the performance of a wind turbine with known rotor geometry and airfoil characteristics is predicted. Therefore, this theory is widely used by wind turbine designers and researchers due to its ease of application and computational operation[53]. This theory is also used for designing and determining the performance of any type of rotary wings such as aircraft propellers, helicopter rotors, ship propellers etc. It basically consists of the blade element and momentum theories, whose detailed derivations are given in the next subchapters.

2.1 Momentum Theory

2.1.1 One-Dimensional Momentum Theory

Following the Ref[12], a simple model based on one-dimensional linear momentum theory is used to determine the performance of an ideal wind turbine rotor. In this model, the rotor is represented as an actuator disk in a stream tube (Figure 2-1), whose surface and two cross sections constitute the control volume boundaries. The ideality here comes from the fact that the rotor does not have any friction or a downstream rotating wake. This analysis takes into accounts the following assumptions[12].

- The airflow is incompressible, homogeneous and steady.
- The rotor is a disk with an infinite number of blades and is placed perpendicularly to the freestream velocity or wind speed.
- There is no frictional drag and no rotating wake behind the turbine rotor.
- Uniform thrust is available everywhere over the rotor disk surface.
- The static pressure far before and far after the rotor disk is equal to the freestream static pressure.

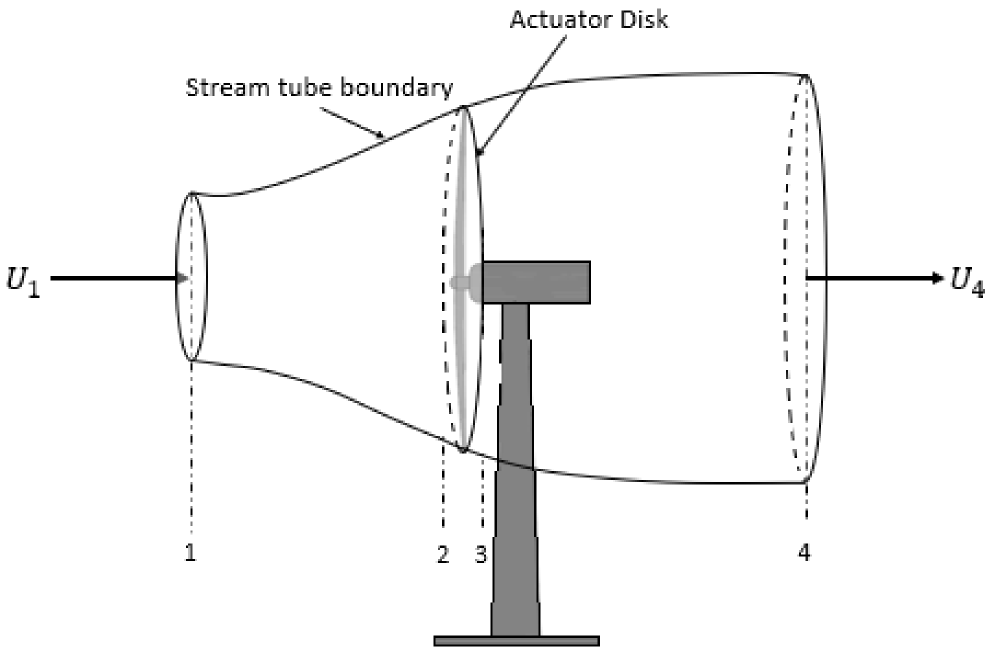

Figure 2-1 Actuator disk model of a wind turbine

With these considerations above, the application of linear momentum conservation principle to the control volume in Figure 2-1 gives the net force, i.e the thrust force, *T*, exerted on the control volume. This force may be formulated as follows[12].

$$T = U_1(\rho UA)_1 - U_4(\rho UA)_4 \quad (2\text{-}1)$$

Where ρ, U and A represent respectively the air density, freestream velocity or wind speed and the cross sectional area of the stream tube, i.e. the rotor disk area. The subscripts denote the corresponding values at those related cross sections. Since there is a steady airflow passing through the rotor disk, the mass flow rate throughout the control volume is fixed and may be calculated by[12],

$$\dot{m} = (\rho U A)_1 = (\rho U A)_4 \tag{2-2}$$

By carrying out some algebraic manipulations using both equations (2-1) and (2-2), the thrust force is obtained as[12],

$$T = \dot{m}(U_1 - U_4) \tag{2-3}$$

The fact that the freestream wind speed,U_1, is larger than the velocity behind the rotor disk, U_4, the thrust force is positive. Further, the Bernoulli equation can be written for the control volumes both upstream and downstream of the rotor disk, respectively as[12],

$$p_{1+}\frac{1}{2}\rho U_1^2 = p_{2+}\frac{1}{2}\rho U_2^2 \tag{2-4}$$

$$p_{3+}\frac{1}{2}\rho U_3^2 = p_{4+}\frac{1}{2}\rho U_4^2 \tag{2-5}$$

The static pressure far upstream, p_1 and far downstream p_4 are the same. In addition, there is no change in velocity passing across the rotor disk. Thus, U_2 and U_3 velocities are equal to each other. The thrust force may be also represented as a net sum of the forces on both sides of the disk as[12],

$$T = (p_2 - p_3)A_2 \tag{2-6}$$

When solved for $(p_2 - p_3)$ using equations (2-4) and (2-5) and plugging that into the equation (2-6), the following equation is also obtained for the thrust force[12].

$$T = \frac{1}{2}\rho A_2(U_1^2 - U_4^2) \tag{2-7}$$

When the equations (2-3) and (2-7) are equated to each other and considering the mass flow rate, $\rho A_2 U_2$, the following relation is derived[12].

$$U_2 = \frac{U_1 + U_4}{2} \tag{2-8}$$

Thus, the wind velocity at the rotor disk is the mean of upstream and downstream wind speeds. An induction factor, which is referred to as axial induction factor and denoted by a, shows the fractional decrease in wind velocity between the freestream wind and the rotor disk. This factor is defined as follows[12].

$$a = \frac{U_1 - U_2}{U_1} \tag{2-9}$$

The velocity at the rotor disk and the velocity far downstream of the turbine are respectively obtained as[12],

$$U_2 = U_1(1 - a) \tag{2-10}$$

$$U_4 = U_1(1 - 2a) \tag{2-11}$$

As seen in the equation (2-10), the total velocity at the rotor is the combination of the wind speed, U_1 and the induced wind velocity at the rotor, $U_1 a$. In addition, an increase in the axial induction factor from zero results in a gradual decrease in both wind speeds of U_2, U_4. For instance, once the axial induction factor becomes $1/2$, the wind speed at the rotor disk becomes half of the freestream wind speed, U_1. On the other hand, the wind speed at downstream of the turbine rotor, U_4 becomes zero. This means that the airflow behind the rotor disk comes to a halt, which causes this simple theory to break down.

The power output from the turbine is obtained by multiplying the thrust force (equation (2-7)) and the velocity of U_2 at the rotor disk[12],

$$P = \frac{1}{2}\rho A_2 U_2 (U_1^2 - U_4^2) \tag{2-12}$$

Substituting equations, (2-10) and (2-11) into (2-12), and then replacing the control volume area at the rotor disk, A_2 and the freestream wind speed, U_1 by respectively A and U, the power output equation becomes as follows[12].

$$P = \frac{1}{2}\rho A U^3 4a(1-a)^2 \tag{2-13}$$

The turbine performance is characterized by the power coefficient, C_p, which is the ratio of rotor power to the power available in the wind. Thus, the power coefficient is[12][14],

$$C_p = \frac{P}{P_{wind}} \tag{2-14}$$

Where the power in the wind is defined as[12][14],

$$P_{wind} = \frac{1}{2}\rho U^3 A \tag{2-15}$$

Using the equations (2-13) and (2-14) and (2-15), the power coefficient,C_p, for an ideal wind turbine is found as follows[12].

$$C_p = 4a(1-a)^2 \tag{2-16}$$

The maximum C_p of an ideal turbine is obtained by plugging $a = 1/3$ into equation (2-15). Here, the value of $a = 1/3$ is a result of a calculation which includes the derivative of equation (2-16) with respect to a, and then equating it to zero. Therefore, the maximum power coefficient for an ideal wind turbine is found as[12],

$$C_{pmax} = 0.5926 \tag{2-17}$$

This maximum C_p value is referred to as the Betz limit. In a similar way, the axial thrust on the rotor disk is found[12] from equations, (2-7), (2-9) and (2-10).

$$T = \frac{1}{2}\rho A U_1^2 4a(1-a) \tag{2-18}$$

This thrust force is used to find the thrust coefficient, C_T, which is defined as the ratio of turbine thrust force to the freestream dynamic force. Therefore, the thrust coefficient for an ideal wind turbine is obtained by[12],

$$C_T = \frac{T}{F_{dynamics}} \tag{2-19}$$

where $F_{dynamics}$ is the dynamic wind force acting on the rotor disk[12],

$$F_{dynamics} = \frac{1}{2}\rho U^2 A \tag{2-20}$$

Therefore, an ideal wind turbine thrust coefficient, C_T is obtained as[12],

$$C_T = 4a(1-a) \tag{2-21}$$

When the axial induction factor becomes 0.5, C_T reaches at its maximum value of 1. Figure 2-2 is plotted for the C_p and C_T curves with respect to axial induction factor,a, using the equations (2-16) and (2-21), respectively.

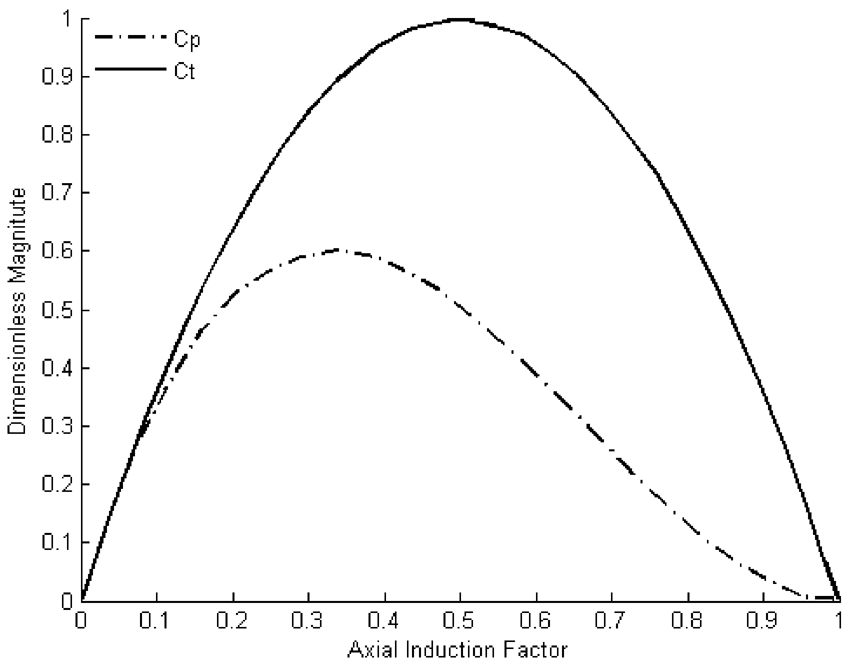

Figure 2-2 Operating parameters for a Betz turbine

As mentioned before, when the axial induction factor goes beyond the value of $1/2$, the ideal wind turbine model is not valid anymore since a highly complex flow pattern occurs at downstream of an actual wind turbine. Accordingly, the thrust coefficient of the turbine reaches up to a value of 2. The flow physics behind this aerodynamic phenomenon is explained in subchapter 2.5. Equation (2-16) gives the maximum C_p of an ideal wind turbine with $a = 1/3$. It is the maximum theoretical power coefficient that an ideal wind turbine may have. The peak of C_p curve in Figure 2-2 is the maximum power coefficient that corresponds to the Betz limit. However, an actual wind turbine has expectedly a lower maximum C_p value than this limit due to the rotating wake behind the turbine rotor, frictions, a certain number of blades, and their respective tip and hub losses etc.[54].

2.1.2 Ideal Horizontal Axis Wind Turbine with Rotating Wake

In one-dimensional linear momentum analysis, a wind turbine has been considered as an actuator disk in a stream tube to determine the performance of an ideal wind turbine rotor. However, when an actual wind turbine rotor rotates, the flow downstream of the turbine turns into a direction opposite to the rotor rotation, which is in reaction to the torque applied by the flow on the rotor. This wake rotation phenomenon is depicted in Figure 2-3.

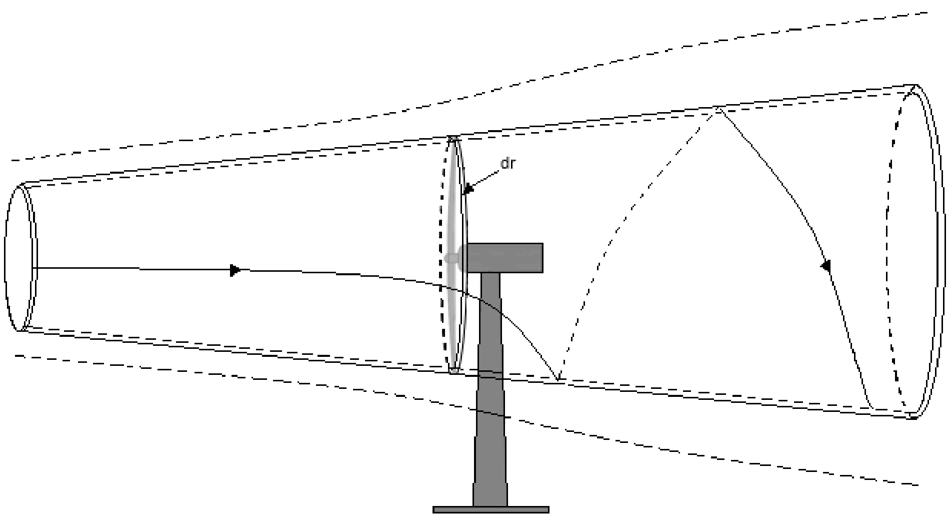

Figure 2-3 Stream tube model of a HAWT with wake rotation

The previous analysis did not include the impacts of wake rotation. Therefore, this approach must be expanded to the case in which the rotating rotor causes an angular momentum, which results in a rotor torque. Thus, the torque is used to obtain the power by considering the rotor speed.

Therefore, following the Ref.[12], the geometry in Figure 2-4 is used to extend the previous analysis to include the wake rotation. The current analysis employs an annular stream tube with a radius r and a thickness, dr. In this analysis, ω represents the angular velocity of the wake flow behind the turbine rotor, whereas **Ω** is the angular velocity of the turbine rotor. An assumption of equality is considered between the pressures in the far wake and in the freestream wind. In addition, wake rotation, the pressure and induction factors are all considered to be a function of rotor radius, r.

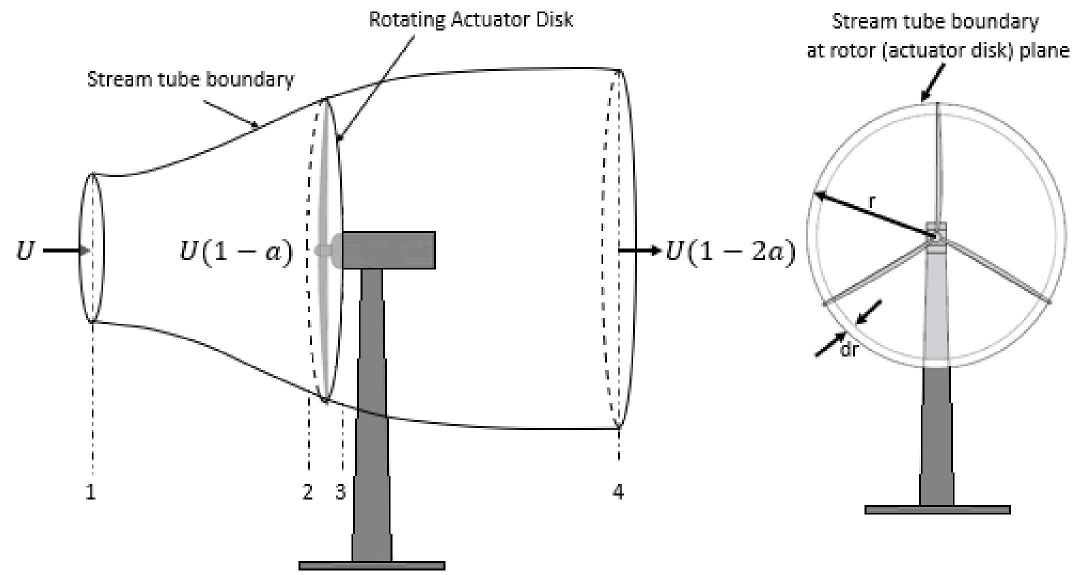

Figure 2-4 Geometry for a HAWT rotor analysis with wake rotation

Therefore, considering a control volume with the same angular velocity of the rotor blades, an expression is derived for the pressure variation across the blades with the application of the energy equation for sections before and after the turbine blades. Across the flow disk, the axial component of velocity is fixed, but the angular velocity of air to rotor blade increases from **Ω** to **Ω**+ω. Therefore, the pressure difference at the cross-sections of 2 and 3 is found as follows[12].

$$p_2 - p_3 = \rho(\Omega + \frac{1}{2}\omega)\omega r^2 \tag{2-22}$$

Therefore, the thrust on an annular element is found as[12],

$$dT = (p_2 - p_3)dA = \rho(\Omega + \frac{1}{2}\omega)\omega r^2 2\pi r dr \tag{2-23}$$

The definition of the tangential induction factor is given as[12],

$$a' = \frac{\omega}{2\Omega} \tag{2-24}$$

Here, tangential induction factor is a non-dimensional quantity which the ratio of rotating wake speed, ω to the rotor speed. Rotating wake speed is much less than the rotor angular velocity. Since this analysis contains the wake rotation, ω, the induced velocity at the rotor is the combination of axial component, Ua and a tangential component in the rotor plane, $\Omega r a'$. Thus, the elemental thrust expression turns into the following[12],

$$dT = \frac{1}{2}\rho\Omega^2 r^2 4a'(1 + a')2\pi r dr \tag{2-25}$$

Apart from the previous linear momentum analysis which considers U_1 as the freestream wind in equation (2-18), the thrust on an annular cross-section is also obtained by the equation (2-26), which utilizes the axial induction factor, a and uses U instead of U_1[12].

$$dT = \frac{1}{2}\rho U^2 4a(1 - a)2\pi r dr \tag{2-26}$$

Equating the two thrust equations (2-25) and (2-26) to each other gives the following relation[12],

$$\frac{\Omega^2 r^2}{U^2} = \frac{a(1 - a)}{a'(1 + a')} \tag{2-27}$$

Where $\Omega r/_U$ is the ratio of a local blade section velocity, r to the freestream velocity, U or referred to as local speed ratio, λ_r. If the same expression is extended to the whole rotor, it is referred to as tip speed ratio, λ and is defined as[12] [14],

$$\lambda = \frac{\Omega R}{U} \tag{2-28}$$

Further, an expression for the rotor torque is derived using angular momentum conservation principle. Therefore, the torque exerted on the rotor, Q, is equal to the change in angular momentum of the wake. For the incremental annular area element, it is written as[12],

$$dQ = d\dot{m}(\omega r)(r) = (\rho U_2 2\pi r dr)(\omega r)(r) \tag{2-29}$$

Employing equation (2-10) and the equation (2-24), the above expression turns into the following[12],

$$dQ = 4a'(1-a)\frac{1}{2}\rho U \Omega r^2 2\pi r dr \tag{2-30}$$

Eventually, the power produced by each element is simply the multiplication of the rotational speed and the elemental torque[12],

$$dP = \Omega dQ \tag{2-31}$$

Integrating the equation (2-31) gives the mechanical power produced by the turbine rotor.

2.2 Blade Element Theory

Up to now, linear and angular momentum conservation principles have been derived to obtain the forces at the blade through the control volume analysis. This section, however, focuses on blade element theory, which refers to an analysis of aerodynamic forces at an element of turbine blades. In this analysis, as seen in Figure 2-5, the turbine blade is divided into a desired number of elements among which the assumption of no interaction is valid.

During the blade element analysis, it should be kept in mind that the lift and drag forces produced by a blade element section are respectively perpendicular and parallel to the relative wind, U_{rel}. The relative wind velocity is the summation of wind velocity vector at the rotor, $U(1-a)$, and the wind velocity due to the blade rotation, which is, again, a vector summation of induced angular velocity, $\omega r/2$ and blade section velocity, Ωr.

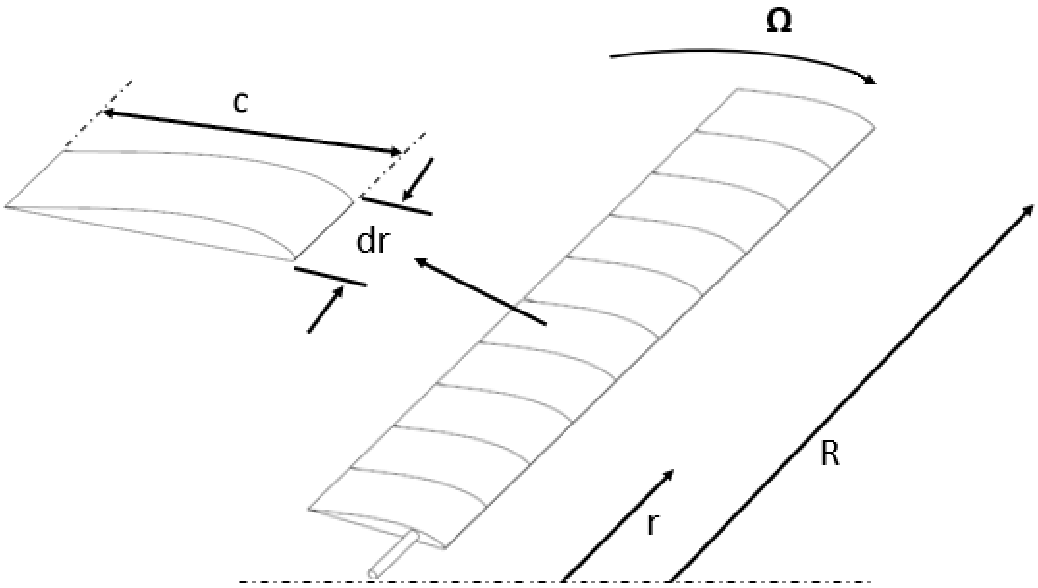

Figure 2-5 Turbine blade division into elements

Therefore, the component of relative wind in the plane of blade rotation is obtained considering the definition of tangential induction factor in (2-24)[12].

$$\Omega r + (\omega/2)r = \Omega r(1 + a') \quad \text{(2-32)}$$

Figure 2-6 shows the blade geometry utilized for the HAWT analysis. It shows some variables related to a blade element. In this figure, $U(1-a)$ is the wind velocity at a blade element, $\Omega r(1+a')$ is the tangential velocity of a blade element due to the blade rotation and induced angular velocity, U_{rel} is the relative wind velocity seen by a blade element, β is the blade pitch angle, the angle of blade tip and the plane of blade rotation. β_T is the elemental twist angle, β_p is the sum of blade pitch and elemental twist angle , α is the elemental AOA, i.e, the angle between the local relative wind and chord line, φ is the local flow angle or inflow angle, i.e the angle between the relative wind and the plane of blade rotation, dF_L is the elemental lift force, dF_D is elemental drag force, dF_N is the elemental normal force to the rotation plane, dF_T is the elemental tangential force to the circle swept by the turbine rotor.

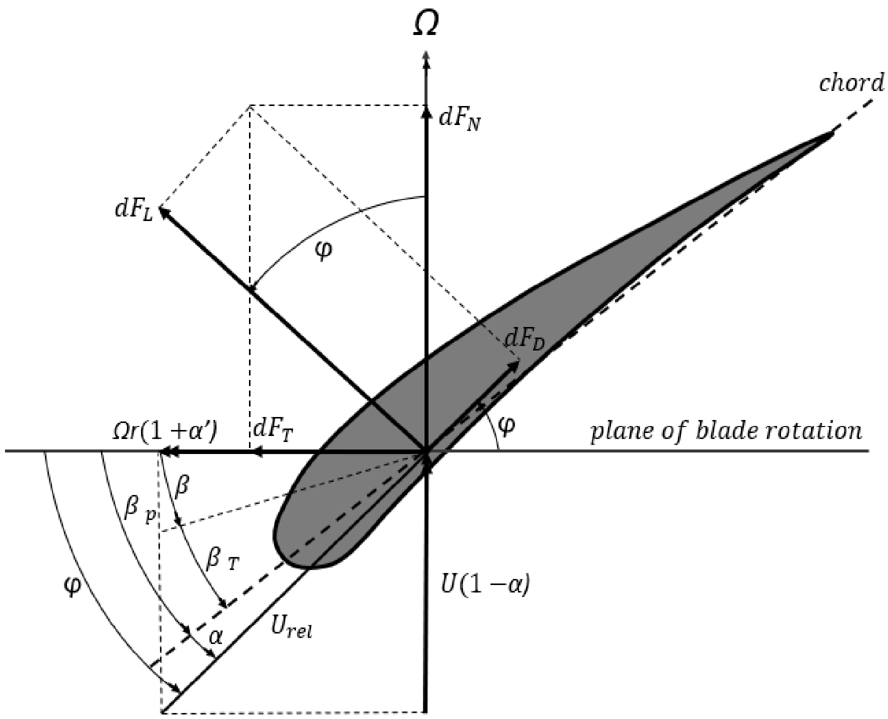

Figure 2-6 Elemental blade forces and specific angles

From the geometry in Figure 2-6, elemental pitch angle, β and AOA, α are obtained respectively as,

$$\beta_p = \beta_T + \beta \tag{2-33}$$

$$\alpha = \varphi - \beta_p \tag{2-34}$$

$$\varphi = \tan^{-1}(\frac{U(1-a)}{\Omega r(1+a')}) \tag{2-35}$$

$$U_{rel} = \sqrt{(U(1-a))^2 + (\Omega r(1+a'))^2} \tag{2-36}$$

Besides, elemental aerodynamic lift and drag forces, which are respectively vertical and parallel to the relative wind, are calculated as[12],

$$dF_L = \frac{1}{2}\rho U_{rel}^2 C_l c dr \tag{2-37}$$

$$dF_D = \frac{1}{2}\rho U_{rel}^2 C_d c dr \quad (2\text{-}38)$$

These elemental aerodynamic forces are later used to achieve the elemental normal (thrust) and tangential forces to the plane of blade rotation[12].

$$dF_N = dF_L cos\varphi + dF_D sin\varphi \quad (2\text{-}39)$$

$$dF_T = dF_L sin\varphi - dF_D cos\varphi \quad (2\text{-}40)$$

Including the effect of blade number, B_n, into these equations, the equations for the elemental total normal and tangential forces turn out to be as follows.

$$dT = dF'_N = B_n dF_N = B_n \frac{1}{2}\rho U_{rel}^2 C_n c dr \quad (2\text{-}41)$$

$$dF'_T = B_n dF_T = B_n \frac{1}{2}\rho U_{rel}^2 C_t c dr \quad (2\text{-}42)$$

where C_n and C_t are normal and tangential force coefficients and are given as,

$$C_n = (C_l cos\varphi + C_d sin\varphi) \quad (2\text{-}43)$$

$$C_t = (C_l sin\varphi - C_d cos\varphi) \quad (2\text{-}44)$$

Therefore, with the effect of local radius, the torque of a blade element is obtained as

$$dQ = r dF'_T = B_n \frac{1}{2}\rho U_{rel}^2 C_t c r dr \quad (2\text{-}45)$$

Integrating the equation (2-45) through the blade span gives the total power of the turbine rotor considering the rotor angular velocity, Ω.

2.3 Blade Element Momentum (BEM) Theory

Blade element momentum, or BEM theory, is a combination of results from both momentum and blade element theories. The theory resumes with four equations, two equations (2-26) and (2-30) from momentum theory and two equations (2-41) and (2-45) from blade element theory. Therefore, both thrust and torque equations for the same turbine rotor must be equal to each other. In this analysis, the following are assumed to be known.

1. Blade number, chord and twist distributions.
2. Elemental blade span and annular thickness.
3. Freestream velocity (or wind speed) and air density.
4. Aerodynamic data of the blade profile(s).
5. Rotor angular velocity for power calculation.

Then, the only unknown variables in the four equations (2-26), (2-30), (2-41) and (2-45) are the axial and tangential factors for the calculation of total torque and thrust of the turbine. To calculate the values of these factors, their equations must be first derived. This is realized using both theories. Considering the geometric relations in Figure 2-6, if the thrust equations (2-26) and (2-41) are equated to each other, and then solved for the axial induction factor, the following equation is obtained as[12],

$$a = \frac{1}{\frac{4\sin^2\varphi}{\sigma C_n} + 1} \tag{2-46}$$

Similarly, if the equations (2-30) and (2-45) are equated to each other, and then solved for the tangential induction factor gives the following[12],

$$a' = \frac{1}{\frac{4 sin\varphi cos\varphi}{\sigma C_t} - 1} \tag{2-47}$$

where σ in equations (2-46) and (2-47) is the local blade solidity and is defined as[12],

$$\sigma = \frac{B_n c}{2\pi r} \tag{2-48}$$

One common method to find these induction factors is to use an iterative method. The basic idea behind this iteration method is as follows.

1. Guess initial values for the induction factors, a and a'.
2. Calculate the inflow angle, φ, by equation (2-35).
3. Calculate the AOA, α by equation (2-34) and then use the corresponding aerodynamic C_l and C_d data.

4. Update a and a' using equation (2-46) and (2-47), respectively.

This process is repeated up until a convergence criterion is satisfied within some acceptable tolerance with respect to previous values. A more advanced iteration process, which is adopted in this thesis study, is explained in detail in subchapter 3.3. When the axial and tangential induction factors are estimated, the total thrust and torque, are calculated using equations from the momentum theory, equations (2-26) and (2-30) or blade element theory, equations (2-41) and (2-45). Therefore, the turbine power is easily obtained by considering the calculated torque and the rotor speed. In the developed MS Bladed simulation model, blade element theory equations, i.e equations (2-41) and (2-45), are used to calculate turbine thrust and torque quantities.

Until now, the momentum theory, blade element theory, and their combination or BEM theory, have been covered in detail. A turbine model based on the derived BEM theory is great enough to represent a simple turbine rotor with straight blades attached to the rotor hub perpendicularly to the rotor shaft (or no preconed blade). However, the wind flow must pass through the rotor in parallel to the rotor shaft or perpendicular to the rotor disk. In addition, the airflow must pass easily through the rotor blades. This corresponds to a turbine operation that the axial induction factors distributed throughout turbine blade span are quite low and therefore the flow pattern could be as seen in Figure 2-8-b. The turbine operating with this flow pattern is said to be operating in the windmill state region. In the subsequent subchapters, some important aerodynamic corrections are defined in order to deal with the invalidity of BEM theory and therefore to extend the theory to represent an actual turbine rotor. With these aerodynamic corrections, the turbine rotor may operate in any operating conditions such as yawed operation toward the wind or highly loaded rotor operation whose flow pattern is also given in Figure 2-8-c. In addition, aerodynamic losses occurring at the blade tips and rotor hub and their total effects should be taken into account since the original theory considers an infinite number of blades. All these corrections allow having a more realistic turbine rotor behavior, resulting in better performance predictions.

2.4 Aerodynamic Corrections for Rotor Hub and Blade Tip Losses

As stated above, an actual wind turbine rotor must also include a hub, tip, and total loss effects because the original BEM theory derived in the previous subchapters consider an infinite number of blades. However, an actual turbine rotor has a finite number of blades, mostly three blades, less commonly two blades. Therefore, there occurs a pressure difference between the upper and lower surfaces of turbine blades, which gets lower and lower close to the blade tips. This reduction in pressure difference occurs due to the airflow on the pressure side that swirls up to the suction side of the turbine blade. This phenomenon generates vortices shed from the blade tips into the wake on the induced velocity field. Therefore, there appear multiple helical structures in the wake. This aerodynamic phenomenon, which is more dominantly available near the blade tips, leads the turbine to produce a lower power output than an ideal wind turbine. This is due to having a lower lift force at the blade tip. Prandtl has modeled this tip loss effect by the equation (2-49). Therefore, Prandtl tip loss factor corrects the assumption of an infinite number of blades because there is the difference between the vortex systems of an infinite and a finite number of blades[11] [55].

$$F_{tip} = \frac{2}{\pi} cos^{-1}(e^{-\frac{B_n}{2}\frac{R-r}{r\,sin\,\varphi}}) \tag{2-49}$$

Likewise, a hub loss correction factor in (2-50) is also utilized due to the similar aerodynamic phenomenon occurring near the rotor hub. These hub vortices decrease the turbine power more[55].

$$F_{hub} = \frac{2}{\pi} cos^{-1}(e^{-\frac{B_n}{2}\frac{r-Rhub}{r\,sin\,\varphi}}) \tag{2-50}$$

Thus, for a given blade element, the local aerodynamics depends upon both tip and hub loss correction factors. In equation (2-51), F stands for the total loss factor, and includes the effects of both losses [55].

$$F = F_{hub} F_{tip} \tag{2-51}$$

The hub loss or tip loss effect or both are introduced here to the BEM theory by plugging them into the momentum equations (2-26) and (2-30). Therefore, new momentum equations including the total loss factor turn out to be as follows[12], [55].

$$dT = 4a(1-a)\rho U^2 F\pi r dr \tag{2-52}$$

$$dQ = 4a'(1-a)\rho U\Omega F\pi r^3 dr \tag{2-53}$$

Afterward, employing the previous methods, the new formulas for the axial and tangential induction factors which include the total loss factor, F turn out to be as follows.

$$a = \frac{1}{\frac{4F\sin^2\varphi}{\sigma C_n} + 1} \tag{2-54}$$

$$a' = \frac{1}{\frac{4F sin\varphi cos\varphi}{\sigma C_t} - 1} \tag{2-55}$$

Thus, new induction factors are affected by the total loss factor, which gives a more realistic rotor behavior than before. In the calculation of both induction factors, the usual practice is to not include the effect of drag coefficient, C_d. This method causes a negligible error when C_d data of an airfoil is very small. However, this is left as an optional choice in the developed MS Bladed simulation model. More importantly, neglecting the C_d effect in the formulas of induction factors does not necessarily require neglecting it in the calculation of elemental normal and tangential forces to the plane of blade rotation. Here, in the current MS Bladed simulation model, C_d effect is not ignored. In addition, it is important to utilize accurate aerodynamic data, C_l and C_d. These data should also include the Reynolds number effect. However, it is common to use a single set of C_l and C_d data at a certain Reynolds number because it in minimal errors. This way of using data depends on the Reynolds number operation range. If the Reynolds number range does not affect the aerodynamic data significantly, then a single set of data may be utilized [56].

2.5 Aerodynamic Correction for Turbulent Wake State

One dimensional momentum theory includes no or very small wake expansion. From the equation (2-11), it is clear that a value of axial induction factor greater than 0.5 gives a negative velocity in the far wake[57]. Therefore, the theory fails when a turbine works in the turbulent wake state or when the axial induction factor increases to one. Thus, the turbine is said to be operating in the turbulent wake state. The flow pattern around the turbine rotor is seen in Figure 2-8-c. In reality, the flow situation is completely different from just a simple change in the velocity direction. The wake at the downstream of the turbine rotor becomes turbulent. Thus, it entrains air from outside the wake region through a mixing process. This phenomenon re-energizes the flow that has passed through the turbine rotor. More explicitly, when a turbine rotor starts operating at high TSR values, its permeability to the airflow is getting lower and lower and therefore it starts pretending to be almost a solid disk. When a high enough TSR is reached, for which the axial induction factor is 1, the turbine behaves anymore as if it were a solid disk. At high TSRs, some of the airflows do not pass through the turbine rotor. There appears a stagnation point just at the front center of the turbine rotor disk, which increases the static pressure there. Thus, the airflow moves radially outwards, and develops a boundary layer, which separates at the turbine rotor disk edge. This aerodynamic phenomenon leads to a low static pressure behind the rotor disk. This drop in static pressure increases as the TSR and the axial induction factor increase. The other parts of the airflows which have passed through the turbine rotor disk encounters the low pressurized region and moves slowly. Therefore, the kinetic energy is not enough to supply the rise in static pressure essential to acquire the ambient atmospheric pressure that must be available in the far wake. The air can only reach the atmospheric pressure level by obtaining energy from the mixing process in the turbulent wake. The shear layer, between the freestream air and the wake, becomes the boundary layer which develops at the front of the disk. This shear layer is unstable and split into turbulence that leads to the mixing and re-energizing of the wake air. Consequently, due to the low pressure behind the turbine rotor as well as the high static pressure at the front center of the turbine rotor disk, the thrust coefficient of the turbine becomes much larger than the predicted value by the original BEM theory during the turbulent wake state or high axial induction operation[58].

Because of the aerodynamic phenomenon explained above, experimental measurements are not consistent with the BEM theory predictions when the axial induction factor exceeds a certain value. This value is referred to as the critical axial induction factor, a_c, and depends on the employed empirical windmill brake state model in the turbulent wake state. An empirical model must be added to the turbine model to correct the thrust coefficient from the momentum theory when the axial induction factor exceeds this critical value. In the literature, there are various empirical corrections between the axial induction factor and the thrust coefficient of wind turbines. These corrections include a parabola or straight lines fitted to the measurements.

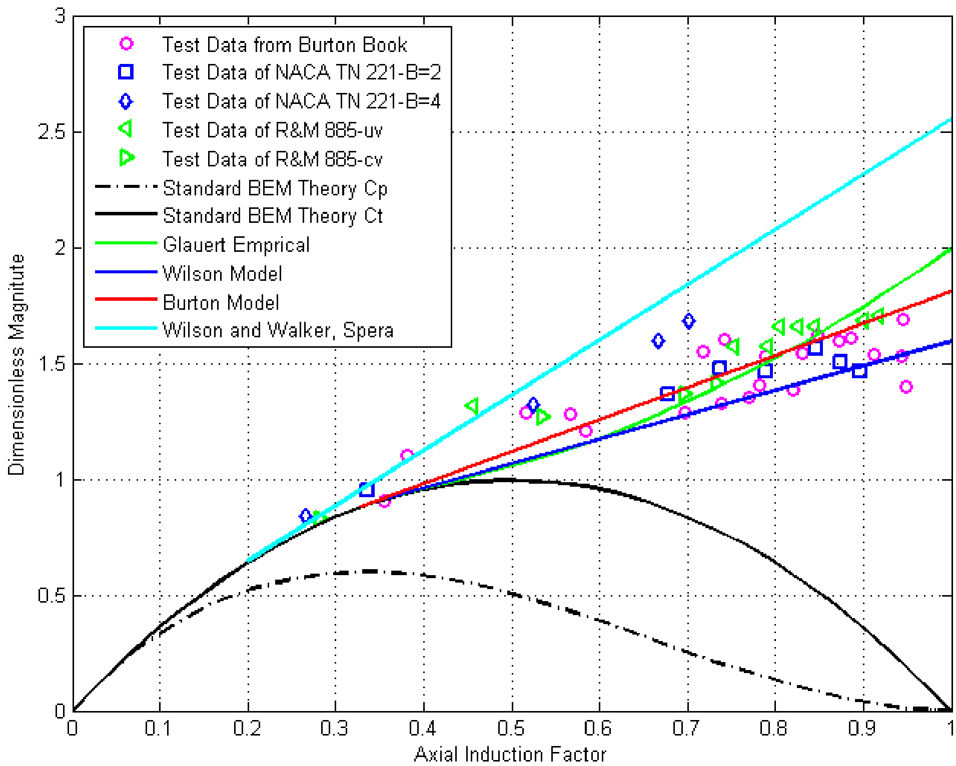

Figure 2-7 Various curve fittings to test data for turbulent wake state

Figure 2-7 shows some test data in the turbulent wake region for a whole rotor. The data, which are quite scattered, are taken from the Ref.[58],[59]. Therefore, the thrust coefficient in the turbulent wake state is not a straightforward function of the axial induction factor. For this reason, in history, quite a few scientists tried to find a curve/relation that predicts the rotor behavior in the turbulent wake state.

For instance, in the 1920s, Glauert fit a parabola to the test data. The parabola starts at the critical axial induction factor of 0.4 and goes through some of the data and terminates at an axial induction factor of 1, which corresponds to a thrust coefficient of 2. The parabola or Glauert's empirical curve was reported in a quadratic form as follows[60] [61].

$$C_T = 0.889 - \frac{0.0203 - (a - 0.143)^2}{0.6427} \tag{2-56}$$

However, tip, hub or total loss factor, which are explained briefly in the previous subchapter, were not taken into account at that time. A wind turbine must also include these loss effects due to vortices shed from both the blade tip and rotor hub. Therefore, later, introducing the loss correction factor into the momentum equation (2-18), therefore into (2-21) as seen in (2-57) caused a numerical problem or a gap between the momentum curve and Glauert's empirical parabola.

$$C_T = 4aF(1 - a) \tag{2-57}$$

This gap created a discontinuity problem when a computer program is used during the iteration process to calculate the new axial induction factor[60] [61]. Later in 1974, Wilson and Lissaman improved a computer program referred to as PROP code to analyze a wind turbine performance. Wilson model, which is a straight line approach, is utilized as a windmill brake state model. The critical axial induction factor or the intersection point with the momentum curve was chosen as 0.368, or 0.37. In between 1981 and 1983, Hibbs & Radkey updated the PROP Code, and renamed the Wilson model as classical momentum brake state model [62]. This model is utilized not only in Wt_Perf program, but also in the current version of PROPID under the name of classical brake state model[63],[61].

In the 1980s, a modification by Hibbs & Radkey and/or Eggleston & Stoddard was applied to the Glauert's empirical formula as well[62] [64] [60]. This modification just lowered the whole empirical curve down, but the gap problem was not removed completely. The modified Glauert's empirical formula was referred to as the advanced brake state model[64] [61]. The gap problem was discussed again later. Buhl simplified this advanced brake state model with a straightforward parabola and employed it in Wt_perf code. The numerical discontinuity problem was solved in the iteration process with the loss factor. But the new fit to the data is not perfect enough, but as suitable as Glauert's empirical equation [60]. Therefore, the relation between the thrust coefficient and the axial induction factor obtained by Buhl with the loss factor became as follows[60].

$$C_T = \frac{8}{9} + \left(4F - \frac{40}{9}\right)a + \left(\frac{50}{9} - 4F\right)a^2 \tag{2-58}$$

In 1984, Wilson proposed the Wilson and Walker model, as previously, a straight line approach. The critical axial induction factor was taken as 0.2. A similar linear concept is also expressed as Spera's correction. In the straight line approach, the selected point of the intersection determines both the line of slope and its equation. Therefore, when the critical axial induction factor, a_c is 0.2, the thrust coefficient passes through the value of 2.56 at an axial induction factor of 1[57] [11]. Similarly, Ref.[58] utilized the same approach and selected a_c as 0.326, which leads the line to pass through a thrust coefficient of 1.816 at an axial induction factor of 1[60]. All these empirical correction curves are depicted in Figure 2-7. Figure 2-8 shows the airflow patterns around a turbine rotor according to the change in the axial induction factor.

The airflow patterns in Figure 2-8 around a turbine give an idea why different correction models have to be used when the axial induction factor increases. Depending on the value of axial induction factor, the turbine operates in different states such as propeller state, windmill state, turbulent wake state, vortex ring state, propeller brake state, which fall in the ranges of axial induction of $(a < 0)$, $(0 < a < 0.5)$, $(0.5 < a < 1)$, $(a > 1)$, $(a \gg 1)$, respectively. The aerodynamical phenomenon occurring around the turbine in turbulent wake state is explained at the beginning of this subchapter.

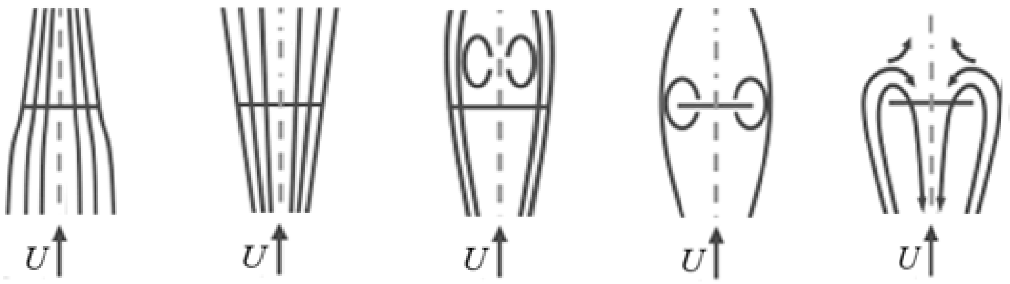

a) b) c) d) e)

Figure 2-8 The airflow patterns around a wind turbine depending on the value of axial induction factor; a) Propeller state b) Windmill state c) Turbulent wake state d) Vortex ring state, e) Propeller brake state[11]

The developed MS bladed simulation model uses the Spera's correction model to deal with the calculations in turbulent wake state operation, i.e calculating the new axial induction factor during the iteration process. The important point is that these above corrections are all empirical relations. In most cases, the axial induction factor never goes above 0.6. In addition, for a perfectly designed blade, the value of the axial induction factor is around 0.33 for most of the operation range. As stated previously, the Spera's correction starts with a straight line approximation that is tangent to the momentum theory thrust parabola at the critical axial induction factor value. Therefore, following the Ref.[57], the slope of this line may be found as follows.

$$\frac{dC_{T_{r,parabola}}}{da} = 4F(1-2a) \tag{2-59}$$

When the critical value for the axial induction factor is substituted into the above equation, the slope is equal to $4F(1-2a_c)$. If a parameter C_{T_1}, which is the maximum value of thrust at $a=1$ is utilized, the equation of the tangent line which touches the parabola at a_c becomes[57]

$$C_{T_{r,linear}} = C_{T_1} - 4F(1-2ac)(1-a) \tag{2-60}$$

Therefore, for a known value of C_{T_1}, the point a_c is found as[57],

$$a_c = 1 - \frac{1}{2}\sqrt{\frac{C_{T_1}}{F}} \tag{2-61}$$

Thus, the tangent equation becomes[57]

$$C_{T_{r,linear}} = C_{T_1} - 4F(\sqrt{\frac{C_T}{F}} - 1)(1 - a) \tag{2-62}$$

Spera's correction uses this tangent's equation when the axial induction exceeds the critical axial induction factor, a_c. Eventually C_{T_r} is calculated with different equations depending on the axial induction value[57] as follows.

$$C_{T_r} = \begin{cases} 4aF(1-a) & once\ \ a \leq 1 - \frac{1}{2}\sqrt{\frac{C_{T_1}}{F}} \\ C_{T_1} - 4F\left(\sqrt{\frac{C_T}{F}}\right)(1-a) & once\ \ a > 1 - \frac{1}{2}\sqrt{\frac{C_{T_1}}{F}} \end{cases} \tag{2-63}$$

In the formulation above, C_{T_1} is used as a parameter. However, a_c may also be employed as a parameter. Then, an equivalent formulation is found as[57],

$$C_{T_r} = 4aF(1 - f_s a) = \begin{cases} 4aF(1-a) & once\ a \leq a_c & i.e\ f_s = 1 \\ 4F(a_c^2 + (1 - 2a_c)a) & once\ \ a > a_c & i.e\ f_s = \frac{a_c}{a}(2 - \frac{a_c}{a}) \end{cases} \tag{2-64}$$

Inverting the equation (2-64) using the equation (2-65) gives the equation (2-66) to calculate the new axial induction factor when it is larger than the critical axial induction factor, $(a > a_c)$[57].

$$C_{T_r} = \frac{(1-a)^2\sigma}{\sin^2\varphi}C_n \tag{2-65}$$

$$a = \frac{1}{2}[2 + H(1 - 2a_c) - \sqrt{(H(1 - 2a_c) + 2)^2 + 4(Ha_c^2 - 1)}] \tag{2-66}$$

Where H is a variable defined for the simplification purpose[57].

$$H = \frac{4F \sin^2 \varphi}{\sigma C_n} \tag{2-67}$$

The value of the critical axial induction factor used by Wilson and Walker as well as Spera is 0.2. However, as stated previously, this value may change depending on the empirical correction model or the selection of a_c. Table 2-1 shows the maximum thrust coefficient and the critical axial induction factor in the context of Spera's correction. Different critical axial induction factor corresponds to a different linear line in the turbulent wake state. For instance, selecting $a_c = 0.37$ corresponds to the empirical model of Wilson and Lissaman which gives similar performance predictions of PROPID program.

Table 2-1 Critical axial induction factor and maximum thrust coefficient in the context of Spera's correction[57]

a_c	C_{T_1}	Note/Reference
0.2	2.56	Wilson and Walker (1984) or Spera (1994)
0.29	2	Glauert's Corrections
0.33	1.186	Fit to Glauert's Experiment
0.37	1.6	Wilson and Lissaman (1974)
0.46	1.17	Flat Disc Hoerner (1965)

As you see in Table 2-1, the critical axial induction factor, a_c may also be chosen as different values. But, Spera's correction is different than that of Glauert and that of Buhl correction, which is a modified version of Glauert correction. Figure 2-7 shows the Glauert empirical correction, except the Buhl correction[60]. As seen from the Figure 2-7, different models give different results in the turbulent wake state. Therefore, they evidently estimate different power and thrust coefficients when the turbine operates in the wake state.

2.6 Aerodynamic Correction for the Skewed Wake Operation

BEM theory breaks down again when the turbine rotor disk operates with a yaw angle toward the freestream wind because the original BEM theory does consider that the wind blows perpendicular to the rotor disk. Operation of the turbine rotor disk with a yaw angle toward the wind causes the downstream wake of the rotor to be skewed with an angle, X. This aerodynamic skewed wake phenomenon is depicted in Figure 2-9, in which U, Λ and Ψ represent the freestream wind, blade azimuth angle and yaw angle of the wind turbine rotor disk plane, respectively. This phenomenon changes the axial induction factor distribution throughout rotor blades. Thus, the axial induction factors must be corrected whenever the turbine rotor disk has been yawed to the wind flow.

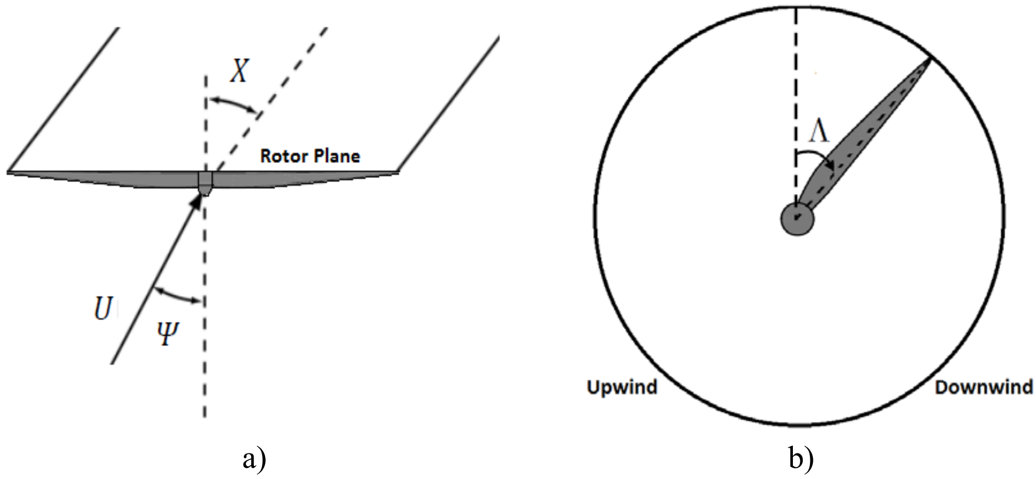

Figure 2-9 Coordinates in skewed wake correction, a) Top view, b) Front view

According to the Figure 2-9, when the azimuth angle, Λ of the turbine blade is 90 degree-angle, the greatest amount of induced velocity occurs on the rotor plane at the most downwind position, the least induced velocity at the most upwind position[55], [65].

In addition, the same aerodynamic phenomenon occurs on a wind turbine with a tilted nacelle or rotor. In one or both of these cases together, the axial induction factor, a, needs to be corrected. In order to add the skewed wake effect, equation (2-68), which is developed by Pitt and Peters (1981), is employed in the developed MS Bladed wind turbine simulation model along with the formulation (2-69) obtained by Burton, which predicts the skewed wake angle. Therefore, the skewed wake formula considering the steady inflow condition is given as[55],

$$a_{skew} = a(1 + \frac{15}{32})\frac{r}{R}\tan\frac{X}{2}\sin\Lambda \tag{2-68}$$

where X is the skewed wake angle, and is approximated by Burton formula as[55]

$$X = (0.6a + 1)\Psi \tag{2-69}$$

In equation (2-68), X stands for the skewed wake angle. It is the angle of actual flow leaving the turbine rotor and is larger than the turbine yaw angle, Ψ. Here, in the MS Bladed simulation model, the skewed wake effect is applied to the axial induction factor after the converge of the iteration process is successfully completed.

When the same equation is used only to deal with the skewed wake due to the nacelle tilt angle, θ. In that case, yaw angle, Ψ is replaced by the tilt angle, θ, in equation (2-69), and the term, $\sin\Lambda$ is replaced by the term, $\cos\Lambda$ in equation (2-68). In the developed simulation model, the selection of nacelle tilt or yaw angle is left optional to the user. Here, it is adjusted to include the skewed wake due to nacelle tilt angle, θ. This selection is made due to the fact the yaw control of wind turbine is not the one of the purposes of this thesis study. Thus, the turbine is always operated with zero yaw angle toward the freestream wind. The same equations (2-68) and (2-69) may also be used to cope with the skewed wake phenomenon accounting both for the tilt angle, θ and yaw angle, Ψ. However, this requires some extra modifications to both equations, (2-68) and (2-69), which is not applied in the developed MS Bladed turbine model.

CHAPTER 3

DYNAMIC MODELING OF WIND TURBINE

Until now, the focus has been on the derivation of BEM theory, aerodynamic corrections for the turbulent wake state and skewed wake operation for a HAWT type turbine. The BEM theory with aerodynamic correction of turbulent wake state, i.e windmill brake state correction, allows to model a HAWT only with a collective blade pitching capability. However, modern turbine blades may move around their own axes, not only as collectively, but also individually. The main reason for the above is that the attitudes of each turbine blade, i.e. precone and tilt angles etc., are not taken into account during the derivation of BEM theory. Instead, the determined total torque and thrust from one blade are simply multiplied by the blade number to obtain the total thrust, torque and lastly the power of the turbine rotor. This procedure may work for a basic turbine with no rotor precone and nacelle tilt angles as well as no yawed turbine operation toward the wind. However, most modern turbines include a precone angle to have a blade-tower clearance, or even variable precones (curved blades) throughout the blade span. Moreover, the blades are attached to the rotor hub with different angles. For instance, for a three-bladed turbine, the angle between the blades is 120 degrees, while, it is 180 degrees for the two-bladed rotor. Rotor blades have different azimuthal orientations and therefore each blade sweeps a different azimuthal angle (with respect to the z-axis of the hub-aligned coordinate system) during turbine operation. Every element of a straight blade sweeps the same azimuthal angle, while each blade element of a swept blade sweeps a different azimuthal angle. In addition, modern turbine nacelles are mostly tilted with a fixed angle in order to increase the blade-tower clearance more. They are also equipped with a yawing mechanism allowing the turbine nacelle or rotor to turn into the freestream wind. Therefore, developing a modern wind turbine simulation model with all of the above properties cannot be realized by just multiplying the one blade torque and thrust by the blade number. This is because of the fact each turbine blade produces a different amount of torque, thrust force, and power due to the above fixed and time-varying structural angles. Thus, in order to develop a simulation model for a highly modern HAWT, particular coordinate systems are required apart from the BEM theory and certain aerodynamic corrections. In the currently developed MS Bladed simulation model, some of the coordinate systems are locally defined to simulate the turbines even with swept/curved blades. However, it requires some more modifications to the model if it is going to be used particularly for swept/curved-bladed turbines. Here, the main focus is on the turbines with straight blades, which are structurally less complex than those with the swept/curved blades.

In addition, the developed MS Bladed simulation model does consider all the turbine components such as a tower, blades, shaft(s) etc. as rigid structures. The model includes the properties of rotor precone and nacelle tilt angles. For the modeling, BEM theory, particular coordinate systems, aerodynamic corrections, Newton second law of motion, a simple generator model, turbine rotor and generator inertias etc. have been employed in order to get a more realistic turbine behavior under various wind speeds.

As mentioned before, for the turbine modeling purpose, BEM theory is largely utilized for turbine aerodynamics due to ease of implementation and computational effectiveness. Wind properties, turbine and rotor geometric features and blade airfoil data are introduced to the developed MS Bladed model as inputs. As outputs, turbine rotor torque, thrust, power, and their coefficients as well as many others are taken from the model depending on the desire. In the developed MS Bladed model, all the aerodynamics and corrections in Chapter 2 as well as the particular coordinate systems and transformation matrices in the subsequent subchapter are used to represent the actual turbine. The coordinate systems are defined using a HAWT drawing and they comply with the right-hand rule. The wind turbine rotor is assumed to be rotating in the clockwise direction when being looked from the front, i.e. looking downwind. Eventually, all the implementations are carried out by Matlab and Simulink software.

3.1 Wind Turbine Coordinate Systems and Transformation Matrices

Transforming a vector quantity such as force, moment etc., from one coordinate system to another coordinate system requires a transformation matrix or multiplication of several matrices. Therefore, the following coordinate systems and transformation matrices are used to model a modern HAWT system.

3.1.1 Inertial and Wing-aligned Coordinate Systems

Figure 3-1 shows the transformation between the inertial coordinate system and wind-aligned coordinate system. The wind angle, β_{wind}, is positive when there is a rotation around +z axis. Both coordinate systems have the same origin and the common z-direction at the center of the tower base. The tower base may be the ground level or the sea-bed level[66].

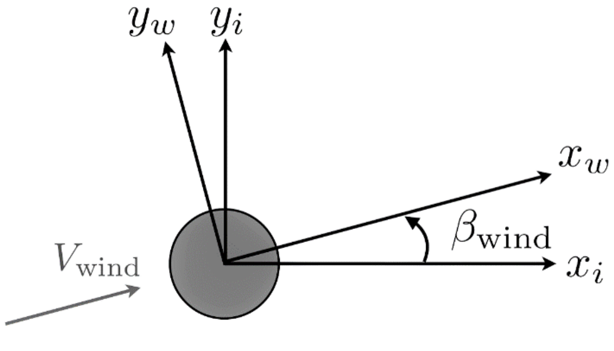

Figure 3-1 Inertial and wind-aligned coordinate systems[66]

In the inertial coordinate system, the x_i-axis may point to any direction when used consistently, but the suitable direction should be the main wind direction. The y_i-axis follows from the right-hand rule, whereas the z_i-axis points up to the tower in the opposite direction of the gravity vector. Similarly, in the wind-aligned coordinate systems, the x_w-axis shows the main wind direction. The y_w-axis follows from the right-hand rule. The z_w-axis, on the other hand, points up to the tower and coincidences with the z_i-axis of the inertial coordinate system[66].

The mathematical relationship between these two coordinate systems is given as follows.

$$O_w x_w y_w z_w = T(\beta_{wind}) O_i x_i y_i z_i \tag{3-1}$$

or

$$O_i x_i y_i z_i = T(\beta_{wind})^T O_w x_w y_w z_w \tag{3-2}$$

Where the $T(\beta)$ is defined as,

$$T(\beta) = \begin{bmatrix} cos(\beta_{wind}) & sin(\beta_{wind}) & 0 \\ -sin(\beta_{wind}) & cos(\beta_{wind}) & 0 \\ 0 & 0 & 1 \end{bmatrix} \tag{3-3}$$

3.1.2 Wind-aligned and Yaw-aligned Coordinate Systems

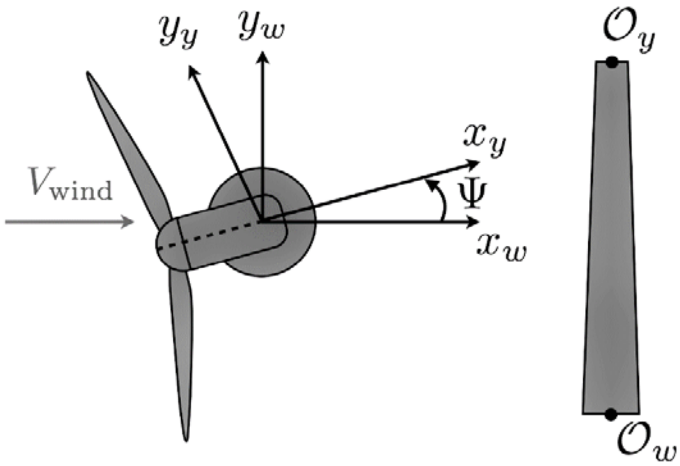

Figure 3-2 Wind-aligned and yaw-aligned coordinate systems[66]

Figure 3-2 depicts the wind-aligned and yaw-aligned coordinates systems. Both of their z-axes are common and opposite to the direction of the gravity vector. However, the wind-aligned coordinate system has the origin, O_w at the tower base, but the yaw-aligned coordinate system has its origin, O_y at the tower top. Therefore, there is a certain height, tower length, between their origins. A rotation around the +z-axis results in a positive yaw angle, Ψ which stays in between -180 and 180 degrees. The relationship between these two coordinate systems is as follows[66].

$$O_y x_y y_y z_y = T(\Psi) O_w x_w y_w z_w \tag{3-4}$$

or

$$O_w x_w y_w z_w = T(\Psi)^T O_y x_y y_y z_y \tag{3-5}$$

where Ψ is given as

$$T(\Psi) = \begin{bmatrix} cos(\Psi) & sin(\Psi) & 0 \\ -sin(\Psi) & cos(\Psi) & 0 \\ 0 & 0 & 1 \end{bmatrix} \tag{3-6}$$

In the yaw-aligned coordinate system, the origin, O_y is the center of the yaw bearing system or the tower top. The x_y-axis lies along the projection of the rotor shaft in the horizontal plane, or is aligned with the rotor shaft when there is no nacelle tilt angle, θ. At a yaw angle of zero, the x_y and x_w axes show the same direction. The y_y-axis follows from the right-hand rule, whereas the z_y-axis points up to the tower and coincidences with the z_w-axis of the wind-aligned coordinate system[66].

3.1.3 Yaw-aligned and Hub-aligned Coordinate Systems

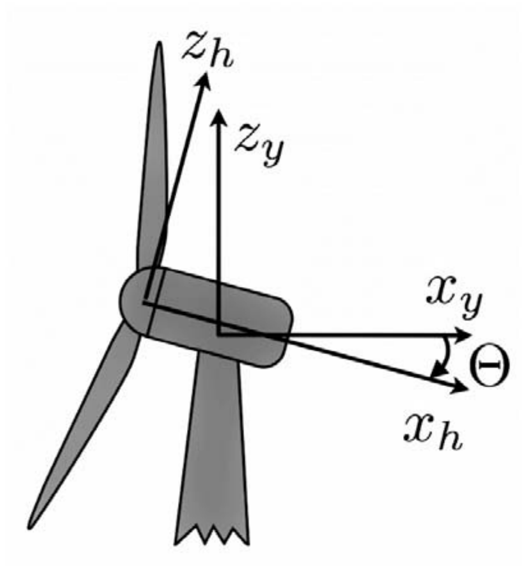

Figure 3-3 Yaw-aligned and hub-aligned coordinate systems[66]

The transformation between the yaw-aligned and the hub-aligned coordinate systems is illustrated in Figure 3-3. Both coordinate systems share a common y-axis. To tilt the rotor up for an upwind wind turbine corresponds to a positive tilt angle, θ around +y axis. The origin of the hub-aligned coordinate system is the center of the rotor hub, O_h. In the hub-aligned coordinate system, the x_h-axis lies along the rotor shaft toward the nominal downwind direction, or it is aligned with x_y when there is no nacelle tilt angle, θ. The y_h-axis coincidences with the yaw-aligned y_y-axis. Finally, the z_h-axis follows from the right hand rule[66].

$$O_h x_h y_h z_h = T(\theta) O_y x_y y_y z_y \tag{3-7}$$

or

$$O_y x_y y_y z_y = T(\theta)^T O_h x_h y_h z_h \tag{3-8}$$

where the $T(\theta)$ is calculated as

$$T(\theta) = \begin{bmatrix} cos(\theta) & 0 & -sin(\theta) \\ 0 & 1 & 0 \\ sin(\theta) & 0 & cos(\theta) \end{bmatrix} \tag{3-9}$$

3.1.4 Hub-aligned and Azimuth-aligned Coordinate Systems

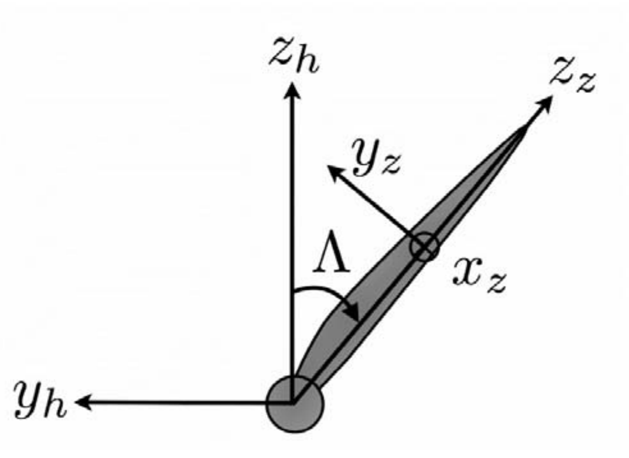

Figure 3-4 Hub-aligned and azimuth-aligned coordinate systems[66]

Figure 3-4 defines the transformation between the hub-aligned and azimuth-aligned coordinate systems. Both coordinate systems use a common x-axis. The azimuth angle, Λ, is positive when there is a rotation around +x-axis. The azimuth angle for every blade element is the same for the straight blades. However, the turbine blades may be designed with variable azimuthal angle throughout blade axis. These blades are referred to as swept blades. Therefore, the azimuth-aligned coordinate system is a rotating coordinate system about x_h and is defined locally in order to deal with the variable-swept blades[66].

$$.O_z x_z y_z z_z = T(\Lambda) O_h x_h y_h z_h \tag{3-10}$$

or

$$O_h x_h y_h z_h = T(\Lambda)^T O_z x_z y_z z_z \tag{3-11}$$

where the $T(\Lambda)$ is given as

$$T(\Lambda) = \begin{bmatrix} 1 & 0 & 0 \\ 0 & cos(\Lambda) & sin(\Lambda) \\ 0 & -sin(\Lambda) & cos(\Lambda) \end{bmatrix} \tag{3-12}$$

Therefore, its origin, O_z is located at the blade pitch axis, local to each blade element. The x_z-axis is aligned with the x_h-axis of the hub-aligned coordinate system. The y_z-axis follows from the right-hand rule. The z_z-axis lies along the projection of the blade from the root to tip in the $y_h - z_h$ plane. It is aligned with the blade only with a precone angle of zero. In any case, straight or swept blades, the azimuth-aligned coordinate system rotates about the x_h axis with the angular speed of the turbine rotor, Ω[66].

3.1.5 Azimuth-aligned and Blade-aligned Coordinate Systems

The transformation defined between the azimuth-aligned and the blade-aligned coordinate systems is seen in Figure 3-5. The y_b and y_z axes show the same direction. The two coordinate systems share the same origin and rotate together. During the rotation, the $x_b - z_b$ and $x_z - z_z$ planes lie in the same plane. The precone angle, Φ is negative when there is a counterclockwise rotation about the +y direction pointing into the page. This negative precone angle keeps the blades away from the tower for an upwind oriented HAWT. In addition, the rotor blades may have variable precone angles along the blade axis, which are referred to as pre-curved blades. The blade-aligned coordinate system is defined locally to each blade element section as the azimuth-aligned coordinate system. The blade rotation is in the negative y-axis[66].

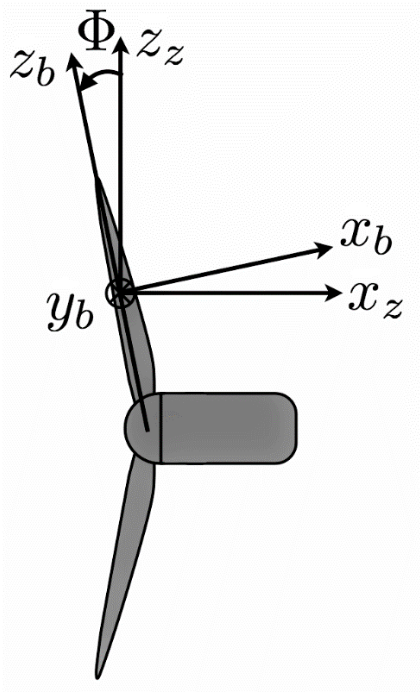

Figure 3-5 Azimuth-aligned and blade-aligned coordinate systems[66]

$$O_b x_b y_b z_b = T(\Phi) O_z x_z y_z z_z \tag{3-13}$$

or

$$O_z x_z y_z z_z = T(\Phi)^T O_b x_b y_b z_b \tag{3-14}$$

Where $T(\Phi)$ is

$$T(\Phi) = \begin{bmatrix} cos(\Phi) & 0 & -sin(\Phi) \\ 0 & 1 & 0 \\ sin(\Phi) & 0 & cos(\Phi) \end{bmatrix} \tag{3-15}$$

The origin, O_b of the blade-aligned coordinate system is at the blade pitch axis and local to the blade section. The x_b-axis follows from the right-hand rule. The y_b-axis points into the page in a direction opposite to the blade rotation. In other words, it lies from the leading edge to the trailing edge of a blade section with no twist angle. The z_b-axis, on the other hand, lies along the blade pitch axis[66].

3.1.6 Blade-aligned and Aerodynamic-aligned Coordinate Systems

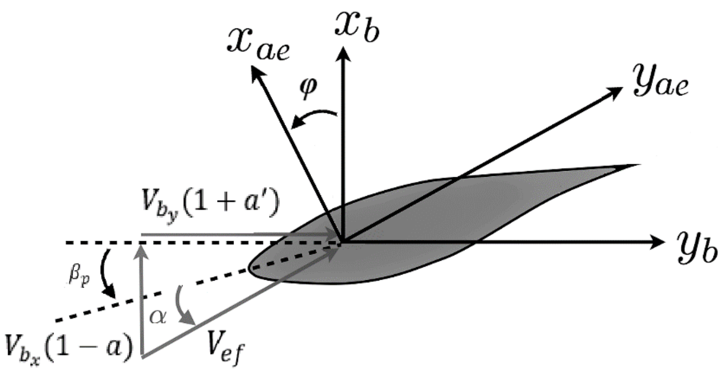

Figure 3-6 Blade-aligned and aerodynamic coordinate systems

Figure 3-6 gives the transformation between the blade-aligned and the aerodynamic-aligned coordinate systems. The z-axes of both coordinate systems point to the same direction. The origin, O_{ae} of the aerodynamic-aligned coordinate system is the blade pitch axis which is the quarter chord location of each airfoil and local to the blade section. The x_{ae}-axis follows from the right-hand-rule. The y_{ae}-axis lies along the effective wind speed. Finally, the z_{ae}-axis points into the page in increasing radius and lies along the blade pitch axis, the same as the z_b-axis. The angle, β_p is the sum of local twist, β_T and blade pitch angle, β, while φ is the inflow angle. Aerodynamic lift and drag forces, dF_L and dF_D are located on the x_{ae} and y_{ae} axes, respectively. On the other hand, no force is considered on z_{ae} axis and the pitching moment of the each blade element acts around the z_{ae} axis.

3.2 Aerodynamic Modeling of a HAWT System

The main purpose in the aerodynamic modeling of a wind turbine is to determine the total thrust, torque and eventually the power of the turbine rotor. As stated before, the standard BEM theory is not capable of predicting the performance of a very basic turbine rotor in all its operation range. Furthermore, modern wind turbines are more complex, with preconed blades, tilted nacelle, or even precurved or swept blades. They have both blade pitching and nacelle yawing capabilities etc. Besides, rotor blades have different azimuthal orientations, i.e. the azimuthal location with respect to x_h-

axis of the hub-aligned coordinate system. Therefore, the aerodynamic model for a modern HAWT must include the previously-mentioned aerodynamic theories, corrections, and particular coordinate systems. However, whatever the properties of the turbine are, the main idea in aerodynamic turbine modeling is to calculate the elemental lift and drag forces first and then the elemental axial and tangential forces at every blade element sections in order to determine the total thrust, torque and lastly the turbine power. Determining these important parameters permit obtaining other turbine parameters easily such as power and thrust coefficients, and their respective curves with respect to TSR and so on. Further, the other forces or moments at any turbine location such as at rotor hub, nacelle, top or bottom of the turbine tower are easily obtained. These processes require rotating and/or non-rotating coordinate systems, aerodynamic equations, dynamic relations, certain lengths etc. Here, the aerodynamic model is developed mainly considering the straight-bladed turbines with precone, tilt angles, blade pitching and nacelle yawing capabilities. Some of the coordinate systems are locally defined for curved/swept bladed turbines such as blade-aligned coordinate system, azimuth aligned coordinate system. Therefore, the following model may be considered as a first step to the modeling of swept/curved bladed turbines. In the following model derivation, the effect of some geometric length and angles etc. particularly belong to the curved/swept bladed turbines may be ignored. This is because of the fact that the main focus is the straight bladed turbines, which has the same precone angle at every blade element section and the same azimuthal angle throughout the same blade, but has a different azimuthal angle for every blade. Therefore, the derived model may require extra more modifications if it is particularly utilized for swept or curved-bladed turbines.

Different from the previous chapters, indicial form or subscripts are used in the turbine modeling since curved/swept blades have a different azimuthal angle and a precone angle at every blade element section. Therefore, the indicial form provides a more compact form and permits not writing the same transformation matrices, force or moment equations as multiple times for each elemental section of every blade.

Therefore, in the modeling, the subscript, i, is used to represent the corresponding blade, such as 1^{th} blade, 2^{nd} blade, and 3^{th} blade etc. The subscript, j, on the other hand, represents the blade element section. For instance, $V_{b_{x_{2,6}}}$ stands for a freestream wind velocity component in the x_b-axis of the blade-aligned coordinate system whose origin is attached to the sixth blade element section of the second blade. Here, the numbering of each blade element section increases from the blade root to tip. Lastly, B_n represents the number of blades in the developed MS Bladed simulation model.

With the above-mentioned statements, the turbine modeling starts firstly with the transformation of freestream wind velocity, V_{wind} at the wind-aligned coordinate system to the blade-aligned coordinate system. This is carried out to calculate the elemental aerodynamic forces, $dF_{L_{i,j}}$ and $dF_{D_{i,j}}$ at the aerodynamic-aligned coordinate system defined at each blade element. As learned from aerodynamic courses, these forces are respectively perpendicular and parallel to the freestream velocity or the relative wind vector. Here, the relative wind, U_{rel} in Figure 2-6 turns out to be the effective wind vector, V_{ef} in Figure 3-6 due to the fixed and time-varying structural angles of modern turbines such as yaw angle, Ψ, nacelle tilt angle, θ, azimuth angle for each blade (or blade element), $\Lambda_{i,j}$ and rotor precone angle (or pre-curve), $\Phi_{i,j}$ etc. Therefore, all these angles must be considered to calculate the effective wind speed, V_{ef} and the induced velocities at the blade-aligned coordinate system. Considering every blade, i and each elemental section, j, the transformation matrix transforming the freestream velocity components from the wind-aligned coordinate system to the blade-aligned coordinate system may be obtained as,

$$T_{bw_{i,j}} = T\big(\Phi_{i,j}\big)^T T\big(\Lambda_{i,j}\big) T(\theta) T(\Psi) \tag{3-16}$$

The explicit form of the matrix, $T_{bw_{i,j}}$ is obtained as follows.

$$T_{bw_{i,j}} = \begin{bmatrix} c\Phi_{i,j}c\theta c\Psi + s\Phi_{i,j}(c\Lambda_{i,j}s\theta c\Psi + s\Lambda_{i,j}s\Psi) & c\Phi_{i,j}c\theta s\Psi + s\Phi_{i,j}(c\Lambda_{i,j}s\theta s\Psi - s\Lambda_{i,j}c\Psi) & s\Phi_{i,j}c\Lambda_{i,j}c\theta - c\Phi_{i,j}s\theta \\ s\Lambda_{i,j}s\theta c\Psi - c\Lambda_{i,j}s\Psi & c\Lambda_{i,j}c\Psi + s\Lambda_{i,j}s\theta s\Psi & s\Lambda_{i,j}c\theta \\ c\Phi_{i,j}(s\Lambda_{i,j}s\Psi + c\Lambda_{i,j}s\theta c\Psi) - s\Phi_{i,j}c\theta c\Psi & c\Phi_{i,j}(c\Lambda_{i,j}s\theta s\Psi - s\Lambda_{i,j}c\Psi) - s\Phi_{i,j}c\theta s\Psi & s\Phi_{i,j}s\theta + c\Phi_{i,j}c\Lambda_{i,j}c\theta \end{bmatrix} \tag{3-17}$$

In the derivation of the above matrix, the x_i-axis of the inertial coordinate system is considered to be pointing into the main wind direction, which is the suitable direction, as stated before. Thus, the wind angle, β_{wind} is not taken into account in the derivation of above matrix, i.e being thought as zero. However, that effect may easily be introduced to the matrix if required.

When the above transformation matrix, $T_{bw_{i,j}}$ is used to transform the freestream velocity, V_{wind} to the blade-aligned coordinate system, the following wind speed components are obtained.

$$\begin{bmatrix} V_{b_{x_{i,j}}} \\ V_{b_{y_{i,j}}} \\ V_{b_{z_{i,j}}} \end{bmatrix} = T_{bw_{i,j}} \begin{bmatrix} V_{w_x} \\ V_{w_y} \\ V_{w_z} \end{bmatrix} \tag{3-18}$$

where V_{w_x}, V_{w_y} and V_{w_z} are the velocity components of the freestream wind speed, V_{wind} at the wind-aligned coordinate system. Therefore, the wind velocity components at the blade-aligned coordinate system are found as,

$$\begin{aligned} V_{b_{x_{i,j}}} = {} & V_{w_x}\big(c\Phi_{i,j}c\theta c\Psi + s\Phi_{i,j}(c\Lambda_{i,j}s\theta c\Psi + s\Lambda_{i,j}s\Psi)\big) \\ & + V_{w_y}\big(c\Phi_{i,j}c\theta s\Psi + s\Phi_{i,j}(c\Lambda_{i,j}s\theta s\Psi \\ & - s\Lambda_{i,j}c\Psi)\big) + V_{w_z}\big(s\Phi_{i,j}c\Lambda_{i,j}c\theta - c\Phi_{i,j}s\theta\big) \end{aligned} \tag{3-19}$$

$$\begin{aligned} V_{b_{y_{i,j}}} = {} & V_{w_x}\big(s\Lambda_{i,j}s\theta c\Psi - c\Lambda_{i,j}s\Psi\big) + V_{w_y}\big(c\Lambda_{i,j}c\Psi + s\Lambda_{i,j}s\theta s\Psi\big) \\ & + V_{w_z}\big(s\Lambda_{i,j}c\theta\big) + \Omega r_{i,j}\, c\,\Phi_{i,j} \end{aligned} \tag{3-20}$$

$$\begin{aligned} V_{b_{z_{i,j}}} = {} & V_{w_x}\big(c\Phi_{i,j}(s\Lambda_{i,j}s\Psi + c\Lambda_{i,j}s\theta c\Psi) - s\Phi_{i,j}c\theta c\Psi\big) \\ & + V_{w_y}\big(c\Phi_{i,j}(c\Lambda_{i,j}s\theta s\Psi - s\Lambda_{i,j}c\Psi) \\ & - s\Phi_{i,j}c\theta s\Psi\big) + V_{w_z}\big(s\Phi_{i,j}s\theta + c\Phi_{i,j}c\Lambda_{i,j}c\theta\big) \end{aligned} \tag{3-21}$$

Note that after the transforming of freestream wind components in the wind-aligned coordinate system to the blade-aligned coordinate system, the effect of blade rotation, $\Omega r_{i,j}\, c\,\Phi_{i,j}$ is also introduced here to be the $V_{b_{y_{i,j}}}$ velocity component. Therefore, the elemental aerodynamic forces, $dF_{L_{i,j}}$ and $dF_{D_{i,j}}$, which are respectively on the x_{ae} and y_{ae} axes of the aerodynamic-aligned coordinate system are obtained using these velocity components, $V_{b_{x_{i,j}}}$ and $V_{b_{y_{i,j}}}$ as well as the axial, $aV_{b_{x_{i,j}}}$ and tangential, $a'V_{b_{y_{i,j}}}$ induced velocities. Eventually, the velocity components at the blade-aligned coordinate systems turns out to be $V_{bx_{i,j}}(1 - a_{i,j})$ and $V_{by_{i,j}}(1 + a'_{i,j})$. These velocity components are used to find the local angle of attack, α by the equation (2-34). This helps to select the corresponding aerodynamic data, C_l, C_d etc. for a particular blade element section. These velocity components are also used to calculate the effective wind speed, V_{ef}. Here, the $V_{b_{z_{i,j}}}$ component is neglected since it is not utilized in the calculation of the above elemental aerodynamic forces, $dF_{L_{i,j}}$ and $dF_{D_{i,j}}$. The calculated elemental aerodynamic forces at the aerodynamic-aligned coordinate system are later transformed to obtain the elemental tangential, $dF_{T_{i,j}}$ and normal, $dF_{N_{i,j}}$ forces to the $y_b - z_b$ plane at the blade-aligned coordinate system using the elemental inflow angle, $\varphi_{i,j}$. These elemental forces may be also referred to as respectively as elemental lead-lag shear and flap shear forces[67]. At the same time, these tangential, $dF_{T_{i,j}}$ and normal, $dF_{N_{i,j}}$ forces are also utilized to calculate the elemental torques, $dM_{T_{i,j}}$ and $dM_{N_{i,j}}$, respectively acting around $x_{b_{i,j}}$ and $y_{b_{i,j}}$-axes considering the local blade length to the hub center. Here, this length is the local radius, $r_{i,j}$ due to the straight blades. These elemental moments, $dM_{T_{i,j}}$ and $dM_{N_{i,j}}$ may be called as elemental lead-lag moments and flap moments, respectively[67]. Therefore, the forces at a blade-aligned coordinate system are defined as follows.

$$F_{bx_{i,j}} = dF_{N_{i,j}} \tag{3-22}$$

$$F_{by_{i,j}} = -dF_{T_{i,j}} \tag{3-23}$$

$$F_{bz_{i,j}} = 0 \tag{3-24}$$

Note that these elemental forces at the blade-aligned coordinate system are obtained by transforming the elemental lift, $dF_{L_{i,j}}$ and drag, $dF_{D_{i,j}}$ forces from the aerodynamic-aligned coordinate system by the inflow angle, φ. However, dF_N equation in (2-39) is kept here to calculate the $F_{bx_{i,j}}$, while the $F_{by_{i,j}}$ is obtained by multiplying dF_T in equation (2-40) by a minus sign. This is due to the fact that the y_b-axis of the newly adopted blade-aligned coordinate system (Figure 3-6) is in the opposite direction to the previously obtained elemental tangential force, dF_T in Figure 2-6. The radial force in the direction of z_b-axis is considered negligible and therefore taken as zero. In addition, the elemental pitch moment or torsion of each blade section is ignored. The elemental lead-lag and flap moments are obtained by the cross product of elemental forces at the blade-aligned coordinate system and their respective local lengths to the rotor hub center as follows.

$$\begin{bmatrix} M'_{bx_{i,j}} \\ M'_{by_{i,j}} \\ M'_{bz_{i,j}} \end{bmatrix} = \begin{bmatrix} 0 \\ 0 \\ r_{i,j} \end{bmatrix} x \begin{bmatrix} F_{bx_{i,j}} \\ F_{by_{i,j}} \\ F_{bz_{i,j}} \end{bmatrix} \tag{3-25}$$

Note that in (3-25), the local length from a blade section to the rotor hub center is taken into consideration for the straight-bladed turbine, i.e. only the local blade radius. Therefore, x and y components are zero. For the curved/swept blades, this length/distance vector should include the x/y components as well. Here, these calculated moments are obtained at the intermediate coordinate systems located at the hub center which are parallel to each blade-aligned coordinate system. Therefore, the elemental moments at these coordinate systems are found as,

$$M'_{b_{i,j}} = -F_{by_{i,j}} r_{i,j}\boldsymbol{i} + F_{bx_{i,j}} r_{i,j}\boldsymbol{j} + 0\boldsymbol{k} \tag{3-26}$$

or

$$M'_{b_{i,j}} = dF_{T_{i,j}} r_{i,j}\boldsymbol{i} + dF_{N_{i,j}} r_{i,j}\boldsymbol{j} + 0\boldsymbol{k} \tag{3-27}$$

Hence,

$$M'_{bx_{i,j}} = dF_{T_{i,j}} r_{i,j} = dM_{T_{i,j}} \tag{3-28}$$

$$M'_{by_{i,j}} = dF_{N_{i,j}} r_{i,j} = dM_{N_{i,j}} \tag{3-29}$$

$$M'_{bz_{i,j}} = 0 \tag{3-30}$$

Now, the elemental forces in equations, (3-22), (3-23), and (3-24) and moments (3-28), (3-29) and (3-30) are to be transformed to the hub-aligned coordinate system to find the total turbine thrust, torque and lastly the power. The transformation matrix between the blade-aligned and hub-aligned coordinate systems are obtained as (3-31).

$$T_{hb_{i,j}} = T(\Lambda_{i,j})^T \, T(\Phi_{i,j}) \tag{3-31}$$

The explicit form in (3-32) shows the effect of each blade element azimuth angle, $\Lambda_{i,j}$ and the rotor precone (or pre-curve) angle, $\Phi_{i,j}$.

$$T_{hb_{i,j}} = \begin{bmatrix} c\Phi_{i,j} & 0 & -s\Phi_{i,j} \\ -s\Lambda_{i,j}s\Phi_{i,j} & c\Lambda_{i,j} & -s\Lambda_{i,j}c\Phi_{i,j} \\ c\Lambda_{i,j}s\Phi_{i,j} & s\Lambda_{i,j} & c\Lambda_{i,j}c\Phi_{i,j} \end{bmatrix} \tag{3-32}$$

Using the transformation matrix in (3-32), the axial force, $F_{h_{x_{i,j}}}$, lateral force, $F_{h_{y_{i,j}}}$ and vertical force, $F_{h_{z_{i,j}}}$ at the hub-aligned coordinate system are obtained as,

$$F_{hb_{i,j}} = T_{hb_j} F_{b_{i,j}} \tag{3-33}$$

More explicitly,

$$\begin{bmatrix} F_{hx_{i,j}} \\ F_{hy_{i,j}} \\ F_{hz_{i,j}} \end{bmatrix} = \begin{bmatrix} c\Phi_{i,j} & 0 & -s\Phi_{i,j} \\ -s\Lambda_{i,j}s\Phi_{i,j} & c\Lambda_{i,j} & -s\Lambda_{i,j}c\Phi_{i,j} \\ c\Lambda_{i,j}s\Phi_{i,j} & s\Lambda_{i,j} & c\Lambda_{i,j}c\Phi_{i,j} \end{bmatrix} \begin{bmatrix} F_{bx_{i,j}} \\ F_{by_{i,j}} \\ F_{bz_{i,j}} \end{bmatrix} \tag{3-34}$$

Thus, the axial, lateral and vertical forces at the hub aligned-coordinate system are then found respectively as,

$$F_{hx_{i,j}} = \, dF_{N_{i,j}} \, c\Phi_{i,j} \tag{3-35}$$

$$F_{hy_{i,j}} = -dF_N s\Lambda_{i,j} s\Phi_{i,j} - dF_{T_{i,j}} c\Lambda_{i,j} \tag{3-36}$$

$$F_{hz_{i,j}} = \, dF_{N_{i,j}} c\Lambda_{i,j} s\Phi_{i,j} - dF_{T_{i,j}} \, s\Lambda_{i,j} \tag{3-37}$$

When these elemental force components of every blade are summed through their blade span, i.e considering the blade number, B_n the following total axial, lateral and vertical forces are obtained at the axes of the hub-aligned coordinate system as below.

$$F_{hx} = \sum_{i}^{B_n} \sum_{j}^{S} F_{hx_{i,j}} \tag{3-38}$$

$$F_{hy} = \sum_{i}^{B_n} \sum_{j}^{S} F_{hy_{i,j}} \tag{3-39}$$

$$F_{hz} = \sum_{i}^{B_n} \sum_{j}^{S} F_{hz_{i,j}} \tag{3-40}$$

Here, F_{hx} corresponds to the total axial force on the rotor hub center, which corresponds to the turbine thrust force. F_{hy} and F_{hz} are total lateral and vertical in-plane forces at the rotor hub[67]. Similarly, the torques at the hub-aligned coordinate system are obtained using the same transformation matrix in (3-32) as follows.

$$M_{h_{i,j}} = T_{hb_{i,j}} M'_{b_{i,j}} \tag{3-41}$$

$$\begin{bmatrix} M_{hx_{i,j}} \\ M_{hy_{i,j}} \\ M_{hz_{i,j}} \end{bmatrix} = \begin{bmatrix} c\Phi_{i,j} & 0 & -s\Phi_{i,j} \\ -s\Lambda_{i,j} s\Phi_{i,j} & c\Lambda_{i,j} & -s\Lambda_{i,j} c\Phi_{i,j} \\ c\Lambda_{i,j} s\Phi_{i,j} & s\Lambda_{i,j} & c\Lambda_{i,j} c\Phi_{i,j} \end{bmatrix} \begin{bmatrix} M'_{bx_{i,j}} \\ M'_{by_{i,j}} \\ M'_{bz_{i,j}} \end{bmatrix} \tag{3-42}$$

Where $M_{hx_{i,j}}$, $M_{hy_{i,j}}$ and $M_{hz_{i,j}}$ are the elemental rotor shaft torque, tilt moment and yaw moment (assuming zero tilt angle)[67] are obtained as,

$$M_{hx_{i,j}} = dM_{T_{i,j}} c\Phi_{i,j} \tag{3-43}$$

$$M_{hy_{i,j}} = -dM_{T_{i,j}} s\Lambda_{i,j} s\Phi_{i,j} + dM_{N_{i,j}} c\Lambda_{i,j} \tag{3-44}$$

$$M_{hz_{i,j}} = dM_{T_{i,j}} c\Lambda_{i,j} s\Phi_{i,j} + dM_{N_{i,j}} s\Lambda_{i,j} \tag{3-45}$$

When these elemental moments are summed through the blade span including the effect of blade number,B_n, the total moments at the hub-aligned coordinate system are

$$M_{hx} = \sum_{i}^{B_n} \sum_{j}^{S} M_{hx_{i,j}} \tag{3-46}$$

$$M_{hy} = \sum_{i}^{B_n} \sum_{j}^{S} M_{hy_{i,j}} \tag{3-47}$$

$$M_{hz} = \sum_{i}^{B_n} \sum_{j}^{S} M_{hz_{i,j}} \tag{3-48}$$

Here, M_{hx} corresponds to the total aerodynamic rotor torque, which drives the electrical generator via the gearbox. The M_{hy} and M_{hz} are respectively the total tilt and yaw moments (assuming zero tilt angle) at the rotor hub, respectively[67]. The aerodynamic torque quantity, M_{hx}, which is used for the dynamic modeling of the turbine in subchapter 3.4, is represented by τ_{aero}. Lastly, turbine power is obtained by the product of this aerodynamic torque, τ_{aero} and the rotor speed, Ω.

Until now, the total forces and torques, which are arisen because of all the blades attached to the rotor hub, are obtained at the hub-aligned coordinate system. During the turbine modeling, the obtained forces and moments at the hub-aligned coordinate system are calculated considering the effects of certain angles such as precone, tilt, yaw etc. In addition, the wind velocity has been considered having three components, V_{w_x}, V_{w_y} and V_{w_z}. However, in nature, wind blows mostly in one direction, which is the x_w-axis of the wind-aligned coordinate system, and other wind components V_{wy} and V_{wz} are quite low. Therefore, these components may be ignored and are taken as zero. Namely, considering the conventional static rotor geometry with the precone and tilt angles exposed to a uniform freestream velocity, V_{wx}, which points in the x_i-axis of the inertial coordinate system[65], the velocity components, $V_{bx_{i,j}}$ and $V_{by_{i,j}}$ at the blade-aligned coordinate systems turn out to be as following. These velocity components are obtained by considering V_{wy} and V_{wz} velocities as zero. Here, uniform freestream velocity, V_{wx} may be represented by U, as previously in Chapter 2. Thus, the following are obtained,

$$V_{bx_{i,j}} = U(\mathrm{c}\,\Phi_{i,j}\,\mathrm{c}\,\theta\,\mathrm{c}\,\Psi + \mathrm{s}\,\Phi_{i,j}(\,\mathrm{c}\,\Lambda_{i,j}\,\mathrm{s}\,\theta\,\mathrm{c}\,\Psi + \mathrm{s}\,\Lambda_{i,j}\,\mathrm{s}\,\Psi)) \tag{3-49}$$

$$V_{by_{i,j}} = U(\mathrm{s}\,\Lambda_{i,j}\,\mathrm{s}\,\theta\,\mathrm{c}\,\Psi - \mathrm{c}\,\Lambda_{i,j}\,\mathrm{s}\,\Psi) + \Omega r_{i,j}\,\mathrm{c}\,\Phi_{i,j} \tag{3-50}$$

Further, the normal and tangential force coefficients for every blade element (equations (2-43) and (2-44)), are calculated inside the iteration process. The relative wind speed, U_{rel} in equation (2-36) turns out to be equation (3-51), which is the effective wind speed, V_{ef} seen by a blade element.

$$V_{ef_{i,j}} = \sqrt{(V_{bx_{i,j}}(1 - a_{i,j}))^2 + (V_{by_{i,j}}(1 + a'_{i,j}))^2} \tag{3-51}$$

Here, due to the straight bladed turbines, $\Phi_{i,j}$ is a scalar quantity, fixed for every blade element section, i.e. $\Phi_{i,j}$= Φ. However, for curved blades, $\Phi_{i,j}$ is different for every blade section and is introduced to the model as an array[66]. Similarly, the azimuthal angle, $\Lambda_{i,j}(\Omega, t)$ swept by a straight blade is same throughout the same blades with respect to the x_h-axis of the hub-aligned coordinate system, but different for every blade due to the certain fixed geometric angle, b between the blades at the roots. Therefore, $\Lambda_{i,j}(\Omega, t)$ may be defined to be equal to $\Lambda^*_{i,j} + \Lambda(\Omega, t) + b_i$ in the turbine model. Here, $\Lambda^*_{i,j}$ may represent the variable azimuthal angles as an array, while $\Lambda(\Omega, t)$ represents the change of blade azimuth angle in time. Therefore, for a straight blade, $\Lambda^*_{i,j}$ may be taken as an array that includes only zeros. Then, $\Lambda_{i,j}(\Omega, t)$ turns out to be equal to $\Lambda(\Omega, t) + b_i$ for straight bladed turbines.

As seen in equation (3.51), the effective wind speed, V_{ef} is a function of rotor precone angle, Φ, nacelle tilt angle, θ, turbine yaw angle, Ψ along with the blade azimuthal location, Λ as well as the induction factors. Similarly, the equation (2-35) for the calculation of inflow angle, φ turns out to be as,

$$\varphi_{i,j} = \tan^{-1} \frac{V_{bx_{i,j}}(1 - a_{i,j})}{V_{by_{i,j}}(1 + a'_{i,j})} \tag{3-52}$$

Therefore, the previou equations, (2-14) and (2-19) for the power coefficient, C_p, and the thrust coefficient, C_T turn out to be the equations (3-56) and (3-57) considering the precone angle, tilt angle as well as the yaw angle.

The rotor precone angle reduces the turbine rotor disk area, whereas the tilt angle and yaw angle of the wind turbine affect the amount of wind passing through the turbine rotor disk area. Therefore, a wind turbine with a tilt angle and a yaw angle to a freestream wind is subjected to a freestream wind speed component normal to the rotor disk rather than the actual freestream wind speed. This situation affects the power of wind passing through the rotor and the dynamic pressure force applied to the turbine rotor. Therefore, these angles must be included to calculate the tip speed ratio, TSR, power coefficient, C_p and thrust coefficient C_T of a turbine with the above properties. Then, the turbine TSR formulation given in equation (2-28) turns out to be as follows[68].

$$\lambda = \frac{\Omega R \cos \Phi}{U \cos \theta \cos \Psi} \tag{3-53}$$

The power available in the wind (equation (2-15)) passing the rotor turns out to be

$$P_{wind} = \frac{1}{2}\rho(U \cos \theta \cos \Psi)^3 \pi (R \cos \Phi)^2 \tag{3-54}$$

The dynamic force due to wind passing through the rotor (equation (2-20)) becomes

$$F_{dynamics} = \frac{1}{2}\rho(U \cos \theta \cos \Psi)^2 (R \cos \Phi)^2 \tag{3-55}$$

The power and thrust coefficients (C_p and C_T) of the turbine with precone and tilt as well as yawed operation are then found respectively by the equations (3-56) and (3-57).

$$C_p = \frac{P}{\frac{1}{2}\rho(U\cos\theta\cos\Psi)^3\pi(R\cos\Phi)^2} \tag{3-56}$$

$$C_T = \frac{T}{\frac{1}{2}\rho(U\cos\theta\cos\Psi)^2\pi(R\cos\Phi)^2} \tag{3-57}$$

Up to now, the modeling of a wind turbine is explained in detail. But, the main issue is to find the elemental aerodynamic forces $dF_{L_{i,j}}$ and $dF_{D_{i,j}}$ at the blade-aligned coordinate system defined at each blade section. These elemental forces, $dF_{L_{i,j}}$ and $dF_{D_{i,j}}$ are calculated by the equations (2-37) and (2-38) using the effective wind speed, V_{ef} which is obtained by the equation (3-51). As explained previously, when these elemental forces are obtained, other forces and moments at other coordinate systems are easily calculated. However, this requires a long process which includes a correction following an iteration process to calculate the axial and tangential induction factors. In the next subchapter, this iteration process is defined in detail.

3.3 Iteration Process and Aerodynamic Corrections to BEM Theory

This subchapter explains the step by step iteration process and the application of corrections to calculate the elemental aerodynamic forces, $dF_{L_{i,j}}$ and $dF_{D_{i,j}}$. In addition, it includes the calculation of elemental torque and thrust of a turbine blade. In this iteration process, one loop iteration is employed to estimate the axial and tangential induction factors. The skewed wake correction to the axial induction factor is applied whenever there is a nacelle tilt or yaw toward the freestream wind. This correction is applied once the iteration process has been completed successfully.

This is summarized as follows.

1. Start the iteration loop by Initializing $a_{i,j}$ and $a'_{i,j}$with zero.
2. Calculate the inflow angle, $\varphi_{i,j}$ by equation (3-52).
3. Calculate the AOA, $\alpha_{i,j}$ by equation (2-34).
4. Calculate the hub loss factor, $F_{hub_{i,j}}$ by equation (2-50).
5. Calculate the tip loss factor, $F_{tip_{i,j}}$ by equation (2-49).
6. Calculate the total loss factor, $F_{i,j}$by equation (2-51).
7. Get the aerodynamic data, $C_{l_{i,j}}$, $C_{d_{i,j}}$ corresponding to the calculated angle of attack, $\alpha_{i,j}$.
8. Calculate the normal and tangential force coefficients, $C_{n_{i,j}}, C_{t_{i,j}}$ by equations, (2-43) and (2-44).
9. Calculate the local solidity, $\sigma_{i,j}$ by equation (2-48).
10. Calculate the axial induction factor, $a_{i,j}$ by equation (2-54).
11. Apply Spera's correction by equation (2-66) and (2-67), if $a_{i,j} \geq a_c$.
12. Calculate the tangential induction factor, $a'_{i,j}$by equation (2-55).

13. If a and a' has changed more than the convergence criterion, go to step 2 and continue to iterate until the criterion is satisfied.
14. Apply the skewed wake correction by equations (2-68) and (2-69) if $\theta_{i,j} > 0$.
15. Calculate elemental lift, $dF_{L_{i,j}}$ and drag, $dF_{D_{i,j}}$ forces by equations (2-37) and (2-38) considering the effective wind speed, $V_{ef_{i,j}}$ instead of relative wind, U_{rel}.
16. Calculate elemental normal (thrust), $dF_{N_{i,j}}$ and tangential, $dF_{T_{i,j}}$ forces to the $y_b - z_b$ plane by equations, (2-39) and (2-40).
17. Transform the elemental normal (thrust), $dF_{N_{i,j}}$ and tangential, $dF_{T_{i,j}}$ forces to the hub-aligned coordinate system via the relation in (3-34).
18. Calculate the elemental torques, $dMF_{T_{i,j}}$ and $dMF_{N_{i,j}}$ considering the local radius, $r_{i,j}$ via the cross product in (3-25).
19. Transform the elemental torques, $dMF_{T_{i,j}}$ and $dMF_{N_{i,j}}$ to the hub-aligned coordinate system via the relation in (3-42).

These elemental forces and moments at the hub-aligned coordinate system are summed throughout each blade span to calculate the total torques and moments at the same coordinate system.

3.4 Dynamic Modeling and Overall Wind Turbine System

In subchapters 3.2 and 3.3, the focus was to determine the thrust, torque and lastly the power of the turbine. In addition to those, calculation of TSR, power and thrust and their respective coefficients, C_p and C_T are also defined at the end of the subchapter 3.2. Here, the aim is to construct the dynamic wind turbine model or MS Bladed simulation model.

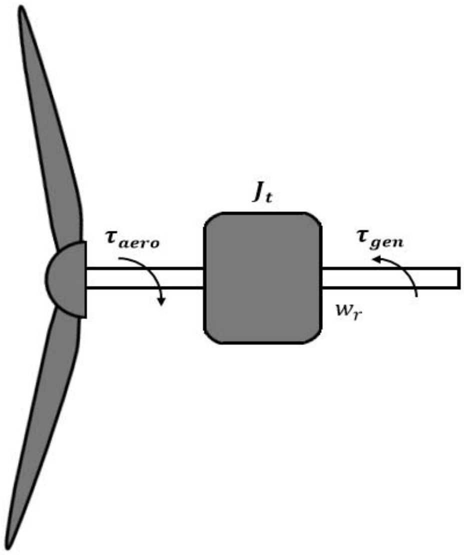

Figure 3-7 Dynamic model of a wind turbine with one mass

First of all, the rotor aerodynamic torque, τ_{aero} acts opposite to the electromagnetic torque of the turbine electrical generator. Assuming the turbine consisting of one single mass with a perfectly stiff and frictionless shaft (Figure 3-7) and using the Newton second law of motion, the dynamic turbine model is represented by a first order differential equation (3-58).

$$J_t\dot{\Omega} = \tau_{aero} - \tau_{gen} \tag{3-58}$$

$$J_t = J_{rotor} + N_{gear}^2 J_{gen} \tag{3-59}$$

Where J_t is the total inertia of the turbine system obtained from the rotor inertia, J_{rotor} and generator inertia, J_{gen} with the effect of gearbox ratio, N_{gear}. Ω is the rotor speed, τ_{aero} is the previously obtained turbine aerodynamic rotor torque, while τ_{gen} is the generator electromagnetic torque on the rotor shaft, LSS. Generator and rotor torques, which acts opposite to each other, are utilized in order to construct the nonlinear MS Bladed simulation model.

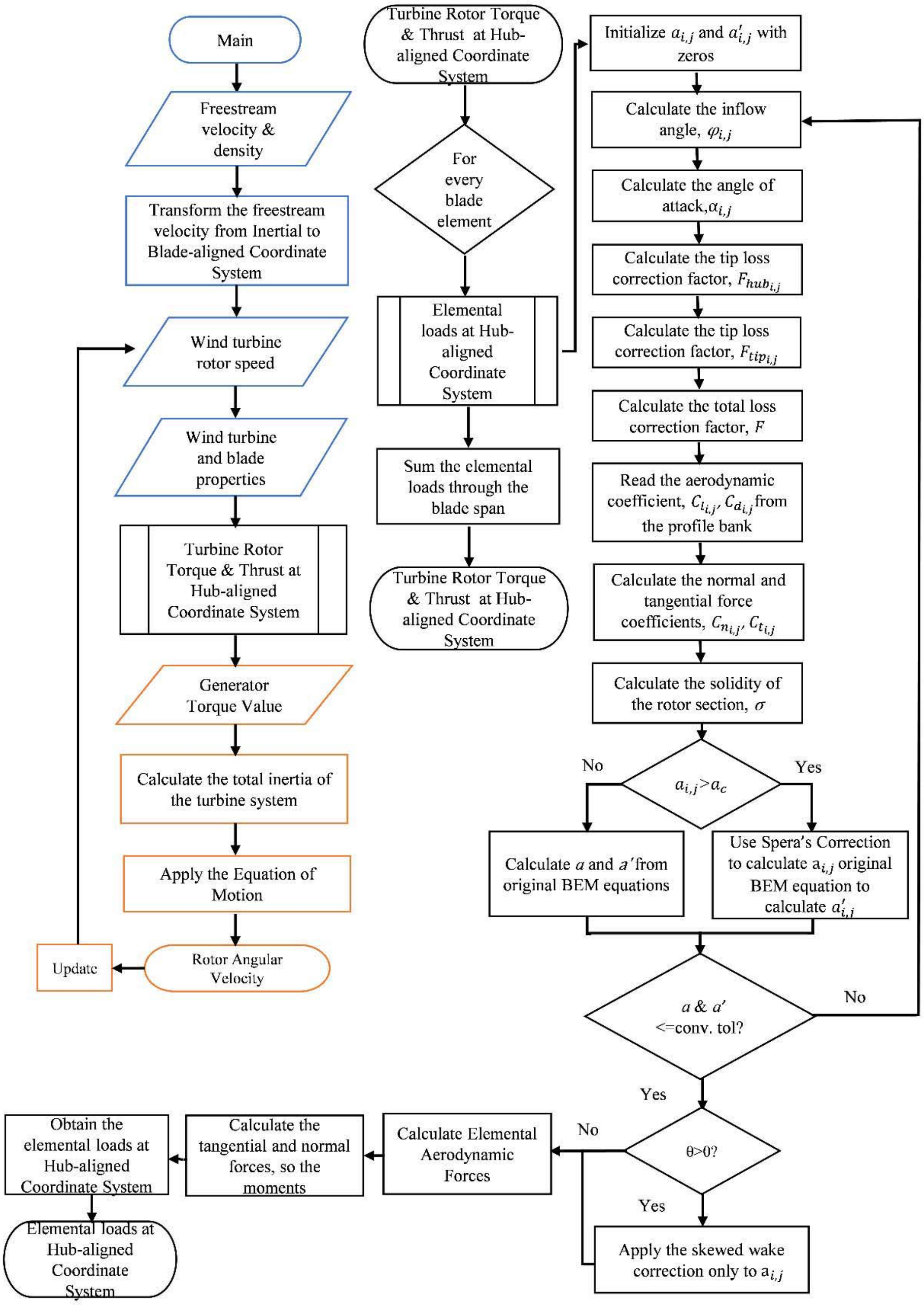

Figure 3-8 Flowchart of the MS Bladed Simulation Model

Figure 3-8 depicts the flowchart of the developed MS Bladed simulation model. Here, the nonlinearity is caused by the rotor aerodynamic torque. The model basically consists of three fundamental parts. Part I, shown in blue color, includes the properties of wind and turbine as well as its rotor properties. Part II, shown in black, deals with the aerodynamics to calculate the turbine total rotor torque and thrust. Lastly, the orange is the Part III, which deals with the dynamic modeling part using both aerodynamic rotor torque, electrical generator torque, and their respective inertias as well as rotor speed.

Eventually, to a certain extent, the aerodynamic part/calculations of the MS Bladed simulation model have similarities to PROP code[69], Wt_Perf [70]and AeroDyn [55] software available in the literature.

The development of MS Bladed simulation model is carried out using MATLAB and Simulink software. Part I and Part II, used together for aerodynamic calculations, are implemented in MATLAB. The model is later validated with different experimental field data or program/models based on BEM theory. The next chapter focuses on the validation process of the developed model in detail. Afterward, the validated (aerodynamic) model was moved into a Simulink block. This Simulink block and Part III are combined with each other in the Simulink software. The developed MS Bladed simulation model works as follows; given the properties of the freestream wind (its level and density etc.), turbine and blade properties (precone angle, tilt angle, blade chord and twist distributions etc.), the iteration process with the skewed wake correction (subchapter 3.3) calculates the elemental forces and moments at the rotor hub, later summing those elemental loads throughout each blade span gives the total loads, forces and moments at the hub center. The force and moment in the direction of the x_h-axis of the hub-aligned coordinate system correspond respectively to the total thrust and torque of the wind turbine. The torque is later used with the generator torque considering the gearbox ratio to construct the dynamic model or simulation model (equation (3-58)). The torque and thrust of each blade may also be obtained separately from the aerodynamic part of the MS Bladed simulation model if required. In addition, from the aerodynamics, it is also possible to obtain spanwise distributions of axially and tangentially induced velocities, inflow angles, angles of attacks, hub and tip loss factors, total loss factor, axial and tangential induction factors, lift and drag forces and their coefficient, tangential and normal forces to the $y_b - z_b$ plane etc.

CHAPTER 4

VALIDATION OF BEM BASED DYNAMIC NONLINEAR WIND TURBINE MODEL

To test the performance of baseline controller algorithms and a new adaptive envelope protection system, validation of the BEM based MS Bladed simulation model have to be realized first. The aerodynamic part of the developed model is validated here. Before elaborating on the details about the validation process, a special short mention about National Renewable Energy Laboratory (or NREL) is due because all the turbines used in this chapter belong to this laboratory.

NREL, located in Golden/Colorado, is a part of the US Department of Energy Office (DOE) for renewable energy and energy efficiency. Initially, the laboratory started working in 1977 as a Solar Energy Research Institute (SERI) and was renamed as NREL, later in 1991. A part of NREL is the National Wind Technology Center (NWTC), which guides the wind industry by realizing applied researches and various tests in a relationship with industrial partners, ranging from small to large turbine manufacturers[14]. NREL has been utilizing the NWTC to carry out different turbine tests. NREL Phase II and Phase III experimental turbine tests are few examples of these tests that this thesis employs for the validation purposes[71].

The validation of the MS Bladed simulation model is realized here using experimental field data and BEM-based program/model predictions of different turbine configurations. These are NREL Phase II and III experimental turbines, NREL Phase VI turbine rotor design with/without blade extension and lastly NREL 5 MW turbine.

A decade after its operational start, NREL began an extensive test program referred to as Combined Experiment in 1987 to explore the complex aerodynamics of wind turbines. The tests with different turbine configurations were started as Phase I and Phase II. Afterward, these tests were extended to include Phase III, IV, V, and VI, under a new name referred to as Unsteady Aerodynamic Experiments (UAE). In these tests, many different modifications to the test setup were conducted according to the needs. Different blade sets consisting of NREL S809 airfoil from the root to tip were utilized through the experiments. These are constant chord/untwisted blades in Phase I [72] and II, constant chord/optimally twisted blades in Phase III, IV[73] and V[74], lastly tapered and nonlinearly twisted blades in Phase VI[75].

As stated above, for the validation purposes, the test results of Phase II and III experimental turbines, rotor design outputs (PROPID) of Phase VI as well as model predictions of Galvani et al.[76] for NREL 5 MW turbine have been utilized. There are common properties of NREL Phase I to Phase VI such as the same airfoil usage through blade sets, i.e NREL S809 profile. During the validation of the MS Bladed simulation model, the blades of all the turbines, except NREL 5 MW turbine, are divided into 20 elements. NREL 5 MW turbine blade is, on the other hand, divided into 17 elements. In all the power predictions, axial and tangential induction limitations, error tolerance or convergence criterion are kept the same. The critical axial induction factor,a_c for the Phase II, III, PROPID performance predictions is taken as 0.37, while it is taken as 0.2 for NREL 5 MW turbine. The selection of this critical axial induction factor, as previously stated in subchapter 2.5, decides the empirical model between the thrust coefficient and axial induction factor in the turbulent wake state. This change has to be carried out because the turbine model developed by Galvani et al.[76] have utilized the critical axial induction factor of 0.2. However, the selection of this critical axial induction as 0.2 has been stepped back to 0.37, later. The justification is thoughtfully investigated in subchapter 4.4.1.

For the NREL Phase II and III turbines, the experimental aerodynamic data between the AOAs of -1 and 18 degrees measured at Reynolds number of $1{,}0.10^6$ are utilized for the predictions of power output[77], [78]. Outside this AOA range, the aerodynamic data are obtained using the Airfoilprep program[79], which employs the Viterna method. This program extrapolates this limited amount of aerodynamic data from -180 to 180 degrees. During the extrapolation, the aspect ratio, or AR, the ratio of blade length over chord length at 80% radius, is selected as 11[80].

For the Phase II and III experiments, NREL utilized the Grumman Wind Stream 33 turbine. It is a three-bladed downwind, stall-regulated HAWT with a diameter of 10 m. Turbine rated power is about 20 kW and a fixed speed of 72 rpm. Appendix A Table A.1 shows the basic specifications of this test turbine. It has the properties of free-yaw and manual full-span pitch control. In order to utilize the turbine for the above test phases, some modifications to the turbine were applied according to the needs. For instance, it was equipped with some special instrumentations to characterize rotating blade aerodynamics, structural response as well as atmospheric inflow conditions. However, the most dominant modification on the turbine was the change of Grumman blades with those of NREL blades consisting of S809 profile[73]. The S809 airfoil is depicted in Appendix A Figure A.1. This airfoil has a low maximum lift, a minimal sensitivity of maximum lift to leading edge roughness as well as a low profile drag [77] [81]. This airfoil was utilized to design the NREL blades for all the test turbines, ranging from Phase I to Phase VI.

In the next subchapters, the blades of NREL Phase II, III and VI turbines are divided into 20 elements, but the AOA distribution is given at the last 17 elements. This is due to the fact that the effect of the first three elements is neglected since they correspond to the hub extension where there is no S809 air profile. However, the blades of NREL 5 MW turbine are divided into 17 element sections.

4.1 NREL Phase II Wind Turbine

NREL Phase II turbine is an experimental three-bladed wind turbine. Turbine blades are in the length of 5.03 m. They are neither twisted nor tapered. They have a constant chord of 0.4572 m throughout the blade span. Turbine rotor does not have a nacelle tilt angle, but a precone angle of 3.25 degrees. In addition, blades have a fixed pitch angle of approximately 12 degrees. Figure 4-1 shows the blade twist and chord distributions of this turbine[71].

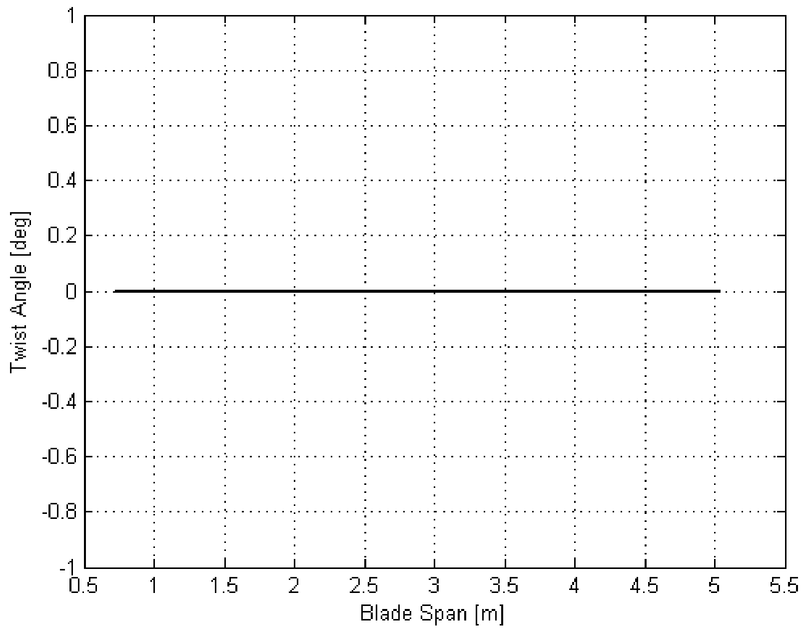

a)

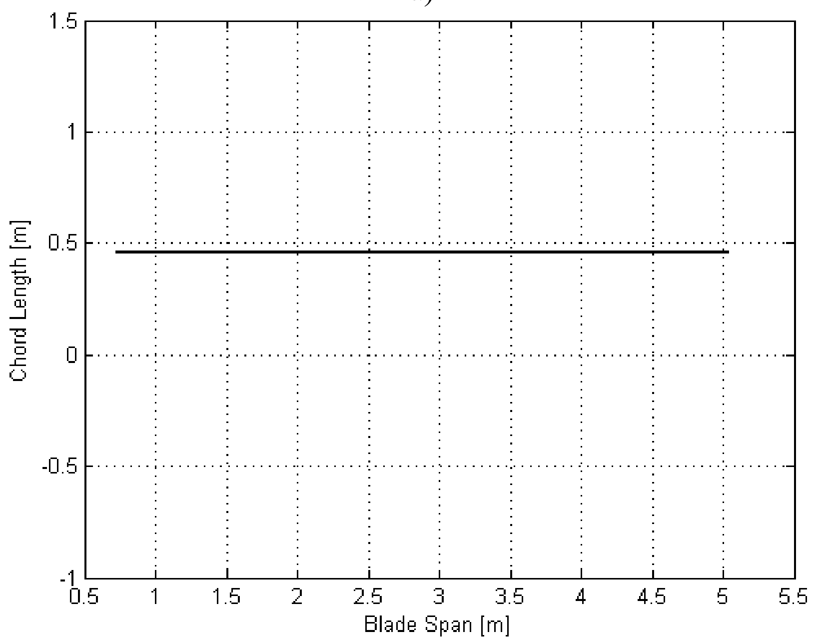

b)

Figure 4-1 Twist and chord distributions of NREL Phase II turbine, a) Twist distribution, b) Chord distribution[71]

Figure 4-2 shows the predicted power output comparison of the current model (MS Bladed model) and the test results of NREL Phase II turbine as well as Ceyhan numerical predictions with respect to freestream velocity or wind speed[82].

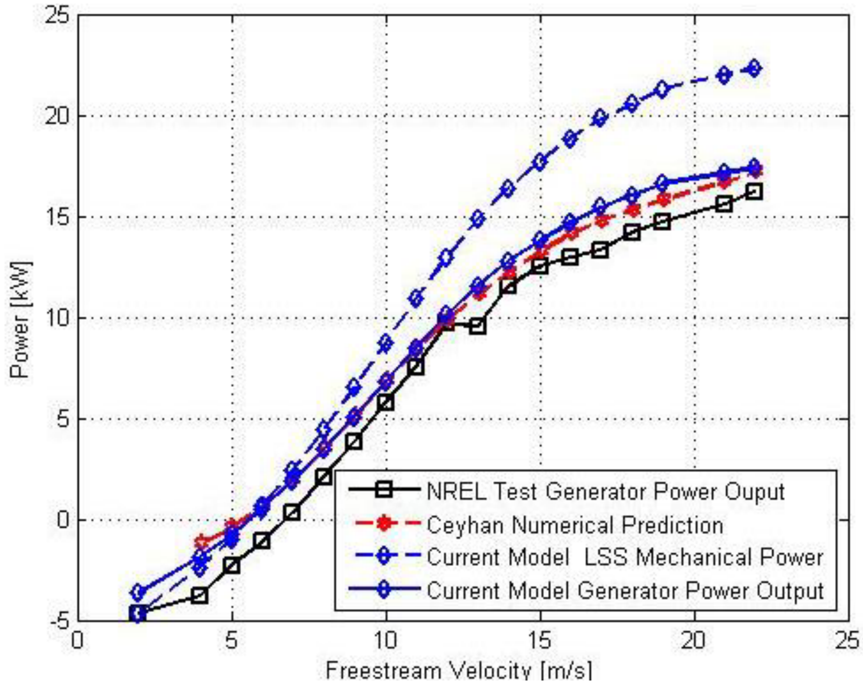

Figure 4-2 Power output comparisons

The solid black curve with square symbols represents the NREL test results. The dashed and solid blue curves with diamond symbols are respectively the currently predicted Low Speed Shaft (LSS) mechanical power or rotor power and electrical generator power. The current MS Bladed model predictions are obtained using the extrapolated experimental aerodynamic data, given in Appendix Figure A.3. The dashed red curve with hexagram symbols is the numerical prediction of Ceyhan[82] with the experimental aerodynamic data. However, due to having some slight difference between the experimental data used in this thesis study and those of Ceyhan, there appears a slight difference between the two predictions especially at higher freestream velocities.

The developed MS Bladed model predicts the performance in term of mechanical rotor power. However, NREL has given the test results in terms of electrical power. Therefore, there should be some mechanical and electrical losses in the turbine system.

NREL test turbine is stated to have an efficiency of fairly fixed and approximately 78% in Ref.[71]. However, the currently developed MS Bladed turbine model considers 100% efficiency in the system. Therefore, when the efficiency of 78% is taken into consideration, the solid blue curve in Figure 4-2 represents the predicted power output of the develop MS Bladed model.

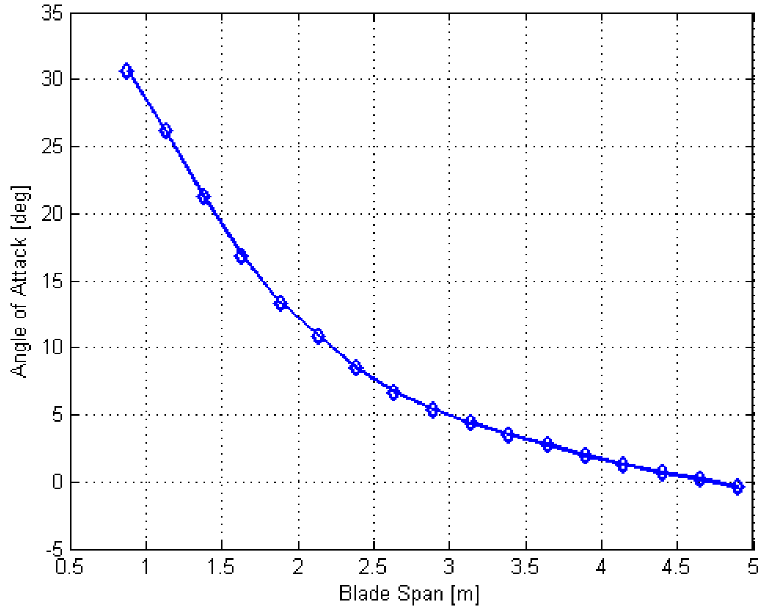

a)

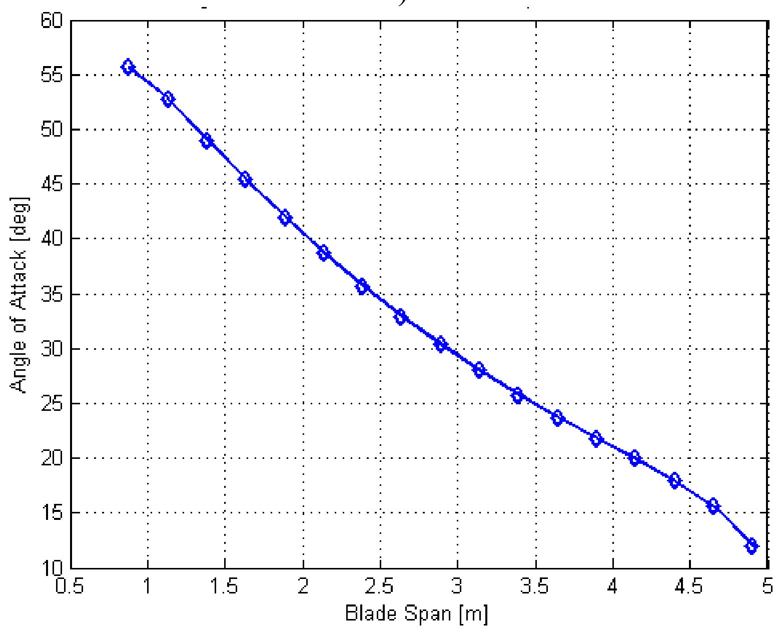

a)

Figure 4-3 Spanwise AOA distributions, a) 8 m/s, b) 21 m/s

When compared, the currently predicted generator power output predictions and the turbine tests give similar results. Starting at around 8 m/s to high wind speeds, the current MS Bladed model predicts the performance with the extrapolated aerodynamic data.

At the wind speed of 8 m/s, only the first three blade elements run above an AOA of above 18 degrees, which corresponds to the extrapolated aerodynamic data. But, at 21 m/s wind speed, the first fourteen elements run above the AOA of 18 degrees. Therefore, few blade elements operate with the experimental data. The AOA distributions at these two wind speeds are seen in Figure 4-3.

Therefore, when the wind speed is increased further, starting from the root section, the most blade element sections run with the extrapolated aerodynamic data. Eventually, at high wind speeds, such as the case in Figure 4-3-b, the estimated performance depends mostly on the extrapolated data. For the NREL Phase II configuration, which employs untwisted and untapered blades, the predicted power output with the extrapolated data is quite satisfactory owing to the closer power predictions to the NREL test results.

4.2 NREL Phase III Wind Turbine

NREL Phase III turbine is also an experimental three-bladed wind turbine. The blades of the turbine are in the length of 5.03 m. They are only twisted, but not tapered. Hence, they have a constant chord of 0.4572 m through the blade span. Turbine rotor does not have a tilt angle, but a precone angle of 3.25 degrees. In addition, the blades have a fixed pitch angle of approximately 3 degrees. Figure 4-4 shows the blade twist and chord distributions of NREL Phase III turbine[71]. The operational angular velocity of the turbine is the same as the Phase II test turbine, i.e. 72 rpm.

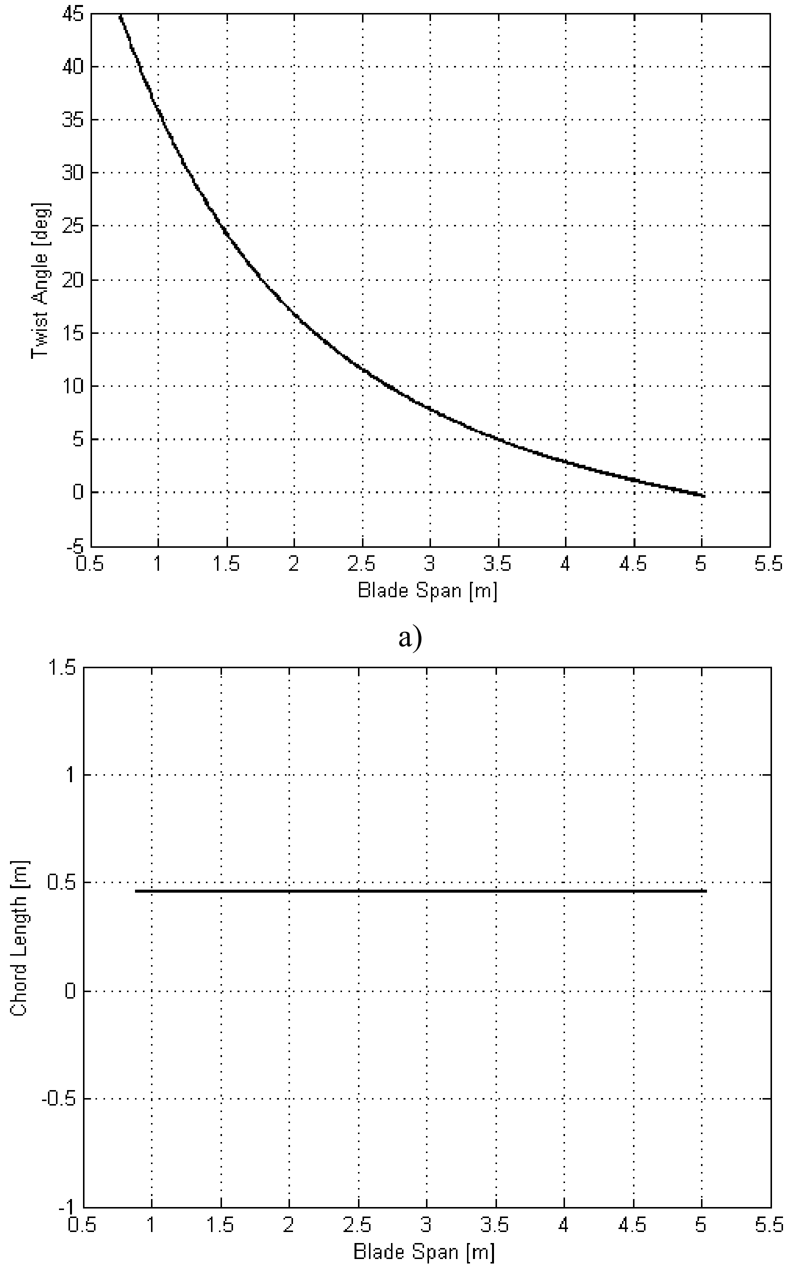

a)

b)

Figure 4-4 NREL Phase III experimental turbine twist and chord distributions, a) Twist distribution, b) Chord distribution[73]

Figure 4-5 shows three different performance results with respect to the NREL tests. As before, the solid black curve with square symbols represents the NREL test results. The red dashed curve with hexagram symbols is Ceyhan's numerical prediction[82], whereas the magenta-colored curve with stars is Polat's[83] numerical prediction.

Both use the same experimental aerodynamic data. As in the Phase II test turbine, the dashed and solid blue curves with diamond symbols in Figure 4-25 are respectively the predictions of the current MS Bladed model for the rotor power and generator power. The same amount of efficiency, 78% in the turbine system is also valid for this test turbine because the only difference is the blade sets. Therefore, the solid blue curve with square symbols is the electrical power output obtained from the current MS Bladed model.

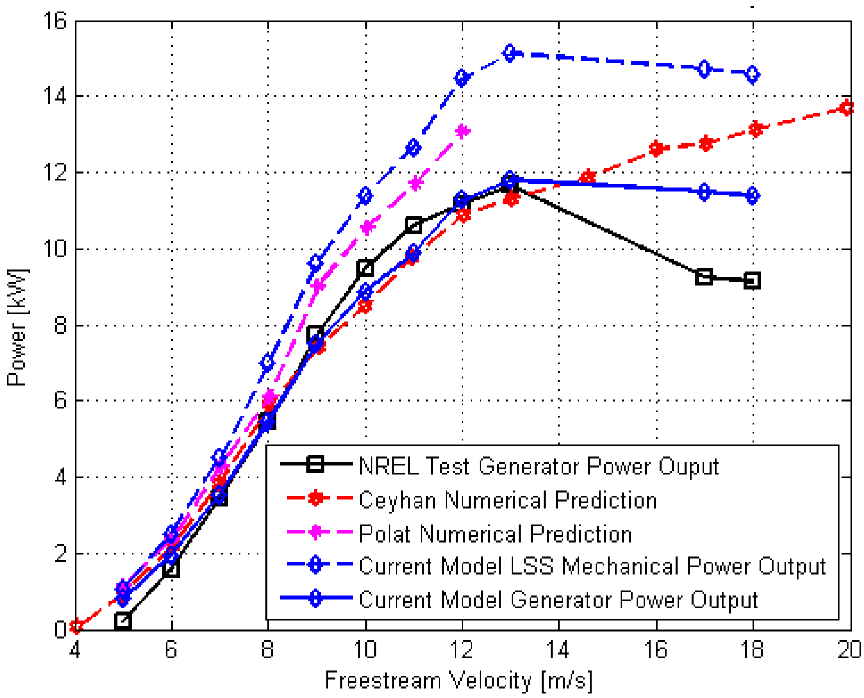

Figure 4-5 NREL Phase III power output comparisons

Although the same extrapolated airfoil data are used as in the case of Phase II turbine power predictions, there appear some differences between the currently predicted generator power and the NREL tests for the Phase III turbine, particularly when the wind speed exceeds the wind speed of approximately 9 m/s. Most of the predicted powers are almost the same except at 5, 10 and 11 m/s freestream winds as well as the wind speeds beyond 13 m/s wind. Therefore, the potential reasons for the difference may be explained as follows.

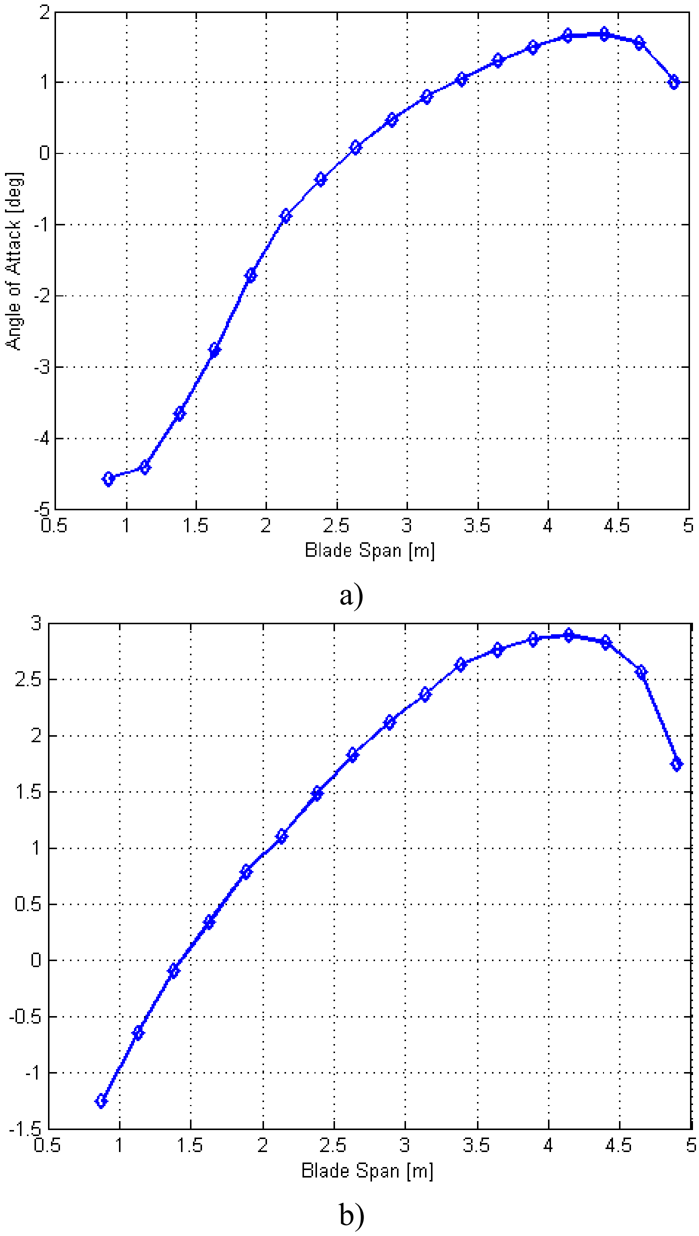

Figure 4-6 Spanwise AOA distributions, a) 5 m/s, b) 6 m/s

At the wind speed of 5 m/s, the AOA distribution is given in Figure 4.6-a. The first five inner blade elements have negative AOAs that utilize the extrapolated aerodynamic data. Thus, the predicted power deviates from the experimental results. However, there is only the first blade element utilizing the extrapolated data at the wind speed of 6 m/s (Figure 4-6-b). Therefore, the currently developed MS Bladed model gives almost the same power outputs as the NREL tests.

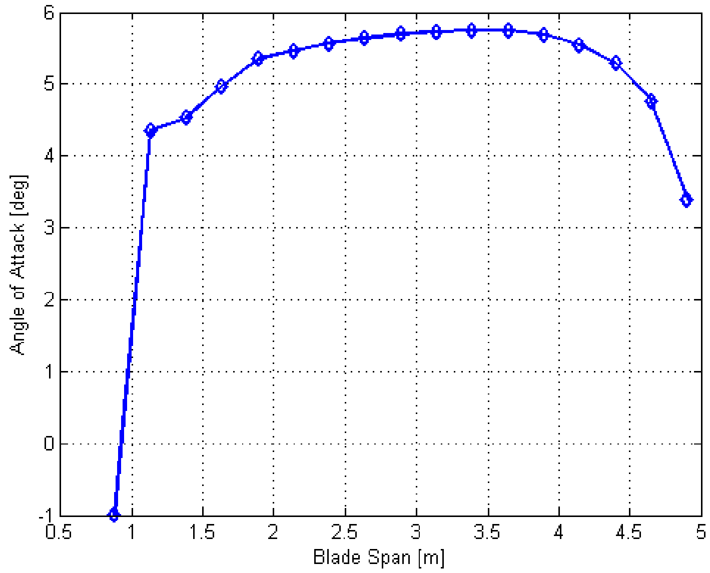

a)

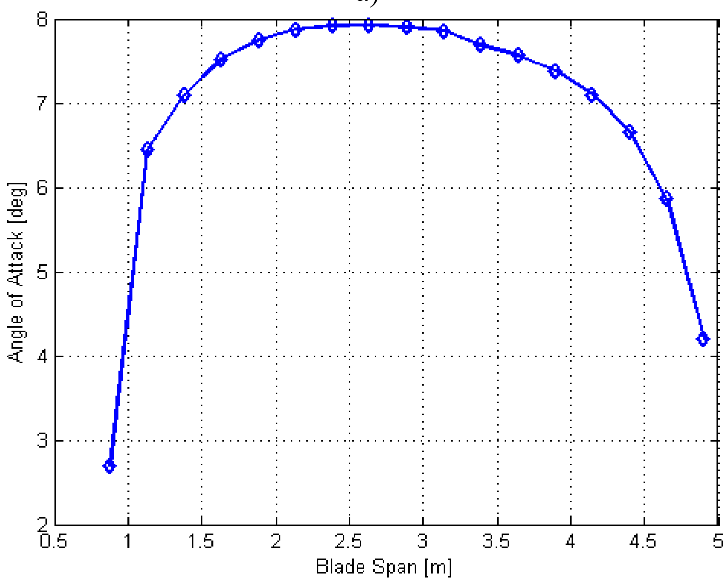

b)

Figure 4-7 Spanwise AOA distributions, a) 8 m/s, b) 9 m/s

Between the wind speeds of 6 and 9 m/s (Figure 4-7), the model predictions and NREL test results are almost the same since the AOAs for all blade sections are under the critical AOA, i.e. airfoil stall angle of 9.22 degrees.

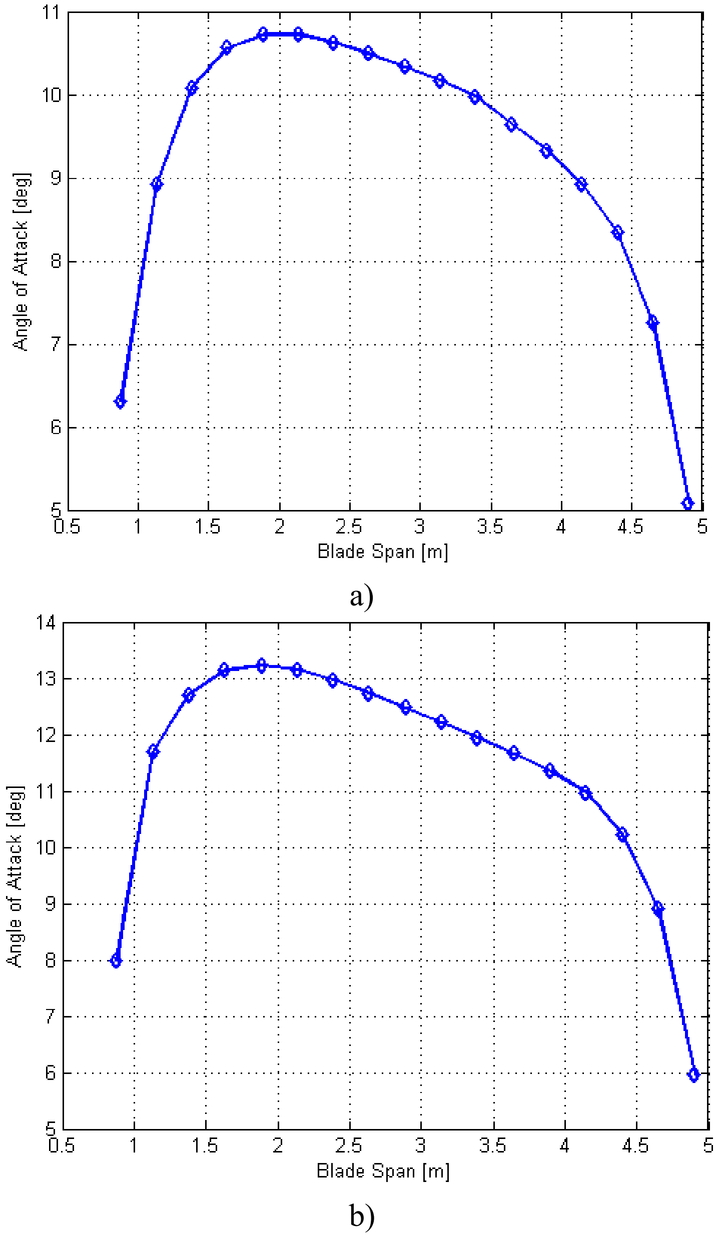

Figure 4-8 Spanwise AOA distributions, a) 10 m/s, b) 11 m/s

However, between the wind speeds of 10 and 11 m/s (Figure 4-8), the predicted powers are less than the test results. At these wind speeds, the AOA distributions are seen respectively in Figure 4-8 (a) and (b). As seen in both figures, most blade elements operate with higher AOAs than the stall angle. Therefore, these blade elements work under the stall conditions. Therefore, this difference may be caused by the complex 3D stall delay effect, which changes the aerodynamic airfoil data through the blade span due to the blade rotation. Therefore, the flow over these elements is probably still attached to the blade airfoil surface, which, in the end, produces larger lift and drag data than the steady 2D tunnel data.

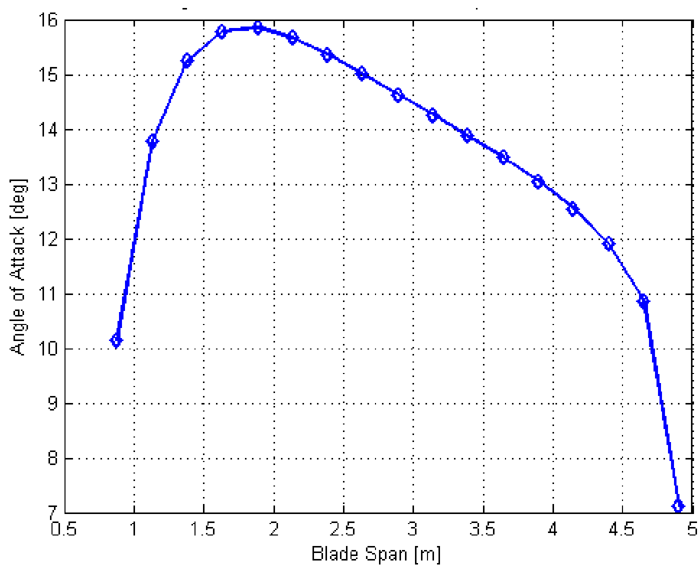

a)

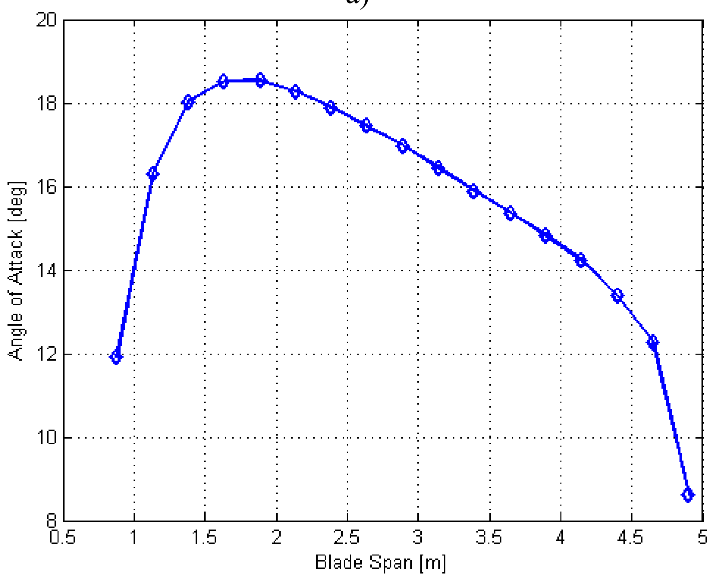

b)

Figure 4-9 Spanwise AOA distributions, a) 12 m/s, b) 13 m/s

At wind speeds of 12 and 13 m/s, the AOA distributions are given in Figure 4-9-a and b, respectively. As seen from the figure, at these two wind speeds, the turbine operates mostly with the measured 2D wind tunnel data that belong to the stalled airfoil.

However, the predicted power output is almost the same as the NREL test results even in stalled conditions. Therefore, probably the total effect of 3D aerodynamics has almost the same effect of 2D steady data along the blade span at these wind speeds.

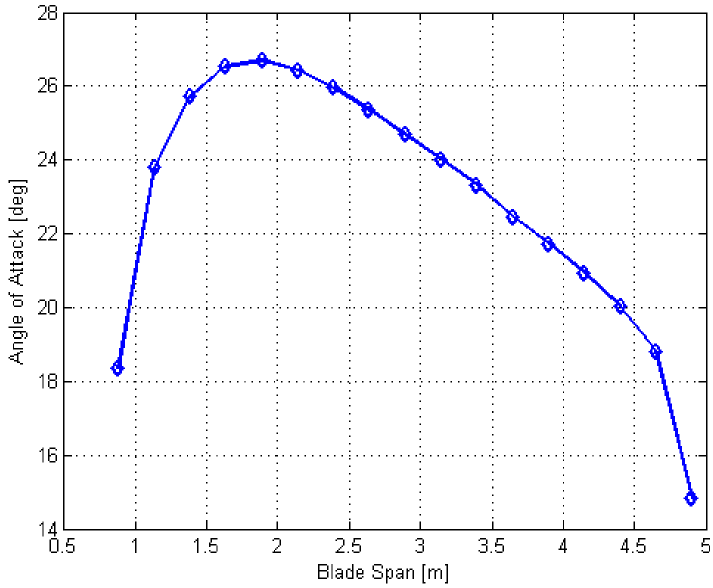

a)

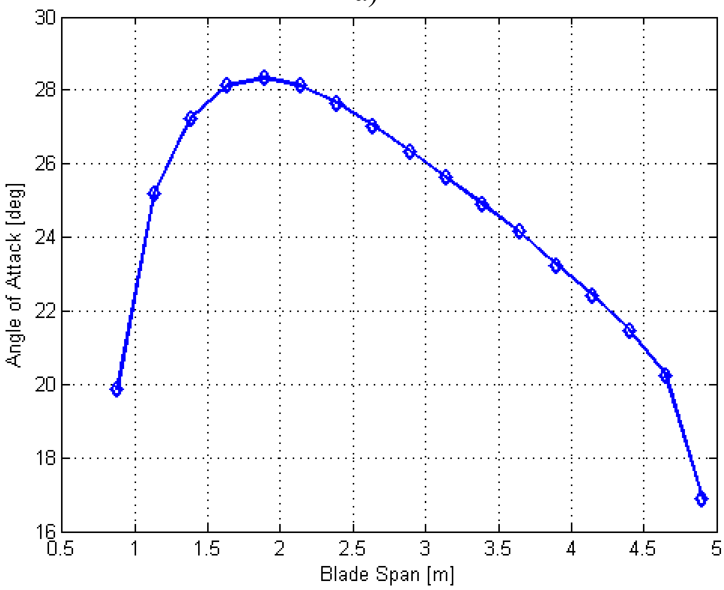

b)

Figure 4-10 Spanwise AOA distributions, a) 17 m/s, b) 18 m/s

Above the wind speed of 13 m/s, the AOA distributions at wind speeds of 17 and 18 m/s are given in Figure 4-10-a and b, respectively. The differences between the predicted powers and NREL tests increase even though the same extrapolated airfoil data are used as in the case of Phase II turbine. The possible reasons may be as follows. The extrapolated aerodynamic data at high wind speeds are not correct enough to predict the power due to the highly twisted blades. At wind speeds of 17 and 18 m/s, all the blade element sections except the last one, run under AOAs that use the extrapolated data. Another similar reason given by Ceyhan is that the local AOA values are higher than the stall angle which decreases the reliability of the aerodynamic data for the high wind speeds.

4.3 NREL Phase VI Wind Turbine

The rotor blade sets for the NREL Phase VI tests were designed by Illinois University Aerospace Engineering using PROPID and PROPGA programs. These are, respectively, an inverse design and analysis method for HAWTs based on BEM PROP code and a genetic algorithm-based optimization method for HAWTs. For the validation purposes, the currently developed MS Bladed model predictions for Phase VI turbine design configurations are also compared with the PROPID performance results. Here, an extra model, referred to as the Corrigan and Schilling post-stall delay[84], [85], is implemented to the extrapolated experimental data which have been used for Phase II and Phase III turbines. When the stall delay effect is not introduced to the aerodynamic data, the power and thrust predictions of the currently developed MS Bladed simulation model are more different than the PROPID results, particularly at moderate and high wind speeds. Therefore, same adjustments, such as activations of the Prandtl tip loss model and the Corrigan and Schilling post-stall delay model, are realized just as the adopted settings in PROPID program during the design of NREL phase VI rotor blades. The performance predictions for various configurations such as baseline three-bladed rotor, and two-bladed rotor at two different rotor speeds etc. are compared with the PROPID predictions given in the design article[86].

Eventually, two different tapered and twisted blades with S809 airfoil profile were designed by Illinois University for ease of comparison with the previous blade sets used for the Phase I to Phase V experiments.

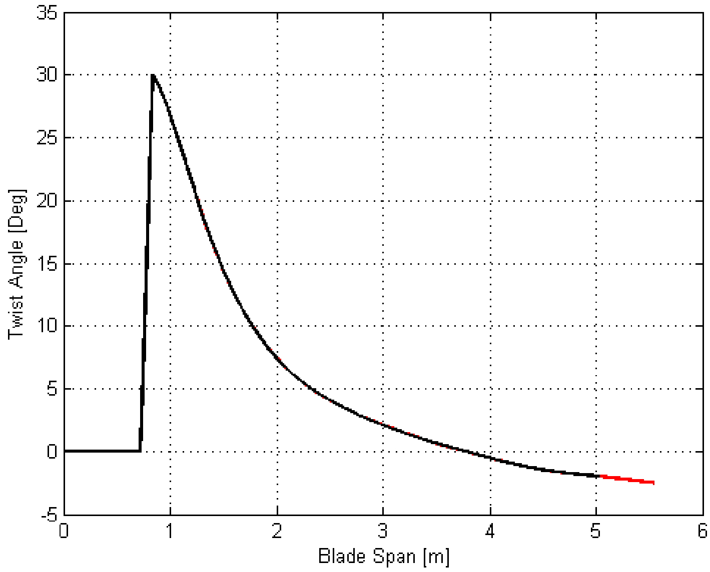

a)

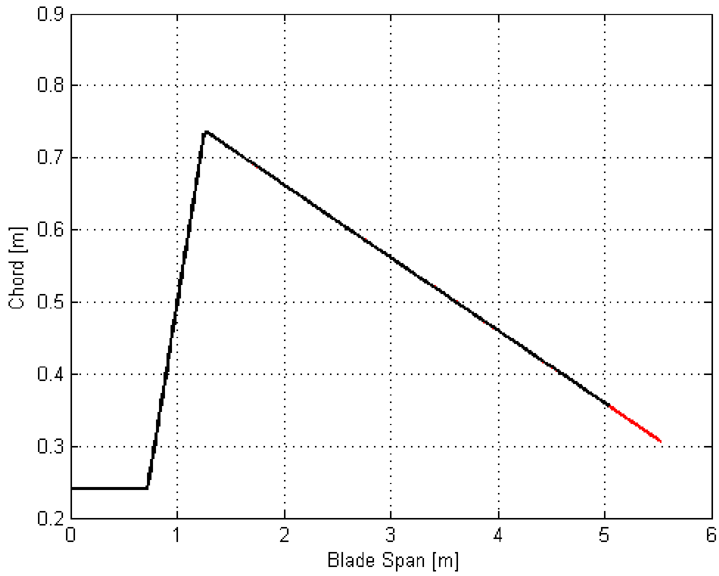

b)

Figure 4-11 NREL Phase VI baseline and extended-blade twist and chord distributions, a) Twist distribution, b) Chord distribution[86]

The first designed blade has the same length of previous blade sets and is therefore referred to as baseline blade, whereas the secondly designed blade is 10% larger with the usage of a span extension, and is referred to as an extended blade. Both turbine blades have the same nonlinearly twisted and linearly tapered region until a span length of 5.03 m. The extension is just 0.5 m in length and is a continuation of the baseline blade. These blades are designed for scientific purposes. Figure 4-11-a and b show the twist and chord distributions of the NREL Phase VI baseline and extended blades, respectively[86]. As seen in both figures, the difference between these two blades is only the blade extension shown in red.

4.3.1 Rotor Configuration with Baseline Blades

Power and thrust predictions of the currently developed MS Bladed model and PROPID program for the baseline rotor case with two or three-bladed configurations with a 5 degree-pitch setting at various fixed rotor speeds are given respectively in Figure 4-13 and Figure 4-14. The solid black curves are the predictions of the PROPID program, while the blue dashed curves are the predictions of the currently developed MS Bladed turbine model. As seen in Figure 4-13-a and Figure 4-14-a, there are large differences between the currently predicted power and thrust outputs and those of the PROPID program, especially at moderate and high wind speeds. This is caused by the unavailability of the stall delay model in the currently developed MS Bladed model. The stall delay model tries to include the effect of 3D stall delay phenomenon to the measured 2D aerodynamic data. This aerodynamic phenomenon occurs during turbine operation due to the rotation of turbine blades. In order to include this effect, the Corrigan-Schilling stall delay model is employed in the PROPID program. When the stall delay model is utilized in the developed MS Bladed model, i.e by applying the stall delay effect to the experimental aerodynamic data, the power and thrust predictions of the current MS Bladed model and PROPID program become much similar as seen in Figure 4-13-b and Figure 4-14-b.

Figure 4-12 shows basically the addition of stall delay effect to the experimental data at two blade span locations considering the currently calculated elemental stall delay angles. The theory behind the Corrigan and Schilling stall delay may be found in Ref.[84], [85]. In addition, Appendix A 1 also briefly explains the stall delay model. Basically, the original experimental data at Reynolds number of 10^6 are shifted at every section as much as the calculated elemental stall delay angle by keeping the lift and drag curve slopes constant.

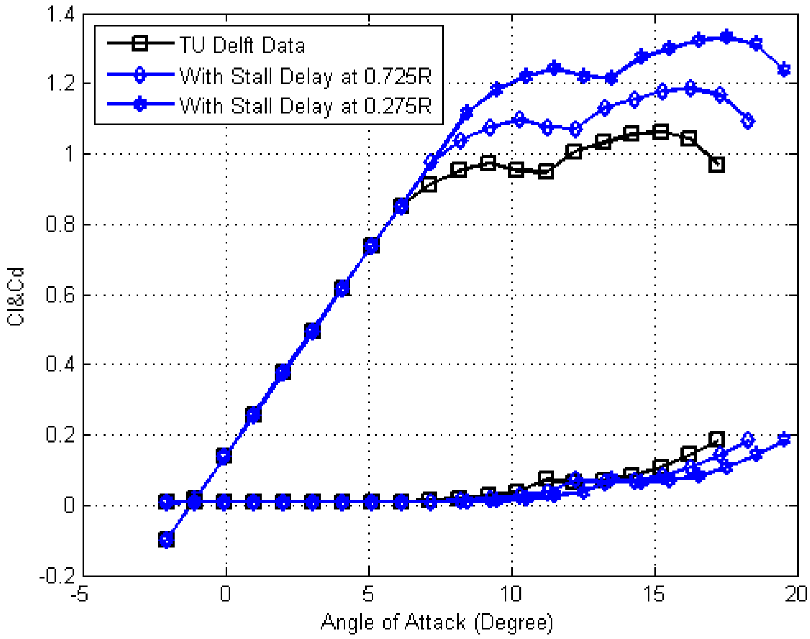

Figure 4-12 Addition of stall delay to the aerodynamic data at Re number of 10^6

The aerodynamic data used in the PROPID program include the effect of Reynolds number as well. During the design process of NREL Phase VI turbine blades, the unknown aerodynamic lift and drag data at unavailable Reynolds numbers are produced respectively by linear and logarithmic extrapolations. Experimental data at different Reynolds numbers are employed for extrapolations. Since the aerodynamic data at the Reynolds number of 10^6 are used for the experimental turbines, Phase II and III, the same extrapolated data are also employed in the current model or MS Bladed model to predict the performance of Phase VI turbine. However, here the stall delay effect is introduced to the Viterna extrapolated data using the Corrigan and Schilling stall delay model as in the PROPID program. This effect is introduced to aerodynamic data starting from the AOA of 6.2 degrees. Above that AOA, all the data includes the stall delay effect. On purpose, the Reynolds number effect, using available aerodynamic data at other Reynolds numbers, is not included to the original data because the design article does not mention precisely about how the data extrapolation based on the Reynolds number was carried out and the data at which Reynolds numbers were used for the blade design. In addition, the application of Corrigan and Schilling stall delay model is not defined explicitly.

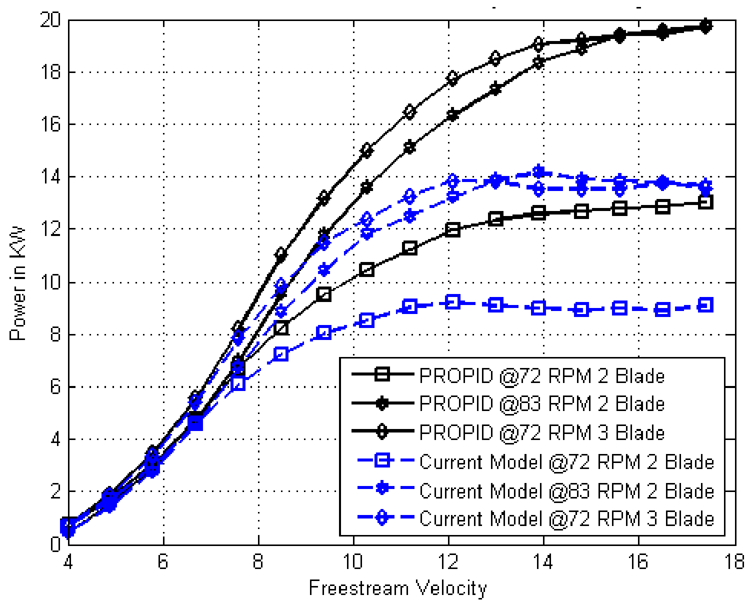

a)

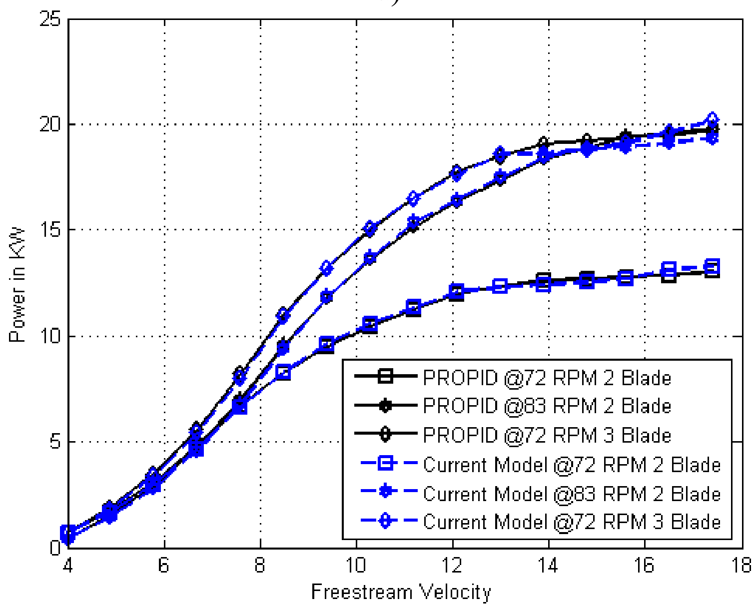

b)

Figure 4-13 Power output comparisons of PROPID program and currently developed MS Bladed model at a pitch angle of 5 degrees, a) With no stall delay effect, b) With stall delay effect

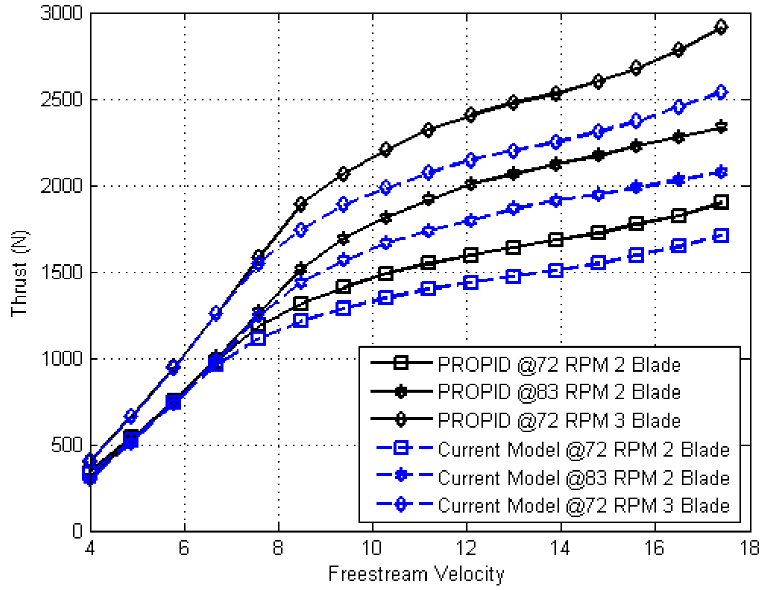

a)

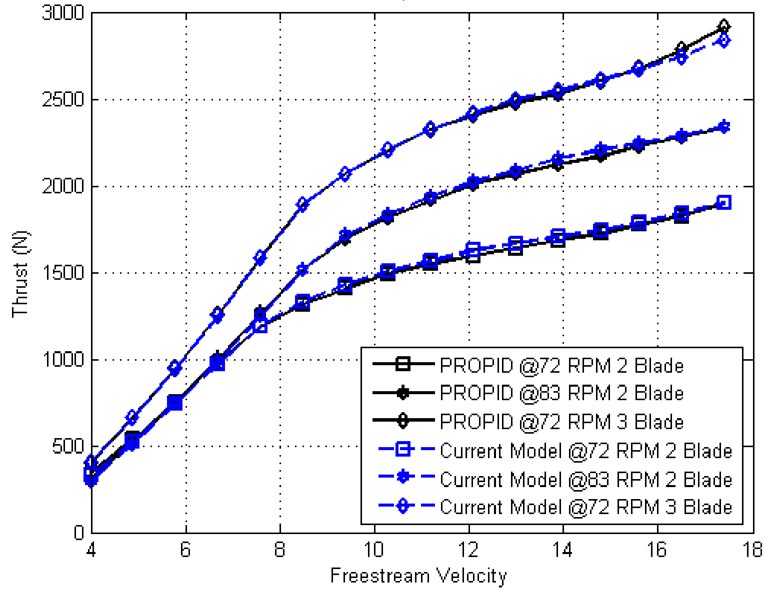

b)

Figure 4-14 Thrust output comparisons of PROPID program and currently developed MS Bladed model at a pitch angle of 5 degrees, a) With no stall delay effect, b) With stall delay effect.

The power and thrust curves for the three different turbine configurations are seen respectively in Figure 4-13-b and Figure 4-14-b. Nevertheless, they are almost the same except very slight differences at high wind speeds.

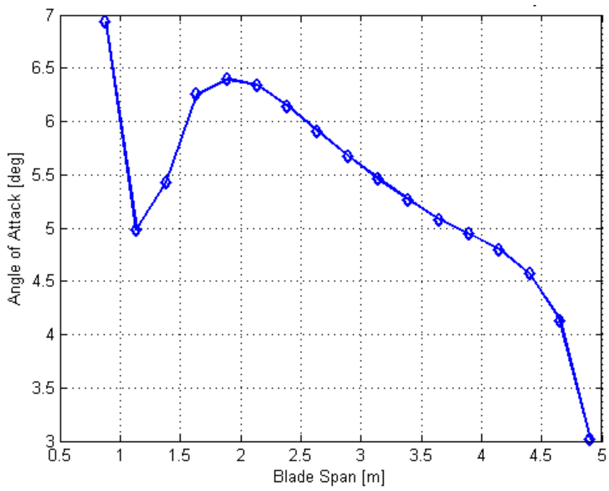

a)

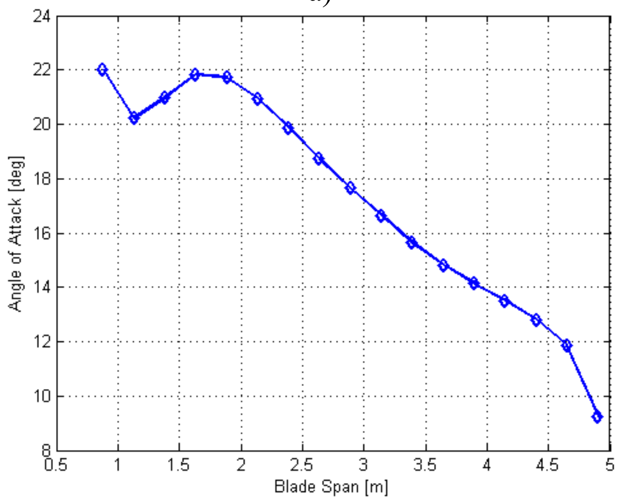

b)

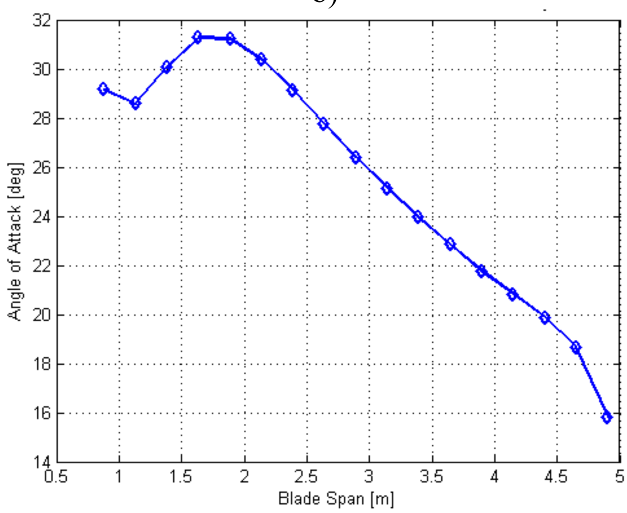

c)

Figure 4-15 NREL Phase VI baseline 2-bladed rotor at 72 rpm, a) 6.4 m/s, b) 12.1 m/s, c) 16.5 m/s

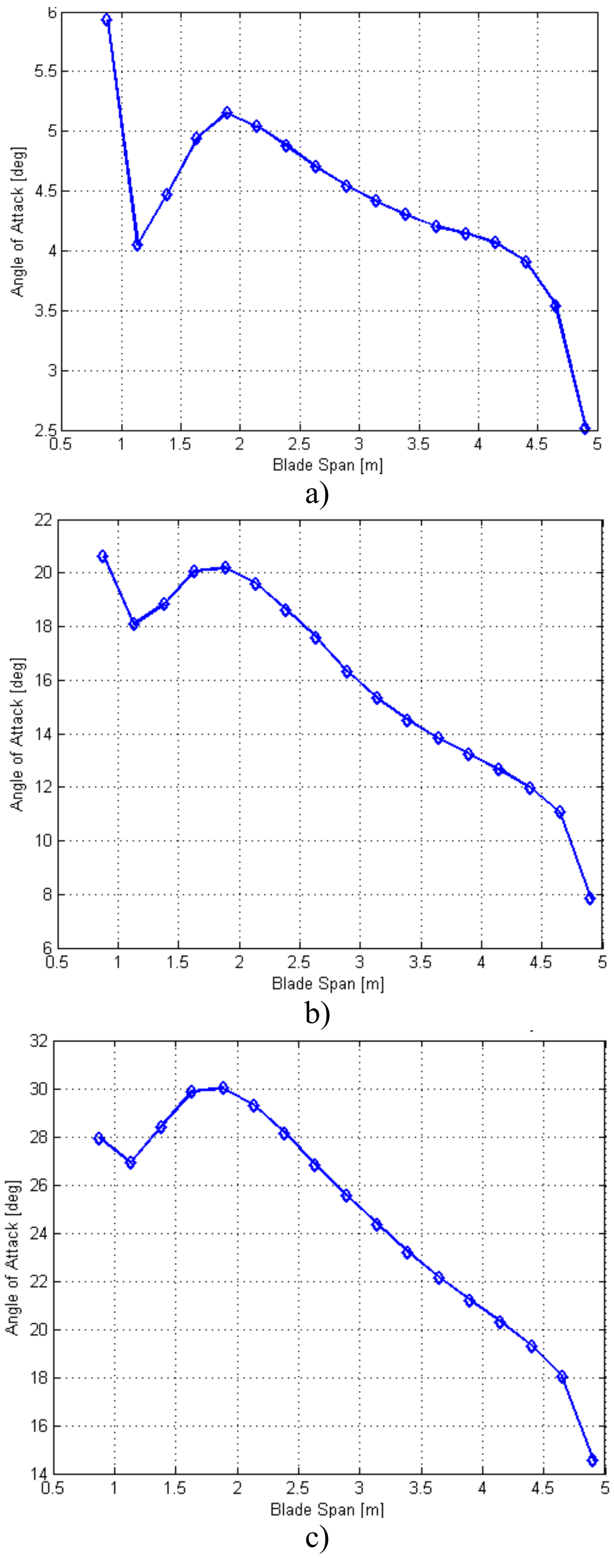

Figure 4-16 NREL Phase VI baseline 3-bladed rotor at 72 rpm, a) 6.4 m/s, b) 12.1 m/s, c) 16.5 m/s

At low wind speeds, the slight difference is potentially caused by the Reynolds number effect since the aerodynamic data utilized by the three turbine configurations at low wind speeds are exactly the pure experimental aerodynamic data without the stall delay effect. This may be understood from their spanwise distribution of AOAs. Figure 4-15-a, Figure 4-16-a, and Figure 4-17-a respectively give the spanwise AOA distributions for the 2-bladed turbine at 72 rpm, 3-bladed turbine at 72 rpm and the 2-bladed turbine at 83 rpm, which are operating at a wind speed of 6.4 m/s. As seen in Figure 4-15-a, most of the AOAs for the 2-bladed turbine at 72 rpm are lower than the AOA of 6.2 degrees. For the other turbine configurations in Figure 4-16-a and Figure 4-17-a, all of the spanwise AOAs are lower than the 6.2 degrees. Therefore, all the turbines at 6.4 m/s use the aerodynamic data without the stall delay effect. The current model and PROPID programs give similar results. Therefore, the slight difference is mostly caused by the effect of Reynolds number.

The slight difference at moderate wind speeds, however, is occurred potentially by not only the Reynolds number, but also the application of stall delay model. Similarly, Figure 4-15-b, Figure 4-16-b and Figure 4-17-b give respectively the spanwise AOA distributions for the 2-bladed turbine at 72 rpm, 3-bladed turbine at 72 rpm and the 2-bladed turbine at 83 rpm, at 12.1 m/s wind speed. As seen in Figure 4-15-b, most of the spanwise locations for the 2-bladed rotor at 72 rpm have different spanwise AOAs which use different aerodynamic data between an AOA of 6.2 degrees and an AOA of approximately 20 degrees. In this range of AOAs, the aerodynamic data includes the stall delay effect (Figure 4-12). The rest of the data are produced by the Viterna method extrapolated data with stall delay effect. For the 3-bladed rotor operating at 72 rpm at the same wind speed, all the AOAs stay in this range of AOAs as seen in Figure 4-16-b. The 2-bladed rotor at 83 rpm uses an AOA distribution (Figure 4-17-b), all of which are in the same range. Therefore, at this wind speed, all the three turbines operate mostly with the stall delay effect. The difference also comes from not introducing the effect of Reynolds number.

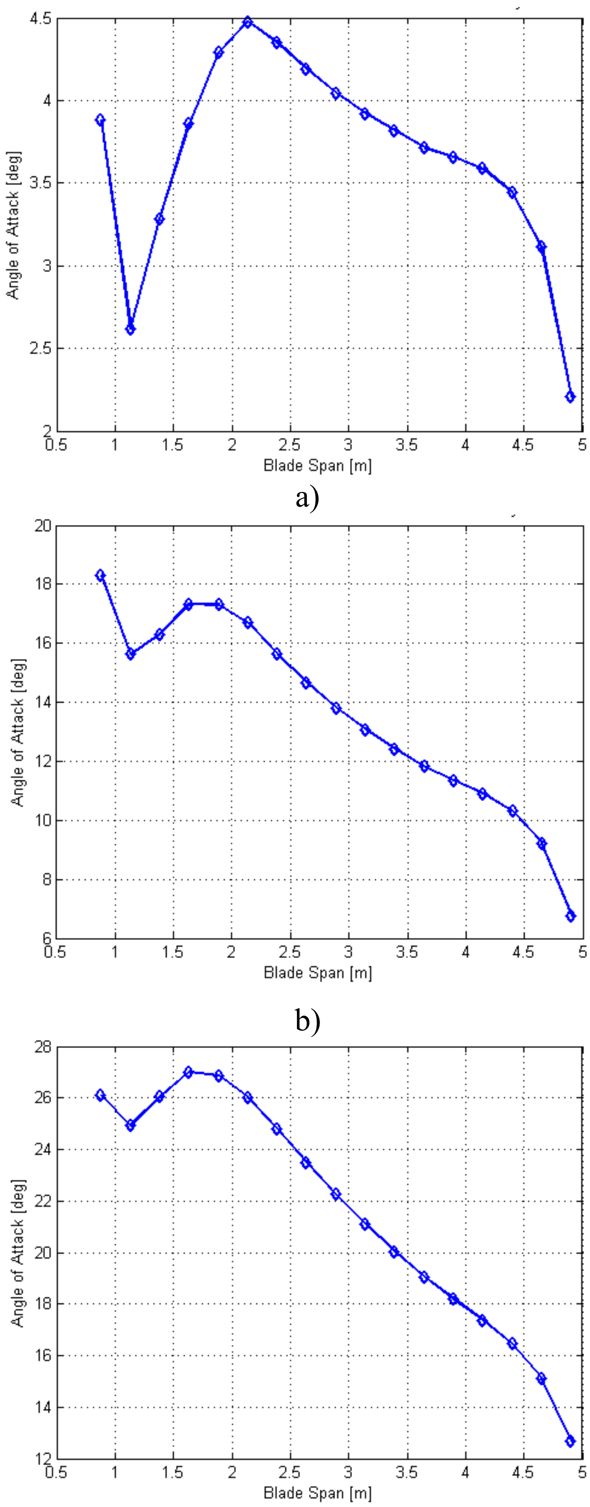

a)

b)

c)

Figure 4-17 NREL Phase VI baseline 2-bladed rotor at 83 rpm, a) 6.4 m/s, b) 12.1 m/s, c) 16.5 m/s

However, at very high wind speeds, the difference is probably caused by the extrapolated aerodynamic data, Reynolds number and the stall delay effect. Again, Figure 4-15-c, Figure 4-16-c and Figure 4-17-c give respectively the spanwise AOA distributions for the 2-bladed turbine at 72 rpm, 3-bladed turbine at 72 rpm and the 2-bladed turbine at 83 rpm at 16.5 m/s wind speed. For all the turbine configurations operating at the wind speed of 16.5 m/s, most of the AOAs are beyond approximately 20 degrees, which are the extrapolated aerodynamic data.

Adopted settings for the convergence tolerance or whether including the drag coefficient effect or not into the calculation of the induction factors both in the PROPID program and the current MS Bladed model potentially may be the other factors. Nevertheless, the obtained results are eventually quite satisfactory for the validation of the currently developed MS Bladed model. The thrust predictions of the current MS Bladed model are better than those of power. At low and moderate wind speeds, there is a very slight difference among the predictions. However, at high wind speeds, the three rotors show some differences, particularly in power outputs. These differences are caused by the usage of different aerodynamic data corresponding to the calculated AOAs as explained in detail above.

4.3.2 Rotor Configuration with Extended Blades

Power outputs of two-bladed configuration with extended blades at two different rotor speeds and two different pitch settings are given in Figure 4-18.

When the stall delay effect is not introduced, the power and thrust predictions are lower than PROPID program results at moderate and high wind speeds (Figure 4-18-a). However, the power and thrust predictions are almost the same at low wind speeds (Figure 4-18-b).

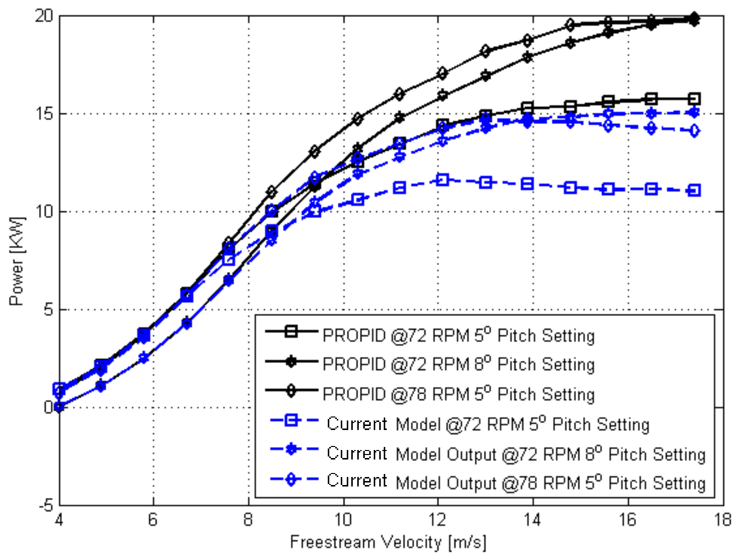

a)

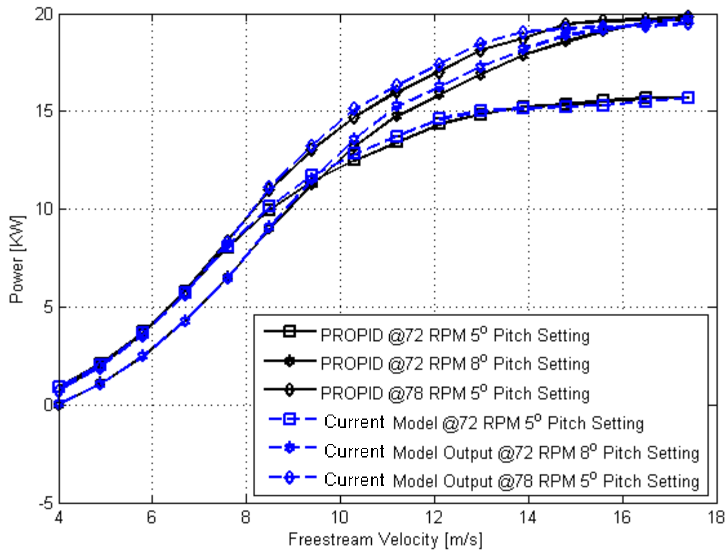

b)

Figure 4-18 Power output comparisons of PROPID program and currently developed MS Bladed turbine model, a) With no stall delay effect b) With stall delay effect

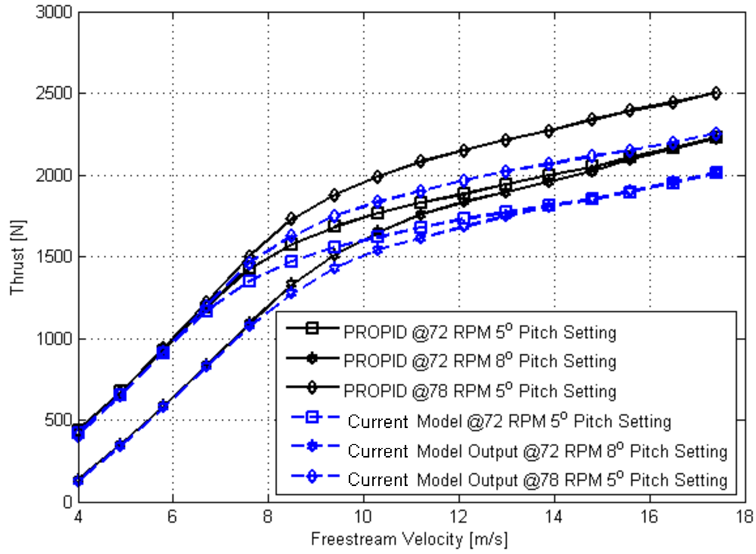

a)

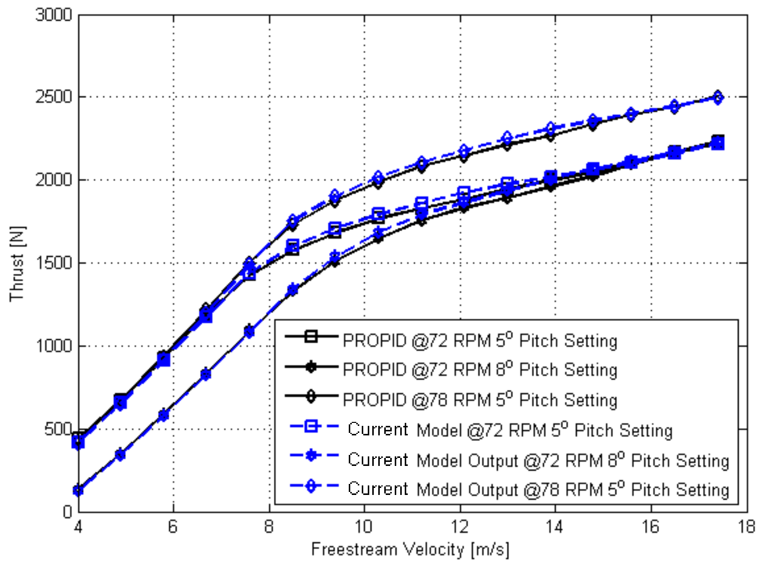

b)

Figure 4-19 Thrust output comparisons of PROPID program and currently developed MS Bladed turbine model, a) With no stall delay effect b) With stall delay effect

Figure 4-18-b and Figure 4-19-b show that all three turbine configurations give closer results at very high wind speeds, compared to the Phase VI with baseline blades. This indicates that the aerodynamic data utilized at low, moderate and high wind speeds are closer to the experimental data utilized during the blade design process.

4.4 NREL 5 MW Wind Turbine

The last turbine used for the model validation is NREL 5 MW wind turbine whose chord and twist distributions are given respectively in Figure 4-20-a and b.

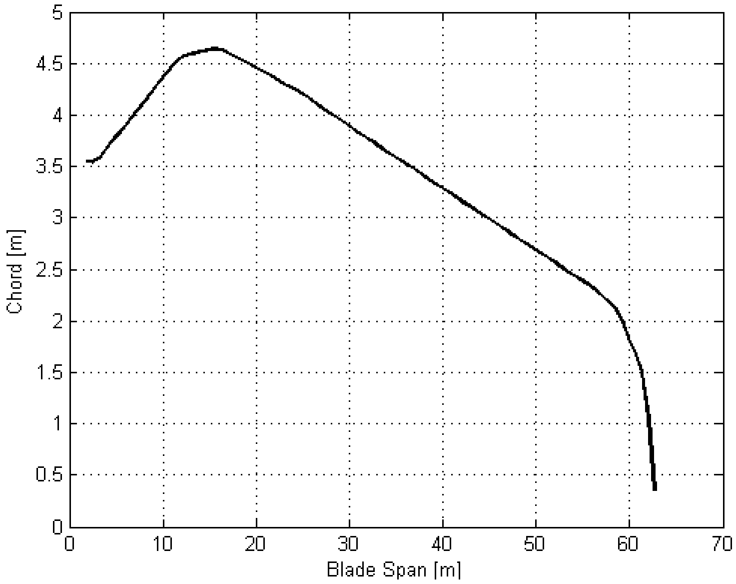

a)

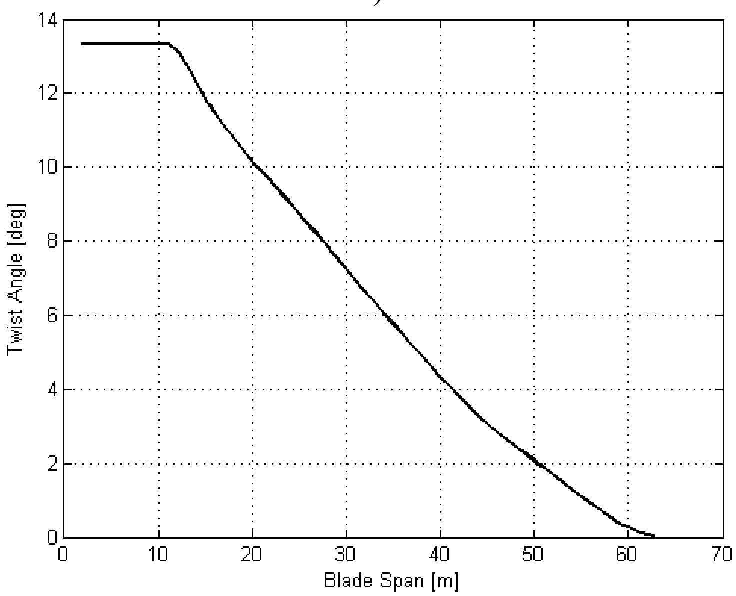

b)

Figure 4-20 NREL 5 MW wind turbine chord and twist distributions,
a) Chord distribution, b) Twist distribution

NREL 5 MW turbine is an upwind, three-bladed, variable-speed, variable blade-pitch-to-feather controlled turbine. It has a precone angle of 2.5 degrees and a tilt angle of 5 degrees. The rotor blade consists of six different airfoils throughout the blade span except for two circular cross sections at the blade root. Here, the utilized aerodynamic data for these airfoils include the effect of 3D stall delay phenomenon and are already extrapolated from -180 to +180 degrees[87]. Some other properties related to NREL 5 MW turbine are available in Ref.[87].

The power outputs of the currently developed MS Bladed model with respect to different freestream velocities at various pitch settings have been also compared to those of Galvani et al. model[76] for NREL 5 MW turbine. The precone and tilt angles are inactivated (adjusted to zero) in the current developed MS Bladed model since the Galvani et al. model[76] does not have these properties, i.e. precone and tilt angles. Therefore, the results given by Galvani et al.[76] belong to NREL 5 MW turbine with no precone and tilt angles. Besides, Galvani et al. model[76] uses the Spera's correction with the critical axial induction factor, a_c of 0.2, while the current MS Bladed model uses this factor as 0.37. These two different factors correspond to different empirical lines i.e. the cyan and blue lines in turbulent wake state (Figure 2-7). Therefore, in order to get similar predictions to those of Galvani et al. model[76], this value of the critical axial induction factor, 0.37 changed into 0.2 while keeping other adjustments same in the current MS Bladed model. Power output comparisons with respect to various wind speeds and different pitch settings are given in Figure 4-21, Figure 4-22, and Figure 4-23. As seen from the results, power outputs of both models at different pitch settings are almost the same at low freestream velocities, but a minor difference at high freestream velocities. The reason may be explained as follows.

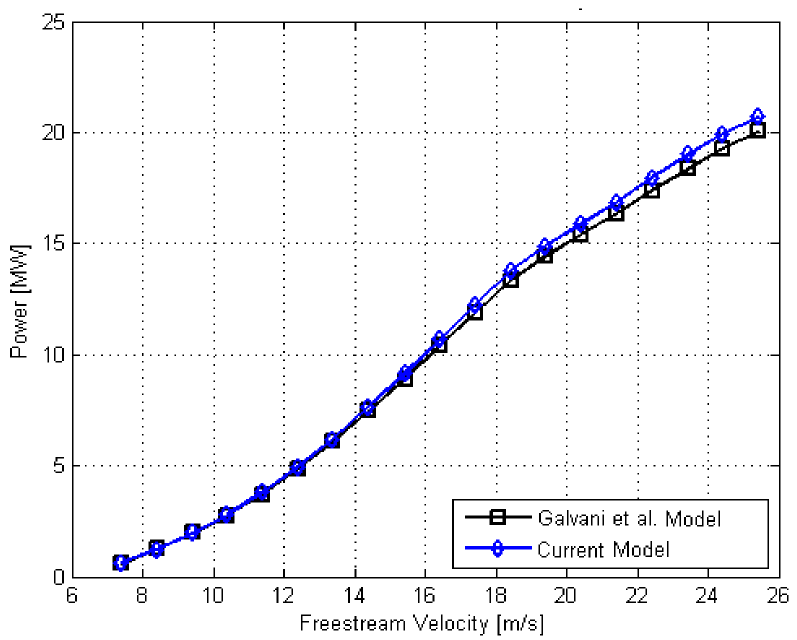

a)

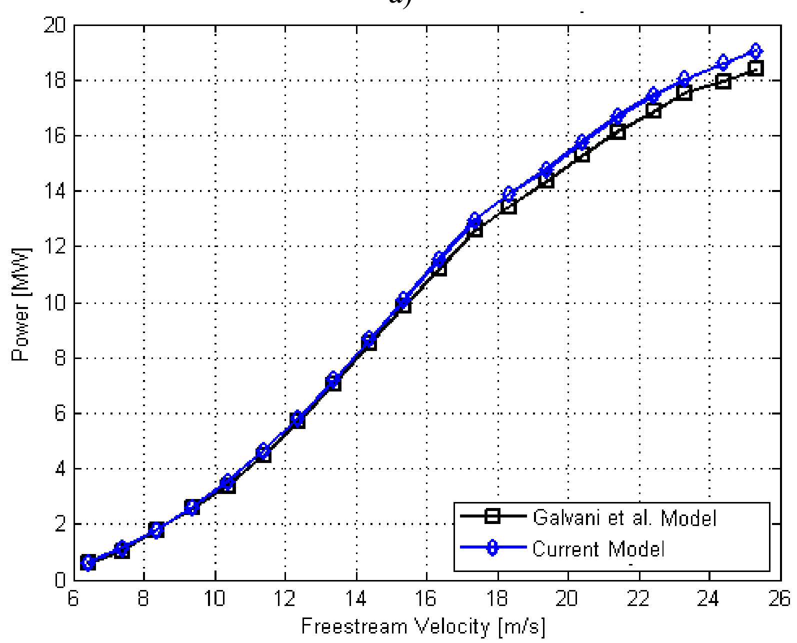

b)

Figure 4-21 Power output comparisons, a) 6-degree pitch setting, b) 4-degree pitch setting

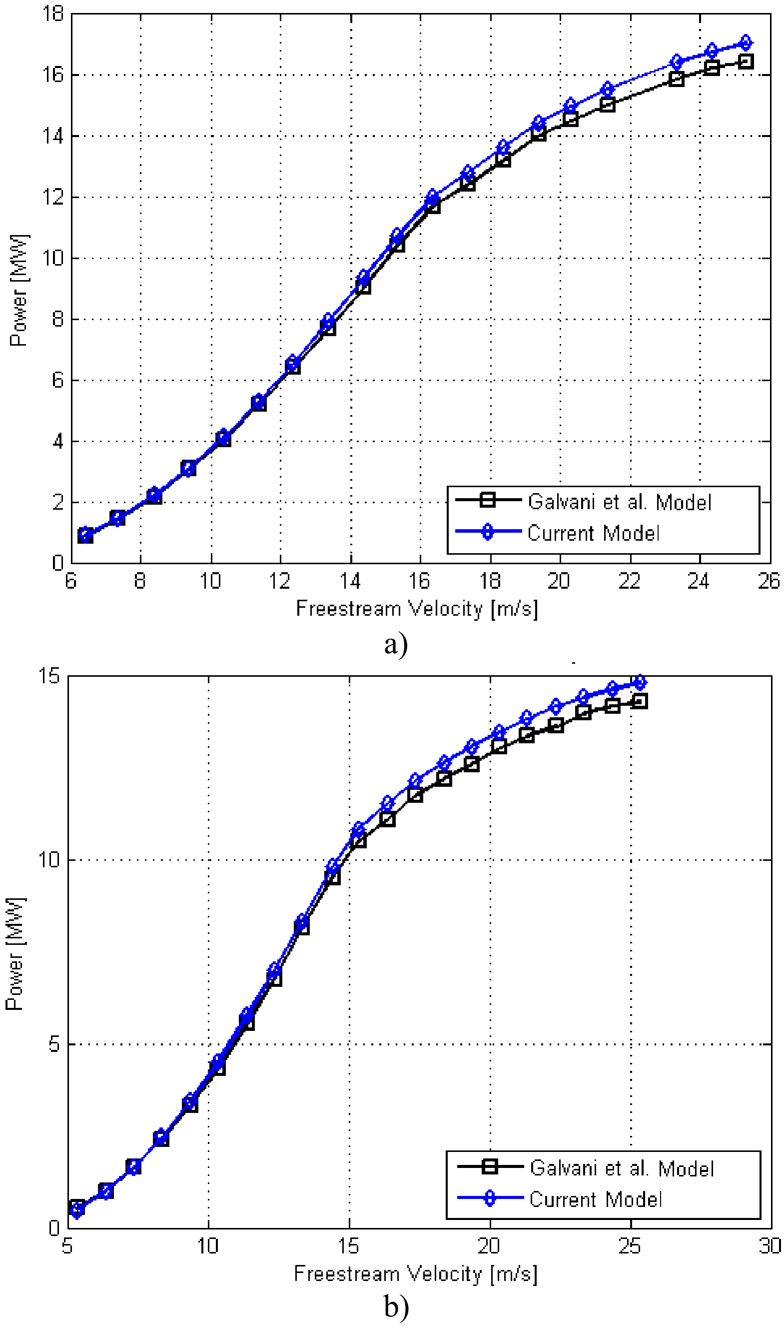

Figure 4-22 Power output comparisons, a) 2-degree pitch setting, b) 0-degree pitch setting

.

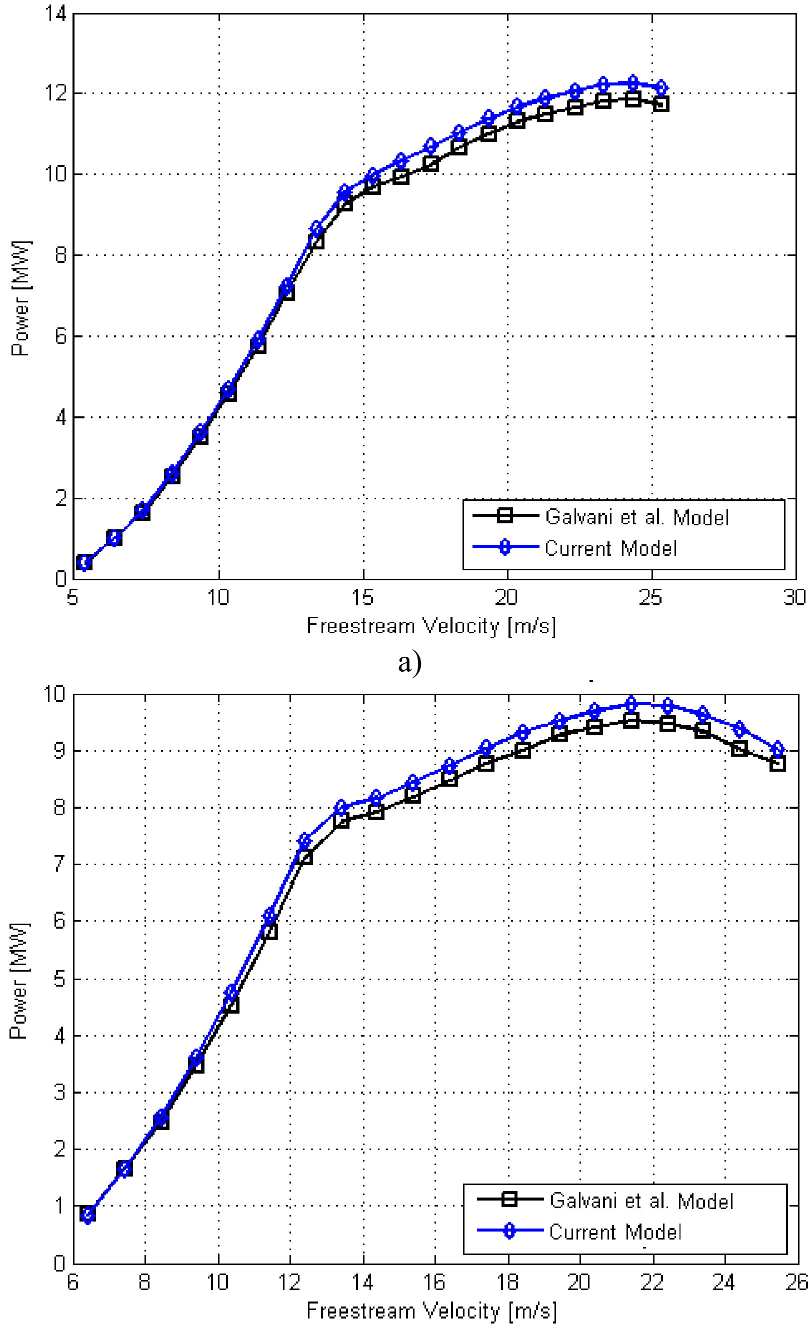

b)

Figure 4-23 Power output comparisons, a) -2-degree pitch setting, b) -4-degree pitch setting

The air density used by Galvani et al.[76] is not given explicitly in Ref.[76]. Hence, assuming the usage of same air density, 1.225 kg/m^3, given in the definition report of the 5 MW wind turbine[87], the reason for the difference is not caused by only one parameter. It is a combination of some parameters such as the value of convergence tolerance criterion, blade element number, and the hub loss correction factor etc. As seen in the last two rows of Table 4-1, the current MS Bladed model uses the convergence tolerance as 0.005, and the blade element number as 17, whereas Galvani et al. model[76] uses these parameters as 0.01 and 100, respectively.

Table 4-1 The difference between wind turbine models

	Current MS Bladed Model	**Galvani et al. Model**	**Explanations**
Hub Loss	+	-	Active in current model
Tip Loss	+	+	Active in both models
Windmill Brake State Model	+	+	Both use Spera's correction with a_c equal to 0.2.
Skewed Wake Effect	+	-	Inactive in current Model
Pitch Angle	+	+	Active in both models
Yaw Angle	+	-	Inactive in current model
Precone Angle	+	-	Inactive in current model
Tilt Angle	+	-	Inactive in current model
Air density	1.225 $\mathrm{kg/m^3}$	Uncertain	Taken from [87]
Convergence Tolerance	0.005	0.01	Models use different convergence value.
Blade Element Number	17	100	Blades are divided into different element numbers.

In addition, Galvani et al. model[76] do not include any model for the correction of the losses at the rotor hub. Thus, some cases have been created to see each of these parameter effects on power output to explore the reason in detail. Blade pitch angles are particularly set to 4 and -4 degrees to see these parameter effects both in positive and negative pitch settings. Table 4-2 summarizes these cases[87]. The comparison is carried out by inactivating some features of the current (MS Bladed) model due to the non-complexity of the Galvani et al. model[76]. Table 4-1 shows the differences between the current MS Bladed model and the Galvani et al. model[76] along with some explanations.

Table 4-2 is prepared as five cases for the discussion of each parameter which causes the difference in power outputs.

Table 4-2 Cases to check the effect of each parameter

	Hub Loss	Precone Angle	Tilt Angle	Convergence Tolerance	Blade Element Number
Case 0	-	-	-	0.01	100
Case I	-	0	0	0.01	17
Case II	-	0	0	0.005	17
Case III	-	0	0	0.01	68
Case IV	+	0	0	0.01	17
Case V	+	0	0	0.005	17

Case 0 corresponds to adopted settings in the Galvani et al. model[76]. Case I is taken as a reference case to compare with other cases. Case II is created to see the effect of convergence tolerance, Case III, the effect of blade element number, Case IV, the hub loss correction effect, and lastly the Case V, the adopted adjustments in the current MS Bladed model.

Figure 4-24 shows the effect of convergence tolerance on power output. As seen in the figure, the tolerance effect is clearly seen at the negative (or low) blade pitch angle, but slightly seen at the positive (or high) blade pitch angle. When the convergence criterion is decreased from 0.01 to 0.005, the power output of the model decreases. Decreasing the convergence tolerance gives more accurate results because of the increase in the sensitivity of the iteration process.

Figure 4-25 depicts the effect of blade element number on power output. The blade element number is increased from 17 to 68. The Galvani et al. model[76] employs a blade element number of 100. As seen in the figure, the blade number has a strong influence on power output at both negative and positive blade pitch angles, especially at high freestream velocities.

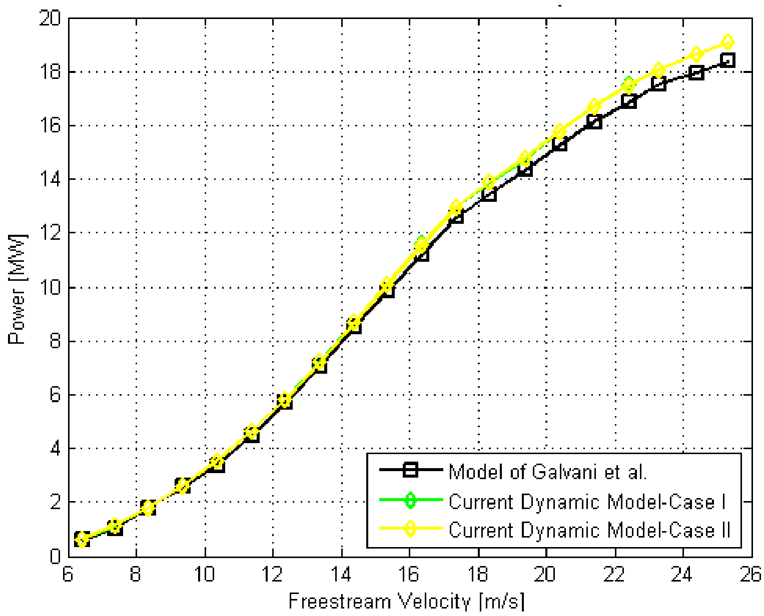

a)

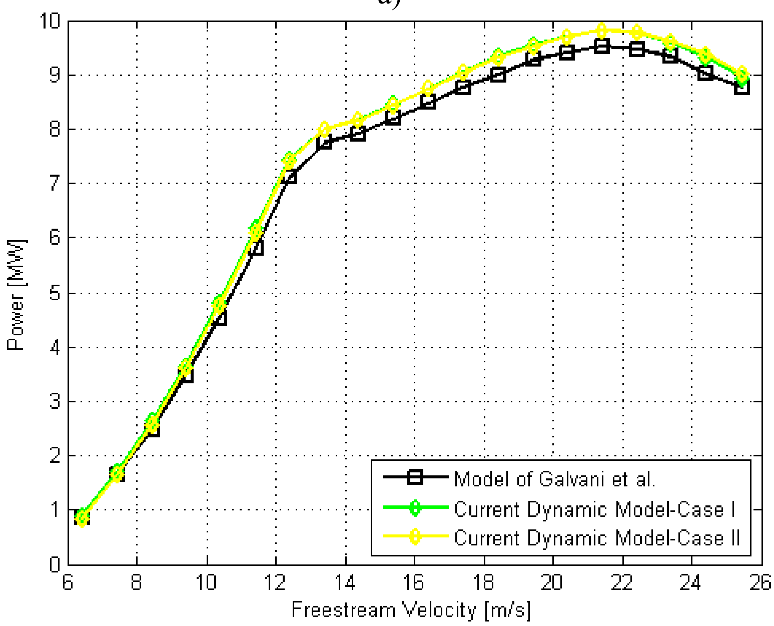

b)

Figure 4-24 Effect of convergence tolerance on power output, a) 4-degree pitch setting, b) 4-degree pitch setting

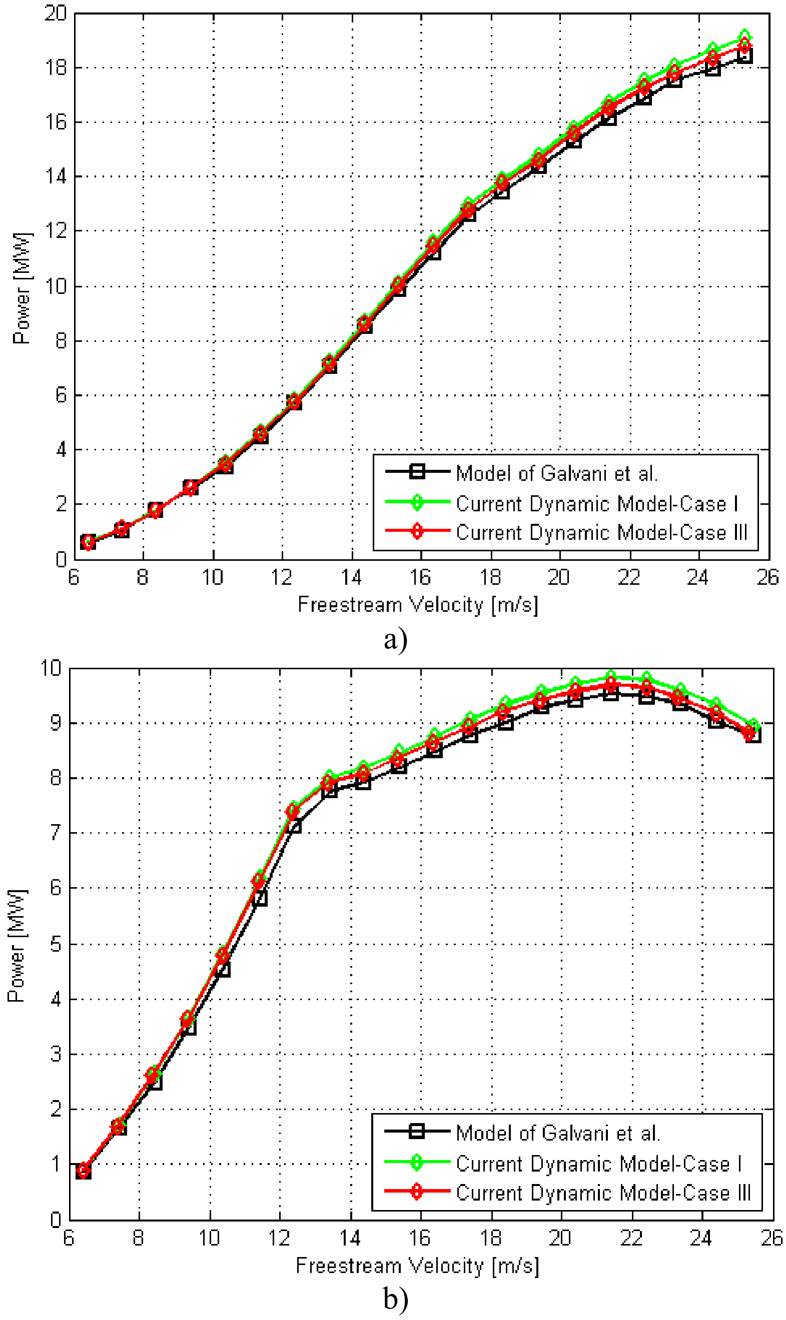

Figure 4-25 Effect of blade element number on power output, a) 4-degree pitch setting, b) -4-degree pitch setting

Increasing the blade element numbers may give a more accurate power output, but it requires more computational power and time. When compared to the effect of selected convergence tolerance criterion, the selected blade number has a much significant effect on power output than the value of tolerance criterion.

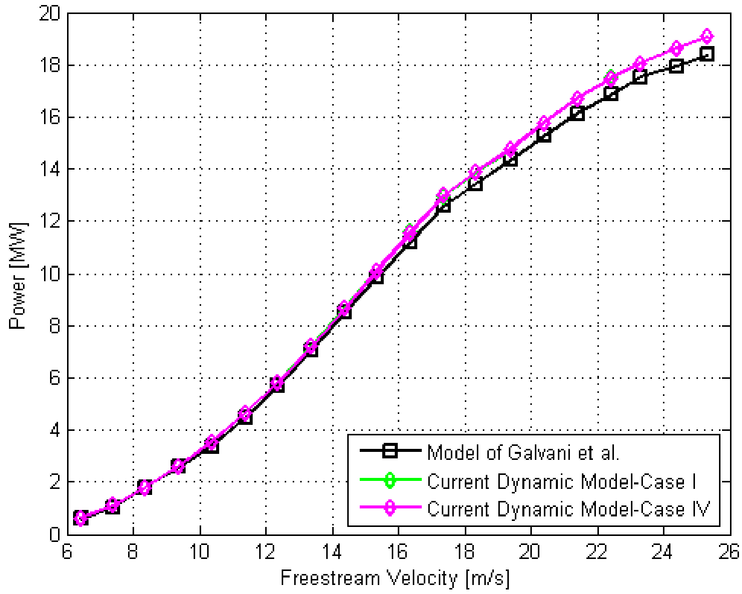

a)

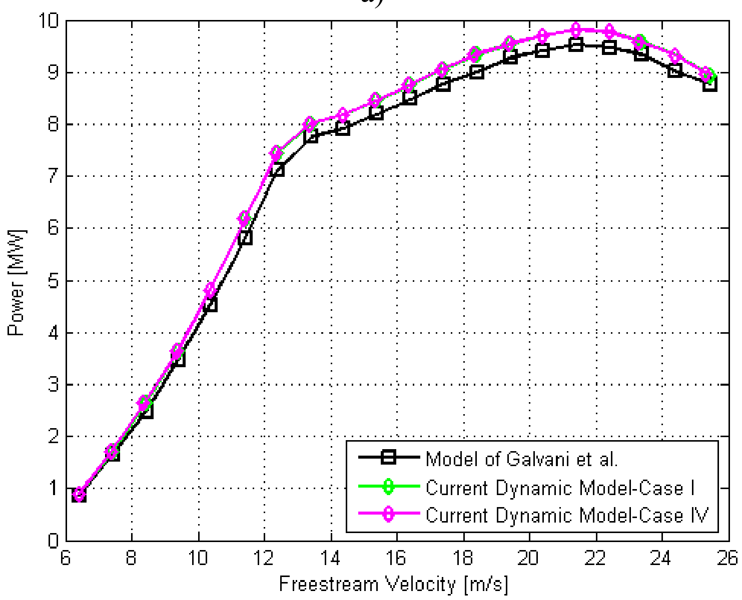

b)

Figure 4-26 Effect of hub loss correction factor on power output, a) 4-degree pitch setting, b) -4-degree pitch setting

The effect of hub loss correction factor on power output is shown in Figure 4-26. Hub loss effect is very small at both pitch angles. Almost no difference is seen at the positive pitch setting, whereas a slight difference is seen at the low pitch setting at highly large freestream velocities. Hub loss factor seems not affecting the turbine power significantly, compared to a reduction of the convergence tolerance value to 0.005.

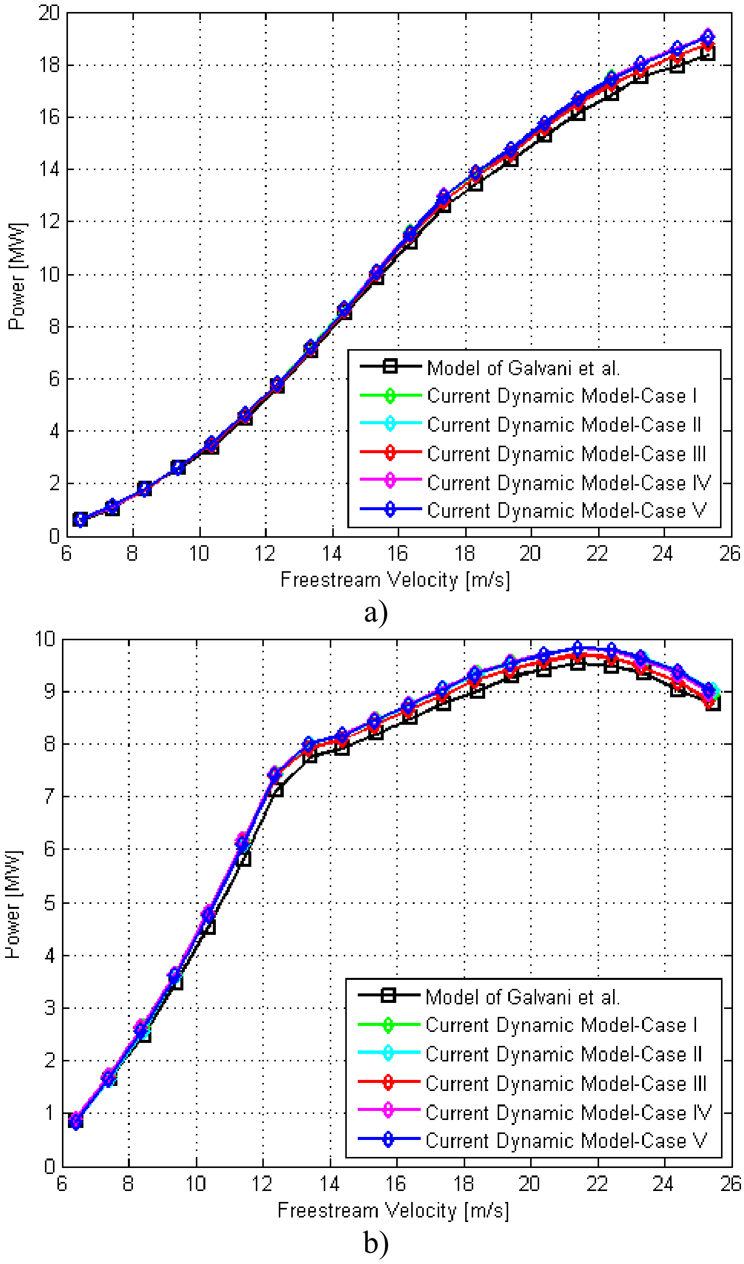

Figure 4-27 The effect of all parameters, a) 4-degree pitch setting, b) -4-degree pitch setting

Furthermore, the Galvani et al. model[76] does not consider the losses at the rotor hub. However, without a hub loss correction model, the turbine rotor is incomplete in an aerodynamical sense. Therefore, it is left as active in the current MS Bladed simulation model. Figure 4-27 shows all the cases together.

Consequently, the difference is a combination of more than one parameter. The most dominant effect on power output is the selected blade element number. When the blade number is increased to around 100, both models give almost the same power outputs. This is very clear that dividing the blade into 68 elements gives a power output between the reference case and Galvani et al. model[76] predictions. However, the blade element number has been kept as 17 in the current thesis study because the increase in blade element number requires more computational power. In addition, the developed MS bladed model is not the same as the Galvani et al. model[76] due to different properties and settings. Moreover, the developed MS Bladed model includes transformation matrices and extra correction models. All these add more complexity, therefore a more computational power. Finally, the difference between power outputs of both models also depends on how the turbine blades are divided into elements, how the integration for the thrust and torque are carried out throughout the blade span and whether the airfoil distributions are carefully taken into account or not. Due to all of above, a minor difference in power output of both models appears at high freestream velocities, while almost no difference is seen at low freestream velocities.

4.4.1 Extraction of Cp and C_T Surfaces from the Turbine Model

For the variable speed operation of wind turbines, Cp-TSR-Pitch surface (or shortly Cp surface) is required to be extracted from the MS Bladed simulation (aerodynamic) model. Here, this is carried out by running the aerodynamic model at various blade pitch angles and different TSR values at the wind speed of 8 m/s.

The Cp surface is particularly important to design the generator torque controller that adjusts the generator electromagnetic torque for operating the turbine rotor at variable rotor speeds due to the varying wind speeds.

Besides, C_T-TSR-Pitch surface (or shortly C_T surface) is also obtained from the developed MS Bladed model during the Cp surface extraction. These surfaces and their contours are seen in Figure 4-28 and Figure 4-29.

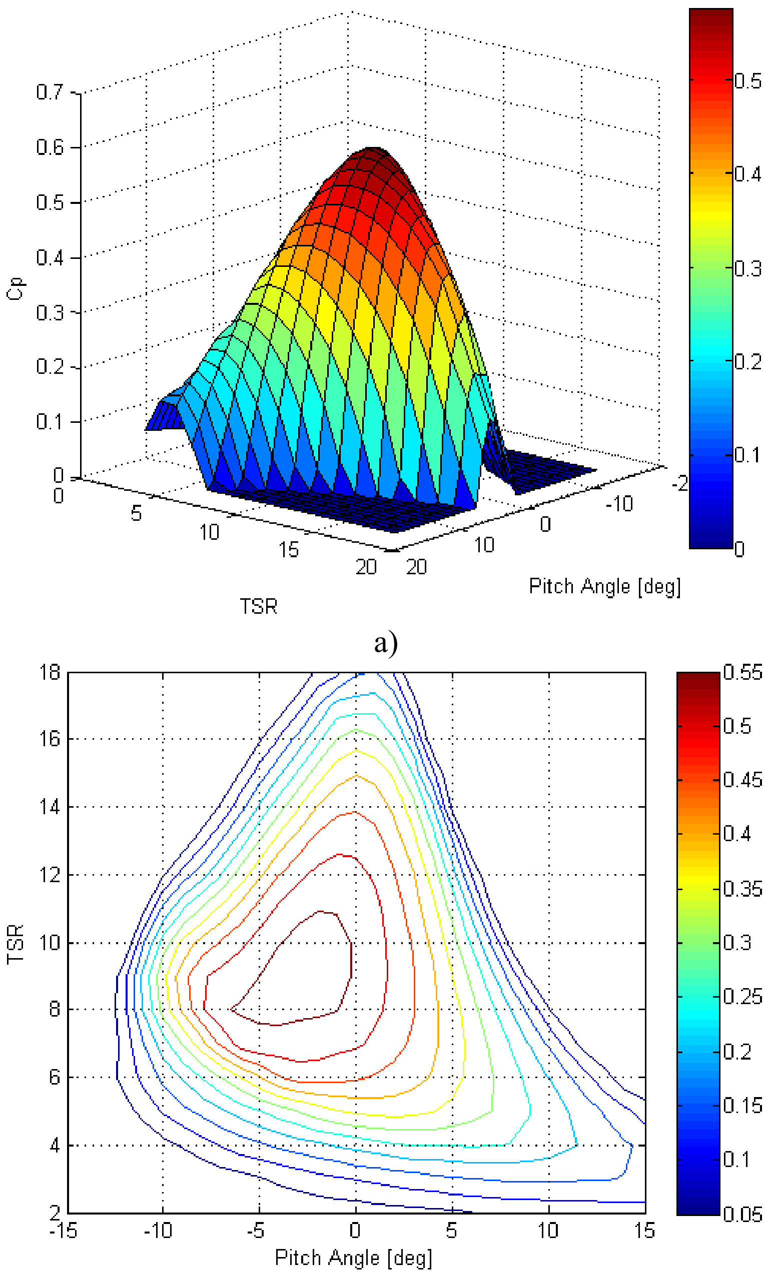

a)

Figure 4-28 Cp surface and its contours, a) Cp surface, b) Cp contours

.

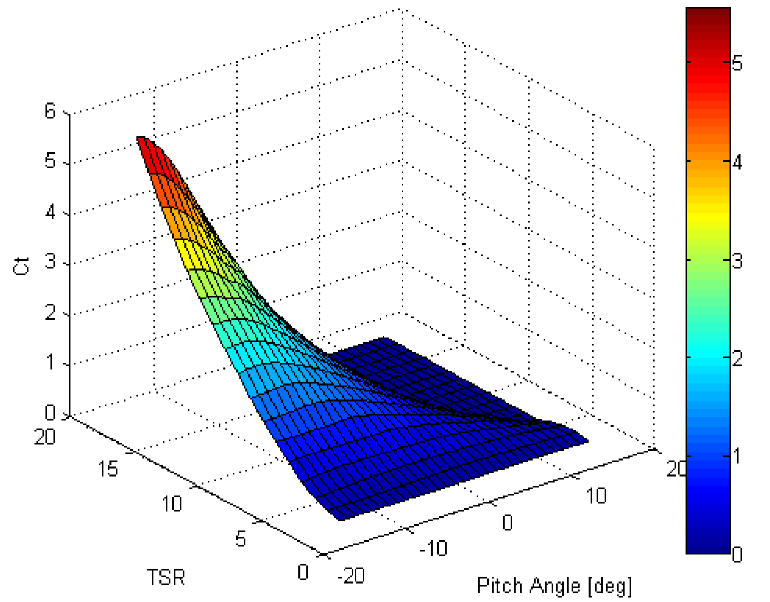

a)

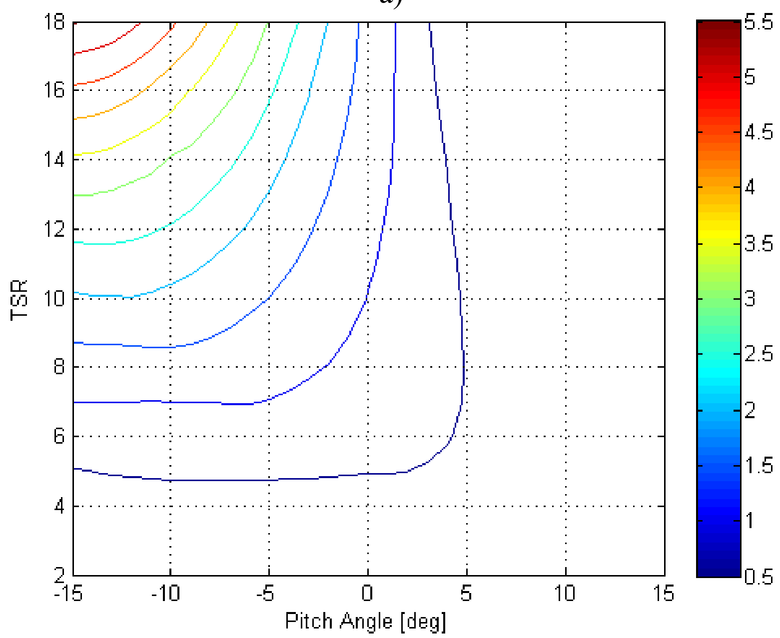

b)

Figure 4-29 C_T surface and contours, a) C_T surface, b) Ct contours

The theory, implementation, and simulation results for the standard generator torque controller designed in this thesis study are extensively investigated in Chapter 5. Here, the negative C_p and C_T values of the extracted surfaces are ignored since negative values of these coefficients state that the turbine generator operates as if it were a motor which draws the electrical energy from the grid[14]. Therefore, this operation of wind turbines is not interesting here for the design of generator torque controller.

In order to extract Cp and C_T surfaces, the rotor speed and blade pitch angles have been varied in such a way that the values of TSR and blade pitch angle are respectively ranging from 2 to 18 and -15 to 15 degrees by an increment size of 1. Such an operation of the current MS Bladed turbine model have eventually resulted in a Cp surface with a peak or C_{pmax} of 0.5741. This value corresponds to a TSR value of 9 and a pitch angle of -2 degrees. The TSR and blade pitch angle that correspond to C_{pmax} value are referred to as the optimum TSR and optimum blade pitch angle or fine pitch angle, respectively. For the same turbine with no precone and tilt angles, Galvani et al.[76] has obtained a C_{pmax} value of 0.5515 that corresponds to an optimum TSR value of 9.0713 and an optimum blade pitch angle of -2.5 degrees. This indicates that Galvani et al.[76] has used different increment sizes for the TSR and the blade pitch angle during the Cp surface extraction. Here, the main reason for obtaining a larger C_{pmax} is due to the adopted settings in the current MS Bladed model such as the blade element number, convergence tolerance criterion etc. It also depends on how the blades are divided into elements, whether the airfoil distributions are taken into account carefully or not, how the integration of elemental forces and moments are realized throughout the blade span. Increment sizes for the TSR and blade pitch angle are also other factors effecting the approximate C_{pmax}. The lower the increment sizes for the TSR and blade pitch angle, the more accurate C_{pmax} and the optimum values can be extracted from the MS Bladed simulation model. Nevertheless, both models give approximately the same optimum TSR and a closer blade pitch angle for the selected increment size of 1. These values are shown in Table 4-3.

Particularly, it is experienced that a less accurate estimation of the optimum TSR value from the model corresponds to a less accurate C_{pmax}. This may result in a situation that a more accurate C_{pmax} of the turbine may appear during the generator torque controller simulations. This situation is caused by the rotor speed variation, causing a change in TSR value due to a changing wind speed. If a step change in wind speed is applied to the controlled MS Bladed turbine model, the generator torque controller varies the generator torque, and therefore the rotor speed in order to obtain the optimum TSR. During the transient response of C_p, there appears a rotor speed giving a TSR value that gives a more accurate C_{pmax} than the estimated value from the turbine model, i.e Cp Surface. This situation occurs due to the fact that the obtained C_{pmax} is less accurate. In such a case, the better way is to reobtain a more accurate C_{pmax} by increasing the resolution for the TSR and blade pitch angle during the Cp surface extraction.

Until now, five different wind turbines have been modeled and the model validations are carried out using the experimental data and program/model power predictions. The reasons for the differences in power outputs have been defined as much as possible for every wind turbine. For the first four turbines, the critical axial induction factor, a_c, is chosen as 0.37 that corresponds to the blue-colored empirical line in the turbulent wake state (Figure 2-7). However, for NREL 5 MW turbine, this critical value had to be changed into 0.2 in order to obtain/validate the turbine model once again with the power predictions of Galvani et al. model[76]. This change is carried out here due to the fact that Galvani et al.[76] has used a different critical axial induction factor, 0.2. This corresponds to a different empirical line shown in cyan color (Figure 2-7). Figure 4-21-Figure 4-23 show the comparison of power outputs of NREL 5 MW turbine with those of Galvani et al. model[76] both considering zero precone and tilt angles.

Table 4-3 Estimated and calculated parameters from different simulation models

	Simulation Model	a_c	C_{pmax}	λ_*	β_*	K_g
Galvani et al.	Model of Galvani et al.	0.2	0.5515	9.0713	-2.5	1410000
Sahin	MS Bladed Model	0.2	0.5741	9	-2	1503900
Galvani et al.	FAST Simulation Model	-	0.48698	7.422	-0.25	2274600

During the development of their model, Galvani et al.[76] has compared the values of some important parameters such as C_{pmax}, optimum TSR and blade pitch angle etc. obtained from their model and those obtained from the FAST simulation model, rather than comparing the predicted power outputs at various wind speeds. Here, FAST (Fatigue, Aerodynamics, Structure and Turbulence) is a simulation model developed by NREL and a widely used simulation tool for HAWTs. It can simulate two or three-bladed conventional HAWTs with rigid and flexible structures. It includes 24 degrees of freedoms, six of which are related to off-shore wind turbines. It is also possible to simulate small wind turbines with rotor-furling, tail aerodynamics etc.[88].

As parameters, Galvani et al.[76] has compared the maximum C_ps, optimum TSRs, optimum blade pitch angles, rotor speeds and lastly generator torque controller gains (Table 4-3). In addition, they have also compared C_p versus blade pitch angle at various TSR values. For the selected parameters in Table 4-3, their investigations show that their model gives quite different results from those of FAST simulation model. They have stated that these differences are derived from the simplicity of their model, compared to the FAST simulation model. Thus, they remarked the importance of FAST simulation model usage for wind turbines. However, these differences are not mainly about the model simplicity. Those are primarily caused by the usage of different empirical correction models for the turbulent wake state (Figure 2-7) where the BEM theory becomes invalid. This is explained further in this chapter with Figure 4-30-Figure 4-32. As seen in Table 4-3, the results of Galvani et al. model[76] and the results obtained from the current MS Bladed simulation model are closer to each other. This is because of the fact that both models use the same empirical model that corresponds to a_c of 0.2(Figure 2-7). However, they are quite different from those of the FAST simulation model obtained by Galvani et al.[76].

Different estimation of C_{pmax} and optimum TSR from the current MS Bladed model has resulted in a different torque controller gain, K_g (Table 4-3) from that of the Galvani et al. model[76], both of which are calculated by equation (5-2). This gain difference produces slightly different optimum operational lines. An optimum operational line indicates how much torque is required from an electrical generator at different generator speeds in order to operate the turbine rotor at C_{pmax} so that the maximum electricity can be generated in the below rated region or Region 2.

Appendix B Figure B.1 shows the above-mentioned operational lines as well as others. The solid black operational line corresponds to the curve using the gain, K_g of Galvani et al.[76], whereas the blue-dashed curve, just above the solid black one, is obtained using the gain, K_g obtained from the current MS Bladed model.

Note that using both equations (5-1) and (5-2) produces an optimum operational line, which indicates the required generator torque as a function of rotor speed, i.e. measured generator torque on the rotor shaft, LSS of the gearbox. Therefore, the operational line corresponds to the optimum generator torque quantity on the rotor shaft for the maximum power generation in Region 2. In this thesis study, equations (5-1) and (5-2) are used for generator torque controller designs. Therefore, the rotor speed and generator torque are obtained from the LSS of the gearbox. Thus, the operational lines in Appendix B Figure B.1 are obtained by taking into the consideration of gearbox effect, N_{gear} to express them in terms of generator speed and generator torque measured from HSS of the gearbox.

Since the current MS Bladed and Galvani et al.[76] models become equivalent after the deactivation of some features such as tilt, precone and yaw angles in the current MS Bladed model, a closer C_{pmax} and therefore the optimum TSR values are obtained at closer blade pitch angles. Thus, the calculated generator torque controller gains and the operational lines in Appendix B Figure B.1 are very close to each other. However, both controller gains (Table 4-3) and therefore the operational lines are lower than the one obtained by Galvani et al.[76] using the FAST model, the red curve in Appendix B Figure B.1. In addition, using FAST simulation model, Jonkman et al.[87] has obtained a gain K_g value less than that of Galvani et al.[76], resulting in a slightly lower optimum operational line for 5 MW turbine as shown in Appendix B Figure B.1.

Appendix B Figure B.1 shows six different operational lines obtained using the current, Galvani et al. and FAST simulation models for the same turbine. The reason for the difference between the current MS Bladed and Galvani et al.[76] models, both having the same a_c of 0.2, has been explored above. However, the potential reason behind the difference between the optimum lines obtained by Galvani et al.[76] and

Jonkman et al.[87] (the red and green operational lines, respectively) should be investigated since those line are obtained using the same FAST simulation model.

Due to the following reasons, the critical axial induction factor, a_c of 0.2 has to be changed back to 0.37, which corresponds to a different empirical line in turbulent wake state (Figure 2-7).

- First of all, the empirical curve (cyan) that corresponds to a_c of 0.2 predicts a higher C_{pmax}, a higher TSR value and therefore a low generator torque controller gain, K_g. Appendix B Figure B.4 shows the controlled power curves based on the estimated maximum C_p of 0.5741, optimum TSR of 9 and blade pitch angle of -2 degrees when the current MS Bladed model uses a_c of 0.2. As seen from the results, there is a quite large difference between the controlled power output of the current MS Bladed model and that of the FAST simulation model in the below-rated region, where the generator torque controller is designed based on Cp surface. Besides, Appendix B Figure B.5 gives generator speed versus torque controller output according to estimated values (Table 4-3) from the Cp surface in Figure 4-28 as well as the designed Region 2.5 transitional torque controller.
- Galvani et al.[76] does not use their estimated controller gain, K_g, and therefore the operational line during the generator torque controller design. Instead, they use the one obtained by Jonkman et al.[87], which is not a correct application. This is probably the main reason why they have obtained a similar controlled power curve to that of the FAST simulation model (Appendix B Figure B.4)
- In addition, the empirical curve (Figure 2-7) that corresponds to a_c of 0.37 gives closer results to those of FAST simulation model. This is explained later in this subchapter.
- Lastly, the developed MS Bladed simulation model should be consistent with the previous model since it is validated against the experimental power outputs of NREL Phase II and III turbines as well as the PROPID power predictions for the NREL Phase VI turbine with baseline and extended blades.

Therefore, NREL 5 MW turbine model with inactivated precone and tilt angles is also operated with the critical axial induction factor, a_c of 0.37, while keeping every other settings same in the model. Figure 4-30-Figure 4-32 show the effect of changing a_c from 0.2 to 0.37 or changing the empirical models.

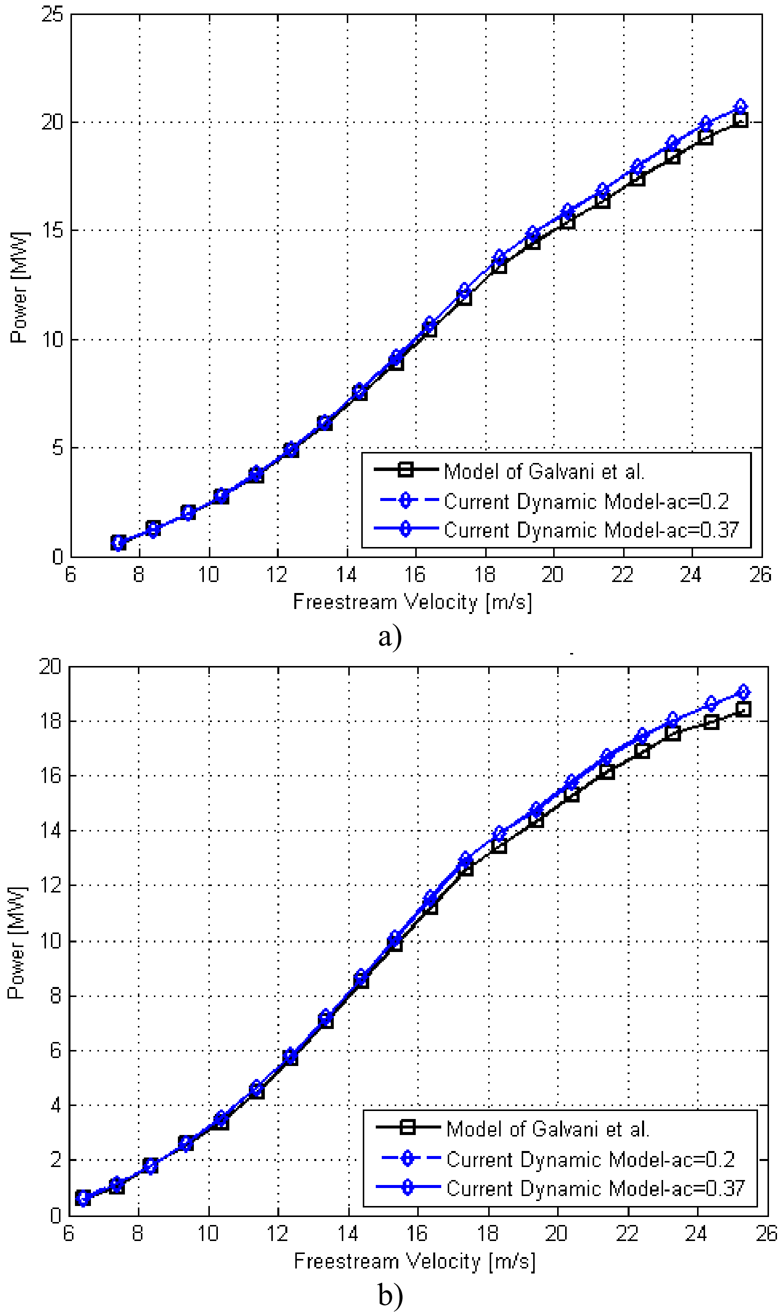

Figure 4-30 Power output comparisons with a_c of 0.37, a) 6-degree pitch setting, b) 4-degree pitch setting

As seen from the results in Figure 4-30 and Figure 4-31-a, there is no effect of changing the a_c on power predictions at high positive pitch angles, but the effect starts appearing at the low positive blade pitch angles close to zero at low freestream velocities. At negative blade pitch angle and low freestream winds, the effect is seen clearly.

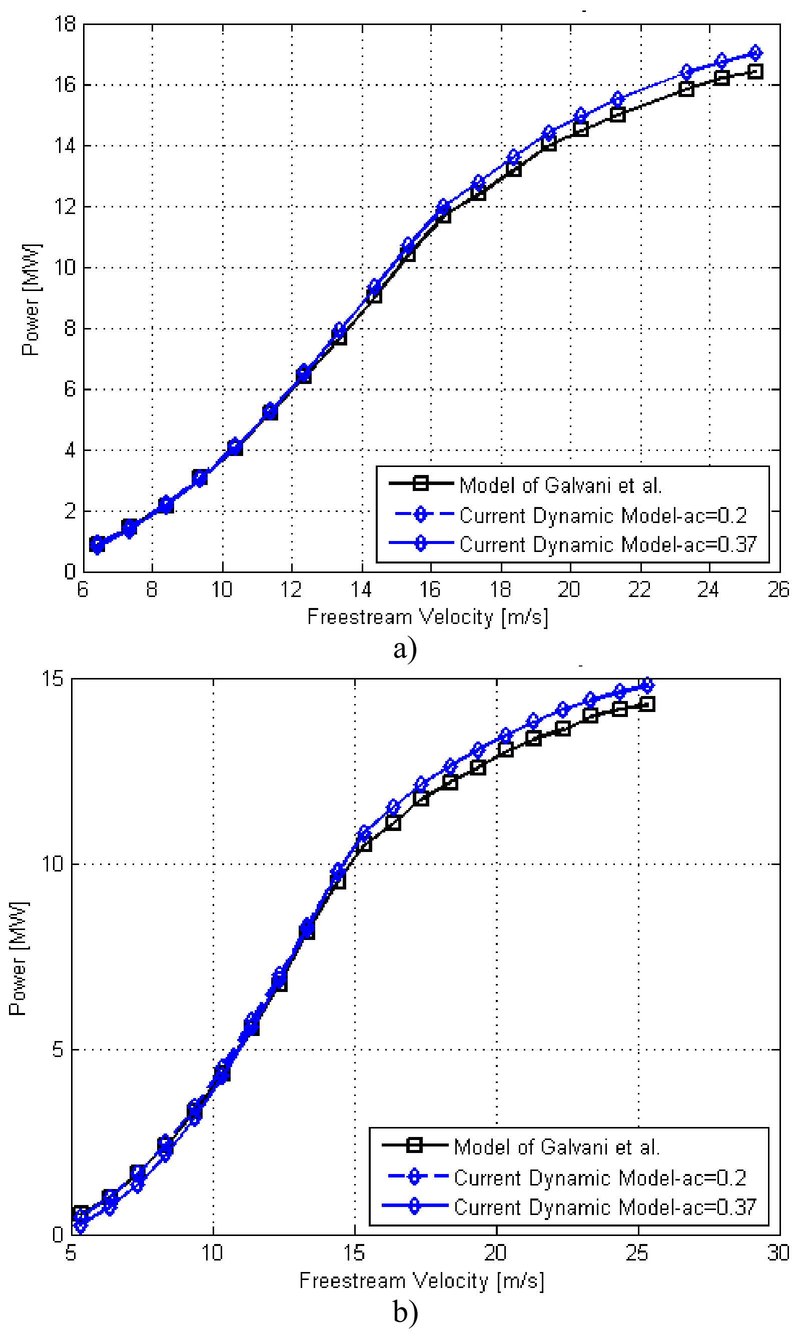

Figure 4-31 Power output comparisons with a_c of 0.37,
a) 2-degree pitch setting, b) 0-degree pitch setting

Therefore, Spera's correction with a_c of 0.2 or 0.37 gives the same results at pitch angles of 6, 4 and 2 degrees. However, the power outputs at low freestream velocities start deviating from the previous results at low pitch angles of 0, -2 and -4 degrees.

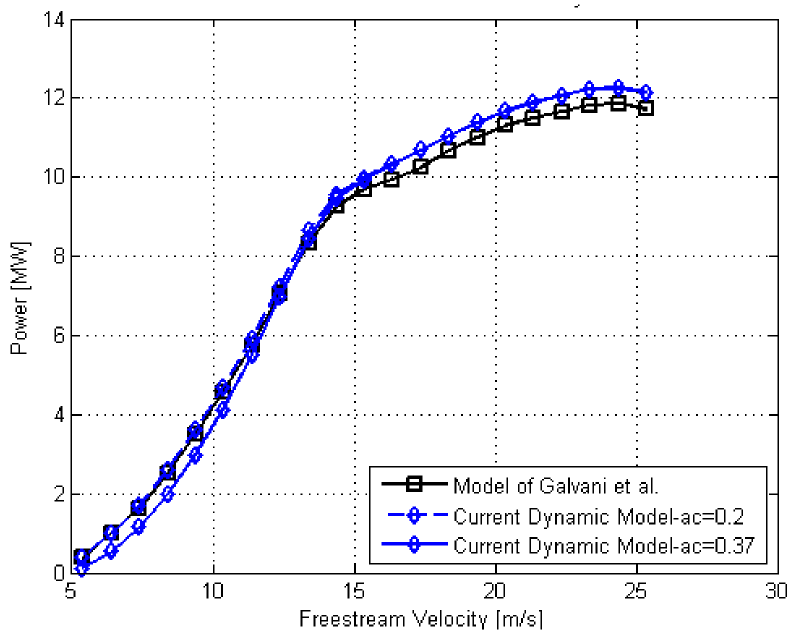

a)

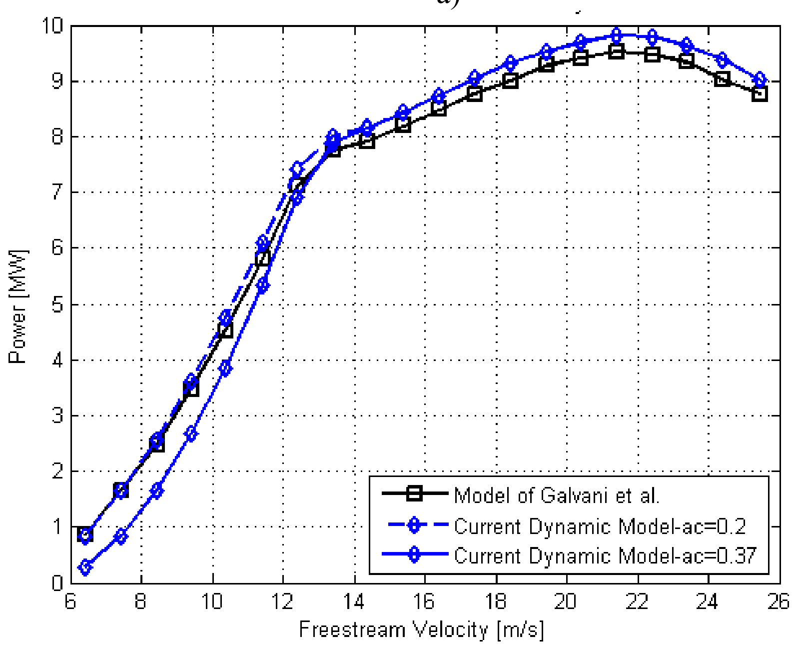

b)

Figure 4-32 Power output comparisons with a_c of 0.37,
a) -2-degree pitch setting, b) -4-degree pitch setting

The more negative the blade pitch angle, the more deviations in power outputs from the current MS Bladed model with a_c of 0.2 appear and shift to the higher freestream velocities. The fact that both models provide the same results at all freestream velocities at the selected pitch settings show that both models run in the windmill state (Figure 2-8-b). Whereas, at low pitch angles and low wind speeds, the current MS Bladed model with a_c of 0.2 and 0.37 operate in turbulent wake state region where different corrections (Figure 2-7) are applied to the BEM theory. Therefore, they predict very different power outputs depending on the utilized empirical correction models.

In addition, Figure 4-33-a shows a comparison of C_p versus blade pitch angle at two different TSR values. These results belong to the current MS Bladed model with a_c of 0.2 and 0.37, Galvani et al. model[76] with a_c of 0.2 and lastly the FAST model obtained by Galvani et al.[76]. Figure 4-33-a shows the results at a TSR of 5.7727, whereas Figure 4-33-b shows the results at a TSR of 7.422. As seen from the Figure 4-33-a, all four predictions of four models are almost the same because the turbine rotor operates in the windmill state. However, when the turbine starts operating in the turbulent wake state(Figure 4-33-b), there appear some differences in predictions. This difference is caused by the usage of different empirical models for the turbulent wake state. The current MS Bladed and Galvani et al.[76] models with a_c of 0.2 provide expectedly similar results. FAST simulation model and the current MS Bladed model with 0.37 produce closer results to each other. However, the Galvani et al.[76] and the current MS Bladed model with a_c of 0.2 differ quite from those of the current MS Bladed model with a_c of 0.37 and FAST model. Therefore, the prediction of the current MS Bladed model with a_c of 0.37 is much better than that of the current MS Bladed model with a_c of 0.2. This is one other important factor forcing to utilize 0.37 as the critical induction factor, a_c.

As mentioned previously in subchapter 4.4, and given in Table 4-1, the number of blade elements used by Galvani et al.[76] is 100. This indicates that Galvani et al.[76] has tried to obtain similar results to those of FAST simulation model. Therefore, they probably increased the blade element number to 100 due to its larger effect on power, and therefore on the turbine C_p, compared to other variables such as convergence tolerance etc.

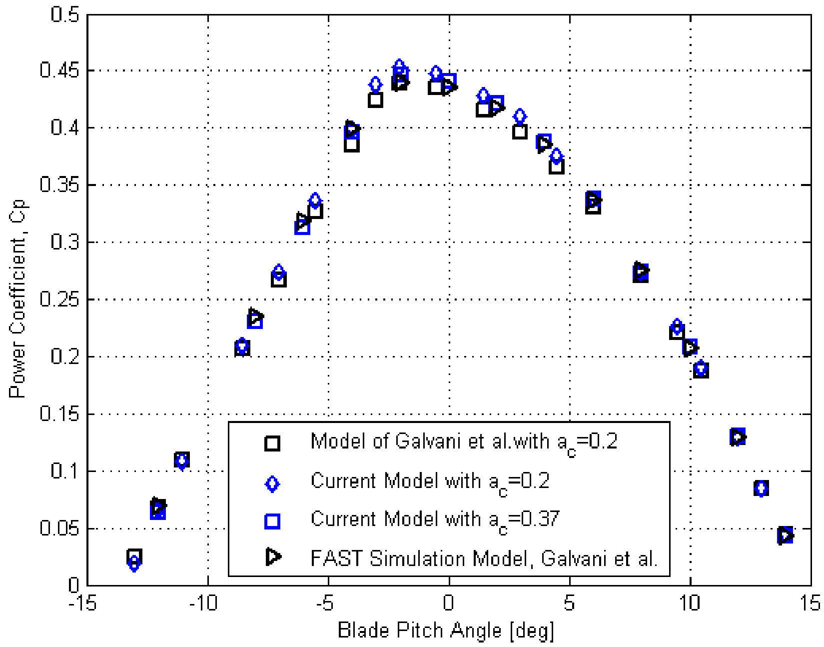

a)

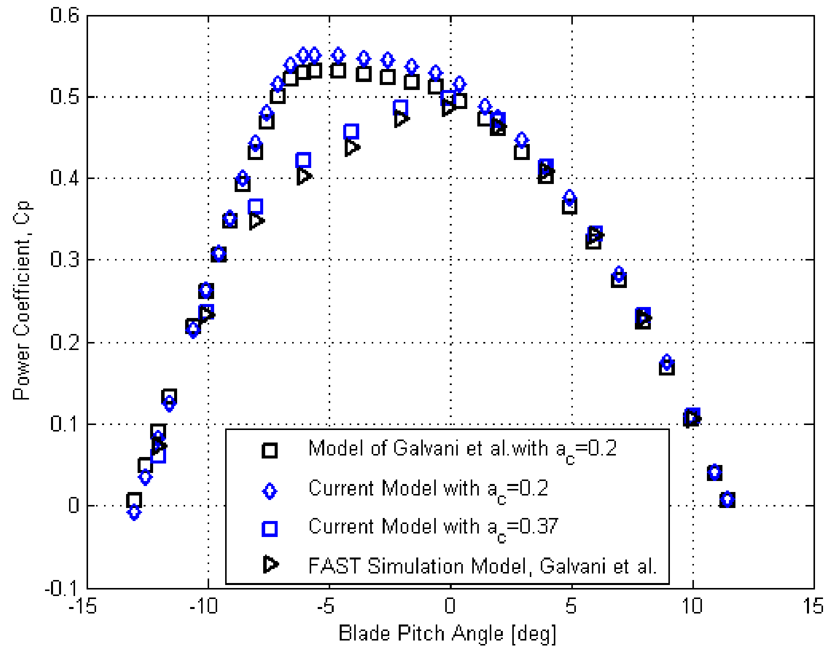

b)

Figure 4-33 Power coefficient versus blade pitch angle,
a) TSR of 5.7727, b) TSR of 7.422

Nevertheless, due to the usage of different empirical models in Galvani et al.[76] and FAST models, they could not achieve closer results to each other. In addition, the original blade element data for NREL 5 MW wind turbine blade are given at 17 different nodes which FAST model and the current MS Bladed model are employed as.

Consequently, the current MS Bladed and Galvani et al. [76] models with a_c of 0.2 gives closer results to each other. However, they both do produce different $C_{pmax}s$, TSRs, and therefore different controller gains, K_g, compared to a highly advanced turbine simulation model, FAST. However, choosing the a_c as 0.37 gives closer results to those of FAST simulation model. For the turbulent wake state, Both Galvani et al. [76] and the current MS Bladed models use the Spera's correction formula. However, FAST simulation model uses Buhl correction formula[55], which is a modified Glauert correction[60]. Because of employing different empirical corrections, there is a slight difference in the estimated results by FAST model and the current MS Bladed model with a_c of 0.37. Nevertheless, the obtained results are quite satisfactory in the sense of obtained C_p versus blade pitch angle in Figure 4-33. Eventually, due to the different empirical corrections, there appear some differences in the C_{pmax} of the turbine. This is also expected for C_T of the turbine according to Figure 2-7.

Therefore, the new Cp and C_T surfaces for NREL 5 MW turbine with no precone and tilt angles are obtained again from the current MS Bladed model with a_c of 0.37. With the new empirical model, both Cp and C_T surfaces have considerably changed. These are respectively shown in Figure 4-34 and Figure 4-35.

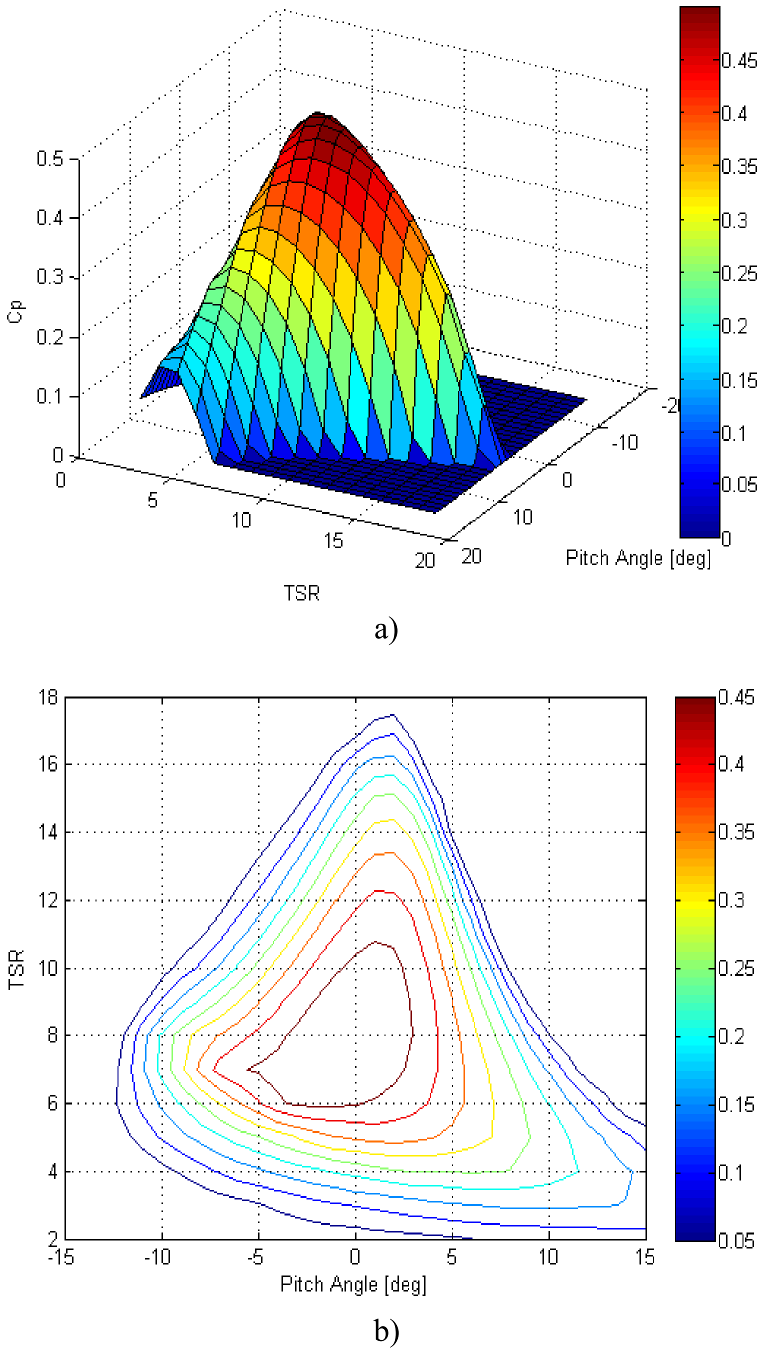

Figure 4-34 Cp-TSR-Pitch surface, a) Cp surface, b) Cp contours

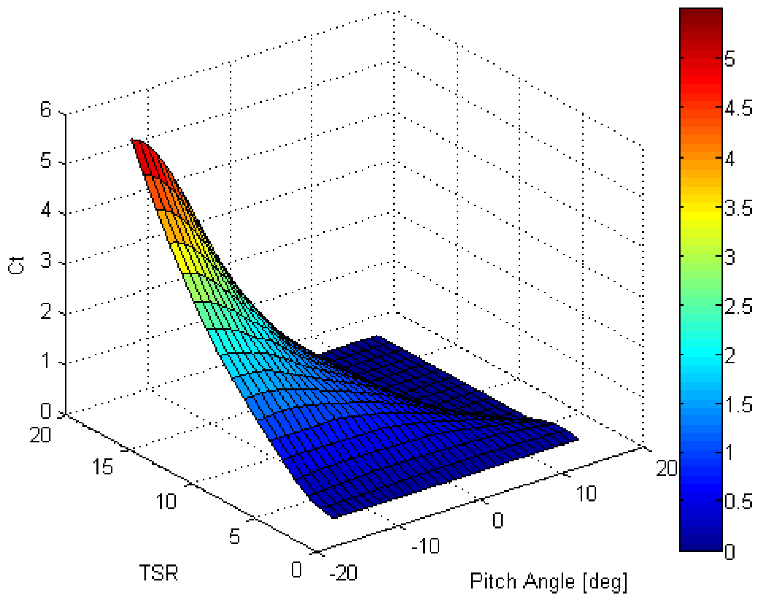

a)

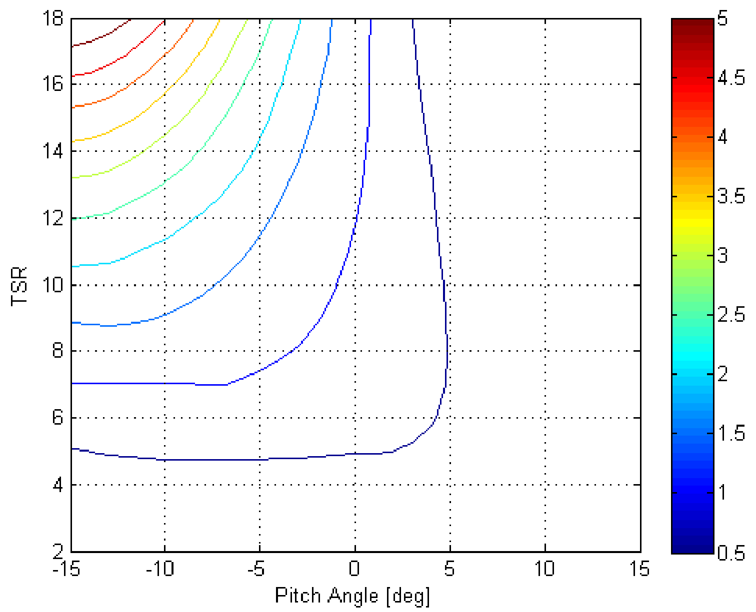

b)

Figure 4-35 C_T surface and contours, a) C_T surface, b) C_T contours

From the new Cp surface, the new values for C_{pmax}, optimum TSR and blade pitch angle are respectively obtained as 0.4984, 8 and 0 degrees. These new results are obtained when the blade pitch angle and TSR are varied respectively with the previous increment sizes of 1. This operation of the currently developed MS Bladed model with

a_c of 0.37 gives closer results to those obtained using the FAST simulation model by Galvani et al.[76]. Further, these new results are also closer to the ones obtained by Jonkman et al.[87]. using the FAST simulation model during the development of 5 MW wind turbine. Table 4-4 gives extra new results along with the previous results in Table 4-3.

Table 4-4 Estimated and calculated parameters from different simulation models

	Simulation Model	a_c	C_{pmax}	λ_*	β_*	K_g
Galvani et al.	Galvani et al. Model	0.2	0.5515	9.0713	-2.5	1410000
Sahin	MS Bladed Model	0.2	0.5741	9	-2	1503900
Sahin	MS Bladed Model	0.37	0.4984	8	0	1858900
Galvani et al.	FAST Model	-	0.48698	7.422	-0.25	2274600
Jonkman et al.	FAST Model	-	0.482	7.55	0	2138800

As seen in Table 4-4, the estimated values using the FAST simulation model, C_{pmax}s, corresponding TSRs and blade pitch angles obtained by the Galvani et al.[76] and Jonkman et al.[87] , are slightly different from each other. Therefore, the small difference in TSR value has fairly effected the controller gain, K_g, which has resulted in different operational lines (Appendix B Figure B.1). The slight difference in between the results of Galvani et al.[76] and Jonkman et al.[87] using the same FAST simulation model is probably caused by the selected increment sizes for the TSR and blade pitch angle or the utilized method during Cp surface extraction because Galvani et al.[76] has identified in their article[76] that the peak of Cp surface is around a TSR of 7.5 and a blade pitch angle of 0 degree, which are very close to the ones obtained by Jonkman et al.[87]. Afterward, they have performed an analysis with higher resolution for the C_{pmax} of 5 MW wind turbine. This analysis has given the C_{pmax} of 0.48698, a TSR of 7.422 and a blade pitch angle of -0.25 degree.

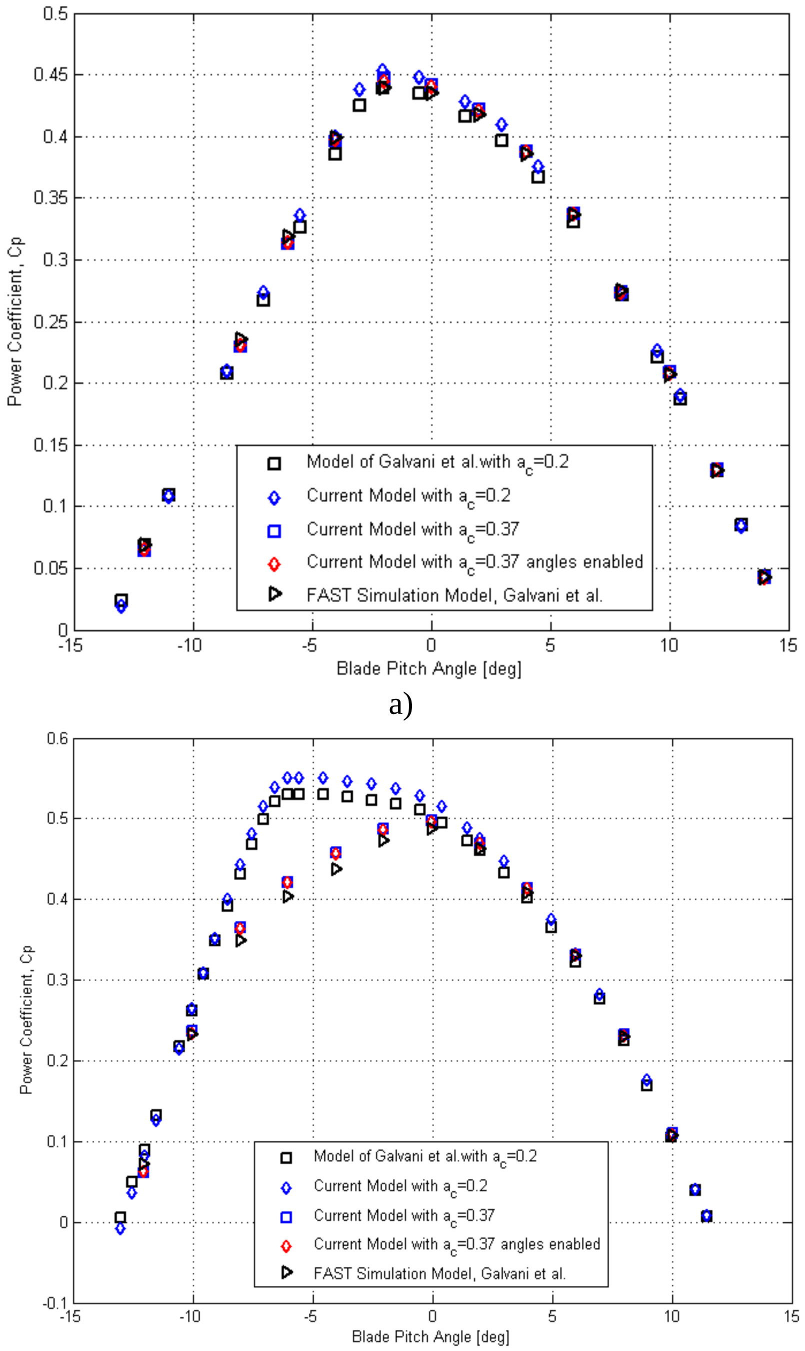

a)

b)

Figure 4-36 Power coefficient versus blade pitch angle,
a) TSR of 5.7727,b) TSR of 7.422

Galvani et al.[76] does not state anything about whether the precone angle and tilt angle of NREL 5 MW wind turbine were active or not during the comparison of their model predictions with those of the FAST simulation model. However, Galvani et. al (Personal Communication, Jan 9, 2018) has obtained these closer results to the results of Jonkman et al.[87] for NREL 5 MW turbine with precone and tilt angles enabled. NREL 5 MW turbine designed by Jonkman et al.[87] has also the properties of precone and tilt angles. According to the Jonkman[68], different obtainment for these values is possible due to different settings or post-processing etc. Jonkman[68] has also stated that the effect of precone and tilt angles on C_{pmax}, TSR and blade pitch angles are expected to be small. Slightly different estimation of TSR values may result in different optimum operational lines due to inverse cubic relation of TSR with the controller gain, K_g in equation (5-2).

Therefore, since the current MS Bladed model is more complex than Galvani et al. model[76], the precone of 2.5 degrees and tilt angle of 5 degrees are activated to examine their effects on the power coefficient versus TSR. The results obtained from the current MS Bladed model for NREL 5 MW turbine with 2.5-degree precone and 5-degree tilt angles are given with the red diamonds in Figure 4-36-a and b. As seen in Figure 4-36, a 2.5 degree-precone and a 5-degree tilt angle have a very slight effect on TSR versus blade pitch angle curve. This supports the above explanation of Jonkman and therefore may be assumed as negligible. Therefore, the difference between the results of Jonkman et al.[87] and Galvani et al.[76] using the FAST simulation model has been probably caused by the different settings, post processing as stated by Jonkman[68]. Another potential reason may be the selected increment size for the TSR and blade pitch angle during the Cp surface extraction.

As mentioned previously, it is important that obtaining C_{pmax} value, and therefore the optimum TSR and blade pitch angle as more accurate as possible appears to be important during the simulation of generator torque controller. Especially, more accurate TSR estimation that corresponds to C_{pmax} is particularly important since an unexpected larger C_p value than the estimated C_{pmax} may show itself during the transient response of C_p to an increasing step wind input. It is experienced that even a difference with the order of magnitude 10^{-4} in value of C_{pmax} has shown itself during the simulation. This has occurred due to the fact that the rotor speed increases to an increasing step wind input, which changes turbine TSR.

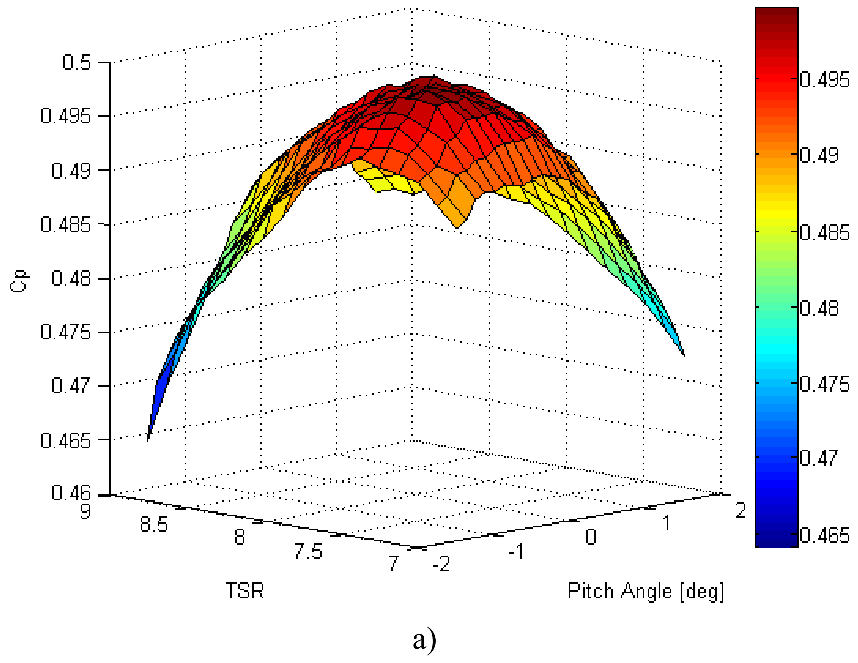

Figure 4-37 Upper part of the Cp surface, a) Cp surface, b) Cp contours

During the transient response of C_p, there appears a short time interval for the rotor speed giving a more accurate optimum TSR at that adjusted optimum blade pitch angle. This gives a more accurate C_{pmax} during the generator torque controller simulation. Simulation results are given in Appendix B to a step wind increase and decrease (Figure B.2-a) at the optimum pitch setting of zero degree (Figure B.2-b) in terms of C_p, rotor speed, TSR(Figure B.3). These simulation results are obtained when the generator torque controller designed using the lastly obtained C_{pmax} of 0.4984, and optimum TSR of 8. In Figure B.3-a, the turbine C_p is seen exceeding the estimated C_{pmax} between 53 and 64 seconds. Therefore, there is a more accurate C_{pmax} than the estimated C_{pmax} in Table 4-4 using the current MS Bladed simulation model with a_c of 0.37.

Therefore, the increment sizes both for TSR and blade pitch angles must be decreased in order to find a more accurate C_{pmax}, and therefore a more accurate optimum TSR and a blade pitch angle. Here, the same step size of 1 for TSR and blade pitch angle does not work mainly due to the new correction factor, 0.37, which has a different slope in Figure 2-7. More accurate results are obtained by constraining the region around the peak of Cp surface in Figure 4-34 rather than operating the turbine from TSR of 2 to 18 and -15 to 15 degree pitch angles, which takes a quite large time. Therefore, the constrained region ranges from -1.5 to 1.5 degrees in pitch settings and 7 to 9 in TSR values with the increment size of 0.125. This restricted particular surface (Figure 4-37) is large enough to obtain a more accurate C_{pmax} and optimum TSR as well as blade pitch angle. This is because of the fact that a more accurate C_{pmax} must be located around the previously obtained blade pitch angle of 0 and TSR of 8. Therefore, more accurate results for C_{pmax}, optimum TSR and blade pitch angle are found respectively as 0.4996, 7.5, -0.875 degrees. Now, these new results, particularly TSR, which has caused an exceeding C_p, are very close to those obtained from FAST model by Galvani et al.[76] and Jonkman et al.[87]. The differences, as mentioned above, are caused by the usage of different empirical models in the current MS Bladed and FAST models. Moreover, the torque controller gain, K_g, using the new C_{pmax} and TSR give almost the same optimum operational line as the one obtained by Galvani et al.[76] using the FAST simulation model. The final results obtained from the current MS Bladed model are not expected to be exactly the same as those of FAST model[87] since they use different correction models for the turbulent wake state, but give closer results. In addition, there is a little bit of precone and tilt angles which the FAST model[87] results include. Therefore, the Table 4-5 shows the final values.

Table 4-5 Estimated and calculated parameters from different simulation models

	Simulation Model	a_c	C_{pmax}	λ_*	β_*	K_g
Galvani et al.	Galvani et al. Model	0.2	0.5515	9.0713	-2.5	1410000
Sahin	MS Bladed Model	0.2	0.5741	9	-2	1503900
Sahin	MS Bladed Model	0.37	0.4996	7.5	-0.875	2261500
Galvani et al.	FAST Simulation Model	-	0.48698	7.422	-0.25	2274600
Jonkman et al.	FAST Simulation Model	-	0.482	7.55	0	2138800

To sum up, NREL 5 MW wind turbine is constructed with the use of FAST simulation model, which utilizes the Buhl correction factor. As seen in Table 4-5, the result of the current MS Bladed model using a_c of 0.37 gives closer results to those of FAST simulation model. Galvani et al.[76] has tried to get almost the same results as those of FAST simulation model in terms of maximum C_p, TSR and blade pitch angles. Their reason not to obtain closer results is the simplicity of their model. However, it is due to the usage of different correction models in FAST and their simulation model. As seen above, when a_c of 0.37 is used, closer results to those of FAST model are achieved although the current MS Bladed and FAST models use different correction models.

CHAPTER 5

BASELINE CONTROLLER DESIGNS AND IMPLEMENTATIONS

This chapter focuses on the baseline controller designs and implementations to the operational regions of NREL 5 MW turbine with inactivated tilt and precone angles. Usually, a standard generator torque controller is employed for the below rated region or Region 2 to get maximum power from the turbine. A general block diagram of the turbine system with a generator torque controller is given in Figure 5-1.

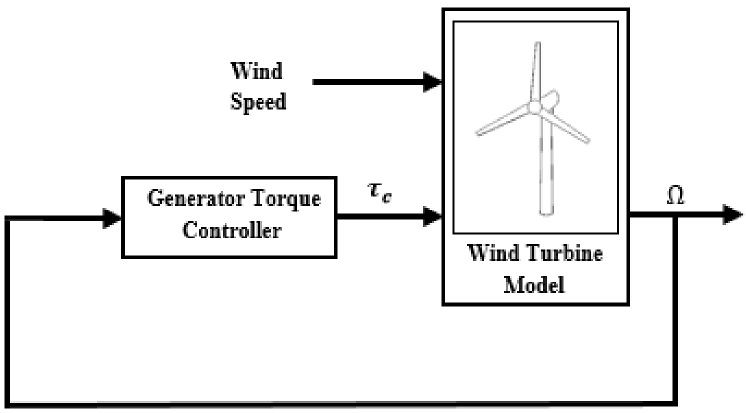

Figure 5-1 Block diagram for generator torque controller

For the above rated region or Region 3, a collective blade pitch controller based on a gain-scheduled Proportional and Integral (PI) strategy is employed in this thesis to regulate the turbine power. The general block diagram of the blade pitch controller with the turbine system model is depicted in Figure 5-2.

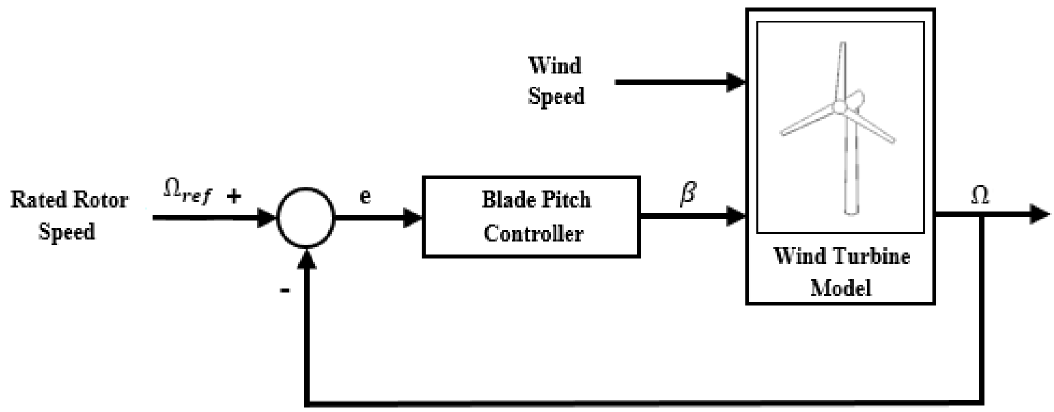

Figure 5-2 Block diagram for blade pitch controller

As seen from the block diagrams in Figure 5-1 and Figure 5-2, the rotor speed is fed back to both controllers. This measurement may be the generator speed (or HSS angular velocity) or the rotor speed (or LSS angular velocity) depending on the designer. However, it is usually the generator speed. The current implementation here uses the rotor speed as feedback to both controllers rather than the generator speed. The switching between the two controllers is carried out dynamically based on generator[36] or rotor speed. In order to realize that, a simple transition region controller referred to as Region 2.5 controller is designed. In addition, there is another transitional region controller referred to as Region 1.5 between Region 1 and Region 2. In the subsequent subchapters, theories and implementations of both controllers to NREL 5 MW turbine are defined, respectively.

5.1 Theory and Design of Baseline Generator Torque Controller for Variable Speed Operation

This subchapter focuses on the standard generator torque controller design using the Ref.[5][14][76] and its implementation to NREL 5 MW turbine. The adopted torque controller utilizes the rotor speed as feedback. Therefore, the control torque, τ_c corresponds to the torque produced by the generator on the rotor shaft, i.e. LSS of the gearbox. Here, the controller is a nonlinear controller and is defined as[5],

$$\tau_c = K_g \Omega^2 \tag{5-1}$$

where Ω and K_g are the rotor speed and the controller gain, respectively. The gain K_g is obtained by the equation (5-2)[14].

$$K_g = \frac{1}{2}\rho A R^3 \frac{C_{pmax}}{\lambda_*^3} \tag{5-2}$$

where ρ is the air density, A rotor disk area, R rotor radius, C_{pmax} maximum power coefficient, λ_* is the optimum TSR that corresponds to the C_{pmax}. The equations for TSR and C_p are respectively given by equations (2-28) and (2-14)[12] [14].

$$\lambda = \frac{\Omega R}{U} \tag{2-28}$$

$$C_p = \frac{P}{P_{wind}} \tag{2-14}$$

where U and P, are wind speed and the power produced by the turbine, respectively. On the other hand, P_{wind}, represents the power available in wind. Wind power is calculated as follows[12] [14].

$$P_{wind} = \frac{1}{2}\rho U^3 A \tag{2-15}$$

Using equation (2-14) and (2-15), equation (5-3) is derived to calculate the turbine aerodynamic power.

$$P = \frac{1}{2}\rho U^3 A C_p \tag{5-3}$$

Turbine aerodynamic power may also be calculated from the equation (5-4)[5].

$$P = \tau_{aero}\Omega \tag{5-4}$$

As stated before, the pitch angles of the turbine blades are set to the optimum pitch angles. This is shown by the equation (5-5).

$$\beta = \beta_* \tag{5-5}$$

As constructed before, the dynamic model of the turbine is basically represented by equation (3-58).

$$J_t\dot{\Omega} = (\tau_{aero} - \tau_c) \tag{3-58}$$

where τ_{aero} is the rotor aerodynamic torque,τ_c control torque, i.e produced by the generator, and J_t the total moment of inertia of the turbine system which includes the inertias of the turbine rotor and generator. Using equations (3-46), (5-3) and (5-4), the rotor torque τ_{aero} is obtained as,

$$\tau_{aero} = \frac{1}{2}\rho A U^2 R \frac{C_p}{\lambda} \tag{5-6}$$

When the rotor torque (τ_{aero}) equation (5-6), and equations (5-1) and (5-2), which are used to obtain control torque, τ_c are plugged into the equation (3-58), and then realizing some algebraic manipulations give the equation (5-7). This equation is used to find the rotor acceleration[5].

$$\dot{\Omega} = \frac{1}{2J_t}\rho A R^3 \Omega^2 \left(\frac{C_p}{\lambda^3} - \frac{C_{pmax}}{\lambda_*^3}\right) \tag{5-7}$$

In equation (5-7), as the total moment of turbine inertia, J_t, air density, ρ, the area swept by the rotor, A, rotor radius, R, and rotor speed, **Ω**, are to be always positive. For rotor acceleration to be positive or negative depends on the expressions in parenthesis, or on the following conditions[5].

I. If $\lambda > \lambda_*$, then $C_p \leq C_{pmax}$, the rotor acceleration is negative. Thus, rotor speed decreases until the rotor TSR, λ, becomes equal to the optimum TSR, λ_*. When the equality, $\lambda = \lambda_*$, is satisfied, the rotor is kept running at the reached rotor speed until the wind speed changes.

II. If $\lambda < \lambda_*$ and $C_p > \frac{C_{pmax}}{\lambda_*^3}\lambda^3$, rotor acceleration becomes positive and therefore the rotor starts accelerating until it reaches at the optimum TSR. When the equality, $\lambda = \lambda_*$, is obtained, the rotor turns constantly at reached rotor speed.

The inequality in condition II may be defined by a function, *N,* which depends on the TSR, λ. This is given by equation (5-8)[5].

$$N = \frac{C_{pmax}}{\lambda_*^3}\lambda^3 \tag{5-8}$$

The derivation of the above theory for the generator torque controller is defined in general. Therefore, when the theory is extended to include rotor precone and nacelle tilt angles considering no yawed operation, the following relations are derived. The generator torque controller gain, K_g, in equation (5-2) turns out to be as follows.

$$K_g = \frac{1}{2}\rho\pi(R\cos\Phi)^5 \frac{C_{pmax}}{\lambda_*^3} \tag{5-9}$$

Therefore, the controller gain, K_g depends on turbine rotor precone angle, Φ, which reduces the rotor disk area, and the optimum TSR, λ_* and C_{pmax}, which are obtained from the simulation model with preconed and tilted rotor. The TSR of turbine with above properties, i.e. precone and tilt angles and without yaw angle effect is calculated by equation (5-10) rather than equation (3-46), which does not includes the effects of precone and tilt angles[68].

$$\lambda = \frac{\Omega R\cos\Phi}{U\cos\theta} \tag{5-10}$$

Besides, the power produced by the turbine is obtained by equation (5-11).

$$P = \frac{1}{2}\rho(U\cos\theta)^3\pi(Rcos\Phi)^2 C_p \tag{5-11}$$

Therefore, the aerodynamic rotor torque (τ_{aero}) in equation (5-6) becomes the equation in (5-12), which is obtained using (5-4), (5-10) and (5-11).

$$\tau_{aero} = \frac{1}{2}\rho\pi(R\cos\Phi)^3(U\cos\theta)^2\frac{C_p}{\lambda} \tag{5-12}$$

Now, when the aerodynamic torque in equation (5-12) and generator control torque in equation (5-1) considering the controller gain, K_g in equation (5-9) are placed into the equation (3-58), a similar form of equation (5-7) is obtained as follows.

$$\dot{\Omega} = \frac{1}{2J_t}\rho\pi\Omega^2(R\cos\Phi)^5\left(\frac{C_p}{\lambda^3} - \frac{C_{pmax}}{\lambda_*^3}\right) \tag{5-13}$$

The air density, pi number and square of rotor speed and rotor radius as well as cosine of precone angle are to be always positive. Therefore, the sign of acceleration depends on the expressions in the parenthesis. Therefore, the previously defined conditions of I and II are still valid for a turbine with preconed and tilted rotor.

In this thesis study, NREL 5 MW turbine with inactivated precone and tilt angles is considered. The value of generator torque controller gain, K_g, is obtained from the turbine Cp surface. As mentioned previously, the developed MS Bladed turbine simulation model is operated at different rotor speeds and various blade pitch angles at a certain wind speed to extract the Cp surface. As stated previously, the wind speed of 8 m/s is utilized for this purpose.

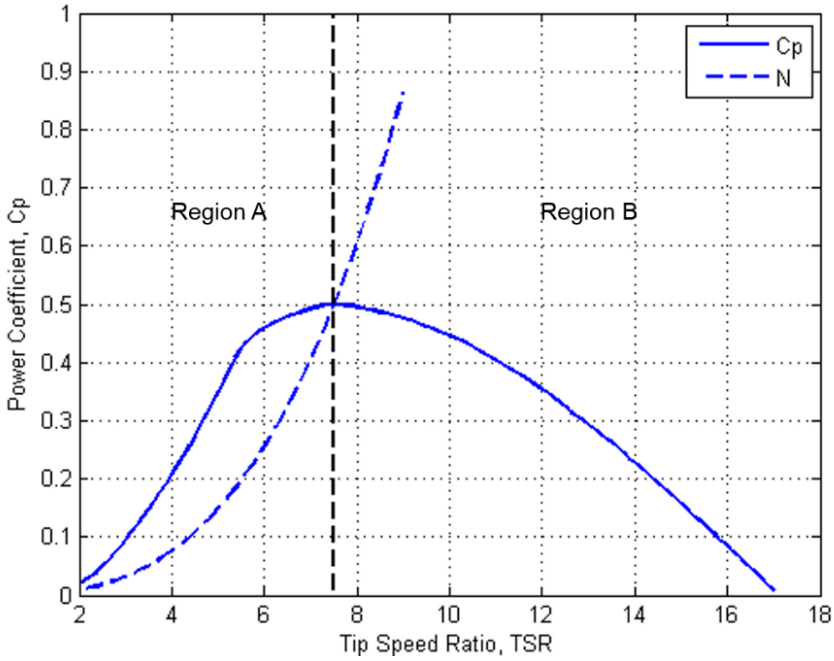

Figure 5-3. C_p versus λ and N versus λ at blade pitch angle of -0.875 degree

Figure 5-3 is obtained from the developed MS Bladed model in order to comment on the rotor speed acceleration or deceleration due to the generator torque control. It illustrates the above conditions of I and II. The joint of both curves coincide at the optimum TSR, λ_* and C_{pmax}. The optimum TSR value, λ_*, is the equilibrium point where the turbine produces its maximum power. At this operating point, the turbine is asymptotically stable[14]. Here, condition I corresponds to an operation in Region B, the area on the right side of the dashed black line. Condition II, on the other hand, indicates an operation in Region A, the area to the left hand side of the dashed black line.

When the turbine is exposed to a change in wind speed, it deviates from its current equilibrium operation, and therefore a change in turbine TSR occurs. Accordingly, the generator torque controller adjusts the control torque, i.e generator torque, such that the turbine can again operate at the optimum TSR, thereby operating the turbine at C_{pmax}. If a turbine operation falls into Region A, the turbine rotor speed increases to reach at the optimum TSR. On the contrary, a falling operation into Region B requires the rotor speed to slow down for obtaining the optimum TSR.

However, the turbine does not always operate at the maximum power coefficient, C_{pmax} and the optimum TSR, λ_*, from cut-in to the rated wind speeds due to the linear transition regions such as Region 1.5 and Region 2.5. In terms of generator speed or rotor speed, these transition regions are narrower than Region 2. As stated before, Region 1.5 is the linear transition region between Region 1 and Region 2. Likewise, Region 2.5 is the transition region between Region 2 and Region 3.

As mentioned previously, Region 1 is the region before the cut-in wind speed, where the generator torque is zero and the turbine does not supply any electrical power. Instead, wind power is used only to speed up the turbine rotor for start-up. In Region 2, however, the turbine works at the maximum power coefficient, C_{pmax} and the optimum TSR, λ_*. Therefore, it produces the maximum power as much as possible. Region 1.5 is a start-up region for the turbine. The lower limit of generator speed in Region 1.5 decides the cut-in wind speed of the turbine, while the upper limit defines the wind speed that the turbine starts producing the maximum power possible. Region 2.5 is the region where the torque slope is the same as the slope of the induction generator used for the turbine[87]. In Region 2, when the wind speed increases, the rotor torque is adjusted in such a way that the rotor speed increases in order to keep the TSR at its optimum value. This permits the turbine to produce maximum power. However, further increasing rotor speed to an increasing wind speed must be limited due to blade tip noise issues and other design constraints such as obtaining the rated torque at the rated speed. The desired rotor speed is reached at a quite low wind speed. Therefore, if the Region 2.5 controller is not added to the MS Bladed simulation model, the rotor speed of the turbine may exceed the rated rotor speed. When the wind speed increases further, it is desired to obtain a larger generator torque which does not allow a further increase in rotor speed. In order to achieve this, a torque-speed ramp or

Region 2.5 transition controller is employed in the torque controller design[24]. For the below rated region, the blades are set to optimum blade pitch angles and simultaneously the generator torque is adjusted to control the rotor speed.

Since this thesis study utilizes the rotor speed as feedback, i.e. the speed sensor being located on the LSS of the gearbox, the torque controller design and the dynamic switching from one region to another is carried out based on the rotor speed. This implementation does not change anything in usual design due to the fact that the generator speed is simply the multiplication of rotor speed, while the generator torque is the division of rotor torque by the gearbox ratio, N_{gear}.

Therefore, Figure 5-4 shows the generator torque controller output. Figure 5-4-a shows the generator torque on the LSS of the gearbox with respect to the rotor speed. This corresponds to the generator torque controller (equations (5-1) and (5-2)) designed in this thesis study. On the other hand, Figure 5-4-b gives the generator's own torque on the HSS of the gearbox, with respect to the generator speed. It is drawn here by considering the gearbox ratio, N_{gear} and the generator speed. Both Figure 5-4-a and b include main and transitional regions, Region 1, 1.5, 2 and 2.5.

Table 5-1 Upper and lower limits for transition regions[87]

	Region 1.5		**Region 2.5**	
	Lower Limit	**Upper Limit**	**Lower Limit**	**Upper Limit**
Rotor Speed [rpm]	6.9072	8.9794	11.7319	11.979
Generator Torque [Nm], on LSS	0	1,999,731.8	3,410,091.17	4,180,100.35
Generator Speed [rpm]	670	871	1138	1,161.963
Generator Torque [Nm], on HSS	0	20,615.8	35,155.57	43,093.81

Table 5-1 gives the lower and upper limits for Region 1.5 and Region 2.5 in terms of generator speed and generator torque on HSS of the gearbox as well as rotor speed and generator torque on the LSS of the gearbox.

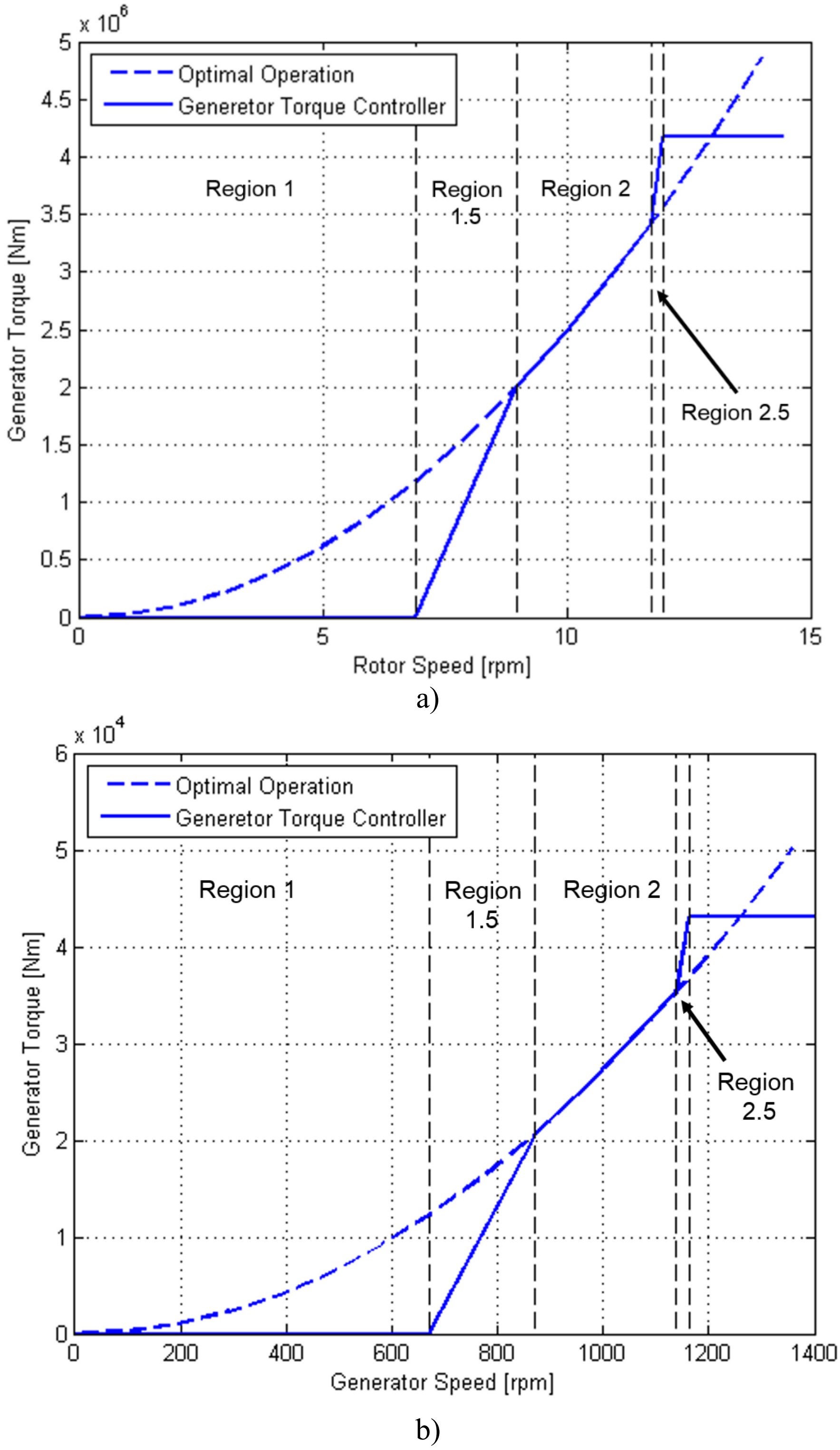

Figure 5-4 Generator torque controller output, a) Generator torque on LSS versus rotor speed, b) Generator torque on HSS versus generator speed

The design of Region 1.5 and 2.5 transition torque controllers is the same and is simply based on equation (5-14)[89].

$$\tau_c = m(\Omega_u - \Omega_l) + \tau_l \tag{5-14}$$

where m is the slope of the linear line in the related transition region and is given as,

$$m = \frac{\tau_u - \tau_l}{\Omega_u - \Omega_l} \tag{5-15}$$

Ω_u and Ω_l are the upper and lower limits of generator or rotor speed in the related regions. Likewise, τ_l and τ_u are the lower and upper borders of generator torques on HSS or LSS of the gearbox or turbine rotor.

Along with the above, in order to deal with undesired power dips whenever the wind speed drops largely in the above rated region, or Region 3, the generator torque is computed as if it were in Region 3 taking into account both the rotor speed and the actual wind speed information. This is realized by introducing these two conditions to the design of the generator torque controller. This helps to minimize the potential power dips in the above rated region.

5.2 Simulations of Baseline Generator Torque Controller

In this subchapter, the simulation of the designed nonlinear generator torque controller is carried out using the developed MS Bladed turbine simulation model. The simulation results are given for 140 seconds. A wind input with a step increasing from 8 to 9 m/s at the 40th second and decreasing from 9 to 8 m/s at 90th second is applied to the developed MS Bladed turbine simulation model with the newly designed generator torque controller. This input is given in Figure 5-5.

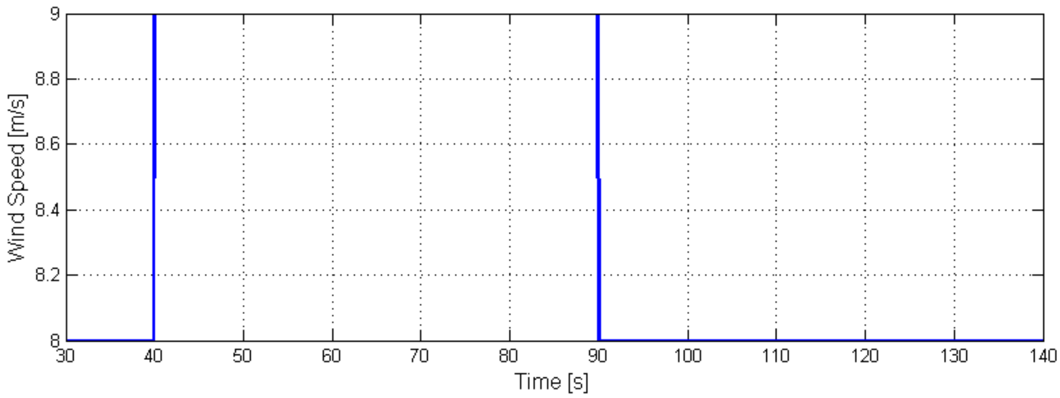

Figure 5-5 Wind speed

.

The blade pitch angles of all the blades (Figure 5-6) are set to the optimum pitch angle of -0.875 degrees (Table 4-5). This is realized by placing a saturation limit to the output of the blade pitch controller, whose design is investigated in the next subchapter. The variation of wind speed (Figure 5-5) changes the turbine TSR, and the turbine C_p.

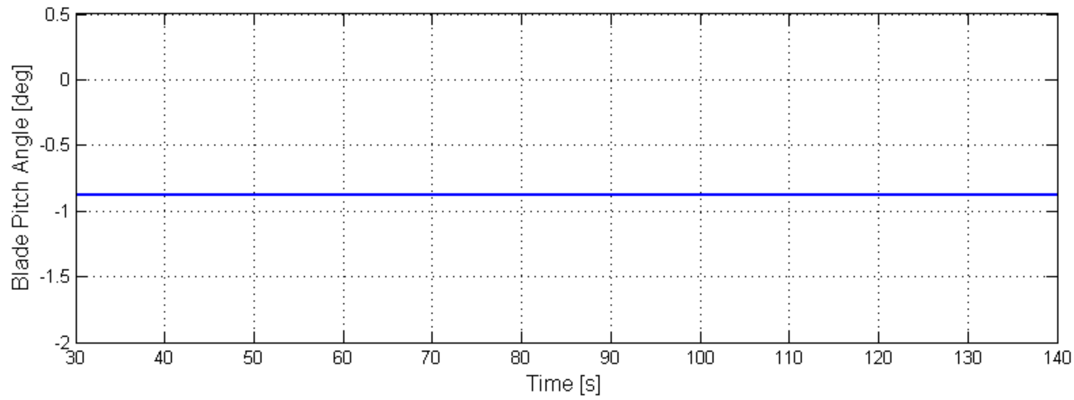

Figure 5-6 Blade pitch angle

Figure 5-7 shows how the generator torque controller adjusts the generator electromagnetic torque in order to let the turbine operate at the optimum TSR and therefore at the maximum C_p. It also shows the change in the aerodynamic rotor torque due to the change in wind speed. As seen in the figure, the rotor torque increases sharply due to the sharp rise in the wind speed input (Figure 5-5). The torque controller increases the generator torque until both torques become equal to each other, i.e. the turbine system reaching at steady-state.

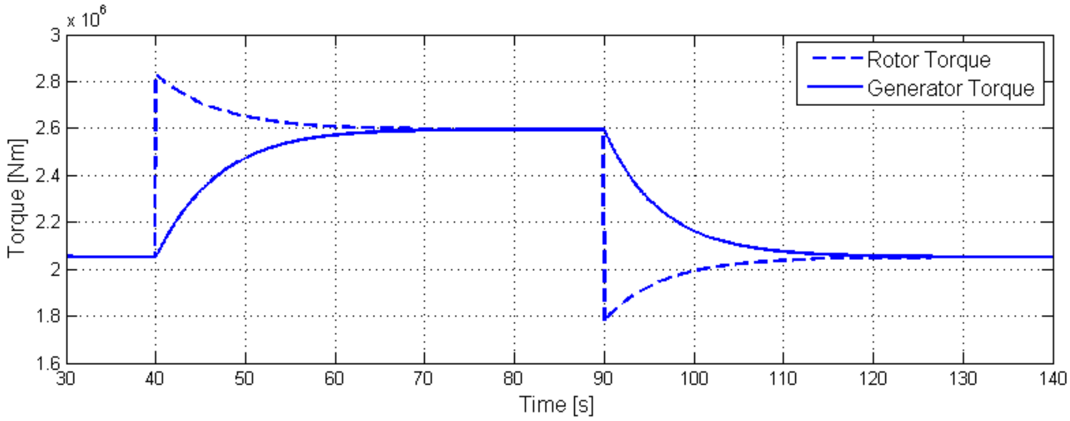

Figure 5-7 Rotor and generator torques

When the aerodynamic and generator torques become equal to each other (Figure 5-7), the turbine rotor operates at a constant rotor speed (Figure 5-8). However, when they differ from one another, the rotor speed increases or decreases until a new steady-state operation is achieved.

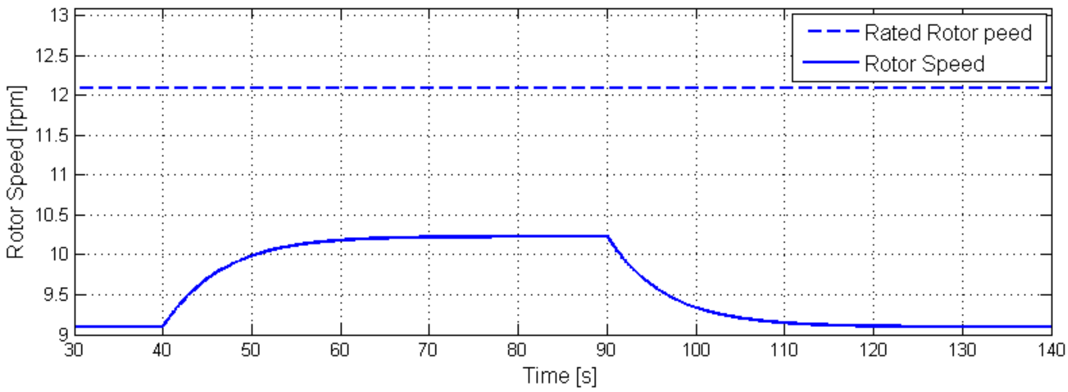

Figure 5-8 Rotor speed

In addition, the changes in TSR, C_p, torque difference, turbine power and turbine thrust force are given respectively in Figure 5-9 to Figure 5-13. Following comments are about how the generator torque controller permits the turbine to generate the maximum power possible at any wind speed in the below rated region.

NREL 5 MW wind turbine with inactivated precone and tilt angles operates at the steady-state condition just before a step increase in wind input at 40th second of the simulation time. With this operational condition, the turbine runs at the optimum TSR of 7.5 and therefore at the maximum C_p of 0.4996 (Table 4-5). The turbine operating at the optimum TSR means a turbine operation at steady-state. At this condition, the rotor rotates at around 9.1 rpm (or 0.953 rad/s) and the wind speed is 8 m/s. However, once an increasing step wind input is applied to the controlled turbine at 40th second (Figure 5-5), the turbine TSR decreases suddenly to the value of approximately 6.6 (Figure 5-9) due to its inverse proportionality of TSR with the wind speed (equations (3-46) or (5-10)). This operation produces a lower C_p than the C_{pmax}(Figure 5-10). Therefore, the turbine operation immediately falls into Region A(Figure 5-3). Therefore, it must satisfy the condition II, stated in subchapter 5.1. Here, the turbine rotor acceleration is positive and therefore the turbine rotor speed is expected to increase. The rotor speed starts increasing from 40th second till 80th second (Figure 5-8) by the generator torque controller to regain the optimum TSR of 7.5 and operate the turbine at the maximum C_p of 0.4996. The rotor speed (Figure 5-8), reaches its steady-state operation within 40s and the turbine operates at the optimum TSR (Figure 5-9) and at the maximum C_p (Figure 5-10).

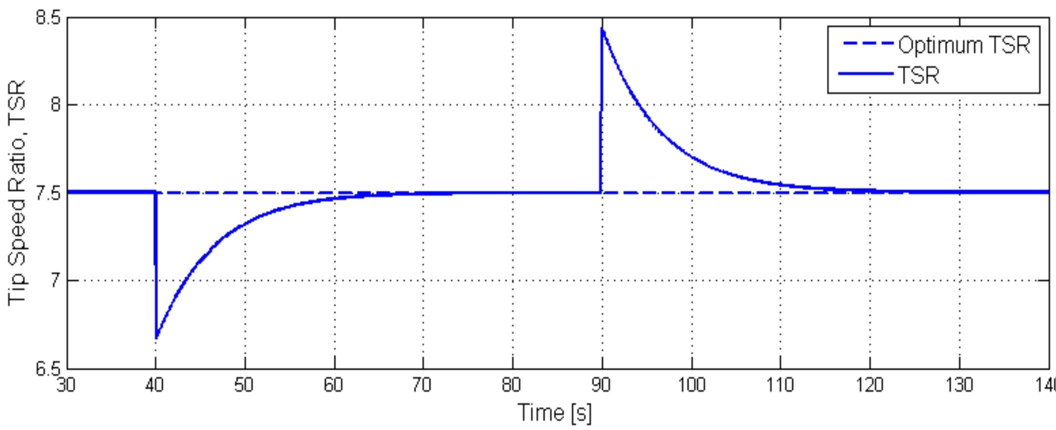

Figure 5-9 Tip speed ratio

In order to achieve the optimum TSR and maximum C_p, the generator torque controller starts increasing the generator electromagnetic torque (Figure 5-7) until it becomes equal to the aerodynamic torque produced by the wind speed of 9 m/s. When the steady-state operation is obtained (Figure 5-7), the turbine operates with the optimum TSR, λ_*. Due to the operation, the turbine operates at the maximum C_p , resulting in maximum power production. Thus, the rotor continues to rotate at the same rotor speed up until a new disturbing wind input is applied to the controlled turbine.

At 90th second (Figure 5-5), the wind input is decreased with a step size from 9 m/s to 8 m/s. Accordingly, the turbine TSR is increased suddenly (Figure 5-9) and becomes approximately 8.45. Therefore, the turbine starts operating with a lower power coefficient, C_p than the C_{pmax} of 0.4996 (Figure 5.10). This operation corresponds to an operation in Region B (Figure 5-3). Thus, the turbine operation should obey the condition I, which requires a negative rotor acceleration and therefore, a decreasing rotor speed. Hence, the generator torque controller starts decreasing the generator electromagnetic torque (Figure 5-7) that decreases the rotor speed (Figure 5-8) to obtain the desired optimum TSR(Figure 5-9), and the C_{pmax}(Figure 5-10). At the steady-state operation, the rotor torque and generator torques becomes again equal to each other (Figure 5-7), which takes a 40 second-time duration to reach the steady-state after a step change in wind speed.

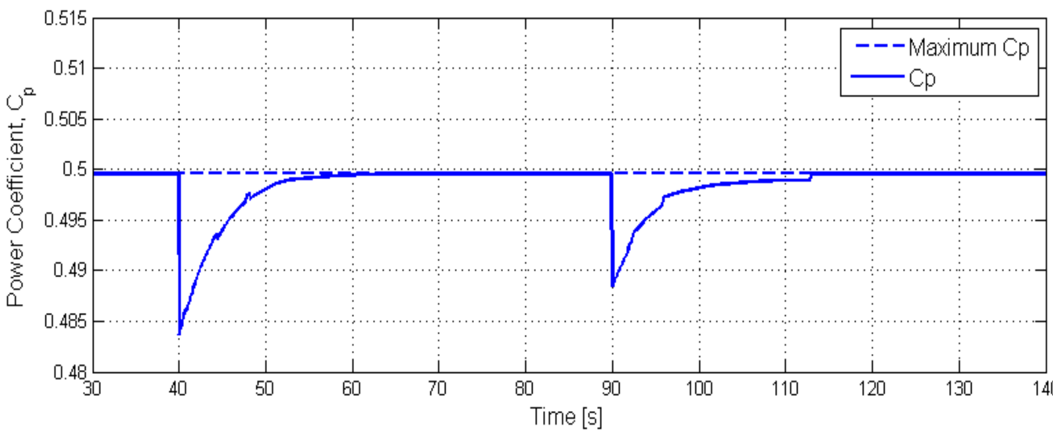

Figure 5-10 Power coefficient

Because of the change in wind speed, thereby the change in turbine TSR in time, the operation with different C_p values are observed during simulations. When the turbine eventually reaches at steady-state operation, it operates at the C_{pmax}, which allows the generation of maximum power. Figure 5-11 shows the torque difference in time between the aerodynamic rotor torque and the generator torque. The difference is larger when the step change is applied to the controlled turbine, but it decreases in time and becomes zero eventually at steady-state.

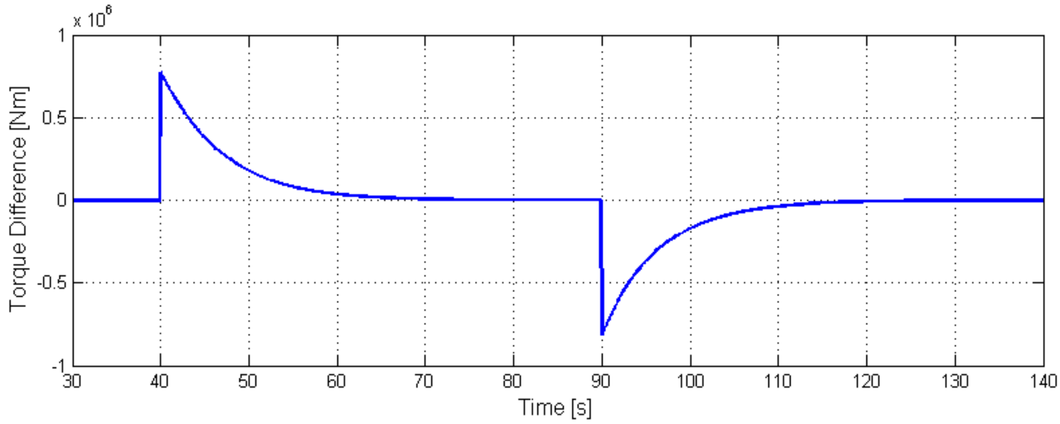

Figure 5-11 Torque difference

The power output of the turbine is seen in Figure 5-12. The produced power never reaches the rated turbine power output of 5 MW since it operates in the partial load region or Region 2. An increasing wind speed results in increasing power output, while a decreasing wind decreases the power output.

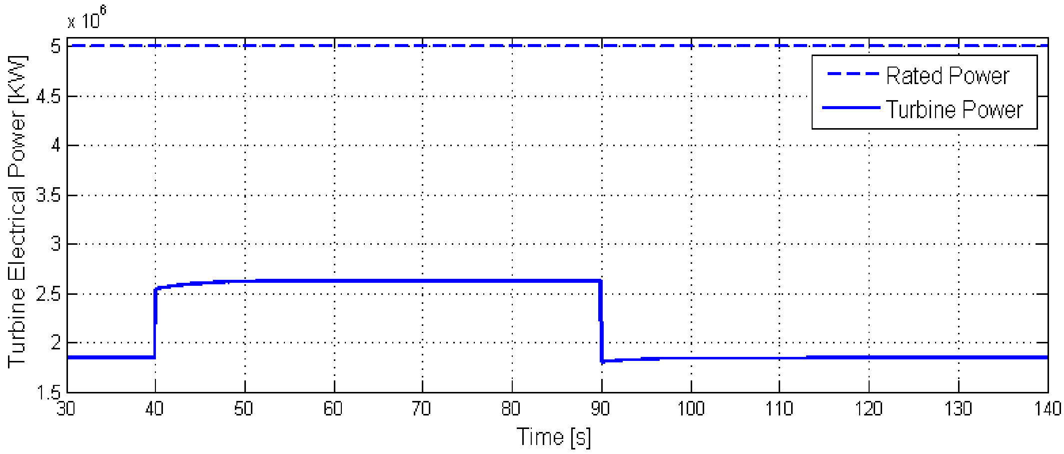

Figure 5-12 Turbine power

The change in the thrust force of the turbine is seen in Figure 5-13. When the wind speed increases, the turbine thrust force increases and vice versa.

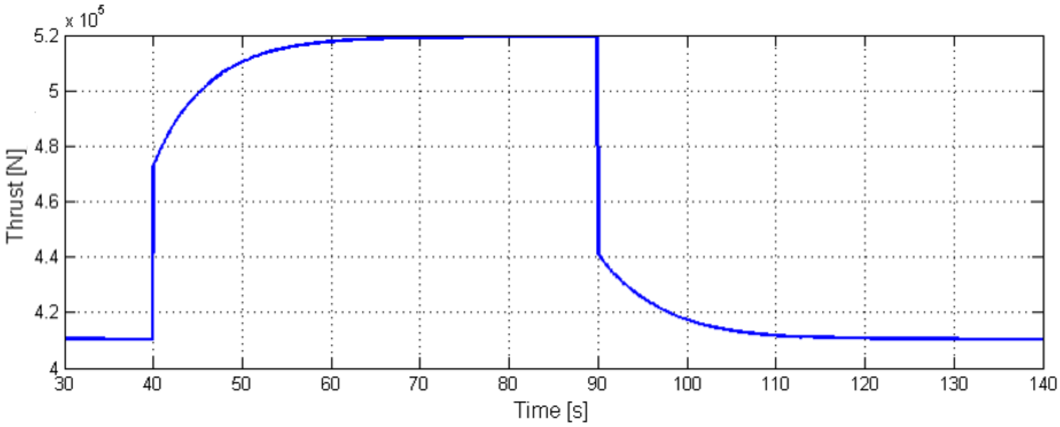

Figure 5-13 Turbine thrust force

As a result, the generator torque controller provides the maximum power generation possible in Region 2. Torque controller permits the turbine to operate at variable rotor speeds to the changing wind speeds. When the wind speed increases, the generator torque and rotor speed increase and vice versa. This way, generator torque controller keeps the turbine to operate at the optimum TSR and the maximum C_p with the blade pitch angles adjusted to optimum blade pitch angle, β_*. Lastly, as mentioned in Chapter 1, this variable speed operation is realized by the power electronics unit. The generator torque controller applied here corresponds probably to an application of Type 4 technology with WRIG generator since the variable rotor speed range is larger than those of Type 2 and 3 technologies.

5.3 Collective Blade Pitch Controller for Rated Rotor Speed Operation

Collective blade pitch control is a method that allows all the turbine blades to move together with the same amount of pitch angles. This control method regulates the turbine power output in the above rated region or Region 3. For this purpose, the same pitch signal from the blade pitch controller is fed to each blade pitch actuator. As stated before, blade pitch control of turbines may be achieved by two active control means, pitching to stall or pitching to feather method.

Although both methods utilize different aerodynamic phenomena, blade stall or blade feathering, they share the same control structure or block diagram. They both use the rotor speed or generally the generator speed to calculate the demanded pitch angles for the pitch actuators. The pitch actuators are limited by constructional constraints such as rate limits, min and max etc. This allows the pitch actuators to travel within certain limits. For a pitch to feather controlled turbine, this ranges from 0 to 90 degrees of pitch angles (or even little negative degrees). Whereas for the pitch to stall turbines, the allowed pitch range lies between -90 to 0 degrees (or a few degree positive pitch angle)[24]. Here, in this thesis study, the pitch angle is limited between -0.875 and 90 degree-pitch angles. A rate limiter of 8 deg/s is also added to the blade pitch control system.

In this section, these two active control methods are defined briefly. But, the second method, pitch to feather, is implemented for NREL 5 MW turbine with inactivated precone and tilt angles. Pitch to feather is designed to due to its common usage in today's wind turbines in wind farms.

Here in this thesis, a gain-scheduled Proportional and Integral (PI)-based pitch to feather controller is designed for power regulation utilizing the Ref.[87] and [89]. The rotor speed is fed back to the collective blade pitch controller, instead of generator speed. The pitch command is determined based on rotor speed error between the rated and measured rotor speed. In order to calculate the gains of the controller, the derived equation of motion for the single DOF turbine system is employed which is given by the equation (3-58).

5.4 Wind Turbine System Linearization for the Above Rated Region

In this subchapter, a gain-scheduled collective blade pitch controller is designed to regulate the rotor speed of a 5 MW wind turbine for the above rated region to produce the rated electrical power. A Proportional and Integral (PI)-based control strategy is adopted to achieve the purpose. In the above rated region, a gain scheduling approach is used since one linear PI-based controller designed for one equilibrium point shows a poorer performance at other equilibrium points in the above rated region. This performance deterioration is demonstrated in Figure 5-17 at a design step toward the gain scheduled-controller design.

Previously, the dynamic turbine or MS Bladed model is represented by the following first order differential equation (3-58).

$$J_t\dot{\Omega} = \tau_{aero} - \tau_{gen} \tag{3-58}$$

This is the nonlinear equation representing the turbine dynamics. Here, for the above rated region, nonlinearity is caused by the aerodynamic torque only since generator torque is kept at its rated value, while for the below rated region, it is due to both aerodynamic torque and generator torque. The turbine system here includes only one state, which is the turbine rotor speed, $\boldsymbol{\Omega}$, measured from the turbine rotor shaft, or LSS as stated before. It is the change of azimuth angle, Λ, of the turbine blades in time. The control inputs to the MS Bladed turbine simulation model are only the blade pitch angles. It allows controlling the blades collectively or individually depending on the purpose. The wind, on the other hand, is a disturbance input to the turbine.

In order to design a linear controller, the nonlinear turbine model needs to be linearized around an equilibrium point. A perturbation technique is a commonly-used approach to linearize a nonlinear system at any desired equilibrium point.

The aerodynamic torque of the turbine rotor is a continuous function and depends on the three variables; rotor speed, $\boldsymbol{\Omega}$, blade pitch angle, β, and lastly the wind speed, U. Thus, following Ref.[90], the aerodynamic torque may be expanded by a Taylor series as,

$$\begin{aligned}\tau_{aero}(U,\Omega,\beta) = \tau_{aero}(U_e,\Omega_e,\beta_e) + \frac{\partial\tau_{aero}}{\partial U}(U-U_e) + \frac{\partial\tau_{aero}}{\partial\Omega}(\Omega-\Omega_e) \\ + \frac{\partial\tau_{aero}}{\partial\beta}(\beta-\beta_e) + \text{HOTs}\end{aligned} \tag{5-16}$$

where U_e, Ω_e, β_e are respectively the values of wind speed, shaft speed, and blade pitch angle at the equilibrium point. $U - U_e = \Delta U,\ \Omega - \Omega_e = \Delta\Omega$ and $\beta - \beta_e = \Delta\beta$ are the perturbations from these equilibrium points. Perturbation is defined as a small deviation of a variable from its equilibrium value at a steady-state operation. Higher Order Terms (HOTs) in equation (5-16) are neglected since the first order Taylor series expansion is enough for the approximation of nonlinear system around an equilibrium point. This approach is valid for the design of classical or advanced linear controllers.

For the above rated region, an equilibrium point for a turbine may be defined as the point at which wind speed and blade pitch angle the aerodynamic torque reaches the rated generator torque at the rated rotor speed. The rated generator torque of 5 MW turbine on the rotor shaft, i.e. on LSS of the gearbox, is determined as 4180074.35 Nm[87]. Thus, the above aerodynamic torque equation may also be written as,

$$\tau_{aero}(U,\Omega,\beta) - \tau_{aero}(U_e,\Omega_e,\beta_e) = \frac{\partial\tau_{aero}}{\partial\Omega}\Delta\Omega + \frac{\partial\tau_{aero}}{\partial\beta}\Delta\beta + \frac{\partial\tau_{aero}}{\partial U}\Delta U \tag{5-17}$$

or,

$$\Delta\tau_{aero} = \frac{\partial\tau_{aero}}{\partial\Omega}\Delta\Omega + \frac{\partial\tau_{aero}}{\partial\beta}\Delta\beta + \frac{\partial\tau_{aero}}{\partial U}\Delta U \tag{5-18}$$

When let

$$\frac{\partial\tau_{aero}}{\partial\Omega} = \gamma\ , \frac{\partial\tau_{aero}}{\partial\beta} = \eta \text{ and } \frac{\partial\tau_{aero}}{\partial U} = \mu \tag{5-19}$$

Equation (5-18) turns out to be

$$\Delta\tau_{aero} = \gamma\Delta\Omega + \eta\Delta\beta + \mu\Delta U \tag{5-20}$$

When the Taylor series expansion is applied to the whole turbine system in equation (3-58), i.e. considering the generator torque, the following is obtained.

$$J_t(\dot{\Omega - \Omega_e}) = \tau_{aero}(\Omega_e,\beta_e,U_e) + \gamma\Delta\Omega + +\eta\Delta\beta + \mu\Delta U - \tau_{gen} \tag{5-21}$$

Here, for the above rated region, the generator torque is assumed to be constant at its rated value. In addition, there is no rotor acceleration at an equilibrium or a steady-state operation since the aerodynamic and generator torques cancel each other at the equilibrium. Thus, for any operation at steady-state,

$$\tau_{aero}(U_e,\Omega_e,\beta_e) = \tau_{gen} \tag{5-22}$$

Since the derivative of rotor speed at an equilibrium point is zero, the system equation is written as,

$$J_t\dot{\Omega} = \gamma\Delta\Omega + \eta\Delta\beta + \mu\Delta U \tag{5-23}$$

Therefore, rotor acceleration at an equilibrium is obtained as,

$$\dot{\Omega} = \frac{\gamma}{J_t}\Delta\Omega + \frac{\eta}{J_t}\Delta\beta + \frac{\mu}{J_t}\Delta U \tag{5-24}$$

where

$$\frac{\gamma}{J_t} = A \tag{5-25}$$

$$\frac{\eta}{J_t} = B \tag{5-26}$$

$$\frac{\mu}{J_t} = B_d \tag{5-27}$$

where A is the system gain, B is the input gain and finally B_d is the disturbance gain. They are respectively the ratios of the partial derivative of aerodynamic torque with respect to rotor speed, blade pitch angle and wind speed to the total inertia of the turbine system.

Since the goal in this part is to design a PI-based collective blade pitch control system, system linearization with PI methodology is first required. Therefore, following the Ref.[89], the perturbation of pitch angle, $\Delta\beta$, is directly related to the perturbation of rotor speed, $\Delta\Omega$ by the equation (5-28).

$$\Delta\beta(t) = K_p\Delta\Omega(t) + K_i\int \Delta\,\Omega(t)dt \tag{5-28}$$

Where K_p and K_i represent the proportional and integral gains, respectively. In addition, the controller output is as follows, $\beta = \Delta\beta + \beta_e$. This controller output is referred to as β_{ref}, later in Chapter 6. Putting the equation (5-28) into the equation (5-24) constructs the closed-loop turbine system with PI strategy as in equation (5-29).

$$\dot{\Omega} = A\Delta\Omega + B\left(K_p\Delta\Omega(t) + K_i\int \Delta\,\Omega(t)dt\right) + B_d\Delta U \tag{5-29}$$

Taking the Laplace Transform of equation (5-29) as,

$$s\Omega = A\Delta\Omega(s) + B\left(K_p\Delta\Omega(s) + \frac{K_i}{s}\Delta\Omega(s)\right) + B_d\Delta U(s) \quad (5\text{-}30)$$

and then carrying out some algebraic manipulations give the closed loop transfer function between the rotor speed, $\Delta\Omega(s)$ and the wind, $\Delta U(s)$ as,

$$G_{CL}(s) = \frac{\Delta\Omega(s)}{\Delta U(s)} = \frac{B_d s}{s^2 + (-A - BK_p)s + (-BK_i)} \quad (5\text{-}31)$$

The denominator of the transfer function or the characteristic equation of the closed loop turbine system gives the information about the system stability considering the controller gains, K_p and K_i. Therefore, by designing K_p and K_i, the desired performance is easily obtained from the turbine system. In order to have a closed loop turbine system stable, both roots of the characteristic equation must be at least negative. Thus, this requires the terms in parenthesis of the characteristic equation to be larger than zero. Thus,

$$-A - BK_p > 0 \quad (5\text{-}32)$$

$$-BK_i > 0 \quad (5\text{-}33)$$

However, in order to achieve the desired response from the system, proper gains should be selected such that the roots of the closed-loop system must pass through a certain root location. This is determined by the desired natural frequency, w_n and damping ratio, ζ for a second order system. The following subchapter 5.5 deals with the selection of these gains according to design requirements.

5.5 Performance and Design of Collective Blade Pitch Controller

Here, a PI-based control methodology is discussed in detail. Firstly, for a selected equilibrium point, the effect of damping ratio on the turbine system response is examined to determine a suitable damping ratio. However, the desired natural frequency is kept the same as in the literature[91]. The damping ratio of 0.8 is determined to give the best performance in terms of settling time at the selected equilibrium point. Later, the blade pitch controller giving the best performance is also tested at other equilibrium points. However, these test simulations have resulted in poorer performance, for which the same is stated by Wright and Fingersh[89] during the NREL CART wind turbine collective blade pitch controller design. NREL CART turbine is a two-bladed upwind oriented turbine with a capacity of 600KW. This turbine is a variable speed variable pitch turbine and is used as a testbed by NREL to study the control systems. It is equipped with a generator with a full power electronics unit which controls the generator torque from a negative rating (motoring) to a positive rating (generating). Power electronics unit gives the rated torque from the generator in the above-rated region and a collective blade pitch control system adjusts the rotor speed. Therefore, a gain-scheduled PI-based controller is designed to have almost the same performance at every equilibrium point in the above rated region. The following are the details of this design process.

In order to design a blade pitch controller, the values of partial derivatives ɣ and η are required to be first determined to find the values of A and B gains at the selected equilibrium point. These gains are explicitly seen in the characteristic equation, i.e., the denominator of the transfer function in (5-31). Here, this process is realized using the currently developed MS Bladed simulation model. The nonlinear aerodynamic turbine model is linearized around the desired equilibrium point. System linearization is carried out using the central difference theorem considering the equilibrium wake assumption.

When the characteristic equation of the closed loop turbine system is considered as a standard second order system in Laplace form as in equation (5-34).

$$s^2 + 2w_n\zeta s + w_n^2 \tag{5-34}$$

Then, equation (5-35) and (5-36) become the relations among the natural frequency, damping ratio, system and input gains as well as controller gains.

$$2w_n\zeta = -A - BK_p \tag{5-35}$$

$$w_n^2 = -BK_i \tag{5-36}$$

Therefore, K_p and K_i gains are obtained by equations (5-37) and (5-38), respectively if the desired natural frequency and damping ratio are already known.

$$K_p = \frac{-2w_n\zeta}{B} - \frac{A}{B} \tag{5-37}$$

$$K_i = \frac{-w_n^2}{B} \tag{5-38}$$

According to the explanations above, Table 5-2 is prepared here for the discussions of controller design and analysis thought this subchapter. It includes information about various equilibrium points in terms of wind, rotor speed, blade pitch angle and rated rotor torque. In Table 5-2, EP represents the equilibrium point.

Table 5-2 Selected equilibrium points for controller design and analysis

Equilibrium Points	Wind Speed (m/s), U_e	Rotor Speed (rpm), Ω_e	Pitch Angle (deg), β_e	Rotor Torque (Nm), τ_e
EP 1	18	12.1	14.9525	4180074.35
EP 2	16	12.1	10.5521	4180074.35
EP 3	13	12.1	6.7206	4180074.35
EP 4	11.5	12.1	2.2792	4180074.35
EP 5	12.6607	12.1	5.9676	4180074.35
EP 6	23	12.1	20.9964	4180074.35

Therefore, EP 1 is taken into account first. One PI-based blade pitch controller is designed for this equilibrium point. During a controller design for a wind turbine, Ref.[91] has suggested utilizing a natural frequency, w_n of 0.6 and damping ratio, ζ of 0.6-0.7 in order to have a satisfactory controller response. By keeping the natural frequency as w_n of 0.6, Wright and Fingersh[89] has selected a damping ratio of 1 for the NREL CART turbine after some trials during the pitch controller design. Therefore, these values, particularly the damping ratio may vary from turbine to turbine. Thus, a similar approach in Ref.[89] is adopted here to find the best damping ratio. Later on, the same damping ratio is kept being used for the further steps in controller designs.

When the turbine model is linearized at the EP 1, the A, B and B_d gains are obtained as follows.

$$A = -0.2401$$

$$B = -1.1672$$

$$B_d = 0.0275$$

Using the above system gain, A and input gain, B and natural frequency, w_n and damping ratio, ζ respectively as 0.6 and 0.7 in equations (5-37) and (5-38) results in a proportional gain, K_p of 0.5140 and an integral gain, K_i of 0.3084. The performance of the pitch controller to a step wind input is investigated considering the time domain response characteristic in term of rise time, settling time, overshoot etc. Figure 5-14 shows the response of blade pitch controlled turbine rotor speed response to a step increasing wind input, rising from 17 to 18 m/s at the 50th second of simulation time. Rotor speed response overshoots slightly the steady-state level when the simulation time is around 57th second and settles down eventually at around 65th second. The rotor speed response to a disturbance wind input looks quite satisfactory in terms of settling time because it only takes a duration less than 15 seconds to settle down.

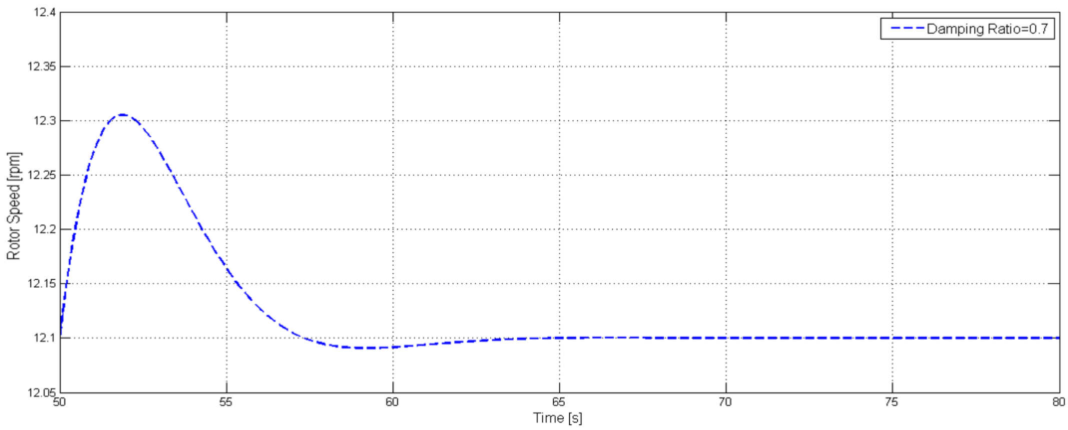

Figure 5-14 Rotor speed response to a step input at damping ratio of 0.7

However, there may be another damping ratio that gives a better rotor speed response than the one obtained in Figure 5-14. To decide an appropriate damping ratio, the value of the selected damping ratio of the closed system is decreased and increased to examine its effect on the response.

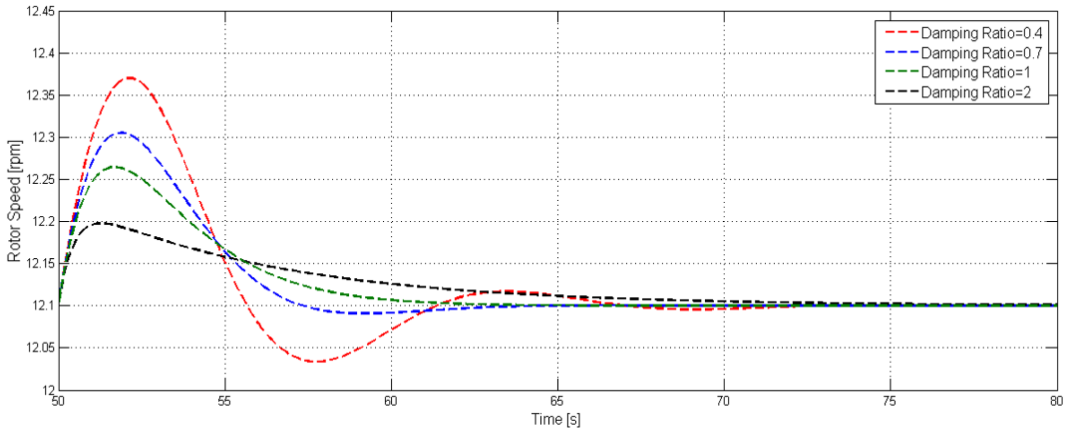

Figure 5-15 Rotor speed response with various damping ratios at EP 1.

Figure 5-15 shows the various rotor speed responses with four different damping ratios; 0.4, 0.7, 1 and 2. As seen from the figure, with the damping ratio of 0.4, the response is an undamped oscillation and takes a quite large time to settle down. Even in 15 seconds, it does not reach its steady-state and is still oscillating. In terms of settling time, the same is also valid for the response with the damping ratio of 2. On the other hand, the damping ratios of 0.7 and 1 demonstrate closer settling times. The response with the damping ratio of 1 gives a closer output to the steady-state around 61^{st} second, whereas the response with the damping ratio of 0.7 gives a closer result to the steady-state around 58^{th} second. However, it overshoots slightly and does not settle down yet in less than 15 seconds. Thus, the damping ratio of 0.7 seems to be the better damping ratio.

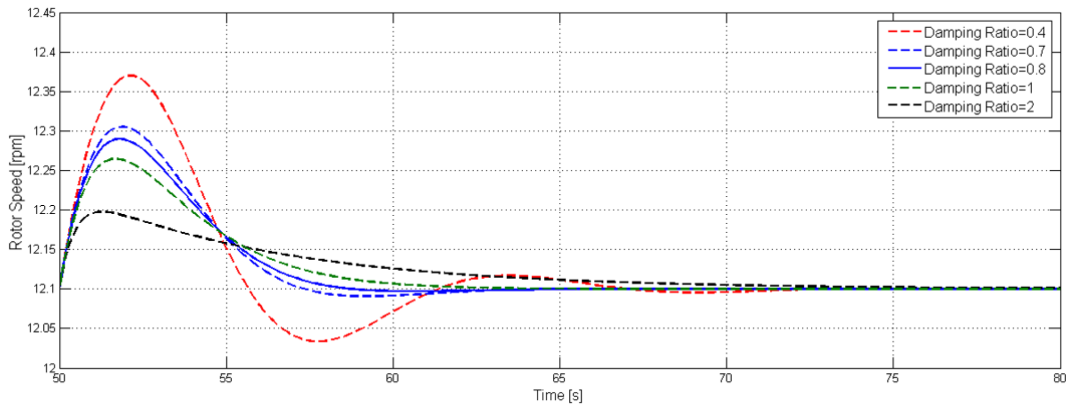

Figure 5-16 The best rotor speed response with a damping ratio of 0.8 at EP 1

But it also seems that selecting a damping ratio between 0.7 and 1 provides a better performance in terms of settling time. Figure 5-16 shows the system response with a damping ratio of 0.8 along with other responses. As seen in the figure, the response with the damping ratio of 0.8 gives the best performance to a step increasing wind input when compared to others.

Table 5-3 shows the corresponding proportional and integral gains of the closed-loop system as well as the system roots when the above-mentioned damping ratios and natural frequency are used during the controller design process.

Table 5-3 Estimation of the best damping ratio

Damping Ratio ζ	**Natural Frequency w_n**	**Proportional Gain K_p**	**Integral Gain K_i**	**System Root 1**	**System Root 2**
0.4	0.6	0.2055	0.3084	-0.24-0.5500i	-0.24+0.5500i
0.7	0.6	0.5140	0.3084	-0.42-0.4285i	-0.42+0.4285i
0.8	**0.6**	**0.6168**	**0.3084**	**-0.48-0.3600i**	**-0.48+0.3600i**
1	0.6	0.8224	0.3084	-0.6	-0.6
2	0.6	1.8505	0.3084	-2.2392	-0.1608

In Table 5-3, when the damping ratio is less than 1, the closed-loop system has complex conjugate roots, which produces an oscillatory rotor response. This oscillatory response typically occurs since the closed-loop system is turned into an underdamped system. However, when the damping ratio is increased to 1, the system operates with repeating roots. Thus, the closed-loop system becomes a critically damped system. Increasing the damping ratio further into 2, the system has two different negative real roots which make the system overdamped. Therefore, the eventual response of the system is determined by the smaller root in magnitude. For all the cases in Table 5-3, the turbine system with the controller is stable due to its negative real part in the system roots. Therefore, it reaches the steady-state condition is ultimately guaranteed.

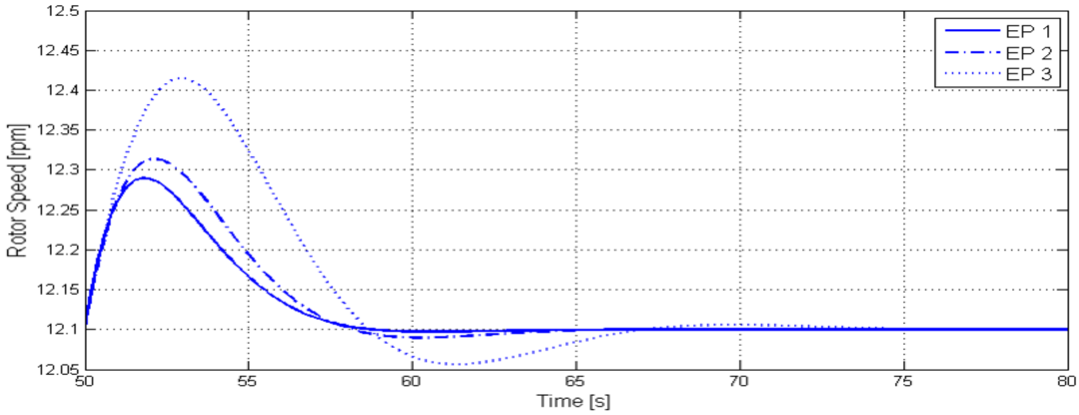

Figure 5-17 Controller performance deterioration at other equilibrium points

Until now, for EP 1, PI-based pitch controller with different gains are considered. It is seen that the best performance is obtained with the damping ratio of 0.8. Therefore, from now on, the damping ratio of 0.8 is kept being used as the desired damping ratio, while the same natural frequency, 0.6, is kept being utilized as before.

When the same controller with K_p of 0.6168 and K_i of 0.3084 is tested at other equilibrium points such as EP 2 and EP 3 (Table 5-2). The performance of the controller gets deteriorated at these equilibrium points, especially at EP 3, which is very close to the rated equilibrium point, i.e. the transition point of Region 2 to Region 3. Figure 5-17 shows the performance deterioration clearly. As seen in the figure, the rotor speed response at EP 3 overshoots largely at around 58th seconds. This performance deterioration occurs due to the change in the control input gain, B with the change in blade pitch angle and wind speed[89]. The value of input gain B is directly related to η, which is the partial derivative of aerodynamic torque, τ_{aero} with respect to the blade pitch angle, β at the rated torque and rotor speed.

Figure 5-18 is obtained using the MS Bladed simulation model and shows the aerodynamic torque curves with respect to various blade pitch settings at different wind speeds. The solid black line represents the rated torque on the LSS of the gearbox. The crossing points of this line with the blue torque curves are the equilibrium points for the open loop turbine system in the above rated region. As seen in this figure, the value of input gain, B, directly related to $\frac{\partial \tau_{aero}}{\partial \beta}$, or changes in magnitude when the blade pitch angle varies. Because of this issue, a controller designed at any equilibrium point does not give the same performance at other equilibrium points, i.e. at lower or higher pitch angles. It arises from the fact that input gain, B differs at every equilibrium point. Thus, in order to move the closed system poles to the desired location, the controller gains are required to be adjusted or scheduled relying on the blade pitch angles. These pitch angles, as seen in Figure 5-18, correspond to different wind speeds at different equilibrium points.

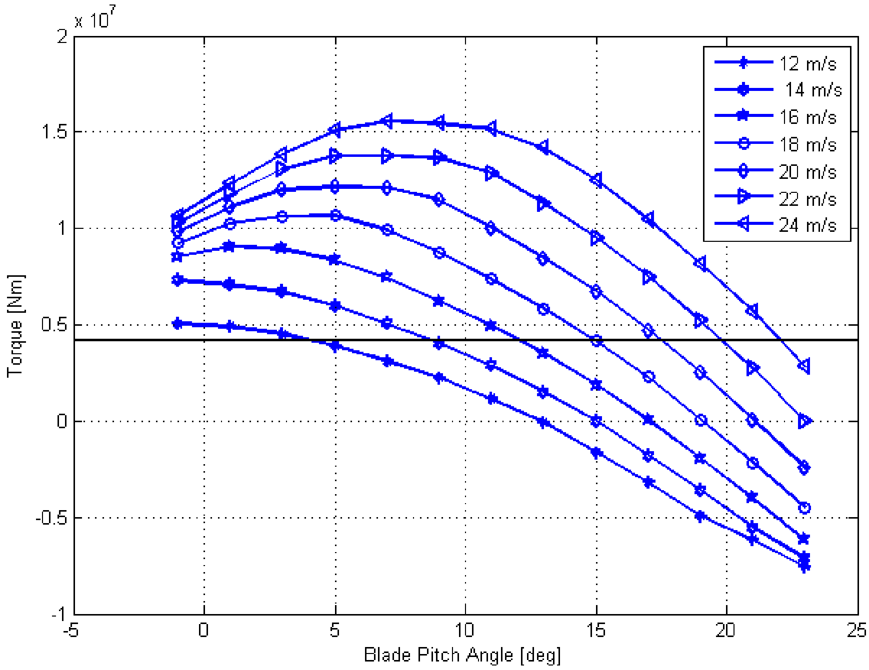

Figure 5-18 Aerodynamic torque versus pitch angle at various wind speeds

Figure 5-18 also shows how much a wind turbine system is nonlinear. For instance, at the wind speed of 24 m/s, at lower pitch angles, the slope of the torque curve is positive, while at high pitch angles, the slope becomes negative. The slope becomes mostly zero when moved from lower pitch angles to higher pitch angles. However, at all the wind speeds and pitch angles, where the rated torque is achievable, all the slopes are negative.

To increase the performance of the designed PI-based pitch controller throughout the above rated region, a gain-scheduled PI-based blade pitch controller is designed and implemented on 5 MW wind turbine. It is explored above that the controller designed for EP 1 does not give the same performance at other equilibrium points, i.e. at EP 2 and 3. In the literature, the gain scheduling of PI methodology is realized by two similar means. These are based on the partial derivative of aerodynamic torque with respect to pitch angle, $\frac{\partial \tau_{aero}}{\partial \beta}$ [89] or rotor aerodynamic power with respect to pitch angle, $\frac{\partial P}{\partial \beta}$ or referred to as pitch sensitivity[87]. For a gain scheduling implementation, both methods use a term referred to as gain correction factor, $GK(\beta)$. By simply multiplying the estimated controller gains with the correction factor, $GK(\beta)$, a superior performance may be achieved from the controller at any equilibrium point all along the above rated region. The equation for $GK(\beta)$ is defined[87], [89] as follows.

$$GK(\beta) = \frac{1}{\left(1 + \frac{\beta}{\beta_K}\right)} \tag{5-39}$$

where β is the blade pitch angle required for the turbine to produce the rated torque at any wind speed when the turbine operates at its rated rotor speed. The finding/definition of β_K is similar and is probably derived from the same idea in both approaches. According to Wright and Fingers[89], β_K is the blade pitch angle where the input gain, B, calculated at an equilibrium point close to the border of Region 2 into 3 has doubled in its value at another equilibrium point further in Region 3[89]. Their application of gain scheduling employs the FAST linearization considering equilibrium wake assumption. However, according to the approach used by Jonkman et al.[87], β_K is defined as the blade pitch angle at which the pitch sensitivity, $\frac{\partial P}{\partial \beta}$ at zero pitch angle has doubled in its value further in Region 3. The partial derivative, $\frac{\partial P}{\partial \beta}$ at zero pitch angle, is obtained by a curve fitting approach to the pitch sensitivities at various pitch angles. The best fit line is used to calculate the pitch sensitivity at zero blade pitch angle and is later utilized for obtaining the β_K value. The pitch sensitivity values are estimated considering the frozen wake assumption rather than equilibrium wake assumption during the linearization process by FAST simulation model realized by Jonkman et al.[87].

$$\frac{\partial P}{\partial \beta}(\beta = \beta_K) = 2\frac{\partial P}{\partial \beta}(\beta = 0) \tag{5-40}$$

Therefore, the blade pitch controller design is started here with the approach employed by Wright and Fingersh[89] initially. According to them, an operating point close to the entry of Region 2 into Region 3 is first selected. This corresponds to the EP 4 in Table 1. Later, β_K is calculated according to the approach they utilized. By a linearization process, following system gain A, input gain, B and disturbance gain, B_d are obtained from the MS Bladed simulation model for NREL 5 MW turbine around the selected equilibrium point, EP 4.

$$A = -0.0554$$
$$B = -0.2658$$
$$B_d = 0.0227$$

When the desired damping ratio and natural frequency are used respectively as 0.8 and 0.6. The proportional and integral controller gains are estimated respectively via the equations (5-37) and (5-38).

$$K_p = 3.4033$$
$$K_I = 1.3544$$

EP 5 is the equilibrium point in Region 3 at which the input gain, B has doubled in its value. This equilibrium point is obtained by means of model linearization. Here, at the EP 5, β_K has a blade pitch angle value of 5.9676 degrees. Therefore, the gain correction factor, $GK(\beta)$, is obtained using this β_K value. The β value in GK formula in (5-39) may be obtained by different ways. Here, the adopted method is the interpolation of pitch angles with respect to wind speeds. For gain scheduling purpose, the above proportional, K_p and integral, K_i gains must be multiplied by the gain correction factor, GK in (5-39).

Figure 5-19 shows the performance of the gain-scheduled PI-based controller at other three equilibrium points, where step increasing wind inputs such as from 12 m/s to 13 m/s and 17 m/s to 18 m/s and lastly 22 m/s to 23 m/s are applied to the controlled MS

Bladed turbine model. Which are, in fact, correspond to EP 3, EP 1 and a newly added equilibrium, EP 6, respectively.

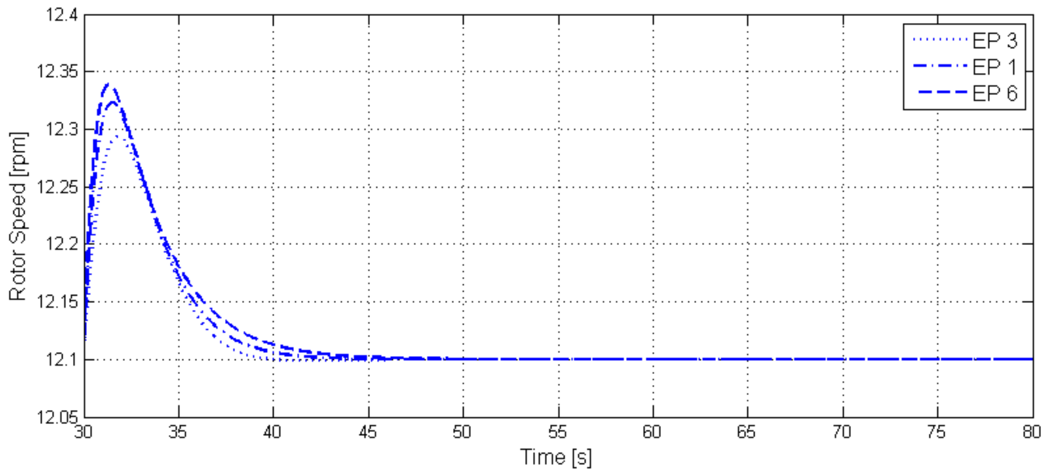

Figure 5-19 Gain scheduled PI-based pitch controller, the damping ratio of 0.8

As seen from the simulation results in Figure 5-19, the gain-scheduled pitch controller demonstrates almost the same performance at three different equilibrium points. This is contrary to the previously demonstrated poor performance of one linear controller (Figure 5-17) at different equilibrium points. The settling times of the rotor speed responses at these equilibriums are around 22 seconds. They are quite satisfactory even though they have slightly different rise and decay rates.

Figure 5-20 shows the change of gain correction factor, GK, whereas Figure 5-21 shows the changes of the controller proportional and integral gains based on GK with respect to blade pitch angle according to the approach of Wright and Fingersh[89].

Another approach to schedule the controller gains is to use the approach used by Jonkman et al.[87]. According to them, the proportional and integral gains are found by equation (5-41) and (5-42). However, these two equations are modified versions of the equations in Ref.[87]. They do not to include the gear ratio effect since the rotor speed is fed here to the controller, rather than the generator speed.

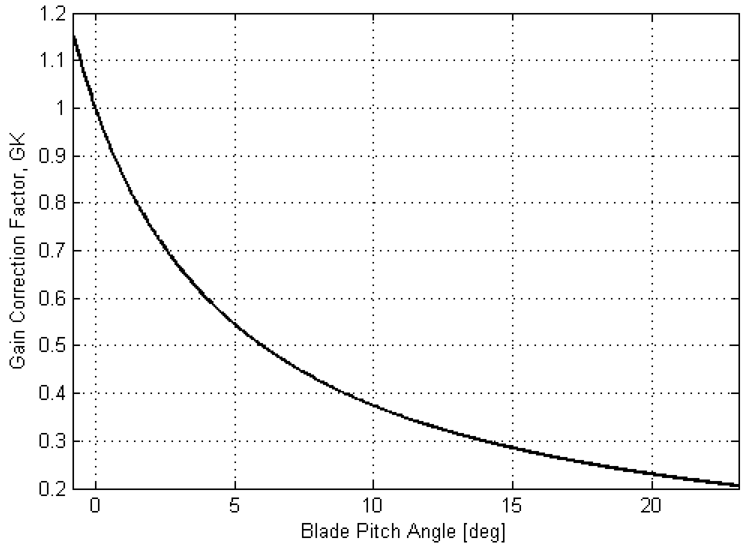

Figure 5-20 Gain correction factor versus blade pitch angle

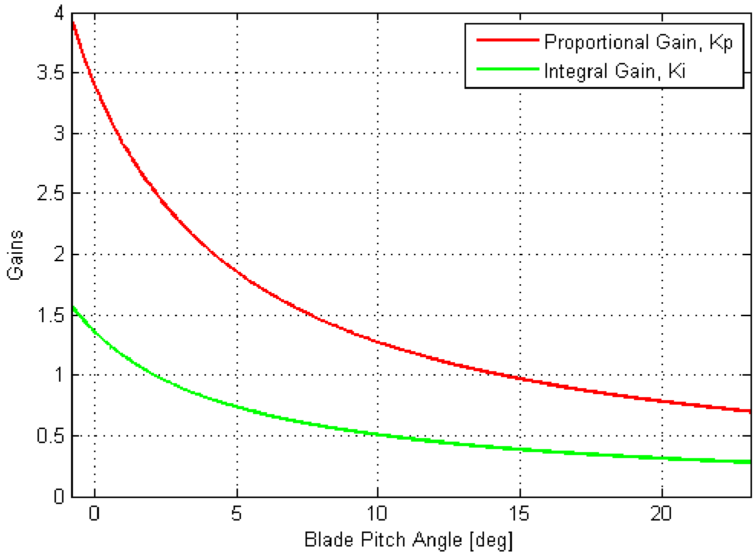

Figure 5-21 Proportional, K_p and integral, K_i gains versus blade pitch angle

$$K_P = \frac{2J_t\Omega_e\zeta w_n}{-\frac{\partial P}{\partial \beta}(\beta = 0)} GK(\beta) \tag{5-41}$$

$$K_I = \frac{J_t\Omega_e w_n^2}{-\frac{\partial P}{\partial \beta}(\beta = 0)} GK(\beta) \tag{5-42}$$

During the blade pitch controller design with the approach of Jonkman et al., a frozen wake assumption must be considered while obtaining the blade pitch sensitivity. This is due to the problem of the PI-based controller gains becoming quite large values around zero-degree pitch angle, which causes a loss of control authority. In addition frozen wake assumption is realized by fixing the elemental axial and tangential induced velocities, $-V_{bx_{i,j}}a_{i,j}$ and $V_{by_{i,j}}a'_{i,j}$ throughout each blade span during the linearization process[92]. However, in the equilibrium wake assumption, there is nothing changed in the MS Bladed simulation model during the linearization process.

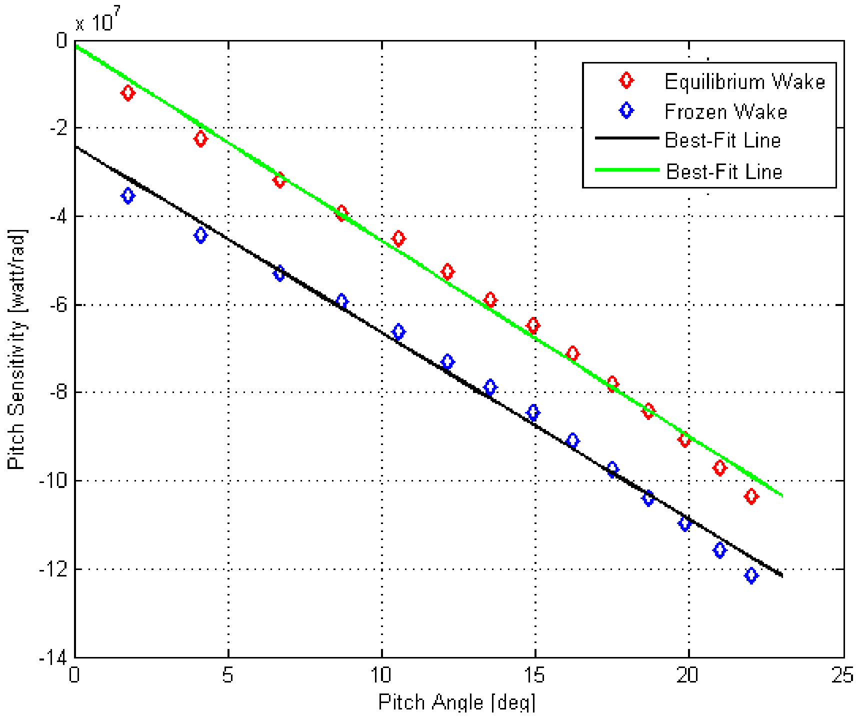

Figure 5-22 Best-fit line of turbine blade pitch sensitivity in Region 3

Figure 5-22 shows the pitch sensitivity versus blade pitch angle with the equilibrium wake and frozen wake assumptions. These are obtained from the developed MS Bladed simulation model and are given respectively by red and blue diamond symbols. Green and black lines are the best fit lines to these sensitivity values.

Table 5-4 gives the pitch sensitivity values in Region 3 obtained at different wind speeds at the rated rotor speed. They are estimated using the MS Bladed simulation model considering the equilibrium wake and frozen wake assumptions.

Table 5-4 Pitch sensitivity values with equilibrium wake and frozen wake

Wind Speed (m/s)	Rotor Speed (rpm)	Pitch Angle, Theta0 (deg)	Pitch Sensitivity, $\partial P/\partial \beta$ (Nm/rad) Equilibrium Wake	Pitch Sensitivity, $\partial P/\partial \beta$ (Nm/rad) Frozen Wake
11.4	12.1	1.7550	-1.2031e+07	-3.5300e+07
12	12.1	4.1478	-2.2355e+07	-4.4414e+07
13	12.1	6.7206	-3.1845e+07	-5.2797e+07
14	12.1	8.7276	-3.9205e+07	-5.9408e+07
15	12.1	10.5480	-4.5075e+07	-6.6269e+07
16	12.1	12.1431	-5.2444e+07	-7.2969e+07
17	12.1	13.5747	-5.9134e+07	-7.8825e+07
18	12.1	14.9525	-6.4757e+07	-8.4693e+07
19	12.1	16.2467	-7.1204e+07	-9.0975e+07
20	12.1	17.4908	-7.8125e+07	-9.7386e+07
21	12.1	18.7130	-8.4307e+07	-1.0377e+08
22	12.1	19.8754	-9.0658e+07	-1.0984e+08
23	12.1	20.9964	-9.7017e+07	-1.1585e+08
24	12.1	22.0646	-1.0362e+08	-1.2162e+08
25	12.1	23.1057	-1.0935e+08	-1.2735e+08

Investigating the performance of gain-scheduled controller designed by the approach used by Jonkman et al.[87] with the same natural frequency, w_n of 0.6 and damping ratio,ζ of 0.8 gives the responses in Figure 5-23 at the same equilibrium points EP 3, 1 and 6.

When the gains are scheduled according to the approach used by Jonkman et al.[87], all the settling times are again around 22 seconds after the same step increasing wind inputs are applied at 30th second of the simulation time. But, all the simulation results have larger peak responses than the ones in Figure 5-19, which are obtained by the approach of Wright and Fingersh[89].

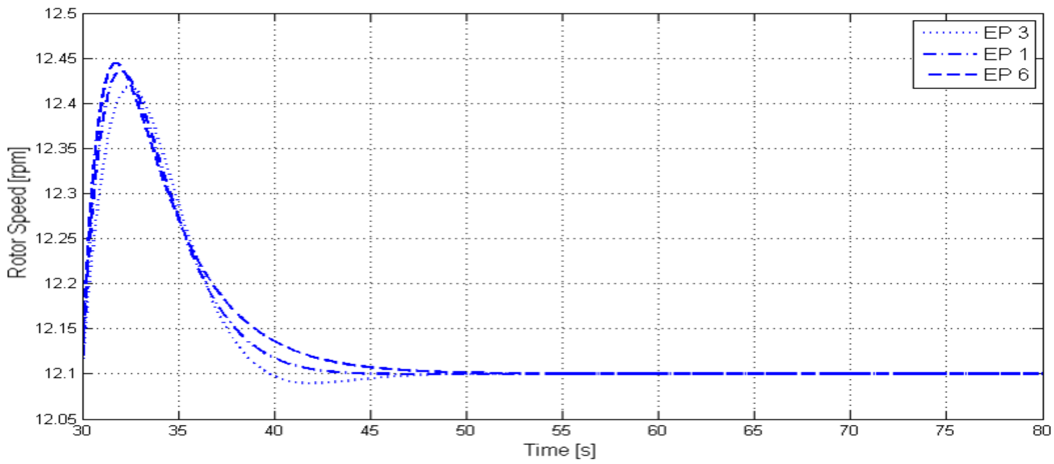

Figure 5-23 Gain scheduled PI-based pitch controller, the damping ratio of 0.8

Figure 5-24 shows the proportional, K_p and integral, K_i gains obtained here according to the approach of Jonkman et al.[87]. They are less than the ones obtained by Wright and Fingers[89] at the same blade pitch angle, β.

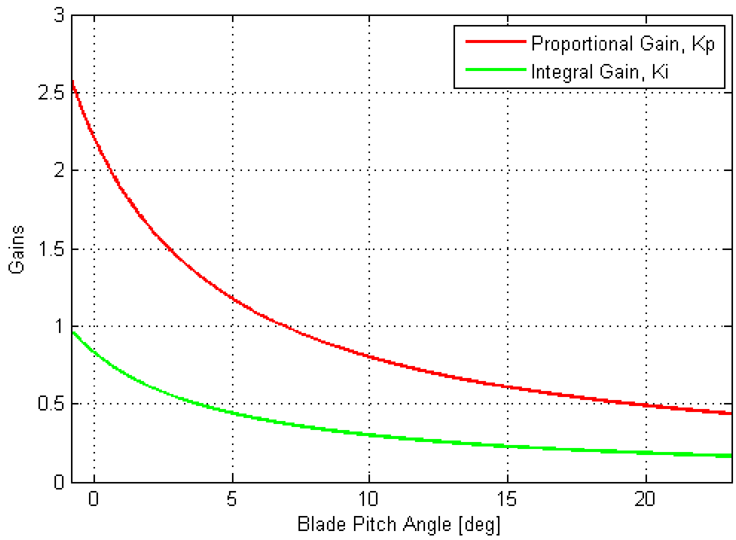

Figure 5-24 Proportional, K_p and integral, K_i gains versus blade pitch angle

5.6 Anti-Windup for Large Rotor Speeds to a Wind Gust

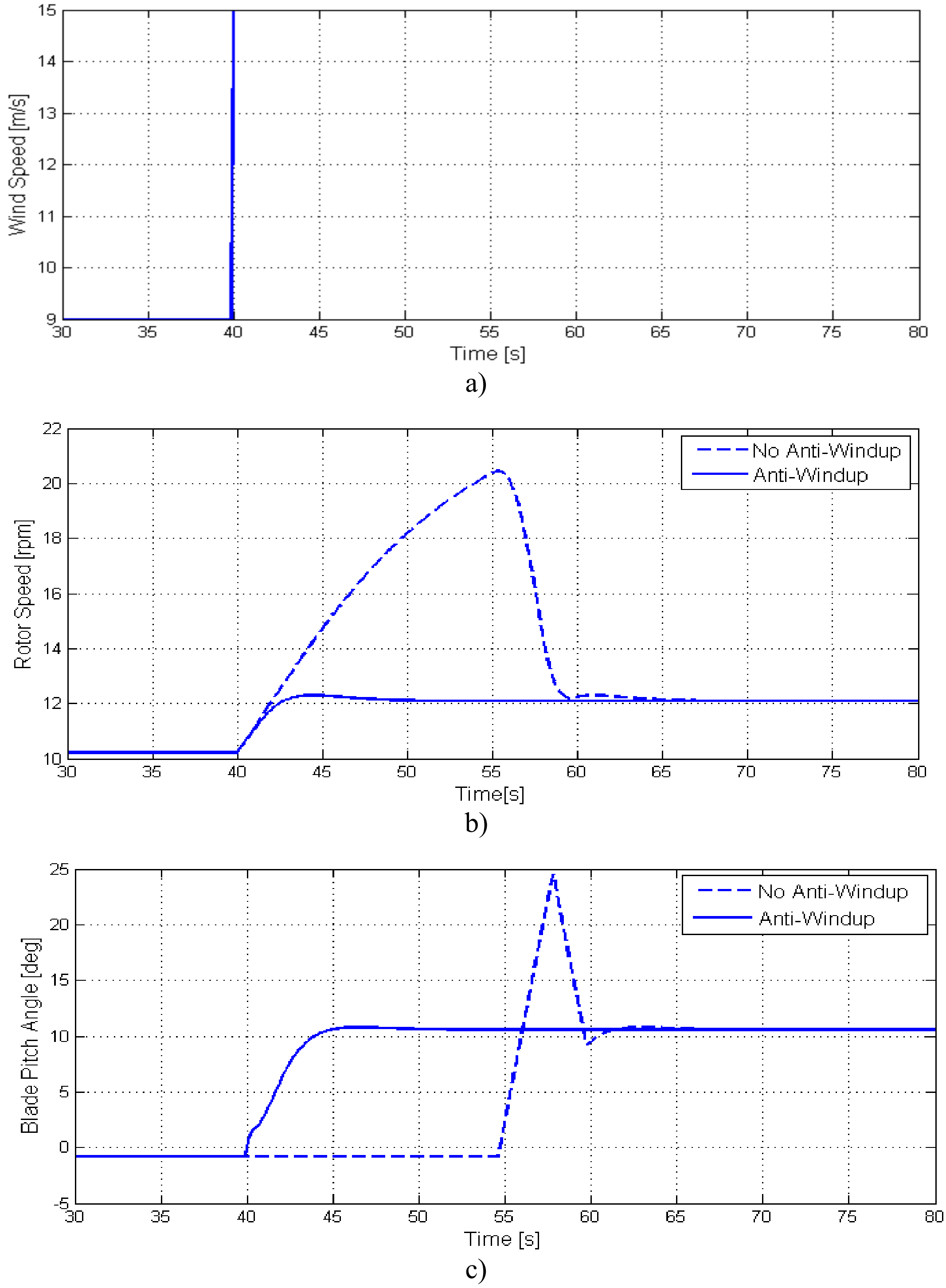

Figure 5-25 Anti-wind up to prevent rotor overspeed, a) Wind speed, b) Rotor speed, c) Blade pitch angle

In the previous subchapter, the focus is given on the design of a gain-scheduled PI-based blade pitch control system. However, there is a problem with the blade pitch control system performance when the turbine is subjected to a wind gust during a Region 2 operation and taking the turbine to Region 3 operation. A similar issue is also seen during the design of the baseline controller for the NREL CART turbine[89]. For instance, Figure 5-25-a shows such a wind gust rising from 9 m/s to 15 m/s at 40th second of the simulation time.

With the application of this wind gust to the controlled MS Bladed turbine simulation model, the rotor speed of the turbine reaches at very large values, starts over speeding (Figure 5-25-b) and reaches a rotor speed almost two times the rated rotor speed at the 56th second of the simulation time. Besides, the blade pitch angle of the turbine increases (Figure 5-25-c) sharply after almost 15 seconds after the gust hits to the turbine. This situation is dangerous for the wind turbine and occurs because of the following reason.

When the turbine operates in Region 2, the blade pitch angle is saturated to -0.875 degree. Therefore, the integrator component of the blade pitch controller takes a negative speed error. Then, the integrator in the pitch controller constantly integrates this negative error. This leads eventually to a negative blade pitch angle, with a saturated pitch angle of -0.875 degree. When the rotor exceeds the rated speed, a positive speed error is fed to the integral part of the controller. In order for this positive speed error to cancel the negative pitch angle effect, which has been accumulated from the integration of these negative errors. There appears a large delay between the moment when the gust hits to the turbine in 40th seconds and the moment when the blade pitch controller response becomes positive at around 55th seconds. These are seen from Figure 5-25-a and c. After around 60th seconds, the blade pitch control systems starts regulating the rotor speed properly. Eventually, in order to get rid of this undesired situation, an anti-windup is added to the controlled MS Bladed turbine model[89].

In the next chapter, simulation results of the designed pitch control system are given to a step by step increasing and decreasing wind input.

5.7 Simulations of the Gain Scheduled Collective Blade Pitch Controller

This subchapter deals with the simulation results for the gain-scheduled PI-based collective blade pitch controller. The controller performance is tested on the developed nonlinear MS Bladed simulation model with the same simulation time used for the generator torque controller. The generator torque controller aims to maximize the turbine power in Region 2 by operating the turbine at its maximum C_p. However, the aim of the collective blade pitch controller is to regulate the turbine rotor speed and therefore the turbine power. Unlike the generator torque control, pitch control system reduces the efficiency of the rotor as the wind speed increases in the above rated region.

Figure 5-26 shows the wind speed applied to the turbine model in time. As you see starting from the 40th second, the wind speed is increased with a step magnitude at every twenty seconds, and then is started to decrease at the 100th second with the same step magnitude at every twenty minute until the end of simulation time.

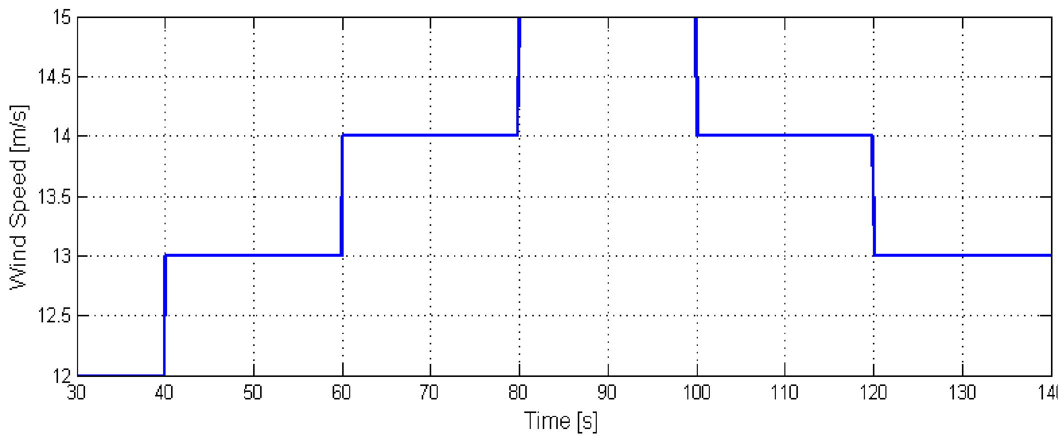

Figure 5-26 Wind speed

The gain scheduled PI-based collective blade pitch controller produces a blade pitch control signal in order to regulate the turbine rotor speed at the rated rotor speed. Whenever the wind speed changes (Figure 5-26), the pitch angles of all the rotor blades vary (Figure 5-27). Thus, the turbine rotor speed is regulated and eventually reaches at the rated rotor speed (Figure 5-28) after the transient response dies out.

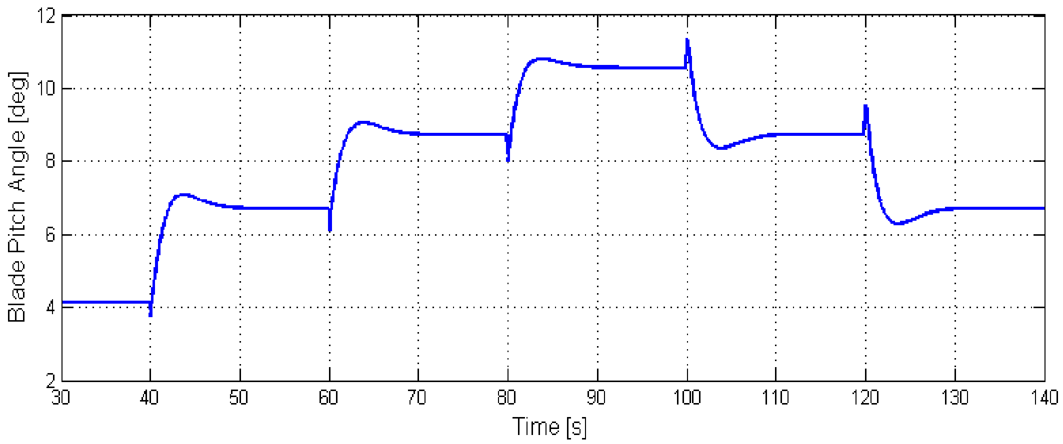

Figure 5-27 Blade pitch angle

When the wind speed increases (Figure 5-26), the blade pitch angle of the turbine increases and vice versa (Figure 5-27). This permits the turbine rotor to operate at the rated rotor speed, which is given as a reference signal to the controller. The most important point here is that the performance of the controller at any wind speed gives almost the same performance (Figure 5-28) due to the gain-scheduled proportional and integral gains.

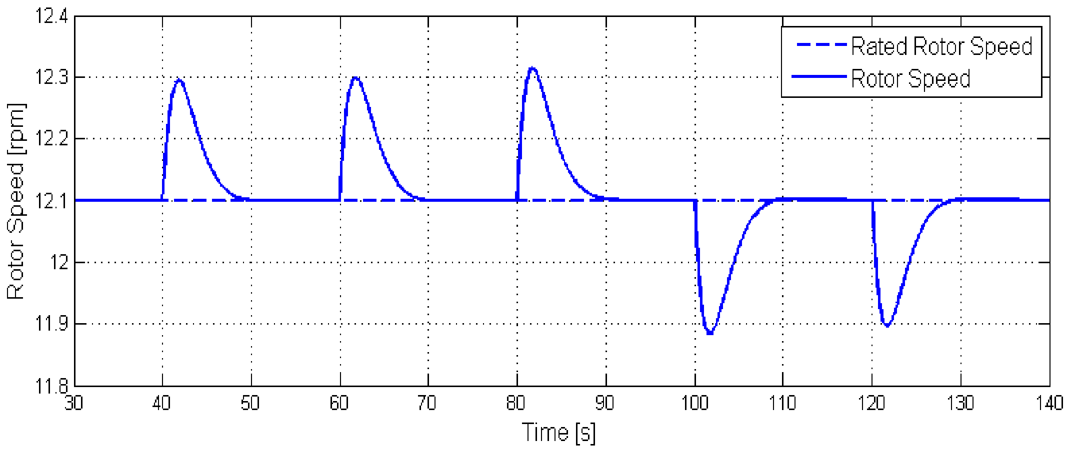

Figure 5-28 Rotor speed

As stated previously, in the above rated region, the electromagnetic torque of the turbine generator is kept constant as shown in Figure 5-29 with the dashed blue line.

The aerodynamic rotor torque of the turbine increases whenever an increasing step change occurs in the wind input. Controlling the blade pitch to feather reduces the AOA of each blade section. This results in the production of lower lift forces, so is the lower aerodynamic rotor torque in spite of increasing wind in the above rated region.

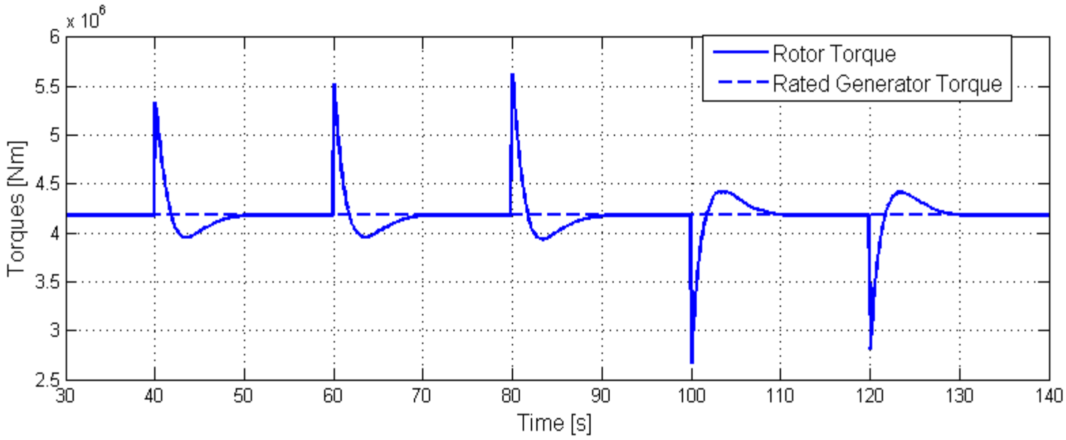

Figure 5-29 Rotor and generator torques

The torque difference between the aerodynamic rotor and generator torques is given in Figure 5-30. Since the generator torque is constant, the change in wind speed affects the aerodynamic torque only (Figure 5-29). Therefore, the torque difference (Figure 5-30) occurs much as soon as the wind speed changes and eventually becomes zero when the transient response dies out.

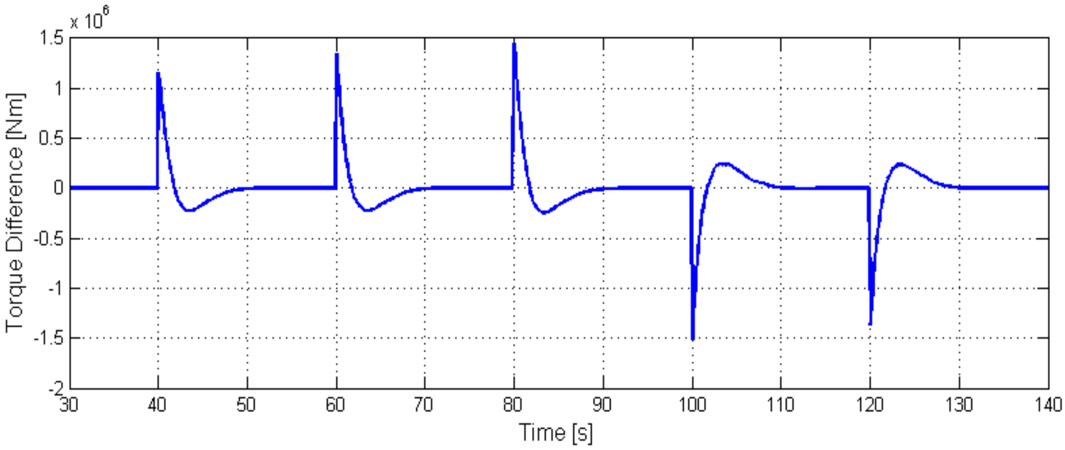

Figure 5-30 Torque difference

The generated electrical power is seen in Figure 5-31. When the turbine operates at an equilibrium point or at a steady-state condition, it produces 5 MW electrical power.

The sudden change in wind speed affects the produced power immediately. Increasing wind speed increases the power output and vice versa. This is, however, a very short duration. Here, the electrical power output is obtained by considering the generator efficiency of 94.4%[87].

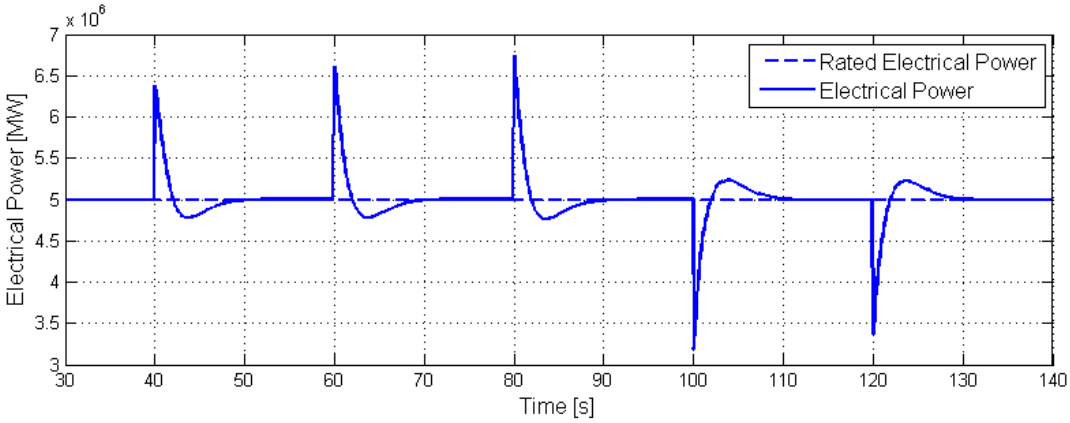

Figure 5-31 Turbine power

Figure 5-32 shows the changes in turbine thrust force. As the wind speed increases, the turbine thrust force decreases and vice versa due to the collective blade pitch control.

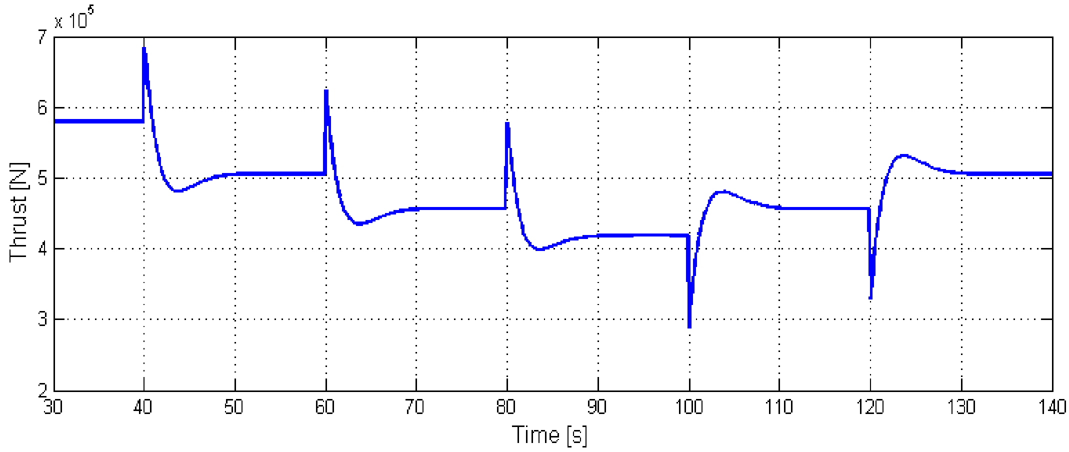

Figure 5-32 Turbine thrust

In Figure 5-33, the power coefficient, C_p decreases with the increasing wind speed, increases with the decreasing wind speed. Therefore, the efficiency of the turbine decreases as the wind speed increases and vice versa.

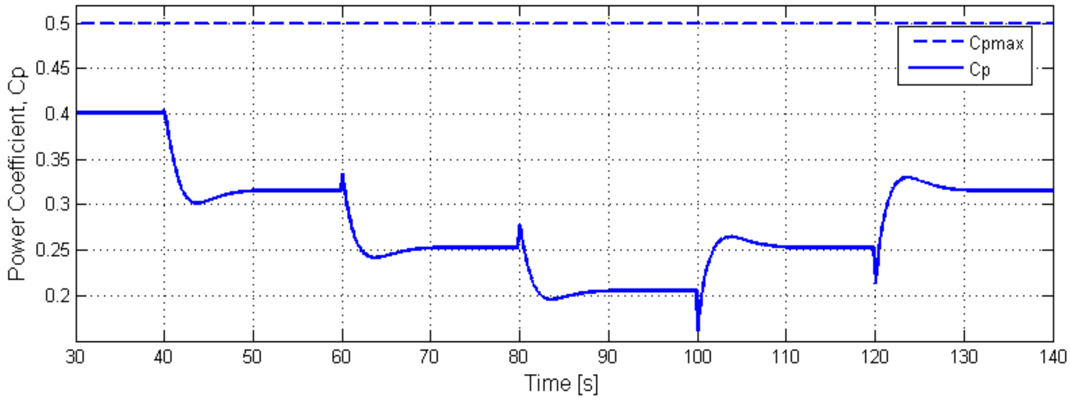

Figure 5-33 Power coefficient

Figure 5-34 shows the changes in turbine TSR. It decreases with the increasing wind speed, increases with the decreasing wind speed. As seen in the figure, it operates with a TSR less than the optimum value in the above rated region. Therefore, the C_p of the turbine is always lower than the C_{pmax} in the above rated region. This is clearly seen in Figure 5-33.

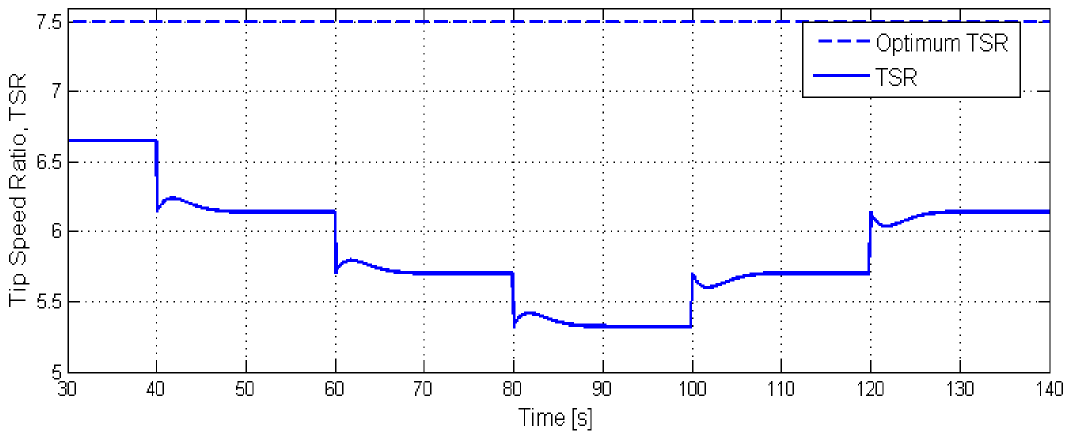

Figure 5-34 Tip speed ratio

5.8 Steady-State Response of the Controlled Wind Turbine

In subchapter 5.2 and 5.7, the responses of both controllers to changing wind speeds are investigated using the MS Bladed simulation model. These responses are given in terms of rotor speed, power, generator torque, blade pitch angle and so on. Here, in this subchapter, the aim is to show the steady-state responses of these turbine variables at various wind speeds starting from the cut-in up to the cut-out wind speed. The cut-in and cut-out wind speeds of NREL 5 MW turbine are 3 m/s and 25 m/s, respectively[87].

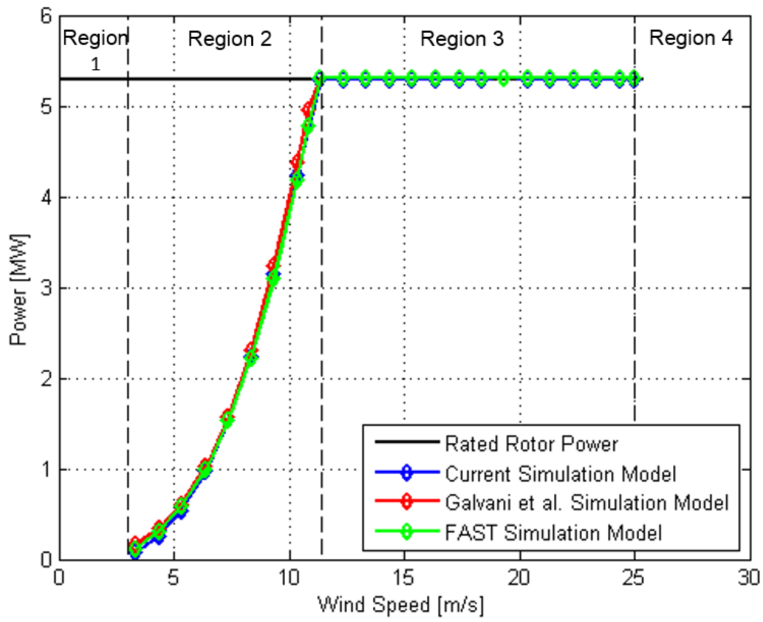

Figure 5-35 Controlled power curves without generator efficiency

.

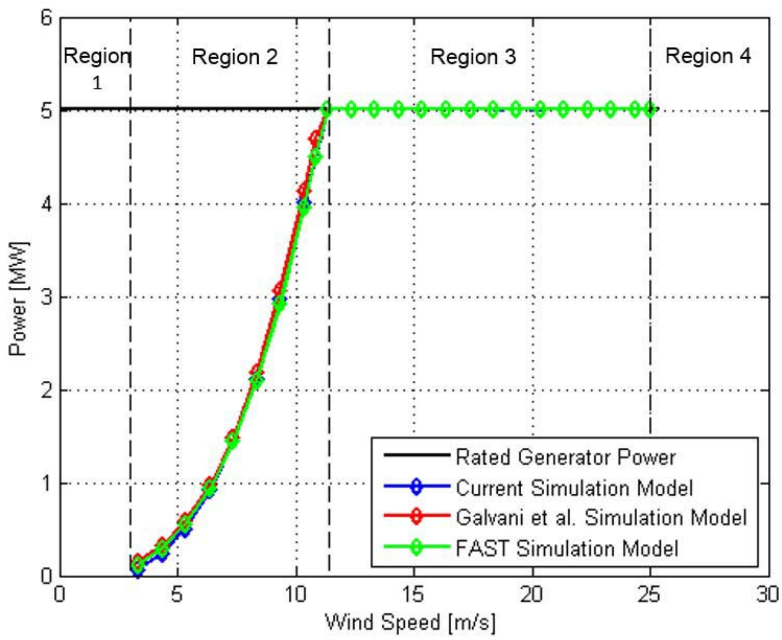

Figure 5-36 Controlled power curve with generator efficiency

Figure 5-35 and Figure 5-36 show respectively the controlled power curves for NREL 5 MW turbine without and with the generator efficiency. As seen in both figures, the current results of the controlled MS Bladed simulation model are almost the same as those of FAST simulation model except a slight difference close to the cut-in wind speed. The slight difference comes from the design of Region 1.5 controller. In Figure 5-4-b, a slightly different torque slope than that of Jonkman et al.[87] is obtained in Region 1.5 utilizing the same generator speeds (Table 5-1) as the borders for Region 1.5. This is occurred due to using different optimum operational lines in Appendix B Figure B.1. As seen in Figure 5-35 and Figure 5-36. The currently obtained controlled power curve in Region 2 is better than the previously obtained controlled power curve in Appendix B Figure B.4. Note that the given green-colored controlled power curve is obtained by Galvani et al.[76] using FAST simulation model. The controlled power curves in Figure 5-36 are obtained considering the generator efficiency. Therefore, due to obtaining pretty good results from the current controlled MS Bladed simulation model similar to those of FAST simulation model, all other turbine variables are also taken from the model at different wind speeds.

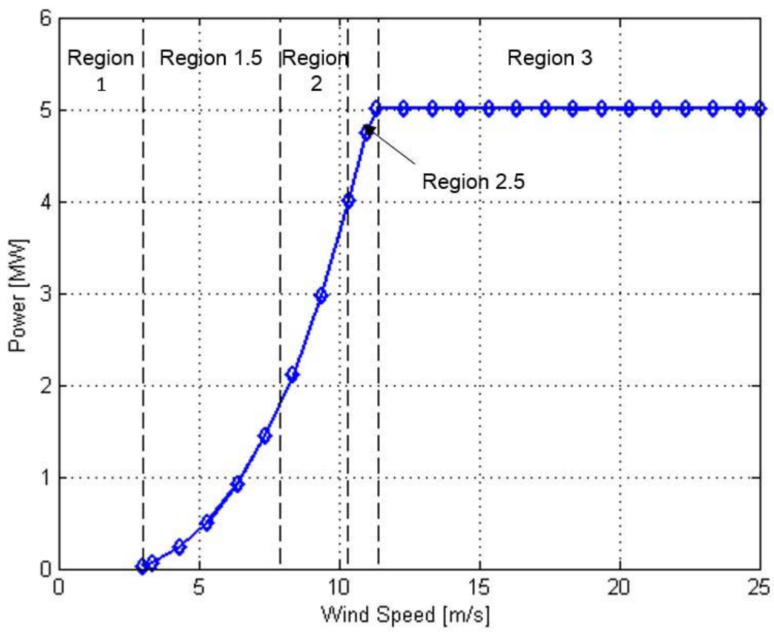

Figure 5-37 Power versus wind speed

Figure 5-37 gives the controlled power curve of the turbine with the generator efficiency included. In the below rated region, the power output of the turbine is less than the rated power because of the unavailability of strong winds. Here, the power is produced with the help of the generator torque controller, which helps the turbine rotor operate at maximum aerodynamic efficiency. Just after the cut-in wind speed, the power output depends on the Region 1.5 transition controller, whereas close to the rated wind speed, 11.4 $^{m}/_{s}$, the power is produced by the Region 2.5 transition controller. Between depends on the pure generator torque controller. In the above rated region, the power output of the turbine is regulated at 5 MW power by the designed collective blade pitch controller.

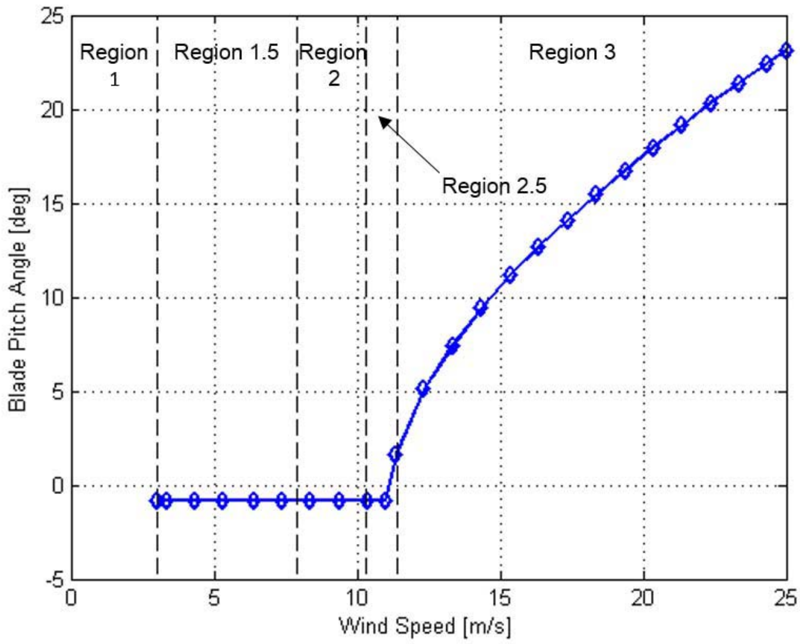

Figure 5-38 Blade pitch angle versus wind speed

Figure 5-38 shows that the blade pitch setting is kept at the optimum angle (Table 4-5) in the below rated region, i.e. Regions of 1.5, 2 and 2.5. However, in the above rated region or Region 3, when the wind speed increases the blade pitch controller increases each blade pitch angle with the same amount to regulate the turbine power. This power regulation corresponds to pitching the blades to feather, which decreases the AOA of each blade element and eventually reduces the elemental lift resulting in decreased turbine power.

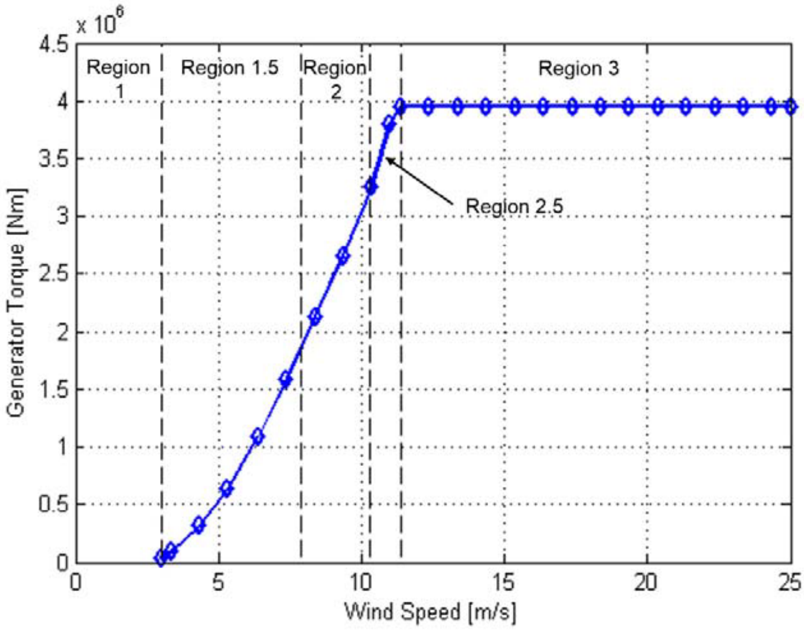

Figure 5-39 Generator torque versus wind speed

The generator torque controller adjusts the generator electromagnetic torque based on the rotor speed according to Figure 5-4-a. Figure 5-39 shows the generator torque controller output measured on the LSS of the generator with respect to the wind speed. The generator torque increases when the wind increases in the below rated region, while in the above rated region, it is fixed at its rated torque value.

Figure 5-40 shows the rotor speed versus wind speed. As seen in the figure, the rotor speed increases due to an increase in wind speed in the below rated region. Close to the rated wind speed, the Region 2.5 controller takes the control action in order not to let the turbine rotor exceed the rated rotor speed due to noise problem of the rotor blade tip speeds etc. This is realized by Region 2.5 torque controller which increases the generator torque sharply as seen in Figure 5-4-a (or Figure 5-4-b). This is referred to as torque speed ramp, as mentioned previously. In Region 3, however, the rotor operates at its rated rotor speed even if the wind speed increases until the cut-out wind speed.

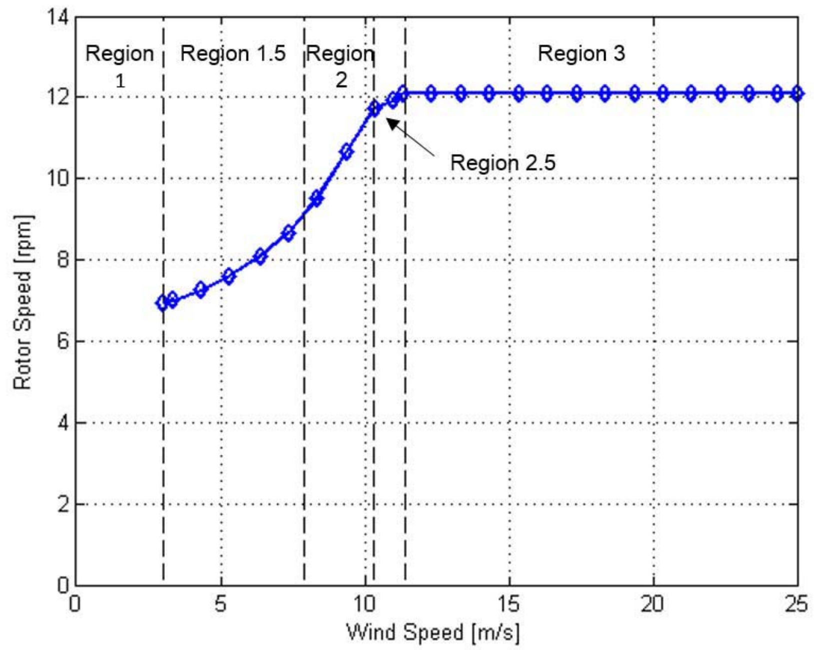

Figure 5-40 Rotor speed versus wind speed

.

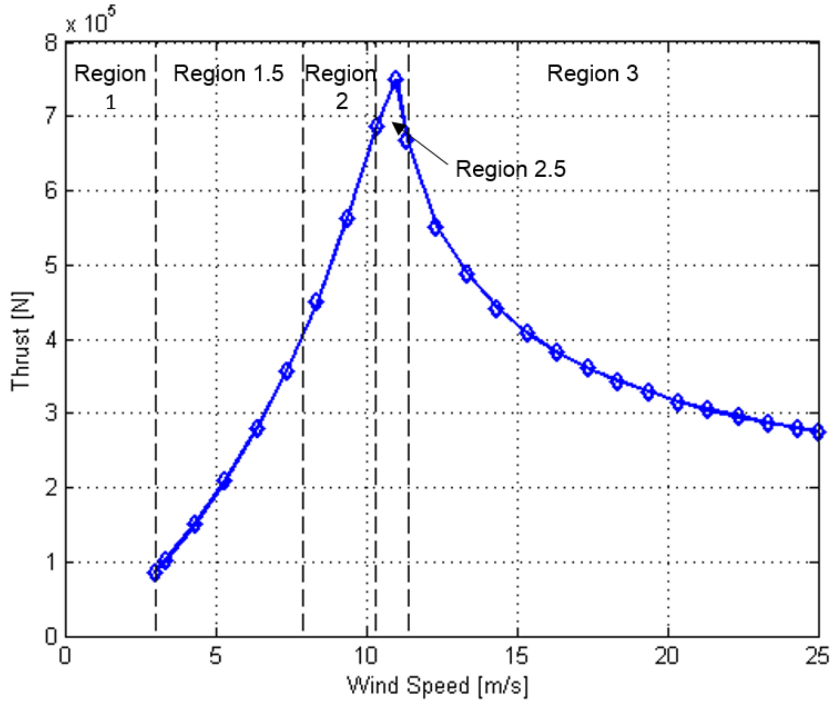

Figure 5-41 Thrust versus wind speed

Figure 5-41 shows how the thrust force of the turbine changes from cut-in to cut-out wind speed. As you see in the below rated region, when the wind speed increases, the thrust force increases. Conversely, in the above rated region, the thrust force decreases when the wind speed increases. The thrust force of the turbine peaks at around rated wind speed.

Figure 5-42 shows the changes in the power coefficient, C_p of the turbine rotor. Just after the cut-in wind speed (Region 1.5), turbine C_p is lower than the maximum C_p, but still the turbine is said to be operating in Region 2. Here, in the below rated region, the aim is to operate the turbine at its maximum C_p. Except for the transition regions, the turbine operates at its maximum C_{pmax}. Therefore, it produces the maximum power possible in Region 2.

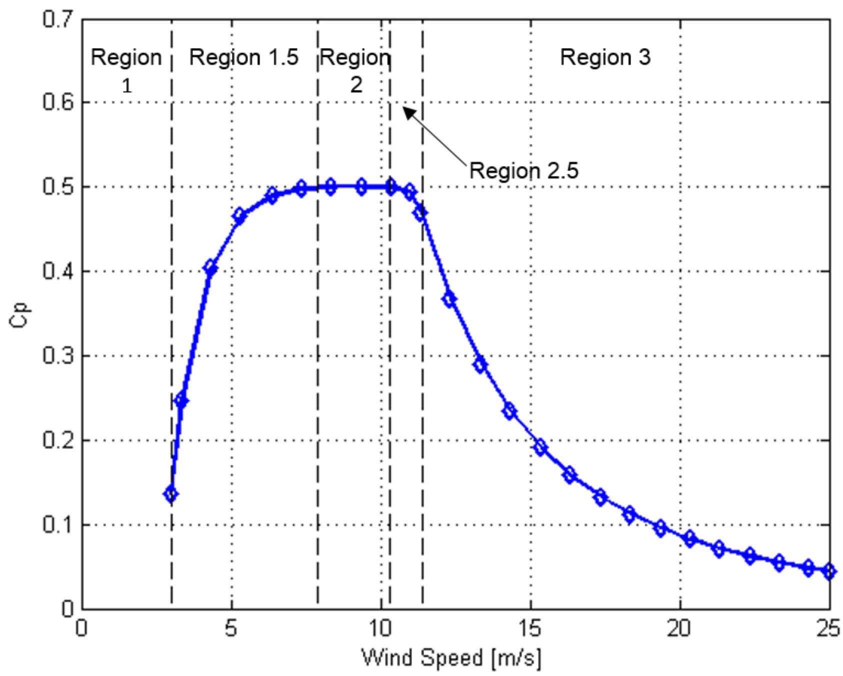

Figure 5-42 Cp versus wind speed

Figure 5-43 shows the change in turbine TSR with respect to wind speed. The turbine TSR decreases mostly with the increase in wind speed. However, in Region 2, the TSR is constant since the turbine operates at optimum TSR value. As stated before, this is achieved by the generator torque controller or power electronics unit. In Region 3, however, it decreases with the increase in wind speed.

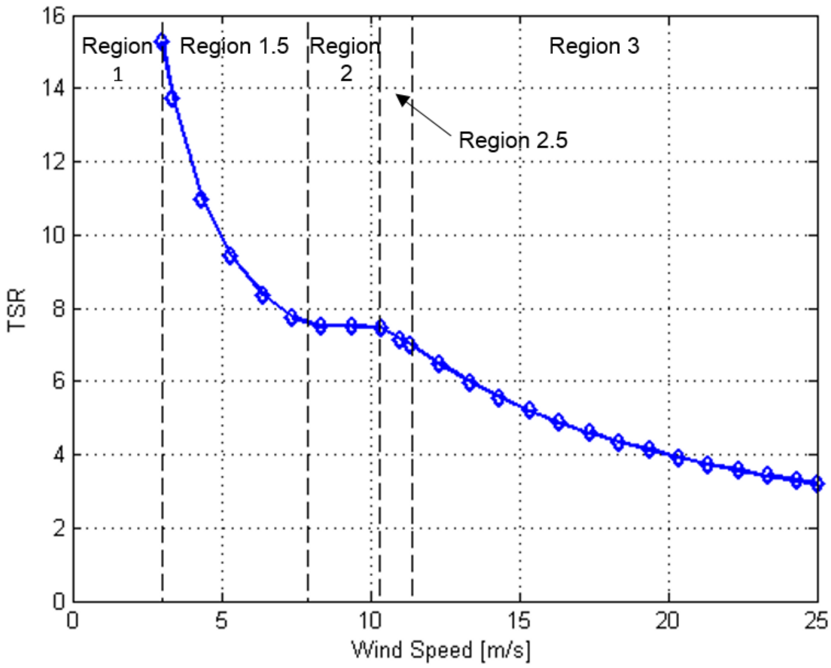

Figure 5-43 TSR versus wind speed

CHAPTER 6

ADAPTIVE ENVELOPE PROTECTION CONTROL SYSTEM FOR WIND TURBINES

In the previous chapter, generator torque and blade pitch controllers were designed, and then their simulations were evaluated in detail. In this chapter, the focus will be on a novel wind turbine envelope protection control algorithm or system. This algorithm is proposed here to protect the controlled turbines between cut-in and cut-out wind speeds, i.e. throughout the below and above rated regions. The algorithm is tested on the controlled MS Bladed simulation model with generator torque and collective blade pitch controller. The proposed approach uses an online learning neural network that adapts to various wind turbines and their operating conditions. Therefore, it may be applied to other types of turbines if required. However, this is not investigated in this thesis study. It is also used for flexibly-structured turbines. The proposed algorithm constantly monitors the current wind and turbine states through a neural network, i.e. learns the turbine situation online and simultaneously predicts the wind speeds that would push the turbine to the pre-defined envelope limits. When necessary, it produces an avoidance action to keep the turbine within a pre-defined limit boundary. Simulations realized on the controlled turbine under normal turbulent winds with different mean values show a promising capability to reduce excessive turbine loadings throughout the entire operational regions, i.e. the below and above rated regions.

Basically, an envelope protection control system keeps a machine within its pre-defined safe operational limits. For a wind turbine, these limits may be the excessive loadings, rotor speed, blade and tower oscillations or other situations considered critical during the turbine design process. In terms of loading, safe operation of a wind turbine is ensured if the critical loads stay within the pre-defined limits. Therefore, a wind turbine envelope protection system must constantly monitor the turbine operating situation in real time. By doing so, it must assure that the turbine operates always within the pre-defined safe limits. In order to do that, the protection system must detect the unsafe operational situations and must carry out a protection/avoidance action whenever the envelope limits are about to be violated.

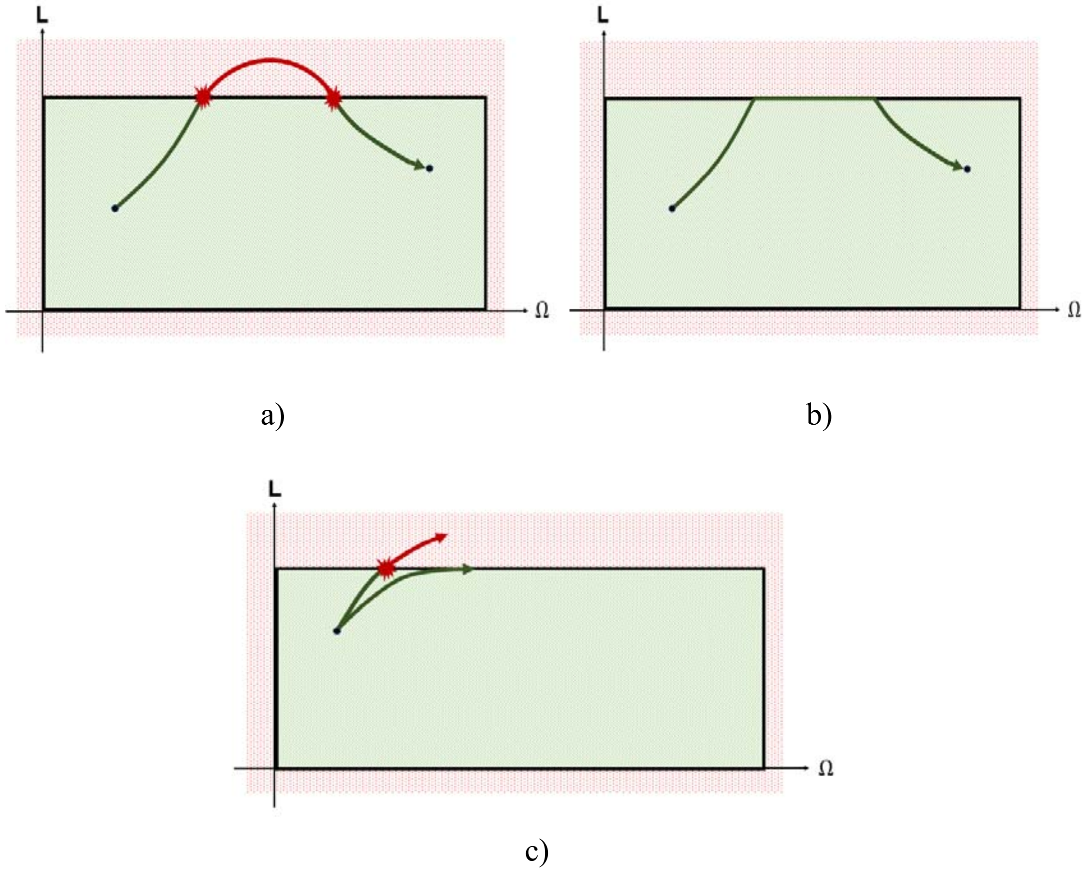

Figure 6-1 Envelope protection concept, a) Exceeding safe operation, b) Riding at the safe boundary, c) Predicting the near future and subsequent action

Figure 6-1 illustrates the conceptual example of an envelope protection control for a machine. Here, as an example, the load, L and rotor speed, Ω are taken into account. The green colored region is turbine safe operational region, while the outside is the unsafe operational region. As seen in Figure 6-1-a, without any envelope protection system, the load of the machine abandons the safe operational region. On the other hand, Figure 6-1-b shows a more desirable machine load response, riding at the safe operational boundary and never exiting into the unsafe domain. This is realized by predicting the near future response of the machine load. As soon as the future crossing of the safe boundary is detected, the envelope protection system takes an avoidance/protection action in order not to allow the machine load response to exit into unsafe operational region. This is illustrated in Figure 6-1-c.

Here, in the proposed system, turbine thrust force is selected as the limit parameter because it is a meaningful proxy for the vital design driving loads on some wind turbine components[45]. Besides, for the pitch to feather controlled turbines, thrust clipping or peak shaving method[35], [36] is utilized to reduce the turbine thrust force around the rated wind speed. This is due to the fact that the thrust forces of the pitch to feather controlled turbines get larger values and peak around the rated wind speed. This thrust peak is seen in Figure 5-41 as the controlled 5 MW turbine uses the pitch to feather technique for power regulation in the above rated region. As seen in the figure, the thrust force of the turbine increases as the wind speed increases in the below rated region, or Region 2. Around the rated wind speed, it reaches at its maximum value. However, it starts to decrease when the wind speed increases in Region 3. This undesired thrust peak is dealt with a method referred to as thrust clipping in the wind power industry. In this method, turbine blades are started to pitching to feather before the rated power is achieved. This limits the turbine thrust force at the expense of lower power output around the rated wind speed. Because the mean value of thrust force is reduced, peak fluctuations are reduced as well[36]. Nevertheless, since this method is off-lined shaped strategy and based on mean wind speed, it does not take into account the current loadings of turbines. Therefore, a more conservative method for thrust reduction is required.

A solution to the above problem is discussed in Ref.[25] and [34] by an online optimization-based algorithm, under the name of wind envelope protection control and wind turbine envelope riding, respectively. This algorithm protects the turbine not only around the rated wind speed, but also throughout the entire operational region, Regions 2, 2.5 and 3. The algorithm considers wind and turbine states and accordingly adjusts the power reference in order to protect the turbine from excessive loadings. This is carried out by varying both blade pitch angle and generator torque, i.e. the controller gain, in the below rated region and adjusting the rotor speed reference in the above rated region while keeping the generator torque at its rated value. The optimization-based algorithm requires the addition of baseline control laws to the reduced wind turbine model both for the below and above rated regions. This may arise a problem which requires the best knowledge of the algorithm used for baseline controllers on different turbines. Otherwise, application/design of the optimization-based algorithm may not be possible.

Here, the new approach, along with giving new capabilities, finds solutions to the above problem as well. The idea of the proposed system is inspired by an adaptive envelope protection system for fly-by-wire manned/unmanned fixed or rotary wing aircraft[47]–[50]. This approach uses an online learning neural network for the adaptation of unmodelled dynamics. Learning is realized in real time. Furthermore, it does not require an a priori training of neural networks using large amounts of data, which would be difficult to generate for all turbine operating conditions. It does not require excessive computation, either. The algorithm can adapt to any wind turbine's operational conditions. The neural network weights are updated in real-time according to an update law based on Lyapunov analysis[49]. A Linearly Parameterized Neural Network (LPNN) is utilized to approximate the nonlinear dynamics of the limit parameter. Weight update laws are designed in such a way that the neural network output eliminates the modeling uncertainty of the approximate limit parameter model. Therefore, the algorithm may potentially be used with various turbine configurations and sizes. Furthermore, this adaptive envelope protection system is rather straightforward to implement. The proposed protection algorithm is independent of the algorithms for baseline controllers unlike the optimization-based algorithms in Ref.[36], [45]. It also allows the turbine to efficiently ride at the desired envelope boundary. In this thesis study, rather than varying both blade pitch angle and generator torque, i.e. the controller gain, in the below rated region and adjusting the rotor speed reference and keeping the rated generator torque in the above rated region, the avoidance is realized only through the variation of the blade pitch reference thereby increasing the blade pitch angle. It is an add-on algorithm to the baseline blade pitch controller only. Therefore, there is no need for the intervention with the generator torque controller, i.e. power electronics unit.

Simulation evaluations have shown that the protection system is capable of keeping the turbine within the pre-defined thrust limit throughout the below and above rated regions, i.e. in Region 1.5, 2, 2.5 and 3. As examples, some of the simulation evaluations are demonstrated here for the below and above rated regions as well as at transition Region 2.5, i.e. around the rated wind speed, at which the turbine thrust force peaks to its maximum value(Figure 5-41). In order to achieve these simulations, three different normal turbulent winds with different mean values of 8, 11 and 15 m/s, are applied to the controlled MS Bladed simulation model with the adaptive envelope protection system.

The following subchapters define the principal parts of the proposed algorithm as well as the algorithm implementation and simulations in detail. Therefore, they respectively focus on the estimations of limit parameter dynamics, envelope wind speed and excessive loadings situation, the limit avoidance method, and lastly the algorithm implementation and simulation evaluations.

6.1 Estimation of Limit Parameter Dynamics with Neural Network

A limit parameter dynamics is a nonlinear function of turbine system states and inputs. This function alters whenever the turbine operating point or configuration changes. The approach here uses a linear approximate limit parameter model along with a neural network to estimate the limit parameter dynamics properly.

Therefore, a general nonlinear wind turbine system may be represented as

$$\dot{x} = f(x, u), \qquad x \in R^n \; u \in R^p \tag{6-1}$$

$$Y = g(x, u), \qquad Y \in R^q \tag{6-2}$$

where x represents the turbine states such as rotor speed, blade pitch angle etc., while u is the input to the wind turbine such as wind speed etc. Y, on the other hand, is the measurable system outputs. Let $y_l \in Y$ be a limit parameter with the following nonlinear equation.

$$y_l = h(x, u) \tag{6-3}$$

Since turbine states have different rise and settling times when, for instance, wind changes are applied, here, wind turbine states are divided into fast and slow states. Here, the blade pitch angle is considered as fast state, while turbine rotor speed is considered as slow state. During a transient response, the fast states are the states that dynamically influence the limiting parameter dynamics. Therefore, the equations for fast and slow states may be written as follows.

$$\dot{x}_s = f_1(x_s, u), \qquad x_s \in R^l \tag{6-4}$$

$$\dot{x}_f = f_2\left(x_f, u\right), \qquad x_f \in R^{n-l} \tag{6-5}$$

The instantaneous value of a limit parameter, y_l for a given input, u may be represented as,

$$y_l = h\left(x_s, x_f, u\right) \tag{6-6}$$

In order to obtain an estimate of limit parameter dynamics, the time derivate of y_l is taken for a constant input:

$$\dot{y}_l = h_{x_s}\dot{x}_s + h_{x_f}\dot{x}_f \tag{6-7}$$

Using equations (6-4) and (6-5), the limit parameter dynamics may be written as

$$\dot{y}_l = r\left(x_s, x_f, u\right) \tag{6-8}$$

When the limit parameter dynamics is written as a function of its value, y_l by assuming the fast states are as fast as the limit parameter dynamics. The final form is obtained as follows[50].

$$\dot{y}_l = r(y_l, x_s, u) \tag{6-9}$$

Therefore, the above equation is a suitable representation of limit parameter dynamics in transient phase. Here, the limiting parameter is assumed to be approximately as fast as the fast states. Therefore, this limit parameter may be a force or moment that is formed by the states and input. Estimation of this actual limit parameter dynamics is a purpose of the algorithm. This is achieved using an approximate linear model of (6-9) and augmenting with neural networks. Thus, let $\hat{y}_l$ be the output of the employed linear approximate model.

$$\dot{\hat{y}}_l = A\hat{y}_l + Bu \tag{6-10}$$

and therefore the actual limit parameter dynamics may also be written as[49]

$$\dot{y}_l = \hat{r} + \xi(y_l, x_s, u) \tag{6-11}$$

where $\xi(y_l, x_s, u)$ corresponds to the modeling error in the limit parameter dynamics, $\hat{r}$ represents the approximate model in (6-10) and therefore, modeling error is

$$\xi = r - \hat{r} \tag{6-12}$$

Since the approximate linear model in (6-10) does not represent the actual limit parameter dynamics, it is augmented here with an adaptive neural network to improve the limit parameter estimation. Thus, the resulting dynamics of the estimate is obtained as (6-13). The block diagram for the online estimation of limit parameter dynamics is seen in Figure 6-2.

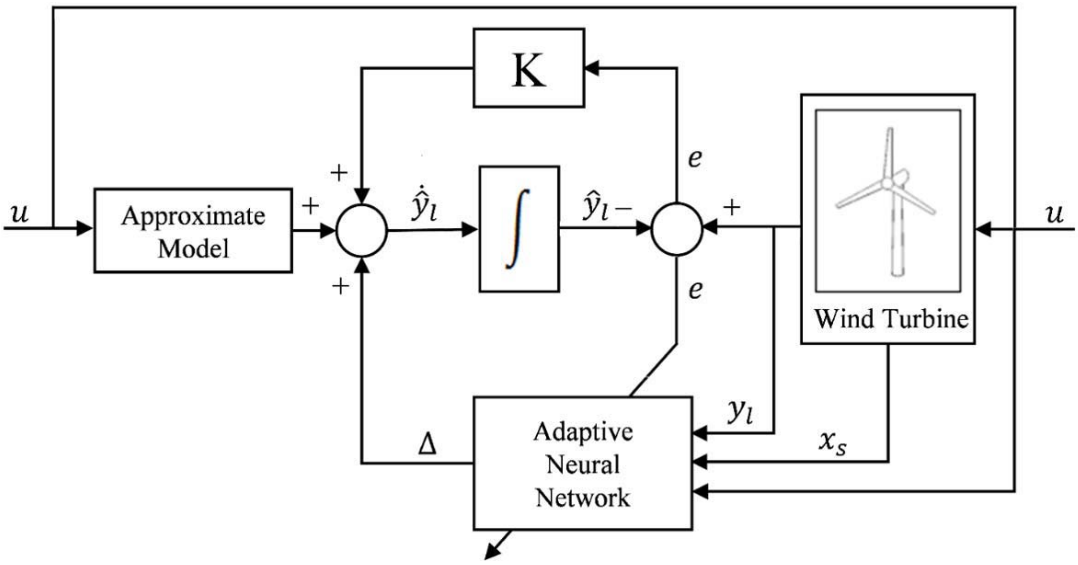

Figure 6-2 Online estimation of the limit parameter dynamics[49][50]

Besides, equation (6-13) includes an error feedback term, i.e. an observer, to provide additional stability to the error dynamics[49], [50].

$$\dot{\hat{y}}_l = \hat{r} + \Delta(y_l, x_s, u) + K(y_l - \hat{y}_l) \tag{6-13}$$

where K is the observer gain matrix and the $\frown$ stands for the estimated variables. The error dynamics is constructed between the actual and the estimated limit parameter. Therefore, the error is defined as,

$$e = y_l - \hat{y}_l \tag{6-14}$$

When the equation (6-13) is subtracted from (6-11), the error dynamics turn out to be[49].

$$\dot{e} = -Ke + \xi - \Delta \tag{6-15}$$

When ξ and Δ cancel each other, the error goes to zero asymptotically. If not, the term $\xi - \Delta$ in (6-15) behaves as a forcing input to the error dynamics[49]. In the formulation of error dynamics, (6-15), $\Delta(y_l, x_s, u)$ is obtained by means of neural networks such as a Single Hidden Neural Network (SHLNN) or a Linearly Parameterized Neural Network (LPNN) etc. Here, as stated previously, a LPPN is employed as an approximator whose design is carried out as[49],

$$\Delta = W^T \delta(\mu) \tag{6-16}$$

where W, δ, μ and Δ represent respectively the network weights, basis functions, input vector and the network output. The network weight update law[49] is given as,

$$\dot{\widehat{W}} = \Gamma\left(\delta e^T P - k\widehat{W}\|e\|\right) \tag{6-17}$$

where k is the e-modification term, Γ is the learning rate of the neural network, e is the error and P is the solution of the following Lypunov equation.

$$(-K)^T P + P(-K) = -I \tag{6-18}$$

and δ is defined as follows[49],

$$\delta(y_l, x_s, u) = D_1 \oplus D_2 \tag{6-19}$$

D_1 and D_2 are the vectors defined considering 1s as the bias terms and $\oplus$ represents the Kronecker product.

$$D_1 = [1\ y_l\ x_s] \tag{6-20}$$

$$D_2 = [1\ u] \tag{6-21}$$

More about the theorem for adaptive neural network update law is available in Appendix B 1.

6.2 Estimation of Envelope Wind Speed and Potential Excessive Loading

Envelope wind speed is predicted by the newly introduced concept of unsteady dynamics. This is caused by the fact that the limiting variable, i.e. thrust force, has an unsteady behavior due to the turbulent wind blowing through the turbine and is always in transient phase. In a supportive way, both fast and slow states do not get their steady state unlike the fast states reaching their steady-state values in dynamic trim concept, while the slow states are still changing in time[47], [49]. Therefore, since the time rate of change of fast states is not zero during turbine operation, and therefore the turbine thrust force. Therefore, the dynamic trim concept seems not a valid choice for the design of envelope protection system for wind turbines.

The estimated envelope wind speed is very different from the actual wind speed due to the fact that it is calculated considering the turbine operating conditions as well as the limit parameter value. The estimation of envelope wind speed is important to determine whether the turbine potentially operates with excessive loadings or not. Here, this wind speed is estimated using the equation of the LPNN augmented limit parameter dynamics in (6-22). Using the limit parameter dynamics in (6-13), the approximate model in (6-10) and the error in (6-14) gives the following[49].

$$\dot{\hat{y}}_l = A\hat{y}_l + Bu + \Delta(y_l, x_s, u) + Ke \tag{6-22}$$

When the desired value of the limit parameter is summited in its place, $\hat{y}_l$ and solved for u. Then, the envelope input which takes the turbine to the limit boundary is obtained as,

$$u_{env} = -B^{-1}\left(Ay_l + \Delta(y_l, x_s, u) + Ke - \dot{\hat{y}}_l\right) \tag{6-23}$$

In (6-23), $\dot{\hat{y}}_l$ is an internal variable and is not measured. However, other variables such as x_s, y_l, and u are measurable variables of wind turbines. In addition, $\hat{y}_l$ is assumed to be a smooth function. In this thesis study, the thrust force, T is chosen to be the limit parameter, y_l, while the wind speed, U and Ω are respectively the input, u to the controlled turbine and the slow state, x_s of the turbine. Then, U_{env} represents the envelope wind speed. In (6-23), $\dot{\hat{y}}_l$ is kept in the above equation to reflect the transient behavior of the limit parameter, which is referred to as unsteady dynamics concept and is introduced newly to the literature with this thesis study. The reason is that the turbine states stay mostly in transient phase due to the turbulent nature of wind. Further, all the turbine states do not get their steady-state because of the turbulent nature of wind. Hence, the time derivative of the fast states is not zero as opposed to in dynamic trim concept, first introduced by Horn et al.[47]. This situation is overcome here with a new concept, referred to as unsteady dynamics. In this concept, none of the states reaches at their steady-state conditions and mostly stay in transient phase.

For a turbine operating with excessive loading, it is expected here that the actual wind speed should be larger than the envelope wind speed. Therefore, an accurate estimation of envelope wind speed is required to decide on accurate loading information, i.e. excessive or not. It is experienced that utilizing the same sign in the selected approximate model for a and b results in an envelope wind speed that gives inaccurate loading information, while the opposite sign gives correct loading information, i.e. an actual wind speed larger than the envelope wind speed corresponds to excessive loading. Besides, the approximate model in (6-28) should be as accurate as possible since the augmented linear approximate model in (6-29) is also utilized to calculate the envelope wind speed as in (6-32).

An approximate model may be selected by utilizing the controlled MS Bladed turbine model, online limit parameter dynamic estimation and the turbine simulation model-aerodynamic model. A selected approximate model may be said to be accurate enough if the envelope wind speed estimated at an instant of time causes the turbine to produce the pre-defined thrust force limit value considering the values of controlled turbine states, rotor speed, blade pitch angle etc., formed by the actual wind speed applied to the turbine at that time instant.

Afterward, comparing the properly estimated envelope wind speed, U_{env} with the actual wind, U gives the information about the turbine loading. The actual wind speed may be obtained by a wind speed sensor, a wind speed estimator or a LIDAR device. When the actual wind is less than the estimated envelope wind speed, the turbine is considered safe, operating below the pre-defined envelope boundary, therefore with low loads. However, once the actual wind speed is larger than the estimated envelope wind speed, the turbine potentially operates with excessive loadings. Thus, having such a situation requires a corrective or avoidance action not to let the turbine exceed the envelope boundary. Relation (6-24), which is adopted here, gives the comparison of the envelope and actual wind speeds and is used to decide the loading, excessive or not.

$$\Delta U = U_{env} - U \tag{6-24}$$

For the limit avoidance, the information, ΔU should be utilized in such a way that it increases turbine blade pitch angles in order to reduce turbine loadings in any case of excessive loading situation.

6.3 Wind Turbine Limit Avoidance

In the literature, the limit avoidance for unmanned systems is realized by two means; control or command limiting[48]. Here, the control limiting technique is used not only for the below rated region; Region 1.5, 2, and 2.5, but also for the above rated region, Region 3. This is realized by adjusting the output of the collective blade pitch control systems, i.e. changing the blade pitch angle reference, β_{ref}. This avoidance method is utilized here only both for the below and for the above rated regions unlike employing different avoidance methods as in Ref.[36], [45]. This makes the proposed method easier to apply to available turbines because of having no intervention with standard generator torque controller, i.e. a power electronics unit in today's wind turbines. None of the turbine controller designs are changed during the implementation of the algorithm since it is an add-on algorithm to the baseline blade pitch controller.

The avoidance, both in the below and above rated regions, is obtained by reducing the turbine power output. This is achieved here by increasing the blade pitch reference, β_{ref}, resulting in increasing the pitch angle, β. In the below rated region, this method reduces the aerodynamic efficiency of the turbine, i.e. operates the turbine away from the maximum power coefficient, C_{pmax}, that the turbine is desired to operate. The avoidance action moves the blade pitch angle away from the fine pitch angle, $\beta \neq \beta_{*}$. Similarly, increasing the blade pitch angle results in power output reduction for the above rated region as well. Therefore, the thrust force of the turbine is reduced throughout these operational regions. The intervention to the blade pitch controller output eventually corresponds to a change in turbine operating point.

Note that in Chapter 5, during the designs of generator torque and blade pith controllers, generator and blade pitch actuator dynamics were not taken into account as in Ref[87]. But here, these dynamics are included to the closed loop turbine system using first order transfer functions with the time constants of 0.1 and 0.2, respectively. The generator torque actuator is assumed to have a faster dynamics. Therefore, the transfer functions between the inputs and outputs of the torque and blade pitch actuators are adopted as follows.

$$\frac{\tau_g}{\tau_c} = \frac{1}{0.1s + 1} \tag{6-25}$$

$$\frac{\beta}{\beta_{ref}} = \frac{1}{0.2s + 1} \tag{6-26}$$

The general block diagram for the turbine limit avoidance is shown in Figure 6-3. As seen in the figure, the envelope protection system intervenes with the output of the blade pitch control system, β_{ref} and thereby adjusting the blade pitch angle, β whenever a limit parameter violation occurs.

From the block diagram, it is easy to understand that the adaptive envelope protection system estimates the amounts of blade pitch angle reference, $\Delta\beta_{ref}$, to be adjusted for protecting the turbine. Here, this amount, $\Delta\beta_{ref}$ is estimated at each instant of time and is obtained by the following relationship.

$$\Delta\beta_{ref} = \varepsilon \Delta U \qquad (6\text{-}27)$$

Where ε and ΔU represents the design parameter for the effective limit avoidance and the comparison of the envelope and actual wind speeds. The amount of $\Delta\beta_{ref}$ should be utilized in such a way that it increases the blade pitch angle reference, β_{ref} i.e. the output of the controller.

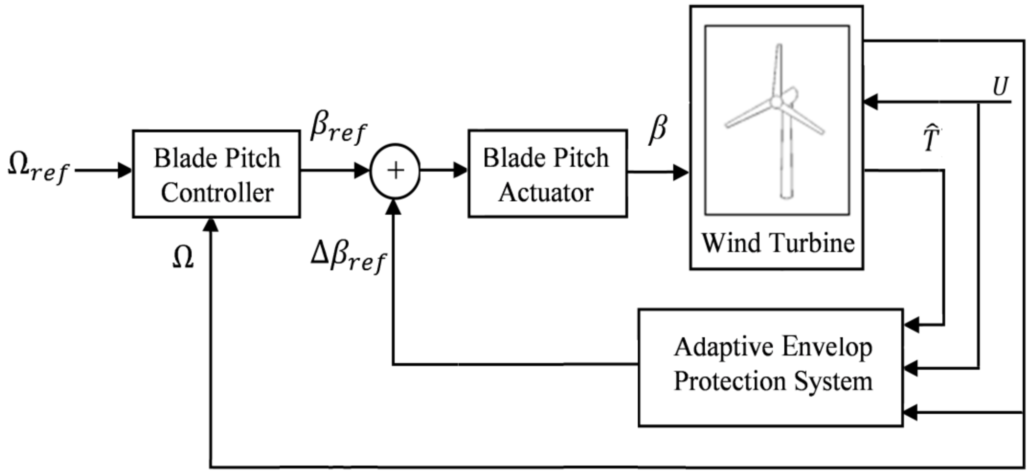

Figure 6-3 Limit avoidance by control limiting technique

Therefore, the sign of the design parameter, ε is selected here as to be negative since ΔU becomes negative when the actual wind speed is larger than the estimated envelope wind speed or when the turbine is outside the safe operational region. This produces a positive $\Delta\beta_{ref}$ information that eventually increases the blade pitch angle. Here, the proposed system protects the turbine only if the turbine is about to exceed the pre-defined envelope boundary.

The main benefit of an envelope protection system is that it allows the turbine to operate at the limit boundary whenever a potential excessive loading occurs. This expectedly allows the turbine to acquire a longer service life. However, the distinctive benefit of the proposed adaptive envelope protection is that it only requires an approximate linear model for the limit parameter estimation, the unmodelled dynamics is handled by neural networks. Furthermore, it is very fast in adaptation to varying turbine operational conditions.

6.4 Algorithm Implementation and Simulation Results

During the design process of the proposed envelope protection system, the following are realized based on the concept described in the above subchapters considering the turbine thrust force, T as the pre-defined limit parameter. Therefore, the approximate model in (6-10) is constructed for the turbine thrust force as follows.

$$\dot{\hat{T}} = a\hat{T} + bU \tag{6-28}$$

where $a = -0.24,\ b = 0.0175,\ U$ is the actual wind input to the turbine. When the above approximate linear parameter dynamics in (6-28) is augmented by the LPNN considering (6-13), the following is obtained for the accurate estimation of the desired thrust limit dynamics.

$$\dot{\hat{T}} = a\hat{T} + bU + \Delta(T, \Omega, U) + K(T - \hat{T}) \tag{6-29}$$

where the turbine rotor speed, Ω, is considered to be a slow state, whereas the blade pitch angle, β to be a fast state.

Table 6-1 Design parameters for the adaptive envelope protection system

Observer Gain, *K*	50
Learning Rate, *Γ*	25
e-modification term, *k*	0.02
Parameter, *P*	0.01
Design parameter, *ε*	-2.5

Therefore, in transient phase, the limit parameter is affected by both fast and slow states. The effect of fast state, i.e. the blade pitch angle, β, is inside the thrust force dynamics considering the thrust dynamics to be a function of limit thrust value, $\hat{T}$. The blade pitch angle is assumed as a fast state as fast as the thrust force. The adopted values of other design variables for the LPNN-based adaptive envelope protection system are given in Table 6-1. Besides, in this thesis study, the vectors in (6-20) and (6-21) are adopted respectively as

$$D_1 = [1\ T\ \Omega] \tag{6-30}$$

$$D_2 = [1\ U] \tag{6-31}$$

Thus, the envelope wind speed, U_{env}, is calculated by plugging the pre-defined limit thrust value, T into the corresponding place of the equation in (6-32). As stated previously, the adopted approximate model in equation (6-28) should be selected in a way that that it can accurately predict the envelope wind speed that pushes the turbine to the desired envelope boundary, i.e. thrust limit. For instance, it is experienced that the parameter, b in equation (6-28) has a dominant effect on the estimation of an accurate envelope wind speed.

$$U_{env} = -b^{-1}\left(aT + \Delta(T,\Omega,U) + Ke - \dot{\hat{T}}\right) \tag{6-32}$$

The above-predicted envelope wind speed, U_{env} is compared with the actual wind speed, U, to obtain the information about the loading of the turbine. This comparison is realized by equation (6-24) for the below and above rated region, i.e. for the entire operational regions. According to the adopted formulations here, a positive estimation of ΔU results in a turbine operation within the safe operational limit. Conversely, a negative value of ΔU corresponds to an operation outside the pre-defined envelope, i.e. with excessive loadings. This ΔU information is used for the protection of the turbine through equation(6-27). Thus, in that case, a proper avoidance action, as defined in subchapter 6.3, must be realized in advance to get rid of the undesired situation.

6.5 Simulation Results of Envelope Protection Control System

After all, the effectiveness of the proposed adaptive envelope protection control algorithm is explored under normal turbulent winds with different mean values both for the below and above rated regions. Wind series is obtained using the SWIFT program developed by ECN[93] according to the IEC61400-I normal turbulence model for a Class IA wind turbine. The turbine thrust force, T, is limited to 0.55 MN. All these investigations have shown that the algorithm has managed to handle with envelope violations under all the normal turbulent winds in the below and above rated regions as well as around the rated wind speed. As examples, three different normal turbulent winds with different mean values are taken into consideration here. These wind speeds have a mean wind of 8, 11 and 15 m/s. These wind speeds fall in the below rated region or Region 2, in the transition region or Region 2.5, i.e. around the rated wind speed, and above rated region or Region 3, respectively. Simulation results are given for a duration of 50 seconds. The neural network weights are selected zero initially. Therefore, just at the beginning of the simulations, weights are adapted online to the turbine operation in few seconds. This may be understood from the rise of weights from zero to the required values for the current wind and turbine states. The protection system is activated at the 10^{th} second of every simulation.

6.5.1 Simulation Results for Below Rated Region

Before focusing on simulation results of the proposed envelope protection system, it would be better to start with showing the limit parameter dynamics estimation, i.e. the thrust force, with the approximate model only (equation (6-28)) and the neural network augmented model (equation (6-29)). Afterward, the proposed adaptive system is activated and simulation results are presented.

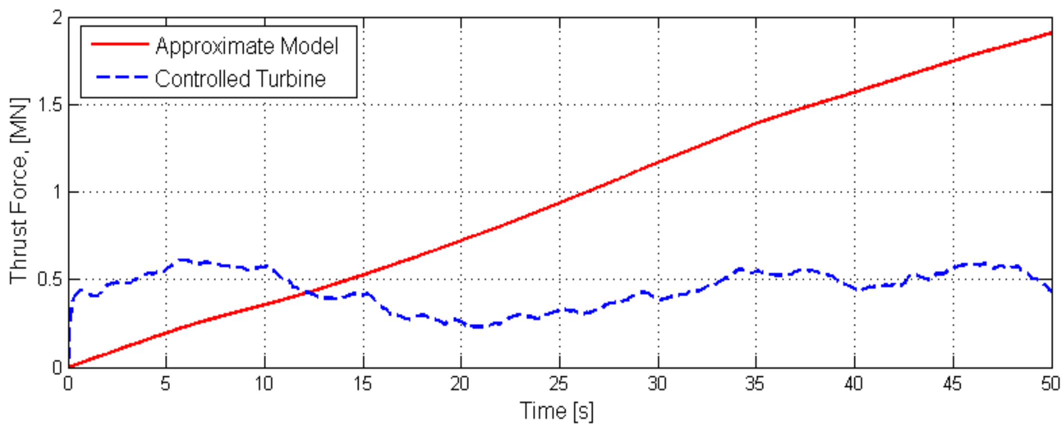

Figure 6-4 Thrust force comparison of controlled turbine and approximate model

As seen in Figure 6-4 above, the thrust force of the controlled turbine cannot be captured since the thrust dynamics is estimated by the approximate linear thrust model. Thus, the thrust response of the controlled turbine is totally different from that of the approximate linear thrust model. However, when the approximate model is augmented with the LPNN, the thrust force estimation is enhanced. There, the thrust forces of both models turn out to be indistinguishable as shown in Figure 6-5.

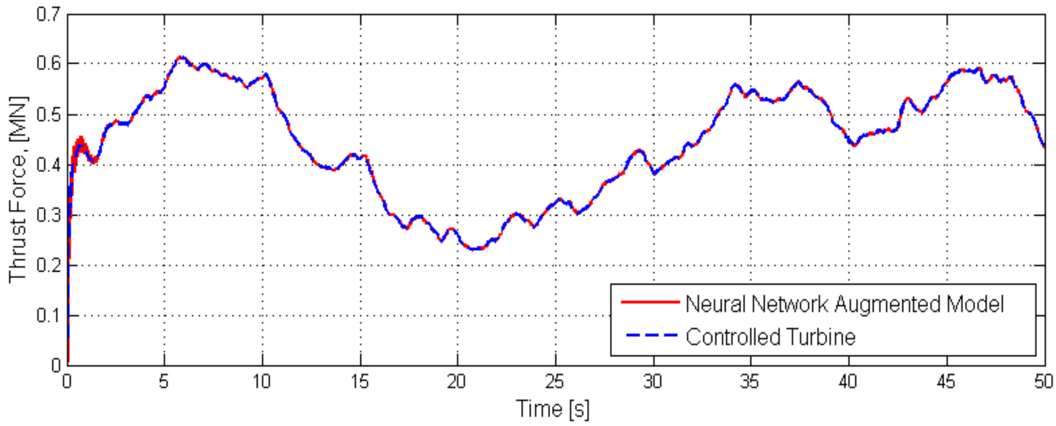

Figure 6-5 Thrust force comparison of controlled turbine and augmented model

Therefore, as the estimation of thrust dynamics is almost the same as those of controlled turbine, the envelope wind speed can be simultaneously calculated through the equation (6-32) by a fixed point iteration method. Note that the algorithm has spent around 2 seconds for adaptation to the turbine operation just at the beginning of the simulation (Figure 6-5). This is due to the fact that the neural network weights are started from zero (Figure 6-9).

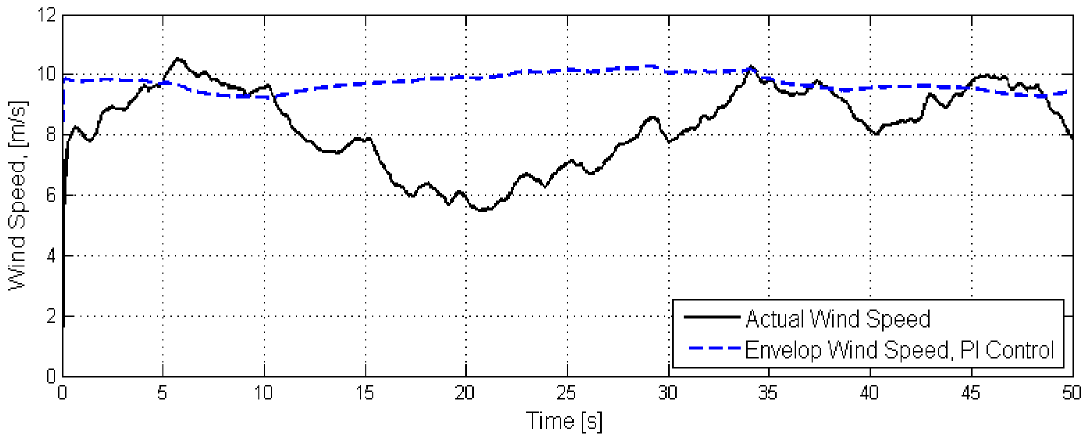

Figure 6-6 Actual and envelope wind speeds

However, in the rest of the simulation time, this adaptation to the changing turbine operating conditions is very fast, which results in almost the same thrust force responses. Figure 6-6 shows the actual wind blowing through the turbine and the estimated envelope wind speed. At the 5th, 34th, 37th and 44.8th seconds, the speed of actual wind exceeds the estimated envelope wind speed. These correspond to excessive turbine loadings. Therefore, the thrust of the turbine exceeds the pre-defined thrust limit of 0.55 MN at those time instants (Figure 6-8).

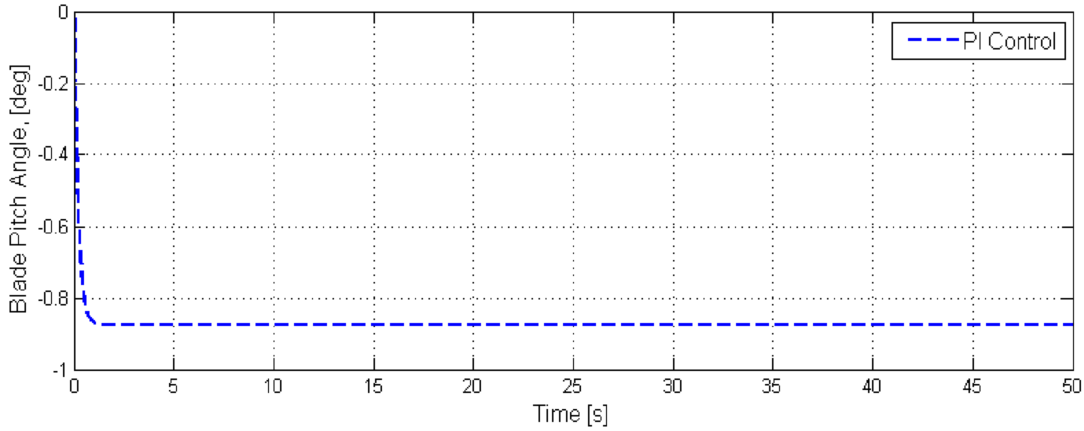

Figure 6-7 Blade pith angle

Since the turbulent wind with a mean of 8 m/s lies in the below rated region, the blade pitch controller maintains the blade pitch angle at its optimum angle, β_* of -0.875 degree (Figure 6-7).

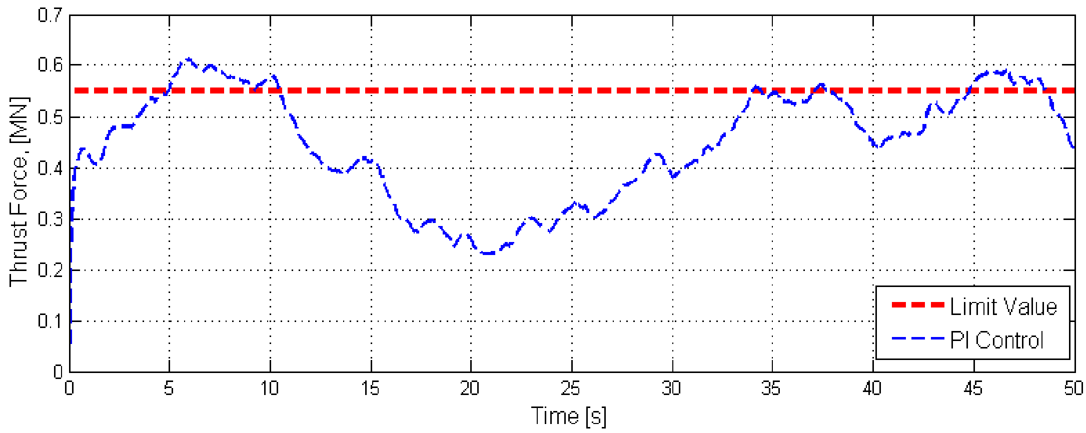

Figure 6-8 Turbine thrust force

In addition, by monitoring wind and turbine states, neural network weights are updated online to capture the accurate thrust dynamics, which allows an accurate envelope wind speed estimation. The changes in neural network weights are seen in Figure 6-9.

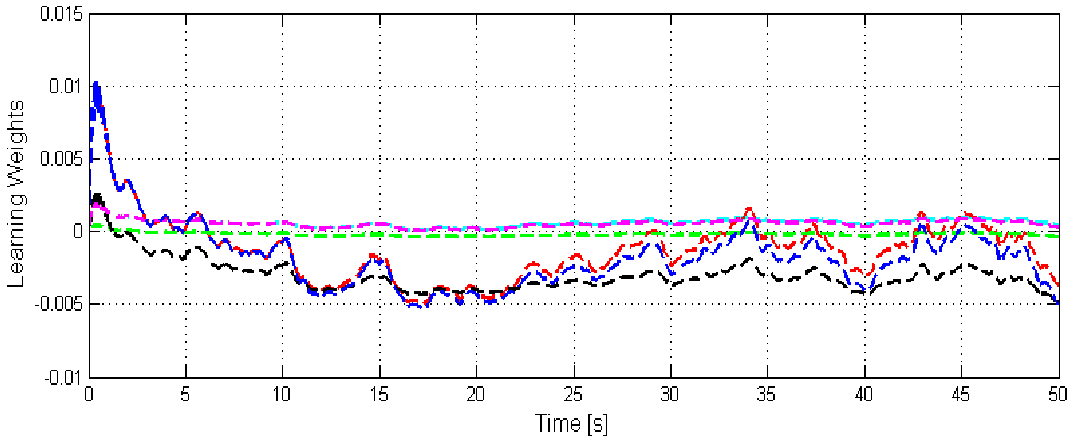

Figure 6-9 Neural network weights

The turbine is in danger, i.e. operating with excessive loads, when the actual turbulent wind speed is larger than the estimated envelope wind speed. This situation occurs at the above-mentioned simulation instants. Once the adaptive envelope protection system is engaged at the 10th second of the simulation time, the system takes a corrective/avoidance action immediately (Figure 6-11) since the turbine is already in danger at that time instant.

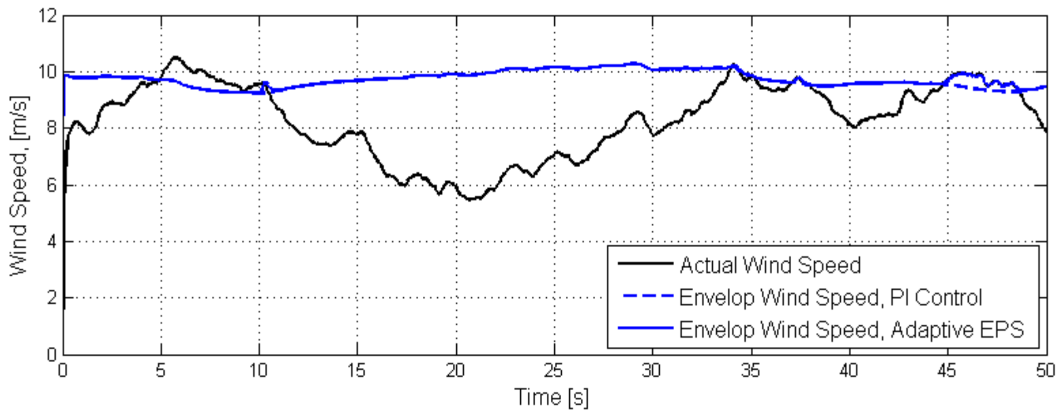

Figure 6-10 Actual and envelope wind speed

This is realized by intervening with the collective blade pitch controller output, i.e. increasing the blade pitch reference, thereby increasing the blade pitch angle. For this reason, there is a slight change in the turbine thrust response at the 10th second of the simulation. This protection action of the system operates the turbine away from the optimum pitch angle, β_* in the below rated region, i.e. reducing the performance or decreasing the C_p of the turbine. Whenever this action is available, the turbine operates at the pre-defined thrust limit until the worst case is disappeared.

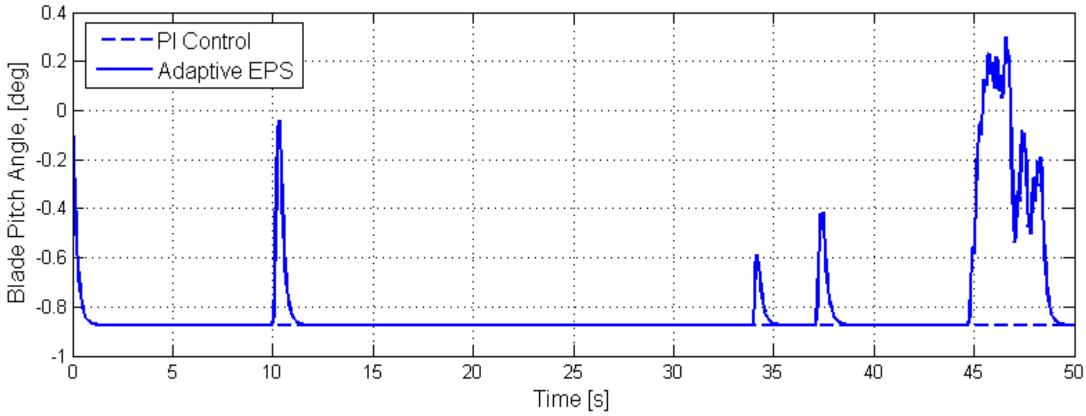

Figure 6-11 Blade pitch angle

Since the envelope protection system constantly monitors the wind and turbine states, it applies corrective actions (Figure 6-11) due to excessive loadings encountered at other simulation times, 34th, 37th and 44.8th as well, thereby protecting the turbine (Figure 6-12). Thus, the turbine rides at the pre-defined thrust limit value of 0.55 MN as seen in Figure 6-12.

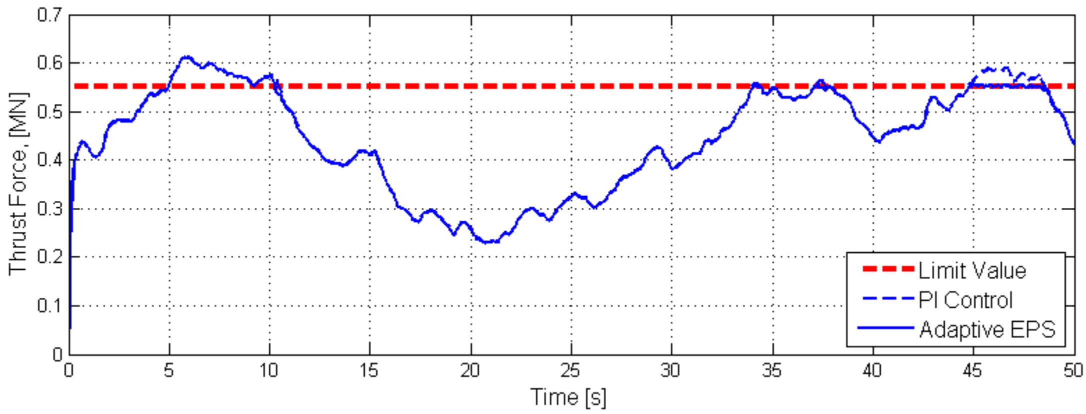

Figure 6-12 Turbine thrust force

As seen in Figure 6-10, the newly calculated envelope wind speed becomes closer to the actual wind speed during turbine protection as the turbine states are changed by the protection system.

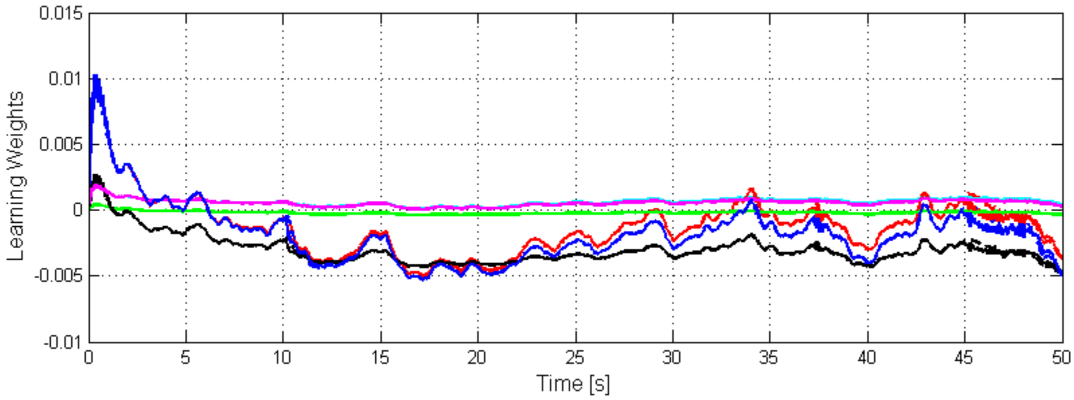

Figure 6-13 Neural network weights

Figure 6-13 depicts the neural network weights with and without envelope protection system. The changes in weights occur only when the avoidance action is present. Dashed ones belong to the case with the gain-scheduled PI-based blade pitch controller only, whereas the solids are the weights when the protection system is active. It is clear that the network weights are adapted automatically to the current turbine operation, i.e. learning the turbine situations in real time.

6.5.2 Simulation Results for Above Rated Region

In the previous subchapter, it was shown that the selected approximate linear model for the thrust force was not capable of predicting the thrust dynamics.

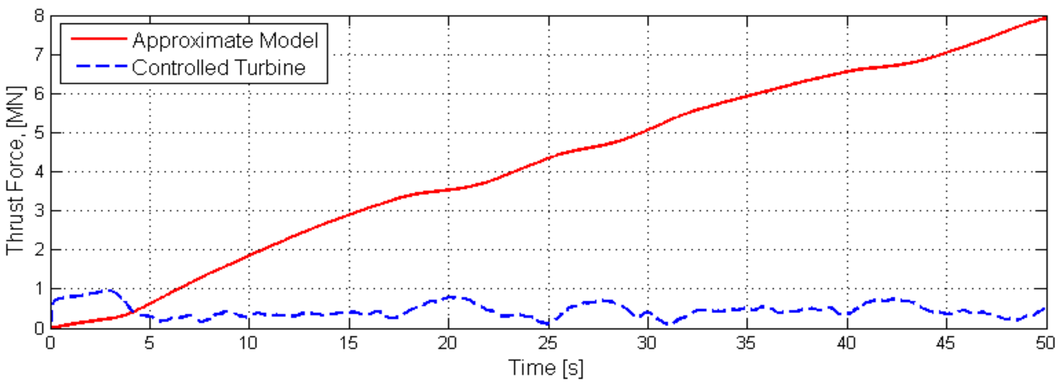

Figure 6-14 Comparison of controlled turbine and approximate model

However, augmenting it with the neural network or the LPNN has resulted in a better estimation of thrust force. Here, the same approximate thrust model is employed and a normal turbulent wind with a mean of 15 m/s is applied to the controlled turbine. As seen in Figure 6-14, the linear approximate thrust model cannot estimate the limit thrust dynamics and give a very different thrust response as before. However, the augmented approximate thrust model can predict the limit thrust dynamics well enough for the above rated region. This allows estimating a proper envelope wind speed.

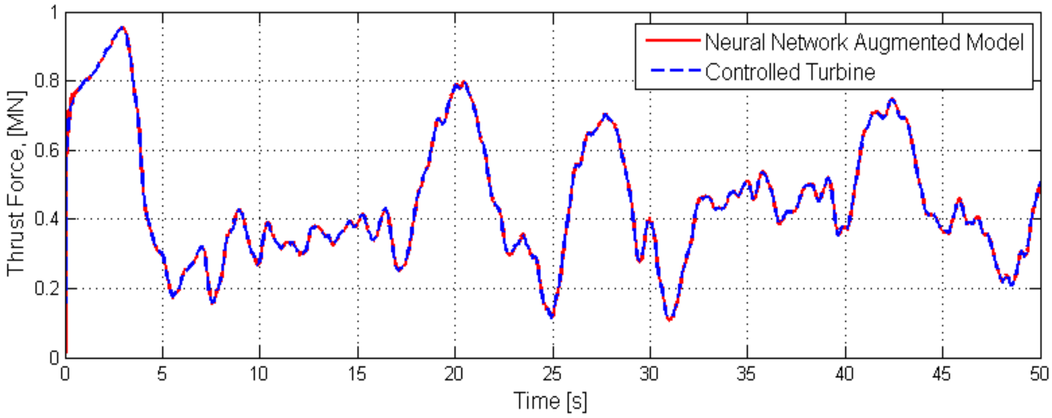

Figure 6-15 Thrust force comparison of controlled turbine and augmented model

Figure 6-16 shows the actual and estimated envelope wind speeds. At the beginning of the simulation, 18.7th, 26.3th and 40.8nd seconds, the actual wind speed exceeds the estimated envelope wind speed. These above time instants, the turbine thrust force exceeds the pre-defined thrust limit of 0.55 MN(Figure 6-18).

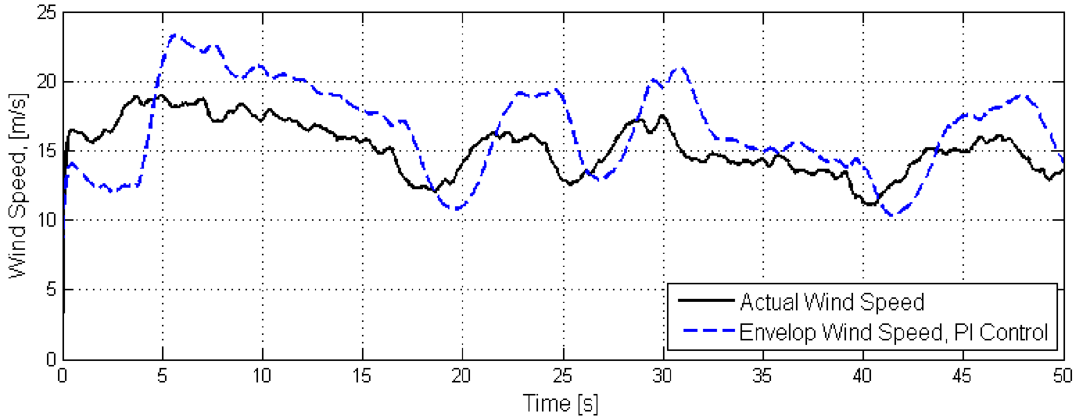

Figure 6-16 Actual and envelope wind speeds

The blade pitch angle of the turbine (Figure 6-17) is adjusted by the gain-scheduled PI-based blade pitch controller due to the fluctuations in the actual wind speed (Figure 6-16).

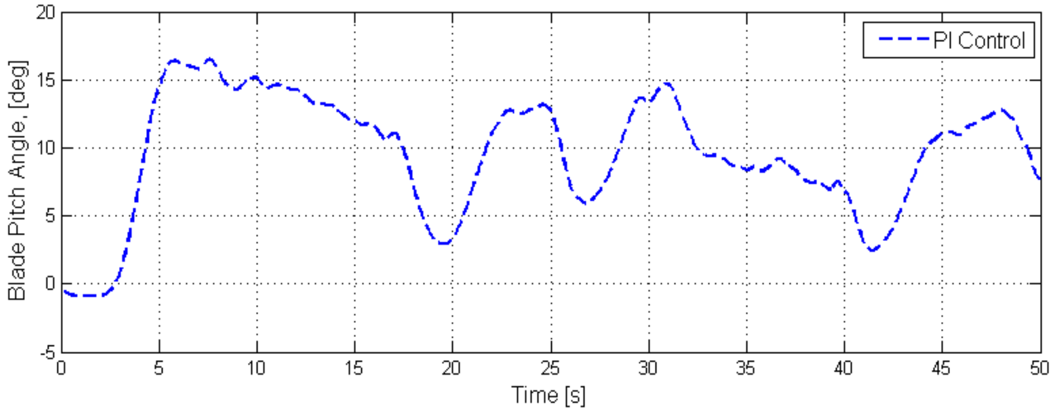

Figure 6-17 Blade pitch angle

As seen in Figure 6-18, the thrust force of the controlled turbine exceeds the pre-defined thrust limit of 0.55 MN. This excessive loading situation, which requires a protection action, occurs four times at the above time instants.

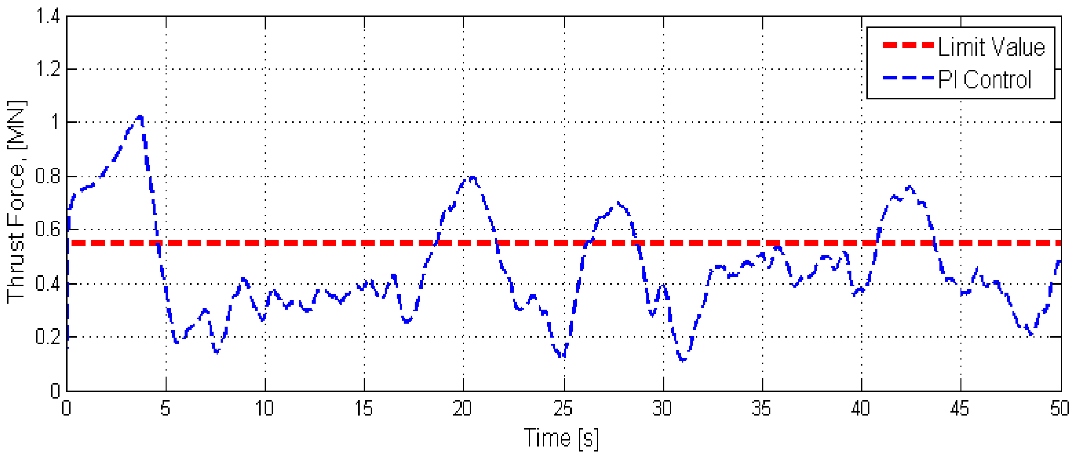

Figure 6-18 Turbine thrust force

The neural network weights are adjusted in real time as in Figure 6-19 in order to predict the limit thrust dynamics (Figure 6-15) and therefore resulting in an accurate envelope wind speed (Figure 6-16).

However, when the adaptive envelope protection system is engaged at the 10th second of the simulation, it does not realize any avoidance action because there is no dangerous situation for the turbine at that time.

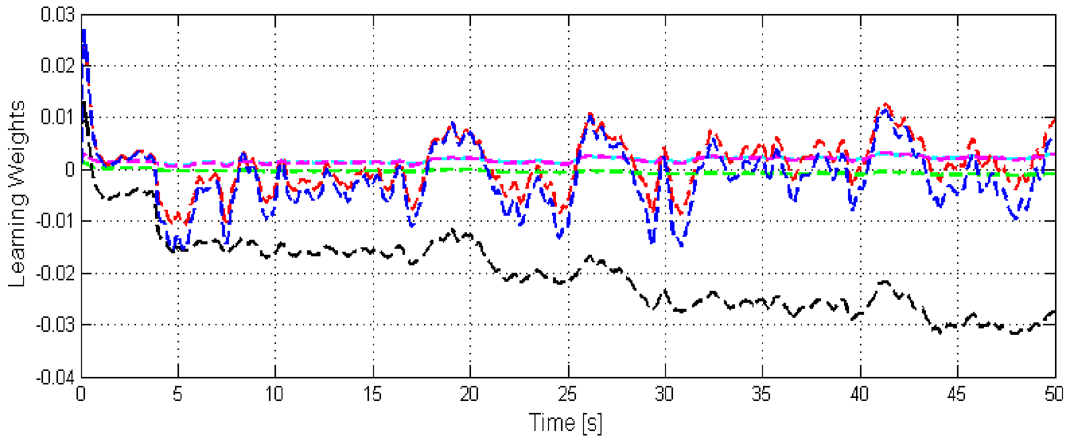

Figure 6-19 Neural network weights

However, the system continues to constantly monitor the wind and turbine states since the adaptation is started with the beginning of the simulation. Thus, neural network weights are adapted online to the turbine operating conditions (Figure 6-23).

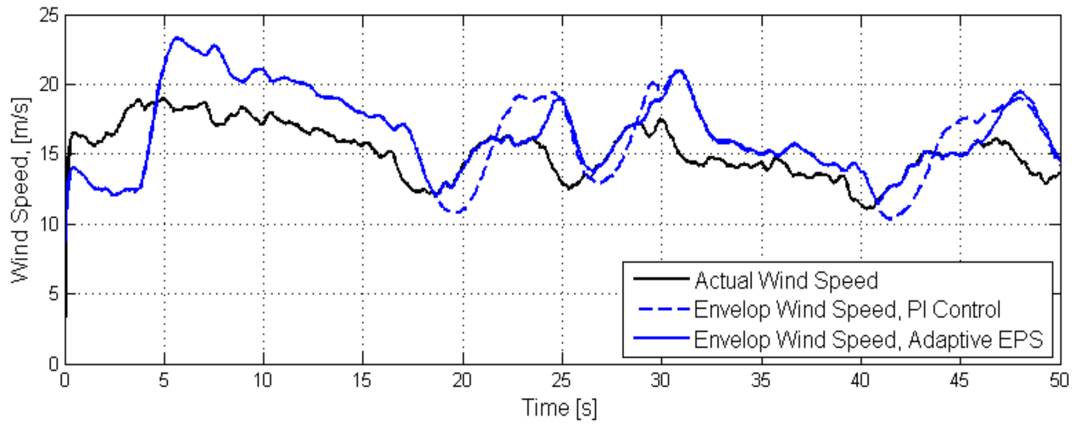

Figure 6-20 Actual and envelope wind speeds

Thus, the system detects the thrust limit exceedance immediately at 18.7th, 26.3th and 40.8th seconds and starts applying avoidance actions at those instants (Figure 6-21). Therefore, it does not permit the turbine to cross the pre-defined thrust limit and rides the turbine at this limit value even after a while the worse operational conditions have vanished. This is caused by the fact the avoidance is carried out by control limiting, which changes the closed loop stability/dynamics due to the interaction with the pitch control system.

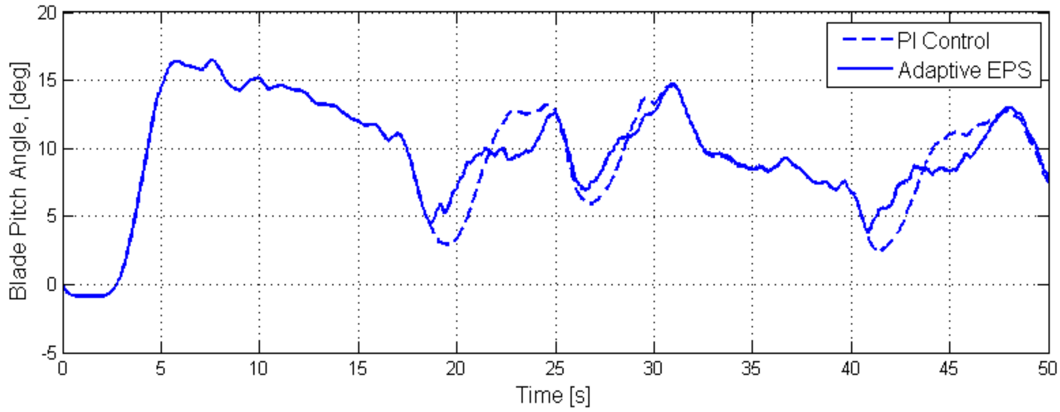

Figure 6-21 Blade pitch angle

Here, as in the below rated region, the proposed protection system prevents the turbine from excessive loading by increasing the turbine blade pitch angle. This is achieved by adjusting the pitch controller output, i.e. increasing blade pitch reference, thereby increasing the turbine blade pitch angle (Figure 6-21). This avoidance changes the turbine operating point. Therefore, the turbine rides at most at the pre-defined thrust limit value whenever an exceedance is about to occur. This is seen in Figure 6-22.

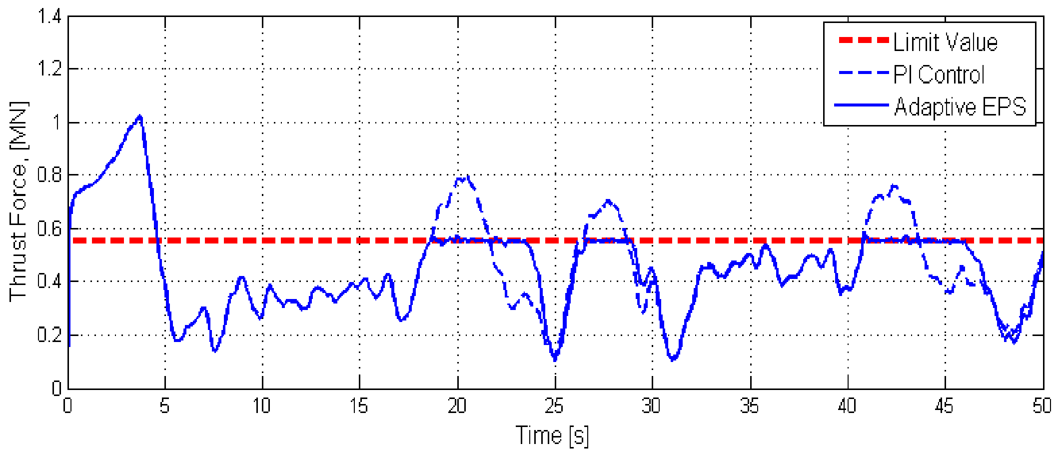

Figure 6-22 Turbine thrust force

As seen in Figure 6-20, during protection, the newly calculated envelope wind speed turns out to be almost the same as the actual wind speed for the above rated region as well. The neural network weights with and without protection cases are seen in Figure 6-23. Dashed weights belong to the case with the gain-scheduled PI-based blade pitch controller only, whereas the solids are the weights when the envelope protection system is active. It is clear that the network weights adjust automatically to the current turbine operating conditions.

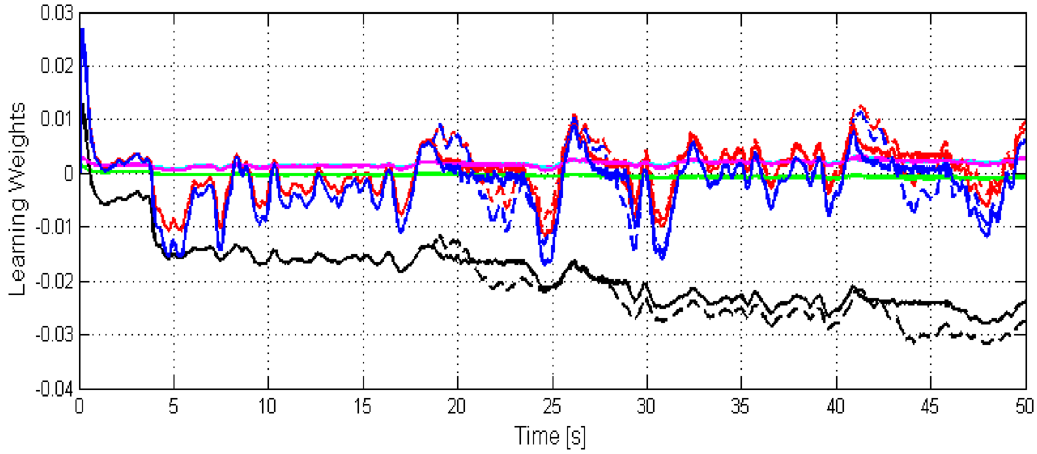

Figure 6-23 Neural network weights

6.5.3 Simulations Results around Rated Wind Speed

Here in this subchapter, the proposed system is tested under a turbulent wind with a mean of 11 m/s. This test is realized at this mean wind speed since the highest thrust force, approximately 0.75 MN, is exerted on the controlled turbine at the steady-state (Figure 5-41). The proposed system will try to keep the turbine thrust force at the pre-defined thrust limit of 0.55 MN.

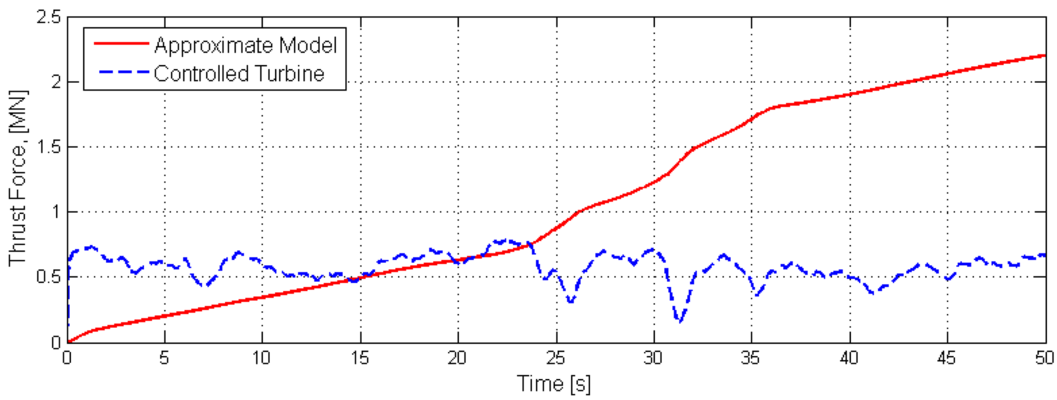

Figure 6-24 Thrust forces of controlled turbine and approximate model

When the normal turbulent wind with a mean of 11 m/s is applied to the controlled turbine with the proposed adaptive envelope protection system, the same approximate linear thrust model without a neural network is lack of predicting the limit thrust dynamics (Figure 6-24). However, as in the below and above region, the augmented thrust dynamics produces almost the same response as that of controlled turbine thrust(Figure 6-25).

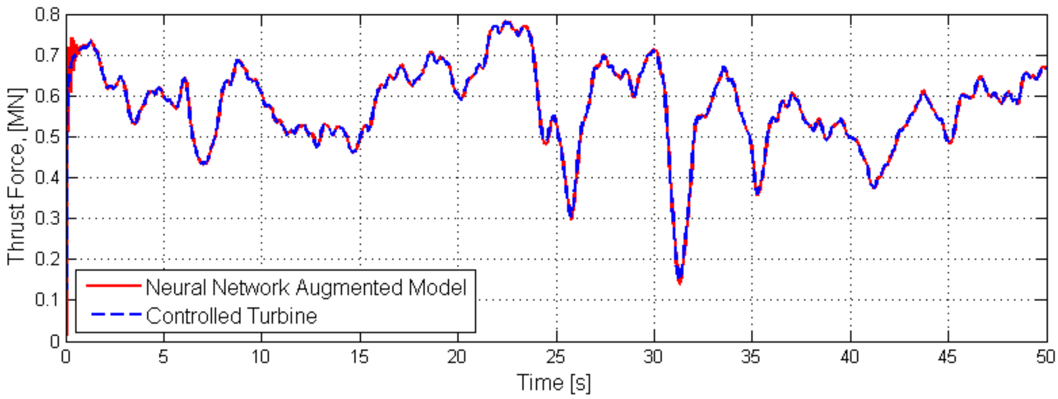

Figure 6-25 Thrust forces of controlled turbine and augmented model

Figure 6-26 shows the actual normal turbulent and estimated envelope wind speeds. As seen in the figure, at most of the simulation instants, the actual wind speed is larger than the estimated envelope wind speed. Therefore, the controlled turbine operates almost always with excessive loading throughout the simulation duration, i.e. exceeding the pre-defined thrust limit of 0.55 MN(Figure 6-28).

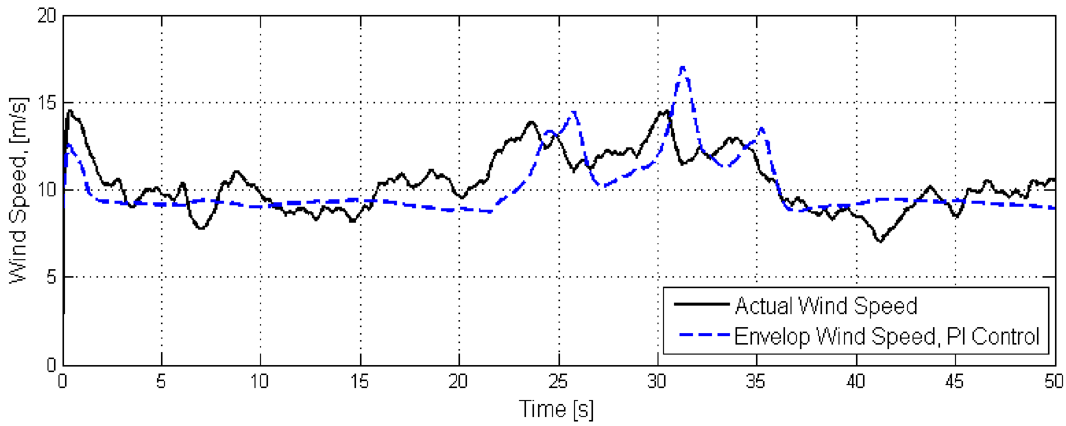

Figure 6-26 Actual and envelope wind speeds

Different from the previous simulation evaluations at 8 and 15 m/s mean speeds, since the selected mean wind speed of 11 m/s lies in the transition region, Region 2.5, i.e.

transition from the below rated region to above rated region. Therefore, due to the turbulent nature of wind, the turbine sometimes operates in the below rated region, and sometimes in the above rated region. This may be easily understood from the change of blade pitch angle in Figure 6-27.

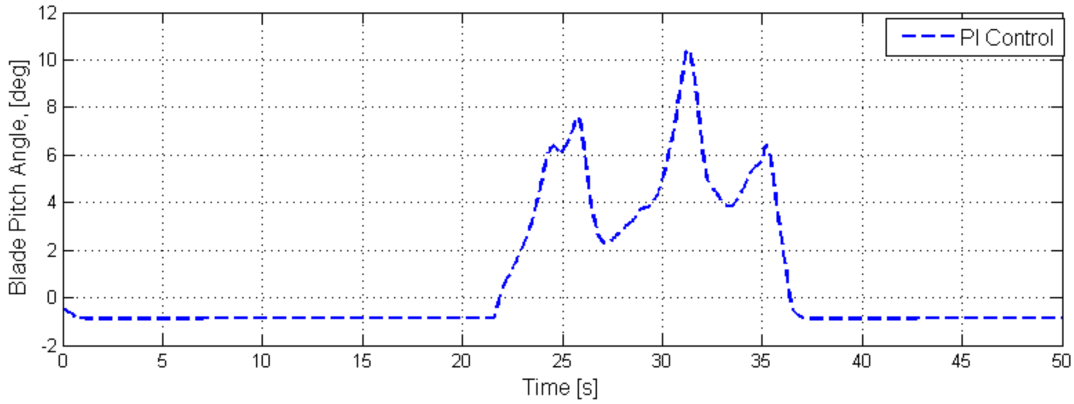

Figure 6-27 Blade pitch angle

As seen in Figure 6-27, between the 21.6th and 36.8th seconds, the turbine operates in the above rated region since the blade pitch angle of the turbine changes with the wind speeds and is different from the optimum blade pitch angle. Therefore, the designed gain-scheduled PI-based pitch controller in Chapter 5 controls the turbine between those time instants. Outside these instants, the turbine blade pitch angle is fixed at the optimum value, β_*, which corresponds to an operation in the below rated region.

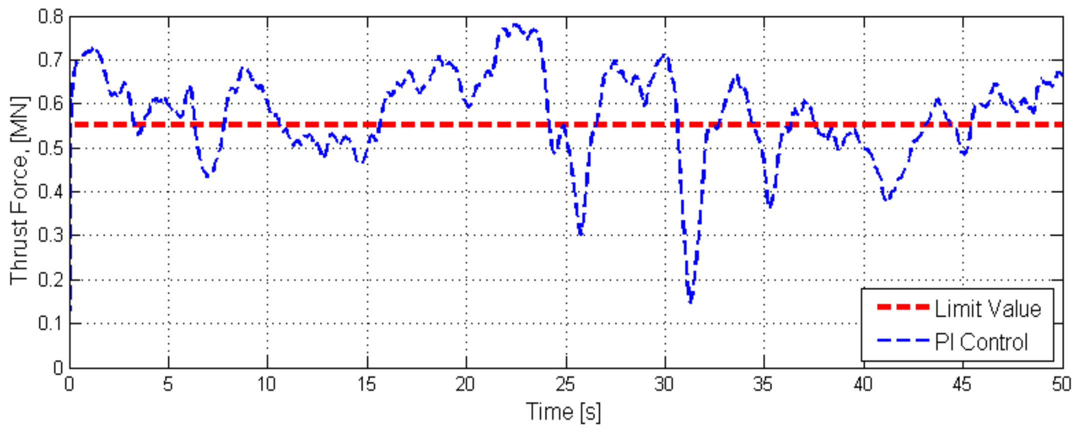

Figure 6-28 Turbine thrust force

Figure 6-28 shows the change of controlled thrust force in time due to the normal turbulent wind with a mean of 11 m/s. As seen in the figure, the turbine thrust force always exceeds the predefined thrust limit value, as opposite to the below and above rated regions. The reason is that the pitch to feather controlled turbine has the maximum thrust force around the rated wind speed, which is certainly much higher than the selected pre-defined limit of 0.55 MN. For instance, in Figure 6-28, it is seen that the turbine reaches a thrust limit force of almost 0.8 MN at around the 22.5th second of the simulation.

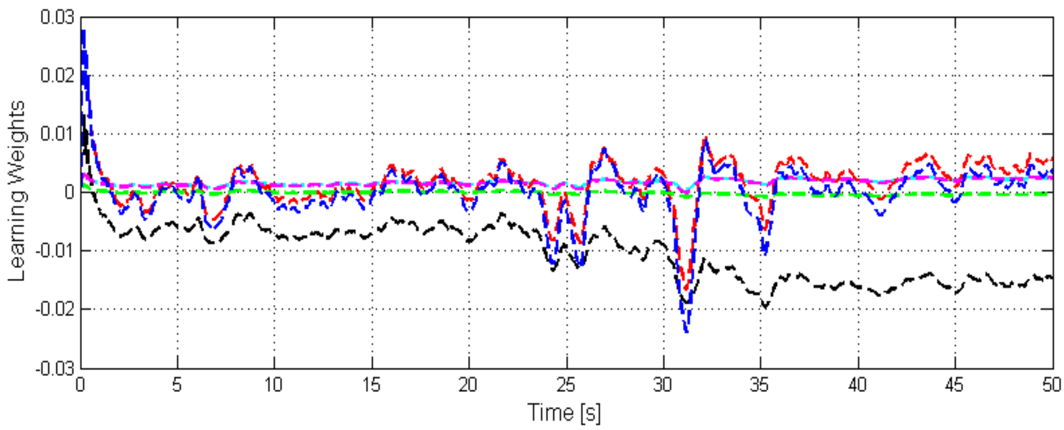

Figure 6-29 Neural network weights

The neural network or LPNN weights are automatically changed as seen in Figure 6-29 to estimate accurate limit thrust dynamics and therefore an accurate envelope wind speed. When the protection system is activated at the 10th second of the simulation time, it applies a protection action by changing the blade pitch angle reference, thereby the blade pitch angle (Figure 6-31).

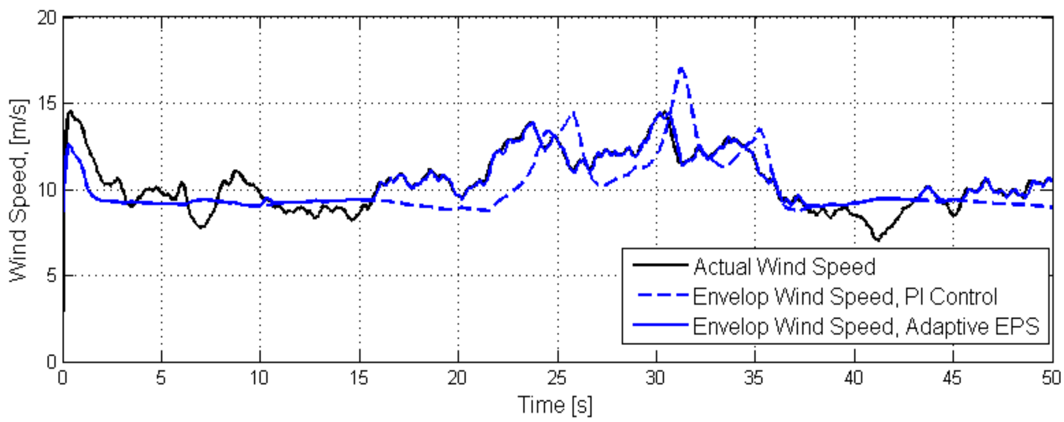

Figure 6-30 Actual and envelope wind speeds

Since the turbine operating conditions vary during protection, the calculated envelope wind speed changes accordingly and turns out to be closer to the actual wind speed during the protection process(Figure 6-30).

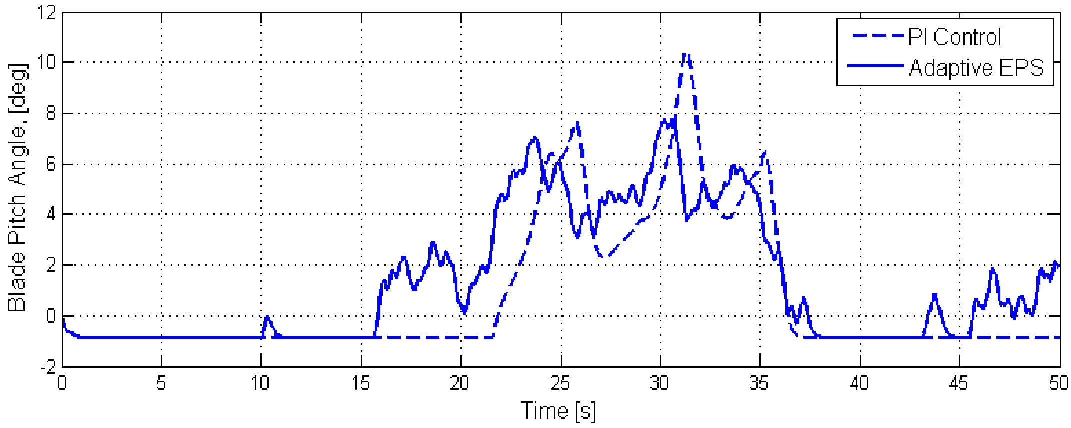

Figure 6-31 Blade pitch angle

Figure 6-31 shows the changes in blade pitch angle when the adaptive envelope protection system is engaged and the avoidance is realized. As seen in the figure, during the avoidance process, the blade pitch angle differs from that of the controlled turbine with baseline controllers.

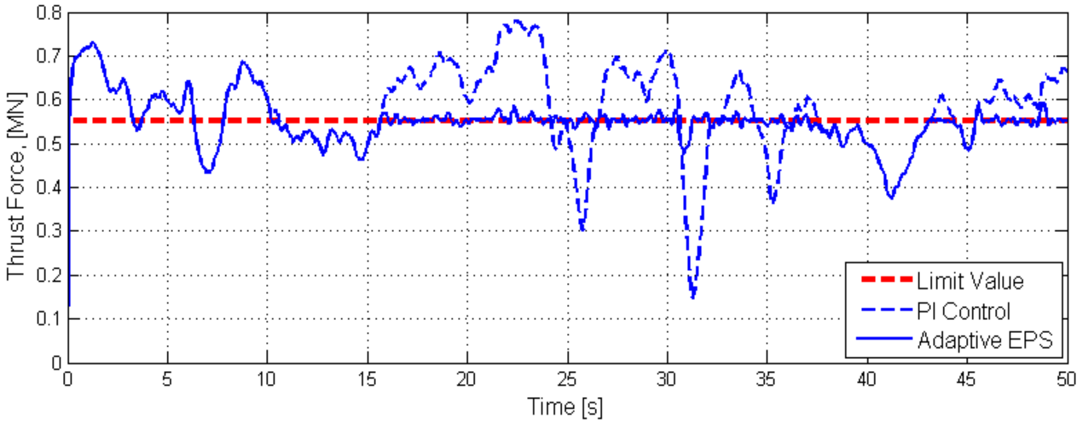

Figure 6-32 Turbine thrust force

Since the protection system adjusts the blade pitch angle in excessive loading situation, the turbine starts riding at the pre-defined thrust limit (Figure 6-32). Therefore, the proposed system is able to keep the turbine within the limit, even in the transition region, where the turbine has the highest thrust force.

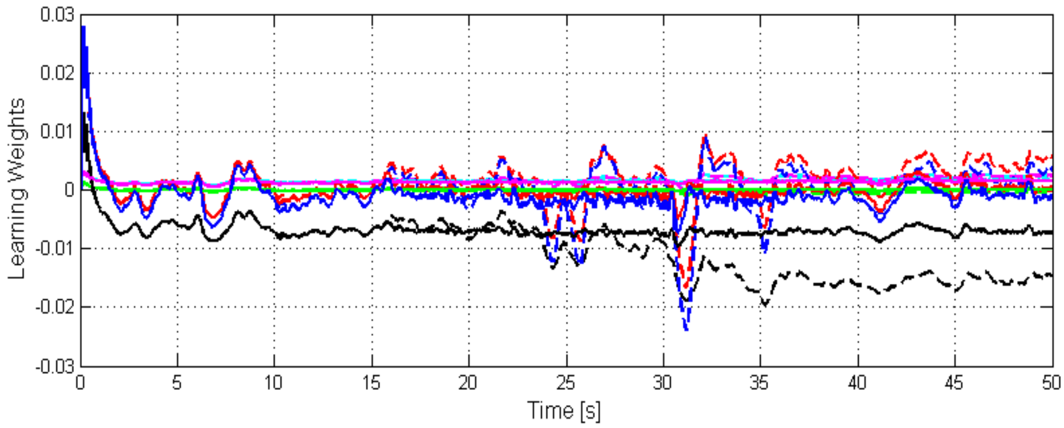

Figure 6-33 Neural network weights

As seen in Figure 6-33, neural network weights are different with and without envelope protection system as in the simulation cases for the below and above rated regions. Dashed weights belong to the controlled turbine, while solids are the weights after the proposed system is activated at the 10th second of the simulation time.

Consequently, the proposed adaptive envelope protection algorithm is utilized here to keep the turbine thrust force within the pre-defined limit thrust value of 0.55 MN from the cut-in to cut-out wind speed. It is explored that the proposed system keeps the turbine within this limit under normal turbulent winds with various mean values throughout the entire operational region. As examples, three of those simulations are presented here at mean wind speeds of 8, 11 and 15 m/s that lie in the below rated, transition and above rated regions, respectively.

Since the proposed algorithm does not allow the turbine to have larger thrust forces at around the rated wind speed, it may be used instead of thrust clipping method. Besides, this algorithm can protect the turbine from excessive loading in between cut-in and cut-out wind speeds. This property probably makes the proposed algorithm more valuable than the thrust clipping method that only works around the rated wind speed. Furthermore, this proposed system is also an alternative to the optimization-based algorithm in Ref.[36], [45]. That algorithm requires the best knowledge of algorithms for the baseline controllers unlike the proposed algorithm here. This may arise a problem since different turbines may have different algorithms for their baseline controllers. This problem has found a solution with the proposed algorithm that does not depend on the baseline controllers.

CHAPTER 7

CONCLUSIONS AND SUGGESTIONS

This thesis study has introduced a novel wind turbine envelope protection system. With the proposed system, the life span of wind turbines is expected to increase since the turbine operates within the pre-defined envelope limits at all times. The proposed novel system utilizes a neural network that adapts to any wind turbine and its operational conditions. Learning is realized online and is quite fast to the changes in wind and turbine states. The proposed system does not allow excessive loadings to occur on turbines throughout the entire operational regions, Regions 1.5, 2, 2.5, 3. The effectiveness of the protection system is demonstrated by means of the simulation results using the developed MS Bladed simulation model with designed baseline controllers. The proposed protection system has managed to keep the turbine safe by the control limiting technique applied to the baseline blade pitch controller output.

In order to achieve the above purpose, a horizontal axis wind turbine (HAWT) simulation model named MS Bladed is first developed using MATLAB and Simulink software. This model has been developed using Blade Element Momentum (BEM) Theory. Some aerodynamic corrections are also introduced to the model where the BEM theory breaks down. Particular coordinate systems are employed in order to include fixed and time-varying turbine structural angles. After the MS Bladed simulation model is developed, experimental or program/model results belonging to different NREL turbines are used for validation purposes. Eventually, the properties of NREL 5 MW turbine is adopted in the MS Bladed simulation model. Baseline controllers such as generator torque and collective blade pitch controllers are designed for 5 MW turbine and their simulation results are evaluated in detail. Afterward, the proposed envelope protection system is designed and added on to the controlled MS Bladed simulation model. Unlike using different methods for the below and above rated regions, the avoidance is realized by only the control limiting technique, i.e. adjusting the blade pitch controller output or the blade pitch reference. This avoidance eventually changes the turbine blade pitch angles. Turbine thrust force is selected as the limit parameter. Whenever the limit violation is about to occur, the proposed algorithm increases the blade pitch angle reference and thus the blade pitch angles, collectively. Therefore, the turbine is prevented from excessive loadings.

Simulation evaluations have shown that the new adaptive envelope protection system demonstrates a promising capability in the below and above rated regions as well as around the rated wind speed under the normal turbulent winds with different mean values. Hence, the algorithm ensures that the turbine operates at most at its thrust limit. Three example cases are shown in this thesis study to prove the effectivity of the proposed algorithm.

The system based on a neural network estimates the limit parameter dynamics, and simultaneously calculates the envelope wind speed that takes the turbine to the envelope boundary. Calculation of envelope wind speed is carried out by the newly introduced concept of unsteady dynamics, which requires the derivative of the limit parameter. This new concept is utilized due to the fact that all the system states stay mostly in transient during turbine operation due to the turbulent nature of wind. Therefore, the time derivative of the fast states is not zero, unlike the case in dynamic trim concept. Turbine condition, operating with excessive loading or not, is determined by comparing the actual wind speed with envelope wind speed. An actual wind speed larger than the estimated envelope wind speed corresponds to the situation of excessive loadings, while the opposite induces lower turbine loadings. With the adaptive neural network, the protection system monitors the wind and turbine states online and adapts to any turbine operation in a very short time. This results in a fast envelope wind speed estimate, resulting in a fast corrective/avoidance action.

This proposed system may also be utilized to limit any of the turbine critical variables. Furthermore, there is no need to precisely know the baseline control algorithms in contrast to the algorithm in Ref.[36], [44], [45]. That algorithm requires the addition of baseline control laws to the reduced wind turbine model. This algorithm is also easier for implementation to the operating turbines as the only intervention is the blade pitch controller output. Furthermore, in contrast to the available methods, such as adjusting generator torque and blade pitch angle for the below rated region, changing rotor speed reference and keeping the generator torque at its rated value for the above rated region, the avoidance here is realized only by adjusting the blade pitch controller output for both operational regions. The collective benefits cited above are likely to make the proposed algorithm more attractive by the wind power industry than the one proposed in Ref.[36], [44], [45]. In addition to those, since the proposed algorithm keeps the turbine within the pre-defined thrust limit around the rated wind speed, it may be utilized instead of the thrust clipping method. It probably would give a better performance than the thrust clipping method since it considers the current turbine loadings in order to not to allow the turbine to operate beyond the pre-defined thrust limit. Exceptionally, it does not only protect the turbine around the rated wind speed, but it also protects the turbine from the cut-in to cut-out wind speed, whenever the pre-defined limit is about to be exceeded due to the turbulent wind applied to the controlled turbine.

This thesis study also covers the wind energy and turbine systems, wind energy usage, current worldwide wind power status, turbine types and their operational principles, with a special focus on HAWTs. In addition, electrical and mechanical HAWT components such as generators, transformers, tower, turbine rotor etc. are also defined in detail.

Following are the suggestions for future work.

1. The developed MS Bladed simulation model may be extended to simulate the turbines with curved/swept blades by applying required modifications to the developed model. These modifications probably would require extra modifications such as local blade lengths in the hub and tip loss models. It

probably would necessitate changes in the approach, i.e. the calculation of torque produced by each blade element with respect to the hub center.

2. The MS Bladed simulation model may be improved to have flexible turbine components such as the tower, blades and so on. Therefore, the performance of the proposed protection algorithm may be tested on the flexibly-structured wind turbines, under different wind conditions, i.e. normal and extreme turbulent wind conditions.

3. The developed MS Bladed turbine simulation model here corresponds to a HAWT model that can simulate the behavior of only the on-shore wind turbines. For instance, by adding the effect of a floating platform to the developed turbine model, it may be extended to simulate even the off-shore wind turbines. The performance of the protection system may also be tested on the off-shore turbines with flexibly-structured components, which are gaining increased attention in today's wind power industry.

4. The proposed algorithm may be compared with the thrust clipping algorithm to investigate the performance difference in the below and above rated regions as well as around the rated wind speed.

5. The proposed algorithm may also be used for increasing the turbine performance rather than limiting the turbine performance. Here, the thrust is limited, but it may be extended to limit other turbine critical variables i.e., rotor speed. The algorithm may be tested to the changes in turbine configurations, rather than the changes in turbine operating conditions, which is tested in this thesis study.

6. The proposed system may be designed by employing other types of neural network such as Single Hidden Layer Neural Network. A different avoidance method may be utilized to limit the turbine thrust force.

7. In the current MS Bladed simulation model, the aerodynamic correction model utilized for the turbulent wake state may be replaced by Buhl correction formula[60] to get an almost the same results as those of FAST simulation model in terms of maximum power coefficient, optimum TSR and optimum blade pitch angle, which decides the maximum electricity generation in the below rated region.

8. Skewed wake formulation in the simulation model may be extended to have the effects of both precone and tilt angles at the same time.

9. The electrical generator and other electrical/electronic components, i.e. power electronics unit-rectifiers and inverters may also be modeled in detail and then added to the turbine simulation model.

10. Lastly, the proposed algorithm here may be implemented to other types of wind turbines such as Darrieus, Savonius and H type turbines if required.

REFERENCES

[1] A. R. Jha, *Wind Turbine Technology*. CRC Press, 2011.

[2] H. Erich, *Wind Turbines-Fundamentals, Tecnologies, Application, Economics*, 2nd Edi. Germany, 2006.

[3] J. Bartl, "Wake Measurements behind an Array of Two Model Wind Turbines," Norges Teknisk-Naturvitenskapelige Universitet (NTNU), 2011.

[4] T. M. Letcher, *Wind Energy Engineering-A Handbook for Onshore and Offshore Wind Turbines*. Elsevier Inc., 2017.

[5] L. Y. Pao and K. E. Johnson, "A Tutorial on the Dynamics and Control of Wind Turbines and Wind Farms," in *2009 American Control Conference*, 2009, pp. 2076–2089.

[6] Z. Shahan, "History of Wind Turbines," 2014. [Online]. Available: http://www.renewableenergyworld.com/ugc/articles/2014/11/history-of-wind-turbines.html. [Accessed: 28-Apr-2017].

[7] M. Whitby, "First V164-8.0 MW turbine installed at Burbo Bank Extension," 2016. [Online]. Available: http://www.mhivestasoffshore.com/first-v164-8-0-mw-turbine-installed-burbo-bank-extension-2/. [Accessed: 02-Apr-2017].

[8] GWEC, "Global Status of Win Power in 2017," 2018. .

[9] A. Abdulrahim, "Experimental investigation of the effects of tip-injection on the aerodynamic loads and wake characteristics of a model horizontal axis wind turbine rotor," Middle East Technical University, 2014.

[10] Festo Didactic, "PLC Applications-Wind Turbine-Job Sheets-Courseware Sample," 2016.

[11] M. O. L. Hansen, *Aerodynamics of Wind Turbines*, 2th Edit. Earthscan, 2008.

[12] J. F. Manwell, J. G. McGowan, and A. L. Rogers, *Wind Energy Explained,*

Theory, Design and Application, Second Edi. John Wiley & Sons Ltd., 2009.

[13] A. Hemami, *Wind Turbine Technology*. Clifton Park, NY 12065-2919 USA: Cengage Learning, 2012.

[14] K. E. Johnson, L. Y. Pao, M. J. Balas, and L. J. . Fingersh, “Control of Variable Speed Wind Turbines-Standard and Adaptive Techniques for Maximizing Energy Capture,” *IEEE Control Syst. Mag.*, vol. 26, no. 3, pp. 70–81, 2006.

[15] P. Duddu, “Top 10 biggest wind farms,” 2013. [Online]. Available: https://www.power-technology.com/features/feature-biggest-wind-farms-in-the-world-texas/.

[16] L. Fortune and Star Co., “Wind Turbine,” 2018. [Online]. Available: http://www.fortuneandstar.com/wind.html.

[17] James, “Global Wind Turbine Control System Market 2018 with Development Factors, Investment Analysis By Top Players Siemens, ABB,” *Paris Ledger*, 2018. [Online]. Available: http://parisledger.com/2018/12/04/global-wind-turbine-control-system-market-2018-with-development-factors-investment-analysis-by-top-players-siemens-abb/.

[18] J. Ament, “Just How Resilient Is The Nation’s Electrical Grid?,” 2017. [Online]. Available: http://www.kut.org/post/just-how-resilient-nations-electrical-grid.

[19] ABB, “Transformers for wind turbine generators,” 2018. [Online]. Available: https://new.abb.com/products/transformers/by-customer-segment/wind/turbine-generators.

[20] Spares in Motion, “Elin 504716,” 2018. [Online]. Available: https://www.sparesinmotion.com/wind-turbine-parts/generators/elin-504716.

[21] rexroth, “Gearbox Exchange Pool,” 2018. [Online]. Available: https://www.boschrexroth.com/en/us/service/service-by-market/renewable-energies/service-products/gearbox-exchange-pool/index.

[22] Innovation Toronto, “‘Small wind’ power plants are blowing strong,” 2011.

[Online]. Available: https://www.innovationtoronto.com/2011/08/small-wind-power-plants-are-blowing-strong/.

[23] "Cloud blowing wind," 2018. [Online]. Available: https://www.shutterstock.com/search/cloud+blowing+wind.

[24] E. A. Bossanyi, "The Design of Closed Loop Controllers for Wind Turbines," *Wind Energy*, vol. 3, no. 3, pp. 149–163, 2000.

[25] R. U. Maheswari and J. Tamilvendhan, "Analysis of Modelling of Active Stall Controlled and Active Pitch controlled Variable Speed Wind Turbines," *Int. J. Mod. Eng. Res.*, vol. 2, no. 4, pp. 2662–2667, 2012.

[26] Y. D. Song, B. Dhinakaran, and X. Y. Bao, "Variable Speed Control of Wind Turbines using Nonlinear and Adaptive Algorithms," *J. Wind Eng. Ind. Aerodyn.*, vol. 85, no. 3, pp. 293–308, 2000.

[27] A. Oudah, I. Mohd, and A. Hameed, "Modern Control Techniques in Wind Turbine," *Int. J. Hybrid Inf. Technol.*, vol. 7, no. 4, pp. 101–122, 2014.

[28] G. Michalke and A. D. Hansen, "Modelling and control of variable speed wind turbines for power system studies," no. June 2009, pp. 307–322, 2009.

[29] A. D. Hansen, P. Sørensen, F. Iov, and F. Blaabjerg, "Centralised power control of wind farm with doubly fed induction generators," *Renew. Energy*, vol. 31, no. 7, pp. 935–951, 2006.

[30] R. W. Erickson and D. Maksimovic, *Fundamentals of Power Electronics*, 'Second Ed. Springer Science, 2001.

[31] K. A. Stol and L. J. . Fingersh, "Wind Turbine Field Testing of State-Space Control Designs," *Technical Report NREL/SR-500-35061*, no. September, Golden, Colorado, 2004.

[32] A. Merabet, J. Thongam, and J. Gu, "Torque and Pitch Angle Control for Variable Speed Wind Turbines in All Operating Regimes," in *10th International Conference on Environment and Electrical Engineering (EEEIC),*

2011, 2011, vol. 1, no. 2, pp. 1–5.

[33] B. Boukhezzar, L. Lupu, H. Siguerdidjane, and M. Hand, "Multivariable Control Strategy for Variable speed, Variable Pitch Wind Turbines," *Renew. Energy*, vol. 32, no. 8, pp. 1273–1287, 2007.

[34] J. Hai, W. Sun, G. Hu, and A. Wu, "The Study on Blade Pitch Control of Wind Power with Gain Scheduling," *Key Eng. Mater.*, vol. 522, pp. 364–368, 2012.

[35] B. Fischer and M. Shan, "A Survey on Control Methods for the Mitigation of Tower Loads," 2013.

[36] V. Petrović and C. L. Bottasso, "Wind turbine envelope protection control over the full wind speed range," *Renew. Energy*, vol. 111, pp. 836–848, 2017.

[37] J. Aho *et al.*, "A tutorial of wind turbine control for supporting grid frequency through active power control," *2012 Am. Control Conf.*, no. March, pp. 3120–3131, 2012.

[38] C. Lim, "Torque Control Methods for Wind Turbines and Their Responses," in *12th International Conference on Control, Automation and Systems*, 2012, no. 2, pp. 1788–1790.

[39] S. Stubkier, H. C. Pedersen, and J. M. Jonkman, "Analysis of load reduction possibilities using a hydraulic soft yaw system for a 5-MW turbine and its sensitivity to yaw-bearing friction," *Eng. Struct.*, vol. 69, pp. 123–134, 2014.

[40] H. Camblong, S. Nourdine, I. Vechiu, and G. Tapia, "Control of wind turbines for fatigue loads reduction and contribution to the grid primary frequency regulation," *Energy*, vol. 48, no. 1, pp. 284–291, 2012.

[41] E. A. Bossanyi, "Individual blade pitch control for load reduction," *Wind Energy*, vol. 6, no. 2, pp. 119–128, 2003.

[42] V. Petrovic, M. Baotic, and N. Peric, "Reduction of wind turbine tower oscillation based on individual pitch control," in *20th Mediterranean Conference on Control & Automation (MED)*, 2012, pp. 1499–1505.

[43] C. L. Bottasso, A. Croce, C. E. D. Riboldi, and M. Salvetti, “Cyclic pitch control for the reduction of ultimate loads on wind turbines,” *J. Phys. Conf. Ser.*, vol. 524, no. 1, 2014.

[44] Petrovic, V., Bottasso C. L., “Wind turbine optimal control during storms,” *J. PhysicsConference Ser.*, 2014.

[45] V. Petrovic and C. L. Bottasso, “Wind Turbine Envelope Riding,” in *AIAA Scitech, 33rd Wind Enery Symposium*, 2015, no. 5–9 January, pp. 1–8.

[46] M. Jelavic, V. Petrovic, M. Barisic, and I. Ivanovic, “Wind turbine control beyond the cut-out wind speed,” in *European Wind Energy Conference and Exhibition*, 2013, p. 7.

[47] J. Horn, A. J. Calise, J. V. R. Prasad, and M. O’Rourke, “Flight Envelope Cueing on a Tilt-Rotor Aircraft Using Neural Network Limit Prediction,” in *American Helicopter Society*, 1998, vol. 1, pp. 1682–1690.

[48] I. Yavrucuk, S. Unnikrishnan, and J. V. R. Prasad, “Envelope Protection for Autonomous Unmanned Aerial Vehicles,” *J. Guid. Control. Dyn.*, vol. 32, no. 1, pp. 248–261, 2009.

[49] I. Yavrucuk and J. V. R. Prasad, “Online Dynamic Trim and Control Limit Estimation,” *J. Guid. Control. Dyn.*, vol. 35, no. 5, pp. 1647–1656, 2012.

[50] S. Unnikrishnan, G. J. Jeram, and J. V. R. Prasad, “Tactile Limit Avoidance Cueing Using Adaptive Dynamic Trim,” in *Proceedings of the American Helicopter Society 60th Annual Forum*.

[51] M. Sahin and I. Yavrucuk, “Dynamical modelling of a wind turbine system with precone and tilt angles,” in *9th Ankara International Aerospace Conference*, 2017, no. 20–22 September, pp. 1–11.

[52] J. N. Sørensen, *General Momentum Theory for Horizontal Axis Wind Turbines, Research Topics in Wind Energy- Volume 4*, Volume 4., vol. 4. Cham Heidelberg New York Dordrecht London: Springer, 2016.

[53] P. Pratumnopharat and P. S. Leung, "Validation of various windmill brake state models used by blade element momentum calculation," *Renew. Energy*, vol. 36, no. 11, pp. 3222–3227, 2011.

[54] J. F. Manwell, J. G. McGowan, and A. L. Rogers, *Wind Energy Explained-Theory, Design and Application*. John Wiley & Sons Ltd, 2002.

[55] P. J. Moriarty and A. C. Hansen, "AeroDyn Theory Manual, NREL/TP-500-36881, Golden, Colorado: National Renewable Energy Laboratory," 2005.

[56] I. Masters, J. C. Chapman, M. R. Willis, and J. A. C Orme, "A robust blade element momentum theory model for tidal stream turbines including tip and hub loss corrections) A robust blade element momentum theory model for tidal stream turbines including tip and hub loss corrections," *J. Mar. Eng. Technol. J. J. Mar. Eng. Technol.*, vol. 10, no. 1, pp. 2046–4177, 2017.

[57] E. Branlard, "Wind turbine tip-loss corrections, Master's Thesis, DTU," 2011.

[58] T. Burton, D. Sharpe, N. Jenkins, and E. Bossanyi, *Wind Energy Handbook*. West Sussex, England: John Wiley & Sons, Ltd, 2001.

[59] R. E. Wilson, P. B. S. Lissaman, and S. N. Walker, "Aerodynamic performance of wind turbines," 1976.

[60] M. L. Buhl, "A New Empirical Relationship between Thrust Coefficient and Induction Factor for the Turbulent Windmill State A New Empirical Relationship between Thrust Coefficient and Induction Factor for the Turbulent Windmill State," 2005.

[61] J. H. Lehr, J. Keeley, and T. B. Kingery, *Alternative Energy and Shale Gas Encyclopedia*. Hoboken, New Jersey: JohnWiley & Sons, 2016.

[62] B. Hibbs and R. L. Radkey, "Calculating Rotor Performance with the Revised 'PROP' Computer Code, AeroVironment, Inc., Report No. PFN-13470W," 1983.

[63] M. S. Selig, "PROPID User Manual-Version 5.3.1." 2012.

[64] D. M. Eggleston and F. S. Stoddard, “Wind Turbine Engineering Design. New York, NY: Van Nostrand Reinhold; pp. 30–35,” 1987.

[65] S. A. Ning, G. Hayman, R. Damiani, and J. Jonkman, “Development and Validation of a New Blade Element Momentum Skewed-Wake Model within AeroDyn,” in *AIAA Science and Technology Forum and Exposition 2015*, 2015, no. January 5-9, 2015.

[66] S. A. Ning, “CCBlade Documentation, Release 0.1.0,” 2013.

[67] R. Van Rooij, “Terminology , Reference Systems and Conventions,” no. October, p. 48, 2001.

[68] J. Jonkman, “Personal Communication,” 2018.

[69] R. E. Wilson and P. B. S. Lissaman, “Applied Aerodynamics of Wind Power Machines,” 1974.

[70] A. D. Platt and M. L. Buhl, “WT_Perf User Guide for Version 3.05.00,” 2012.

[71] J. G. Schepers, A. J. Brand, A. Bruining, and E. Al., “Final report of IEA Annex XVIII : ‘Enhanced Field Rotor Aerodynamics Database’, ECN-C-02-016,” 2002.

[72] C. P. Butterfield, W. P. Musial, and D. A. Simms, “Combined Experiment Final Report- Phase I, NREL/TP-257-4655, Golden, Colorado: National Renewable Energy Laboratory,” 1992.

[73] D. A. Simms, M. M. Hand, L. J. Fingersh, and D. W. Jager, “Unsteady Aerodynamics Experiment Phases II – IV Test Configurations and Available Data Campaigns, NREL/TP-500-25950,” 1999.

[74] M. M. Hand, D. A. Simms, L. J. Fingersh, D. W. Jager, and J. R. Cotrell, “Unsteady Aerodynamics Experiment Phase V: Test Configuration and Available Data Campaigns, , NREL/TP-500-29491, Golden, Colorado: National Renewable Energy Laboratory,” 2001.

[75] M. M. Hand *et al.*, “Unsteady Aerodynamics Experiment Phase VI : Wind

Tunnel Test Configurations and Available Data Campaigns, NREL/TP-500-29955, Golden, Colorado: National Renewable Energy Laboratory," 2001.

[76] P. A. Galvani, F. Sun, and K. Turkoglu, "Aerodynamic Modelling of the NREL 5-MW Wind Turbine for Nonlinear Control System Design: A case Study Based on Real-Time Nonlinear Receding Horizon Control," *Aerosp. 2016*, 2016.

[77] D. Somers, "Design and Experimental Results for the S809 Airfoil, NREL/SR-440-6918, Golden, Colorado: National Renewable Energy Laboratory," no. January 1997, p. 103, 1997.

[78] M. Selig, "S809 Experimental data from Delft wind tunnel," 2017. [Online]. Available: http://m-selig.ae.illinois.edu/propid/raj/wtprep/polardata-html/airfoil1.html. [Accessed: 01-Jun-2017].

[79] NREL, "Airfoilprep," 2014. [Online]. Available: https://nwtc.nrel.gov/AirFoilPrep.

[80] J. Tangler and J. D. Kocurek, "Wind Turbine Post-Stall Airfoil Performance Characteristics Guidelines for Blade-Element Momentum Methods," in *43rd AIAA Aerospace Sciences Meeting Meeting and Exhibit*, 2005, no. January 10-13, 2005.

[81] B. S. Gerber, J. L. Tangler, E. P. N. Duque, and J. D. Kocurek, "Peak and Post-Peak Power Aerodynamics from Phase VI NASA Ames Wind Turbine Data," vol. 127, no. May, pp. 192–199, 2005.

[82] Ö. Ceyhan, "Aerodynamic Design and Optimization of Horizontal Axis Wind Turbines by Using BEM Theory and Genetic Algorithm," Middle East Technical University, 2008.

[83] O. Polat, "Genetic Algorithm Based Aerodynamic Shape Optimization of Wind Turbine Rotor Blades Using a 2-D Panel Method With a Boundary Layer Solver," Middle East Technical University, 2011.

[84] J. J. Corrigan and J. J. Schillings, "Emprical Model for Stall Delay Due to

Rotation," *Am. Helicopter Soc. Aeromechanics Spec. Conf.*, p. 8.4-1 to 8.4-15, 1994.

[85] J. L. Tangler and M. S. Selig, "An Evaluation of an Emprical Model for Stall Delay due to Rotation for HAWTs," in *Windpower 97*, 1997, no. June 15-18.

[86] P. Giguere and M. S. Selig, "Design of a Tapered and Twisted Blade for the NREL Combined Experiment Rotor," 1999.

[87] J. Jonkman, S. Butterfield, W. Musial, and G. Scott, "Definition of a 5-MW Reference Wind Turbine for Offshore System Development," 2009.

[88] J. M. Jonkman and M. L. B. Jr, "FAST User ' s Guide," 2005.

[89] A. D. Wright and L. J. Fingersh, "Advanced Control Design for Wind Turbines Part I : Control Design, Implementation, and Initial Tests," *Tech. Rep. Natl. Renew. Energy Lab.*, no. March, p. 98, 2008.

[90] A. Wright, "Modern Control Design for Flexible Wind Turbines," no. July, 2004.

[91] M. H. Hansen, A. Hansen, T. J. Larsen, S. Øye, P. Sørensen, and P. Fuglsang, "Control design for a pitch-regulated , variable speed wind turbine, Risø-R-1500(EN),Risø National Laboratory," Roskilde, Denmark, 2005.

[92] J. M. Jonkman and B. J. Jonkman, "FAST modularization framework for wind turbine simulation: Full-system linearization," *J. Phys. Conf. Ser.*, vol. 753, no. 8, 2016.

[93] D. Winkelaar, "SWIFT Program for Three-Dimensional Wind Simulation Part 1: Model Description and Program Verification,Technical Report No. ECN-R-92-013," Petten, The Netherlands, 1992.

[94] NREL, "Nrel's S809 Airfoil Graphic and Coordinates," 2017. [Online]. Available: https://wind.nrel.gov/airfoils/shapes/S809_Shape.html. [Accessed: 31-May-2017].

[95] A. J. Calise, N. Hovakimyan, and M. Idan, "Adaptive Output-Feedback Control for Nonlinear Systems using Neural Networks," *Automatica*, vol. 37, pp. 1201–1211, 2001.

APPENDICES

APPENDIX A

This Appendix includes the information about NREL turbines and aerodynamic data of their airfoil(s).

Table A.1 shows the basic properties of experimental turbine used for NREL Phase I to Phase V.

Table A.1 Test turbine basic specifications[71]

Turbine Type	HAWT
Rotor Location	Downwind
Blade Number	3
Rotor Diameter	10.06 m
Root Extension	0.723 m
Rotor Type	Fixed Speed
Power Regulation	Stall-Regulated
Operational Angular Speed	71.63 rpm
Tilt Angle	0 degrees
Cone Angle	3.25 degrees
Cut-in Wind Speed	6 m/s
Cut-out Wind Speed	NA (stall control)
Rated Power	19.8kW

Figure A.1 shows the NREL's S809 airfoil used for the turbines Phase I-Phase VI.

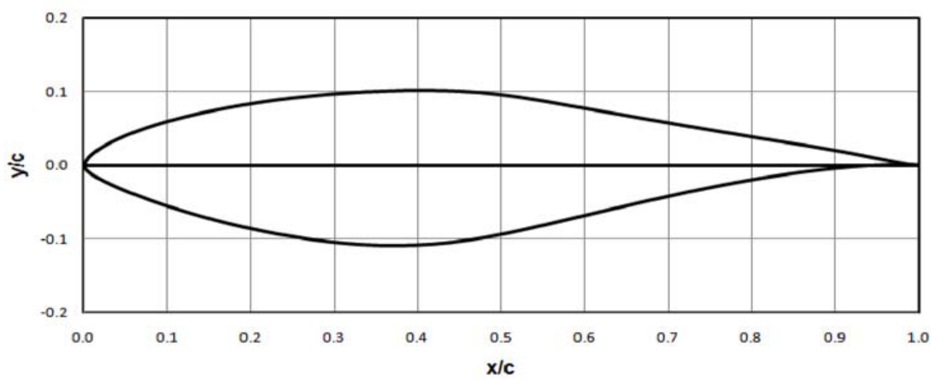

Figure A.1 NREL's S809 airfoil[94]

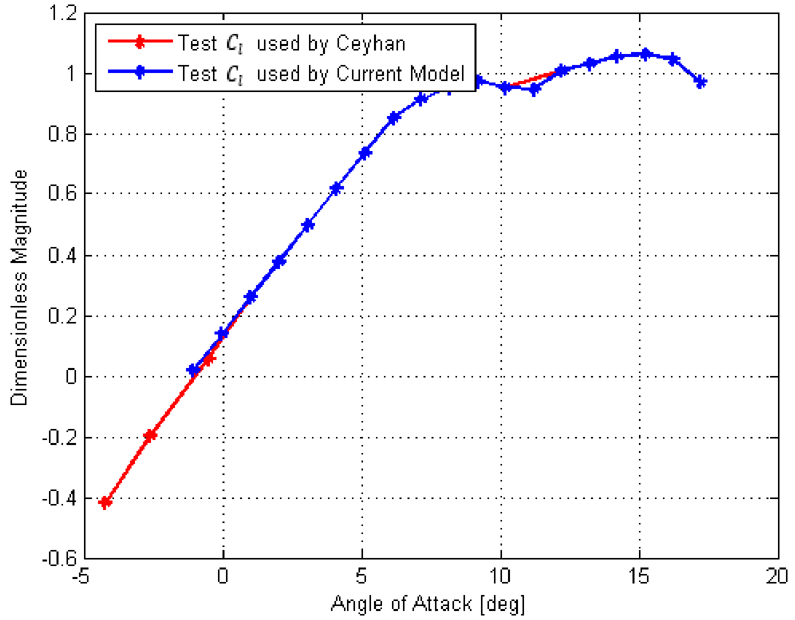

a)

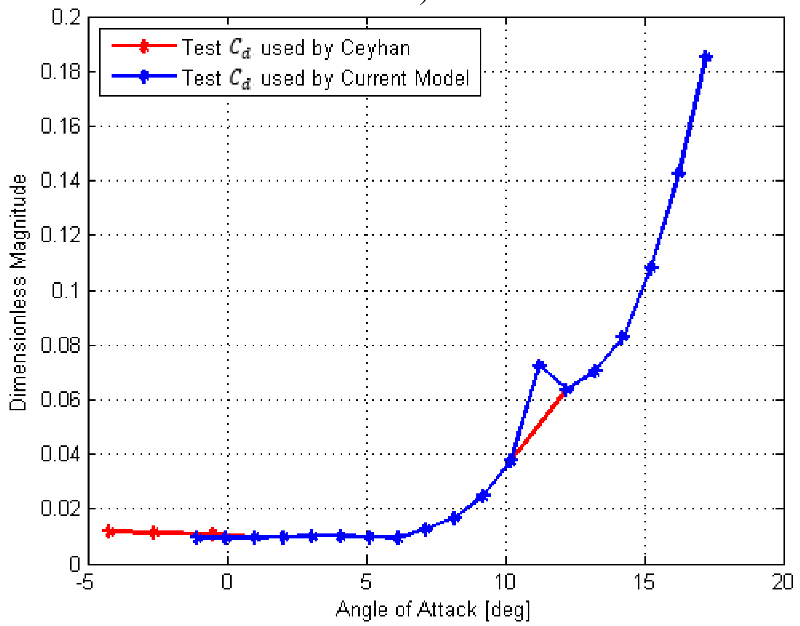

b)

Figure A.2 Aerodynamic data at the Re number of 10^6, a) C_l data, b) C_d data[78], [82]

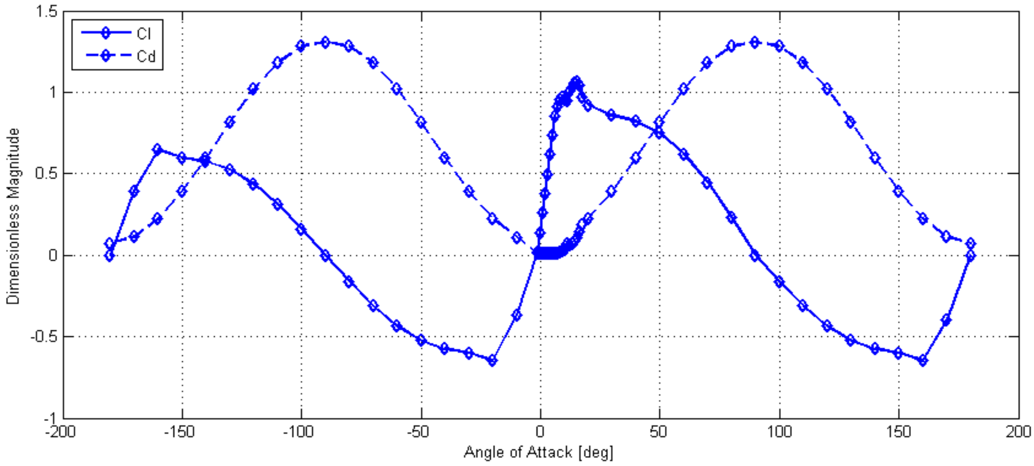

Figure A.3 Extrapolated aerodynamic data at Re number of 10^6,$C_{d,90}$ of 1.308

1 Corrigan and Schilling stall delay model

The Corrigan and Schilling stall delay model[84], [85], used in PROPID program, includes the effect of radial pressure gradient, centrifugal as well as the Coriolis forces. In this model, the amount of stall delay depends on the local solidity. Therefore, the blade elements with a higher local solidity has a higher stall delay than the one with lower local solidity. Basically, in the selected stall delay model, a stall delay angle is calculated for every blade element section. The resultant stall delay angle is employed to modify the airfoil aerodynamic data. This stall delay angle, $\Delta\alpha$ for every element is calculated by the following equation.

$$\Delta\alpha = \left(\alpha C_{l,max} - \alpha C_{l0}\right)\left[\left(\frac{K'\theta_{TE}}{0.136}\right)^n - 1\right] \qquad \text{(A.1)}$$

where n is a constant and usually chosen to be between 0.8 and 1.6. But, the usual value for n that fits well with the experiments is 1. Therefore, this value is selected to calculate the stall delay angle, $\Delta\alpha$. K' is the velocity gradient and there is a universal relation between the K' and the ratio of the local chord to local radius. This is formulated as below.

$$\frac{c}{r} = 0.1517K'^{-1.084} \qquad \text{(A.2)}$$

where θ_{TE} is approximately equal to the ratio of local chord to local radius.

NREL 5 MW TURBINE

Table A.2 Blade aerodynamic properties of NREL 5 MW turbine[87]

Node	R Nodes (m)	Twist Angle (°)	DR Nodes (m)	Chord Length (m)	Airfoil Type
1	2.8667	13.308	2.7333	3.542	Cylinder1
2	5.6000	13.308	2.7333	3.854	Cylinder1
3	8.3333	13.308	2.7333	4.167	Cylinder2
4	11.7500	13.308	4.1000	4.557	DU40_A17
5	15.8500	11.480	4.1000	4.652	DU35_A17
6	19.9500	10.162	4.1000	4.458	DU35_A17
7	24.0500	9.011	4.1000	4.249	DU30_A17
8	28.1500	7.795	4.1000	4.007	DU25_A17
9	32.2500	6.544	4.1000	3.748	DU25_A17
10	36.3500	5.361	4.1000	3.502	DU21_A17
11	40.4500	4.188	4.1000	3.256	DU21_A17
12	44.5500	3.125	4.1000	3.010	NACA64_A17
13	48.6500	2.319	4.1000	2.764	NACA64_A17
14	52.7500	1.526	4.1000	2.518	NACA64_A17
15	56.1667	0.863	2.7333	2.313	NACA64_A17
16	58.9000	0.370	2.7333	2.086	NACA64_A17
17	61.6333	0.106	2.7333	1.419	NACA64_A17

According to the Ref.[87], the aerodynamic data for all airfoil types in Figure A.4, A.5 and A.6 were prepared in AirfoilPrep v2.0 program. Firstly, the stall delay of Selig and Eggars method was utilized to correct lift and drag coefficients between 0° and 90° angles of attack. Afterward, Viterna method was utilized to correct the drag coefficients for the same angle of attack range considering an aspect ratio of 17. Besides, the “DU” refers to Delft University, while “NACA’’ refers to National Advisory Committee for Aeronautics[87].

Table A.3 Properties of NREL 5 MW turbine[87]

Turbine Type	HAWT
Rating	5 MW
Rotor Orientation	Upwind
Rotor Configuration	3 Blades
Rotor Diameter	126 m
Hub Diameter	3 m
Control	Variable Speed, Collective Pitch
Cut-in Wind Speed	3 m/s,
Rated Wind Speed	11.4 m/s,
Cut-Out Wind Speed	25 m/s
Cut-in Rotor Speed	6.9 RPM
Rated Rotor Speed	12.1 RPM
Rated Tip Speed	80 m/s
Tilt Angle	5º
Pre-cone Angle	2.5º
Drivetrain	High Speed, Multi-Stage Gearbox
Rated Rotor Speed	12.1 RPM
Rated Generator Speed	1173.7 RPM
Gearbox Ratio	97:1
Electrical Generator Efficiency	94.4 %
Hub Inertia about Low Speed Shaft	115926 kg m^2
Generator Inertia about High-Speed Shaft	534.116 kg m^2

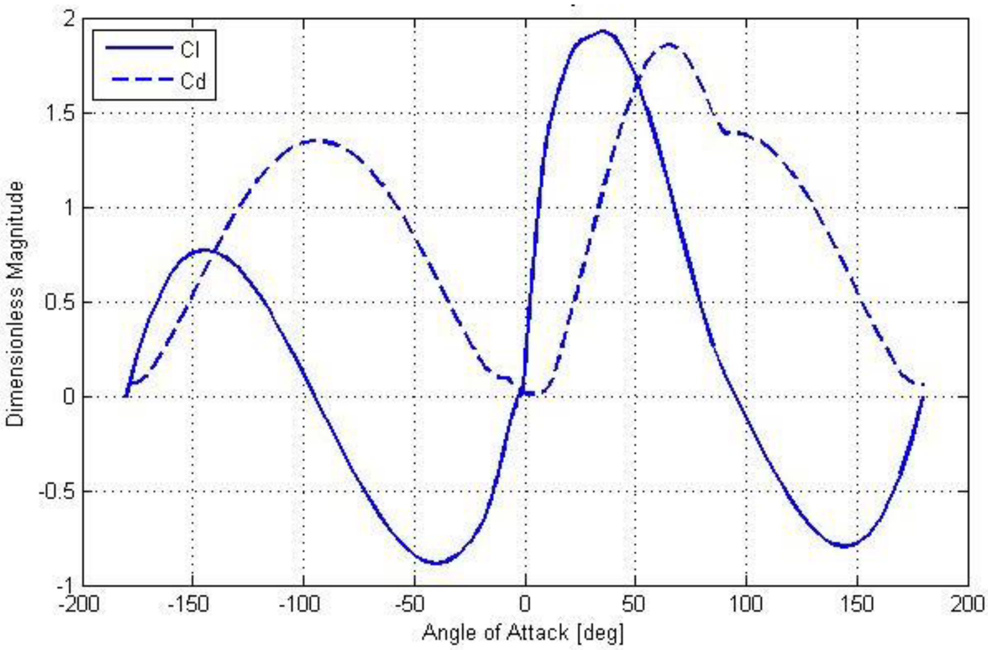

a)

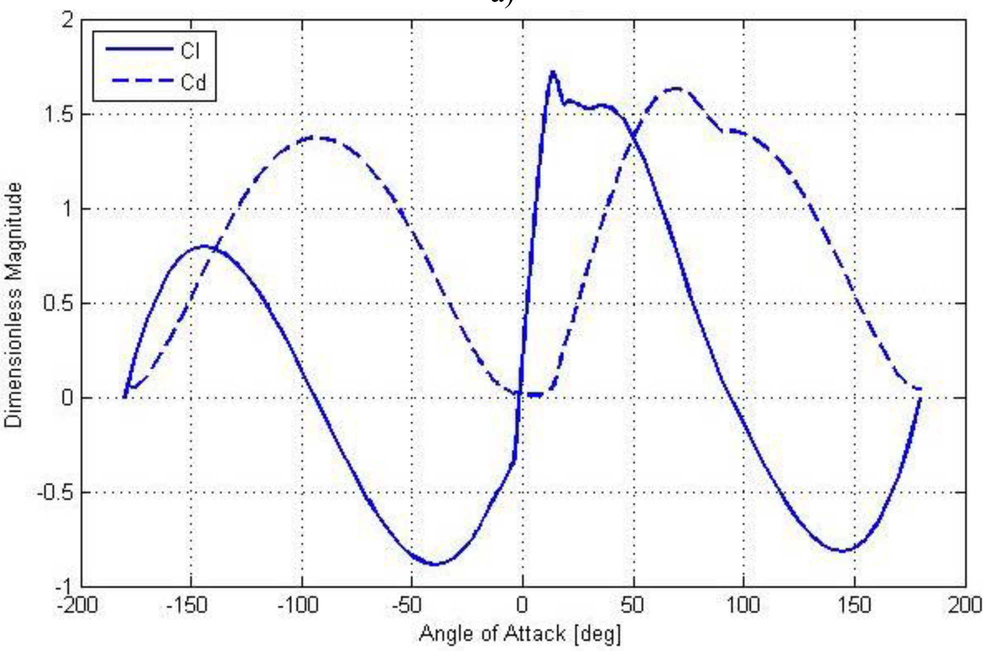

b)

Figure A.4 Aerodynamic data, a) DU40A17, b) DU35A17[87]

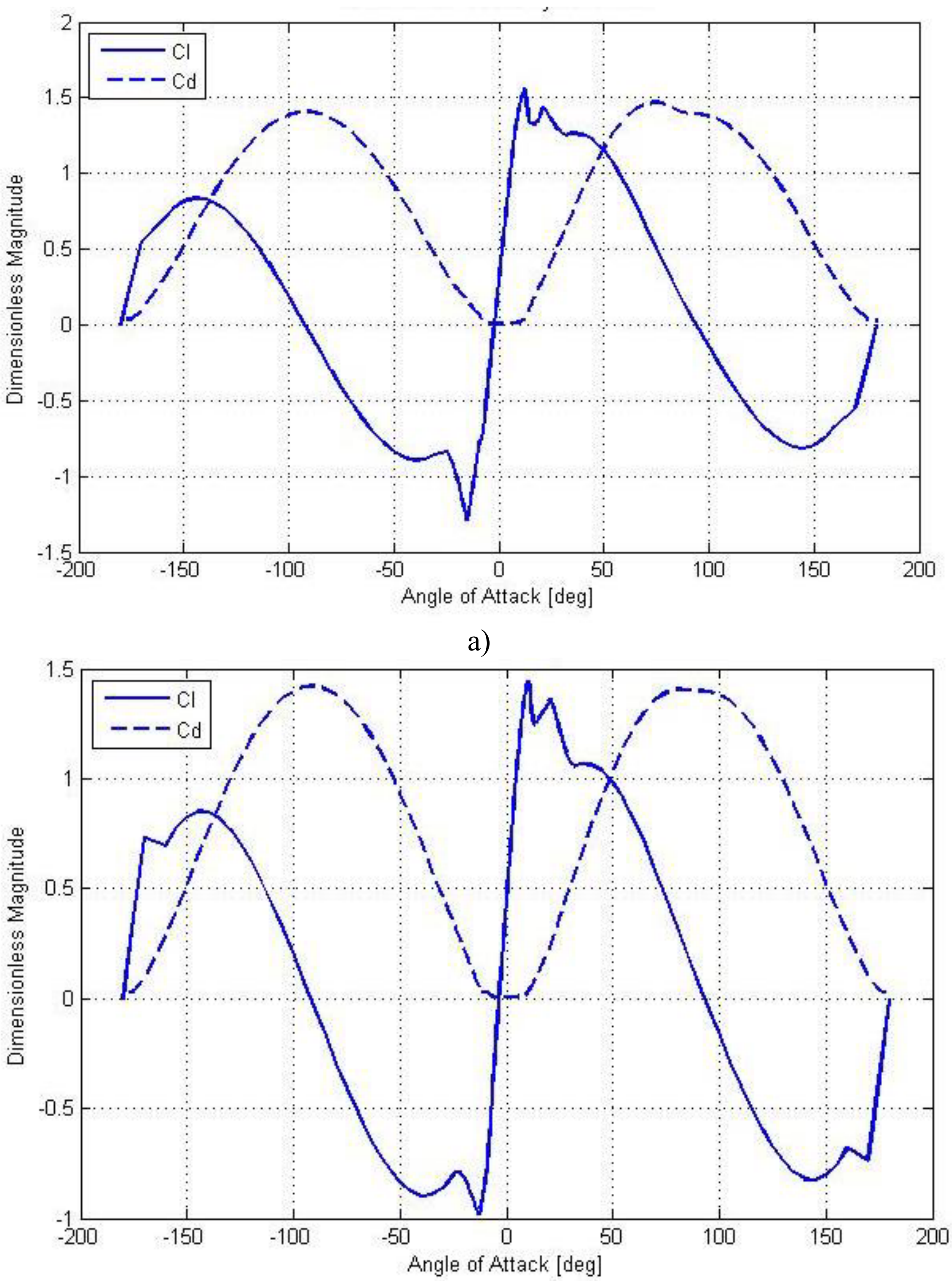

a)

b)

Figure A.5 Aerodynamic data, a) DU30A17, b) DU25A17[87]

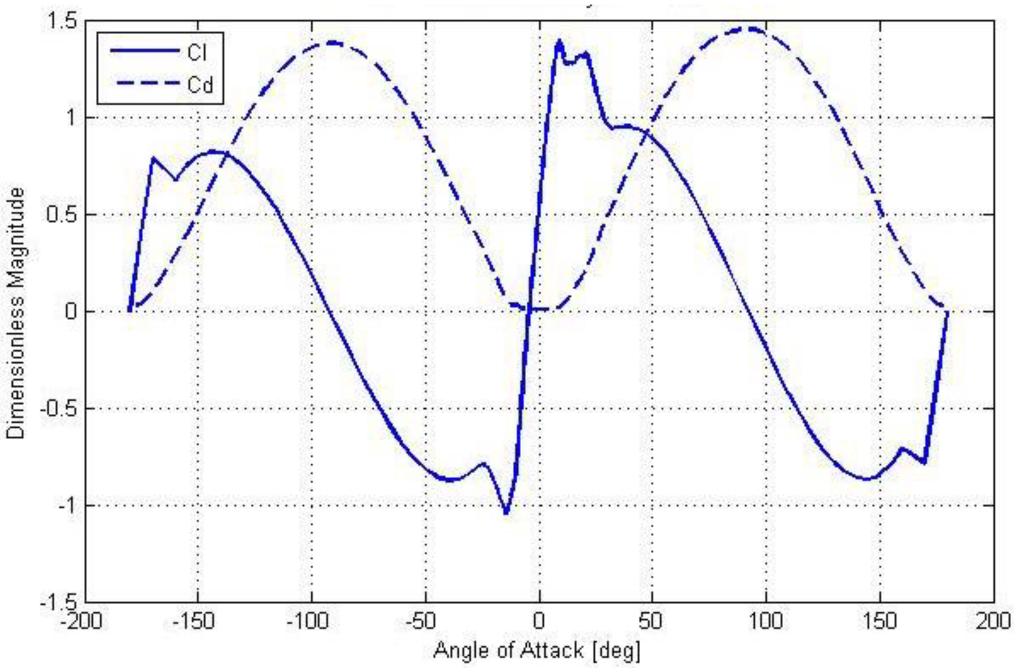

a)

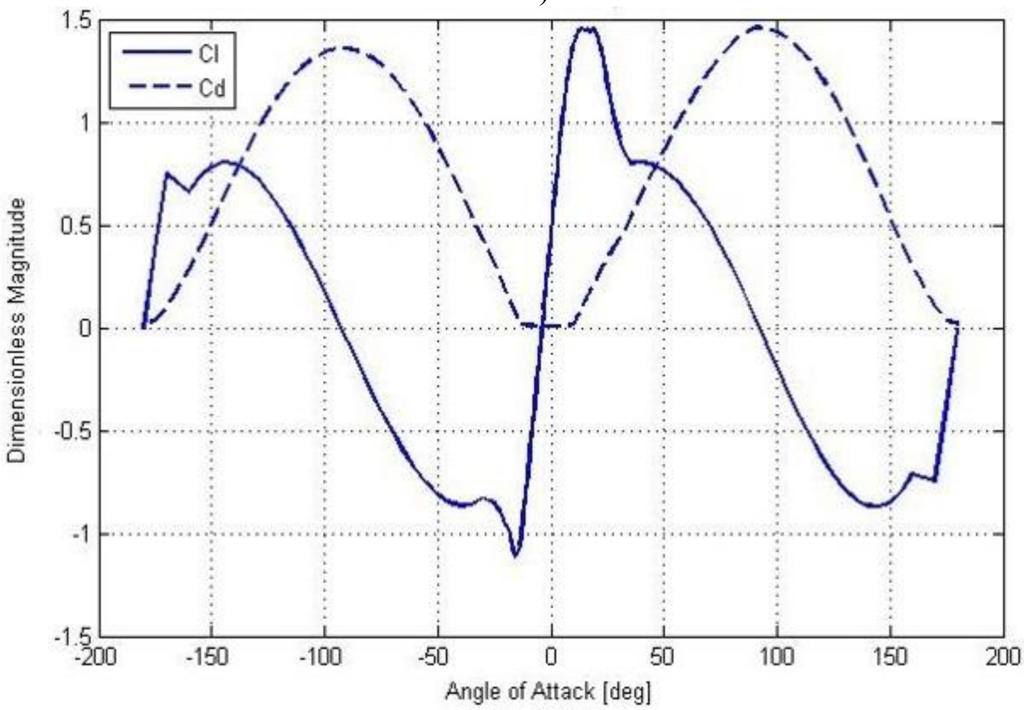

b)

Figure A.6 Aerodynamic data, a) DU21A17, b) NACA64A1[87]

APPENDIX B

This Appendix provides the information about the baseline controller design process. It also defines the theorem for the neural network update law.

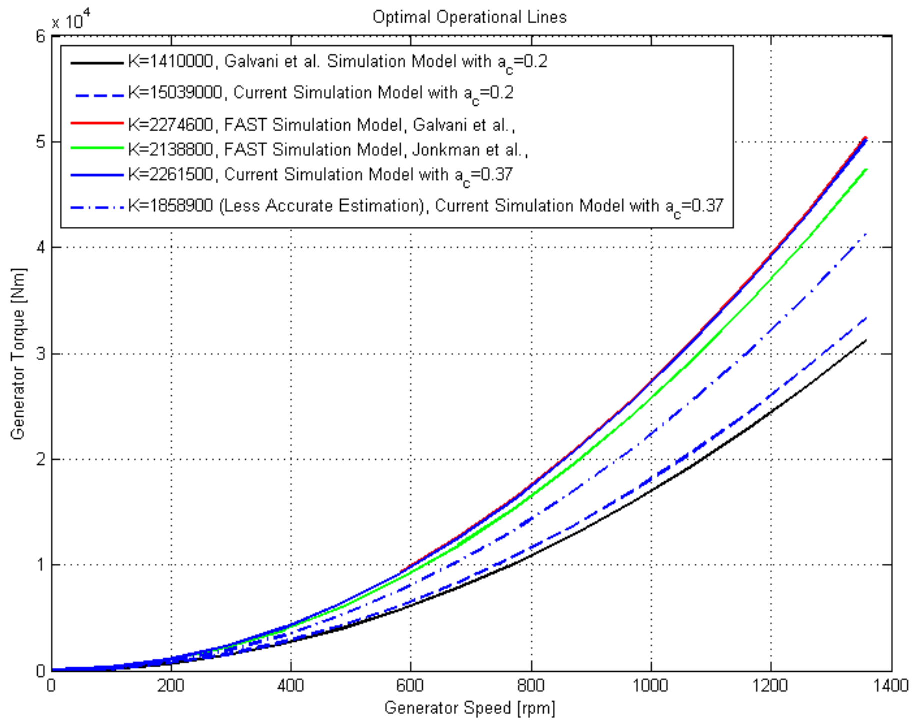

Figure B.1 Optimum operation lines[76], [87]

Figure B.2 shows the input applied to the MS Bladed simulation when the generator torque controller is designed based on the information such as C_{pmax} of 0.4984, TSR of 8 and β_{*} of 0 degree.

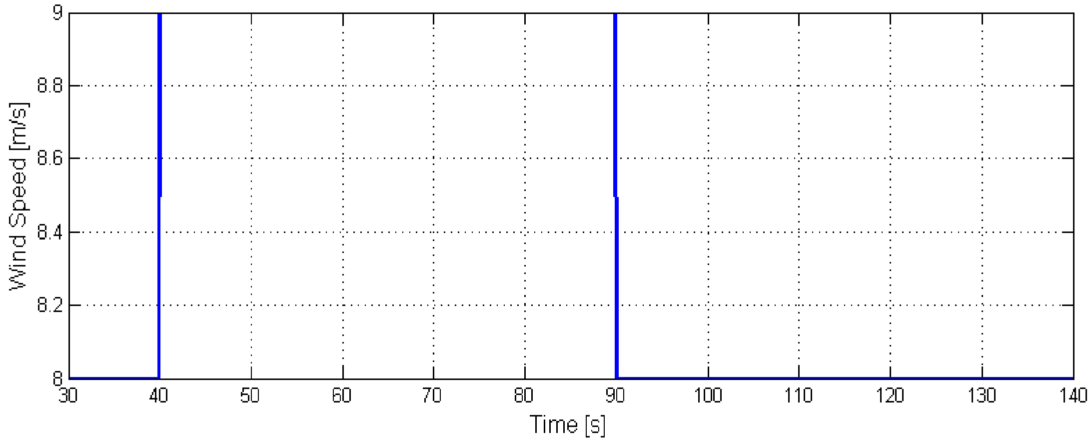

a)

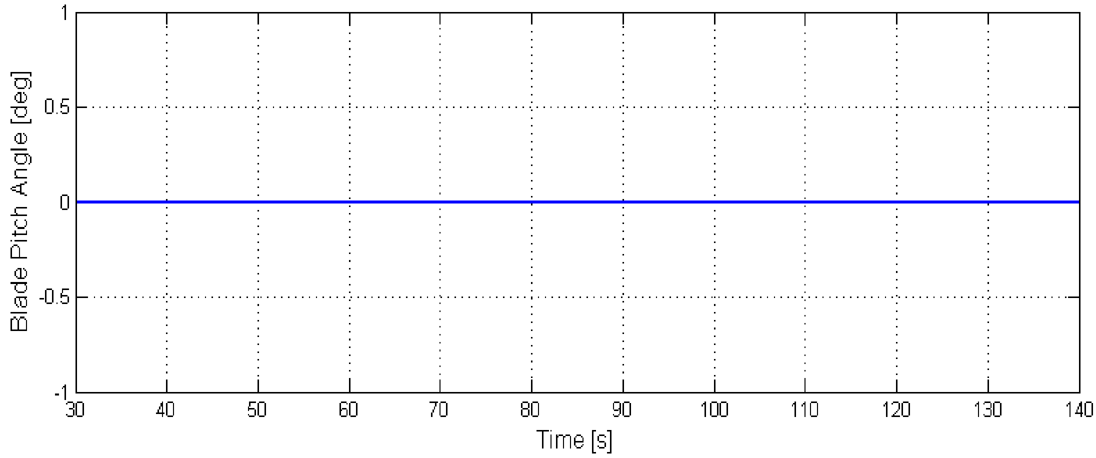

b)

Figure B.2 Inputs to simulation model, a) Wind speed, b) Blade pitch angle

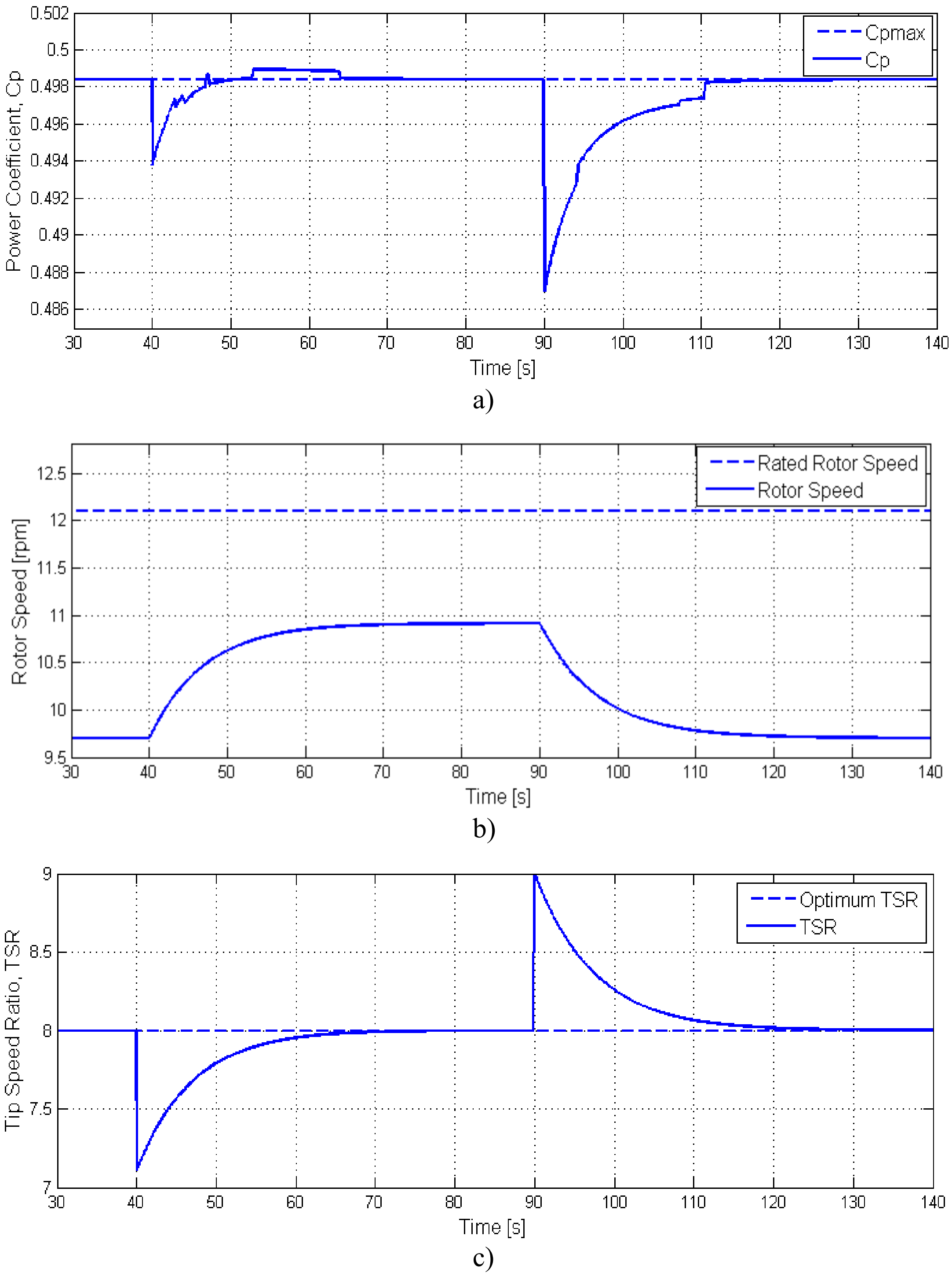

Figure B.3 Simulation results, a) Power coefficient, b) Rotor speed, c) Tip Speed Ratio

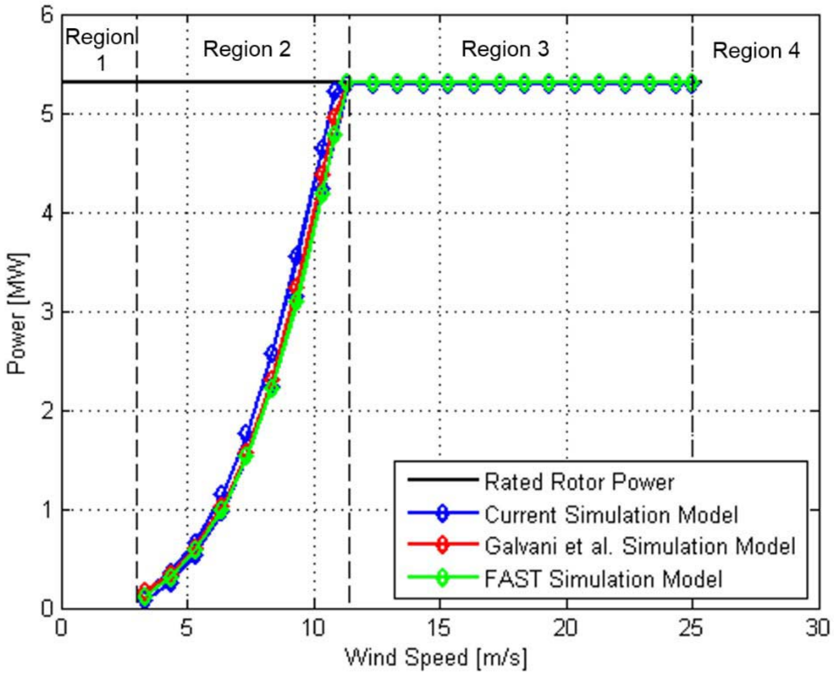

a)

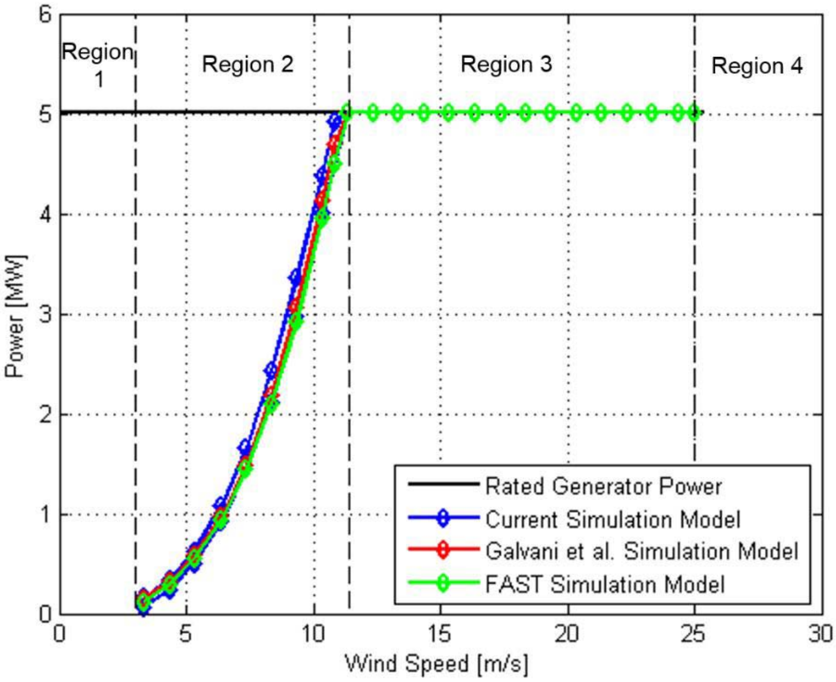

b)

Figure B.4 Controlled power curves, a) Rotor power versus wind speed, b) Generator power versus wind speed

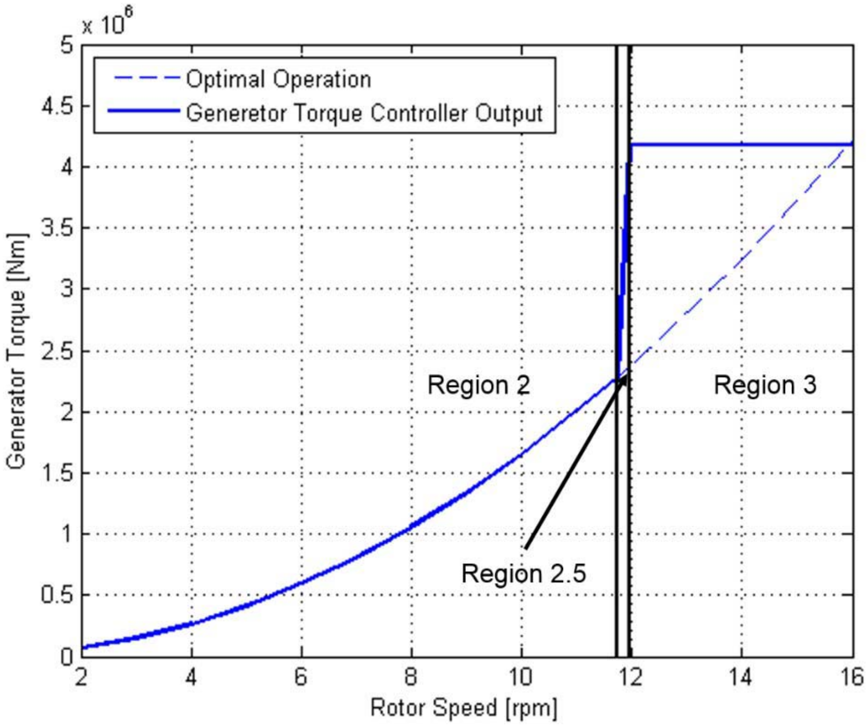

Figure B.5 Region 2.5 Transition controller

1. Theorem for Neural Network Update Law

Following Ref.[49], various function approximations may be utilized for constructing the nonlinear function, Δ. Here, this nonlinear function is approximated by an online learning adaptive neural network, i.e., an LPNN, which is given follows.

$$y = W^T \delta(\mu) \tag{B.1}$$

Where y is the network output, W includes the neural network weights, δ are the network basis functions, μ is the input vector. In addition, $y \in R^r$, $\mu \in R^q$, $W \in R^{rxb}$, $b \geq q$. Since LPNNs are universal approximators[95], vector function $\delta(.)$ may be chosen as a basis over the domain of approximation. Therefore, a function $f(\mu) \in \varrho^r$, $\mu \in \mathfrak{J} \subset R^q$, may be expressed as

$$f(\mu) = W^T \delta(\mu) + \epsilon(\mu) \tag{B.2}$$

where $\epsilon(\mu)$ is the bounded functional reconstruction error. The function f is said to be within ϵ^* range of the network when there are constant weights, W^*, and $\epsilon^* \geq ||\epsilon||$, where $\epsilon^* \geq 0$ is real constant. An LPNN or Δ^* is represented using suitable basis functions as

$$\Delta^* = (W^*)^T \delta(\mu) \tag{B.3}$$

and W^* stands for the optimum network weights which deals with the modeling error of the augmented dynamic model in (6-22). Following Ref.[49], with the $\epsilon^* \geq 0$, there are constant weights and the modeling error may be approximated by an LPNN over a compact set, such that

$$\epsilon^* \geq ||\epsilon|| \tag{B.4}$$

and

$$\xi = \Delta^* + \epsilon \tag{B.5}$$

Therefore, design the LPPN as,

$$\Delta = \widehat{W}^T \delta(\mu) \tag{B.6}$$

Where $\widehat{W}$ are the estimates of W^* and μ is the vector with suitable inputs of Δ function. Therefore, the weight estimation errors are given as

$$\widetilde{W} = W^* - \widehat{W} \tag{B.7}$$

Lastly, considering P be the solution of following Lyapunov equation.

$$(-K)^T P + P(-K) = -I \tag{B.8}$$

Theorem: In addition, the LPNN weights tuning may be defined as

$$\dot{\widehat{W}} = \Gamma(\delta e^T P - k\widehat{W}||e||) \tag{B.9}$$

Where P satisfy the above Lyapunov equation, k is the gain for the e-modification term. Therefore, for learning rates of $\Gamma_{min} < \Gamma < \Gamma_{max}$, where Γ_{min} and Γ_{max} are the lower and upper bounds and $k > 0$, the weight estimation error of (B.7) and the estimation error of (6-15) are eventually bounded[49].

More detail about the proof of the theorem is found in Ref.[49]. Finally, the e-modification term is added into the update law to gain extra damping to the weight update law in B.9.

CIRRICULUM VITAE

PERSONAL INFORMATION

Surname, Name: Şahin, Mustafa
Nationality: Turkish
Date and Place of Birth: 06.06.1986, Erdemli, Mersin.
Marital Status: Single
Phone: +90 5438639125
E-mail: musahin33@gmail.com

EDUCATION

Degree	**Institution**	**Year of Graduation**
Scientific Prep. School	Department of Aerospace Engineering, Middle East Technical University, Ankara	2011-2012
Master Degree	Department of Civil Aviation, Graduate School of Natural and Applied Science, Erciyes University, Kayseri	2009-2011
Bachelor Degree	Department of Aircraft Electrical and Electronics/Avionics, (Valedictorian), School of Civil Aviation, Erciyes University, Kayseri	2005-2009
English Prep. School	School of Foreign Languages, Erciyes University, Kayseri	2004-2005
High School	Erdemli Technical High School, Department of Electricity, (Valedictorian)	2000-2004

ACADEMIC AND WORKING EXPERINCE

Year	Place	Enrollment
2018-	METU Center for Wind Energy, Middle East Technical University, Ankara	Instructor
2013-2018	Department of Aerospace Engineering, Middle East Technical University, Ankara	Graduate Research Assistant
2012-2013	Department of Aircraft Technologies, İzmir Aeronautical School, University of Turkish Aeronautical Association, İzmir	Instructor, Founder Chairman
2009-2012	Department of Aviation Management, Ali Cavit Çelebioğlu School of Civil Aviation, Erzincan University, Erzincan	Instructor
2009-2009	My Technic Aircraft MRO Services, Sahiba Gökçen International Airport, Istanbul	Aircraft Avionics Maintenance Engineer
2004-2009	Arven Construction Industry, Kayseri	Electrician Foreman, Subcontractor
2003-2004	Yıldırım Electric, Mersin	Electrician Master
2002-2003	Özen Electric, Mersin	Technical Staff
2000-2002	Yıldırım Electric, Mersin	Technical Staff

RESEARCH INTEREST

Wind Turbine Aerodynamics, Modeling, Control and Protection, Wind Turbine Electricity Generation, Electrical Machines and Controls, Unmanned Aerial Vehicles and Applications, Flight Mechanics and Control, Aircraft Electrical Systems, Aircraft Instrumentation and Avionics Systems, Aircraft Communication and Navigation Systems, Aircraft Maintenance, Repair and Overhaul.

FOREIGN LANGUAGES

English

INTERNATIONAL JOURNAL ARTICLES

1. Mustafa ŞAHİN, İlkay YAVRUCUK, Adaptive Envelope Protection Control for Below and Above Rated Regions of Wind Turbines, Journal of Wind Energy (under review)

NATIONAL JOURNAL ARTICLES

1. ŞAHİN, M., YILDIRIM, T., Toros Sedirinin İnsansız Hava Aracıyla Ekilmesi Doğa Bilimleri Dergisi Özel Sayısı, 26-28 Ekim 2011, Kahramanmaraş.

INTERNATIONAL CONFERENCE PAPERS

1. ŞAHİN, M., YAVRUCUK, İ., Dynamical Modeling of a Horizontal Axis Wind Turbine System with Precone and Tilt Angles, 9. Ankara International Aerospace Conference, AIAC 2017, 20-22 September 2017.

2. SAHİN, M., GUNDUZ N, EREN, O., SAHBAZ, M., ÇAKIN U., KURTULUS, D. F., 'Performance Analysis of a Micro-scale Model Helicopter Rotor in Hover Flight, 8. Ankara International Aerospace Conference, AIAC 2015, 10-12 September 2015.

3. ŞAHİN M., EKİCİ, M., DEMİRCİ, H., 'An Extensive Structural Maintenance Problem caused by Corrosion on an Aircraft', 7. Ankara International Aerospace Conference, AIAC 2013, 11-13 September 2013.

4. ŞAHİN, M., YILDIRIM, T., Application of a Fixed-Wing Unmanned Aerial Vehicle (UAV) in Reforestation of Lebanon Cedar (Cedrus Libani A. Rich)", 6.

Ankara International Aerospace Conference, AIAC 2011, September 14-16, 2011, Ankara.

NATIONAL CONFERENCE PAPERS

1. SAHİN, M., YAVRUCUK, İ., Değişken Hızlı Rüzgar Türbinlerinin Kısmı ve Tam Yük Bölgeleri için Kontrolcü Tasarımı, 9. Yenilenebilir Enerji Kaynakları Sempozyumu ve Sergisi, YEKSEM 2017, Antalya.
2. SAHİN, M., YAVRUCUK, İ., Rüzgar Türbinin Dinamik Modellenmesinde Belirli Parametrelerin Güç Eğrisi Tahminine Etkilerinin İncelenmesi, 9. Yenilenebilir Enerji Kaynakları Sempozyumu ve Sergisi, YEKSEM 2017, Antalya.
3. ŞAHİN, M., EKİCİ, M., DEMİRCİ, H., Boeing 737-300 Tipi Yolcu Uçağında Gerçekleştirilen Korozyon Kaynaklı Büyük Çaplı Yapısal Tamir Örneği, 12-14 Eylül 2012, Hava Harp Okulu, İstanbul.
4. ŞAHİN, M., YILDIRIM, T., Toros Sedirinin İnsansız Hava Aracıyla Ekilmesi, I. Akdeniz Orman ve Çevre Sempozyumu, 26-28 Ekim 2011, Kahramanmaraş.

OTHER PAPERS

1. ŞAHİN, M., Uçaklar Neden 400 Hz Elektrik Enerjisi Kullanır? Siwep Havacılık Dergisi, Sayfa 65-66, Haziran 2010, TALTA Aylık Havacılık Dergisi sayı:37, sayfa: 15-17, Ocak 2011.

SEMINARS

1. ŞAHİN, M., “Erzincan Üniversitesi Sivil Havacılık Yüksekokulu”, Erzincan Üniversitesi Başöğretmen Salonu, Tanıtım Semineri, 03 Kasım 2010, Erzincan.
2. ŞAHİN, M., “Unutulmuş Bir Efsane Nuri DEMİRAĞ”, Seminer, Erzincan Üniversitesi Başöğretmen Salonu, 19 Nisan 2010, Erzincan.